



1 Global Carbon Budget 2021

2
3 Pierre Friedlingstein^{1,2}, Matthew W. Jones³, Michael O'Sullivan¹, Robbie M. Andrew⁴,
4 Dorothee, C. E. Bakker⁵, Judith Hauck⁶, Corinne Le Quéré³, Glen P. Peters⁴, Wouter
5 Peters^{7,8}, Julia Pongratz^{9,10}, Stephen Sitch¹¹, Josep G. Canadell¹², Philippe Ciais¹³, Rob B.
6 Jackson¹⁴, Simone R. Alin¹⁵, Peter Anthoni¹⁶, Nicholas R. Bates¹⁷, Meike Becker^{18,19}, Nicolas
7 Bellouin²⁰, Laurent Bopp², Thi Tuyet Trang Chau¹³, Frédéric Chevallier¹³, Louise P. Chini²¹,
8 Margot Cronin²², Kim I. Currie²³, Bertrand Decharme²⁴, Laique M. Djeutchouang^{25,26}, Xinyu
9 Dou²⁷, Wiley Evans²⁸, Richard A. Feely¹⁵, Liang Feng²⁹, Thomas Gasser³⁰, Dennis Gilfillan³¹,
10 Thanos Gkritzalis³², Giacomo Grassi³³, Luke Gregor³⁴, Nicolas Gruber³⁴, Özgür Gürses⁶, Ian
11 Harris³⁵, Richard A. Houghton³⁶, George C. Hurtt²¹, Yosuke Iida³⁷, Tatiana Ilyina¹⁰, Ingrid T.
12 Luijkx⁷, Atul Jain³⁸, Steve D. Jones^{18,19}, Etsushi Kato³⁹, Daniel Kennedy⁴⁰, Kees Klein
13 Goldewijk⁴¹, Jürgen Knauer^{12,42}, Jan Ivar Korsbakken⁴, Arne Körtzinger⁴³, Peter
14 Landschützer¹⁰, Siv K. Lauvset^{19, 44}, Nathalie Lefèvre⁴⁵, Sebastian Lienert⁴⁶, Junjie Liu⁴⁷,
15 Gregg Marland^{48,49}, Patrick C. McGuire⁵⁰, Joe R. Melton⁵¹, David R. Munro^{52,53}, Julia E.M.S.
16 Nabel^{10,54}, Shin-Ichiro Nakaoka⁵⁵, Yosuke Niwa^{55,56}, Tsuneo Ono⁵⁷, Denis Pierrot⁵⁸, Benjamin
17 Poulter⁵⁹, Gregor Rehder⁶⁰, Laure Resplandy⁶¹, Eddy Robertson⁶², Christian Rödenbeck⁵⁴,
18 Thais M. Rosan¹¹, Jörg Schwinger^{19, 44}, Clemens Schwingshackl⁹, Roland Séférian²⁴,
19 Adrienne J. Sutton¹⁵, Colm Sweeney⁵³, Toste Tanhua⁴³, Pieter P. Tans⁶³, Hanqin Tian⁶⁴,
20 Bronte Tilbrook^{65,66}, Francesco Tubiello⁶⁷, Guido van der Werf⁶⁸, Nicolas Vuichard¹³, Chisato
21 Wada⁵⁵, Rik Wanninkhof⁶⁸, Andrew J. Watson¹¹, David Willis³, Andrew J. Wiltshire⁶²,
22 Wenping Yuan⁶⁹, Chao Yue¹³, Xu Yue⁷⁰, Sönke Zaehle⁵⁴, Jiye Zeng⁵⁵

23
24 ¹ College of Engineering, Mathematics and Physical Sciences, University of Exeter, Exeter EX4 4QF,
25 UK

26 ² Laboratoire de Météorologie Dynamique / Institut Pierre-Simon Laplace, CNRS, Ecole Normale
27 Supérieure / Université PSL, Sorbonne Université, Ecole Polytechnique, Paris, France

28 ³ Tyndall Centre for Climate Change Research, School of Environmental Sciences, University of East
29 Anglia, Norwich Research Park, Norwich NR4 7TJ, UK

30 ⁴ CICERO Center for International Climate Research, Oslo 0349, Norway

31 ⁵ School of Environmental Sciences, University of East Anglia, Norwich Research Park, Norwich NR4
32 7TJ, UK

33 ⁶ Alfred-Wegener-Institut, Helmholtz-Zentrum für Polar- und Meeresforschung, Am Handelshafen
34 12, 27570 Bremerhaven

35 ⁷ Wageningen University, Environmental Sciences Group, P.O. Box 47, 6700AA, Wageningen, The
36 Netherlands

37 ⁸ University of Groningen, Centre for Isotope Research, Groningen, The Netherlands

38 ⁹ Ludwig-Maximilians-Universität München, Luisenstr. 37, 80333 München, Germany

39 ¹⁰ Max Planck Institute for Meteorology, Bundesstr. 53, 20146 Hamburg, Germany

40 ¹¹ College of Life and Environmental Sciences, University of Exeter, Exeter EX4 4RJ, UK

41 ¹² CSIRO Oceans and Atmosphere, Canberra, ACT 2101, Australia

42 ¹³ Laboratoire des Sciences du Climat et de l'Environnement, LSCE/IPSL, CEA-CNRS-UVSQ, Université
43 Paris-Saclay, F-91198 Gif-sur-Yvette, France

44 ¹⁴ Department of Earth System Science, Woods Institute for the Environment, and Precourt Institute
45 for Energy, Stanford University, Stanford, CA 94305–2210, United States of America

46 ¹⁵ National Oceanic & Atmospheric Administration, Pacific Marine Environmental Laboratory
47 (NOAA/PMEL), 7600 Sand Point Way NE, Seattle, WA 98115, USA



- 1 ¹⁶ Karlsruhe Institute of Technology, Institute of Meteorology and Climate Research/Atmospheric
- 2 Environmental Research, 82467 Garmisch-Partenkirchen, Germany
- 3 ¹⁷ Bermuda Institute of Ocean Sciences (BIOS), 17 Biological Lane, Ferry Reach, St. Georges, GEO1,
- 4 Bermuda
- 5 ¹⁸ Geophysical Institute, University of Bergen, Bergen, Norway
- 6 ¹⁹ Bjerknes Centre for Climate Research, Bergen, Norway
- 7 ²⁰ Department of Meteorology, University of Reading, Reading, UK
- 8 ²¹ Department of Geographical Sciences, University of Maryland, College Park, Maryland 20742, USA
- 9 ²² Marine Institute Ireland, Galway, Rinville, Ireland
- 10 ²³ NIWA, Union Place West, Dunedin, New Zealand
- 11 ²⁴ CNRM, Université de Toulouse, Météo-France, CNRS, Toulouse, France
- 12 ²⁵ Department of Oceanography, University of Cape Town, Cape Town, 7701, South Africa
- 13 ²⁶ SOCCO, Council for Scientific and Industrial Research, Cape Town, 7700, South Africa
- 14 ²⁷ Department of Earth System Science, Tsinghua University, Beijing, China
- 15 ²⁸ Hakai Institute, Heriot Bay, BC, Canada
- 16 ²⁹ National Centre for Earth Observation, University of Edinburgh, UK
- 17 ³⁰ International Institute for Applied Systems Analysis (IIASA), Schlossplatz 1
- 18 A-2361 Laxenburg, Austria
- 19 ³¹ North Carolina School for Science and Mathematics, Durham, North Carolina, USA
- 20 ³² Flanders Marine Institute (VLIZ), InnovOceanSite, Wandelaarkaai 7, 8400 Ostend, Belgium
- 21 ³³ European Commission, Joint Research Centre, 21027 Ispra (VA), Italy
- 22 ³⁴ Environmental Physics Group, ETH Zürich, Institute of Biogeochemistry and Pollutant Dynamics
- 23 and Center for Climate Systems Modeling (C2SM), 8092 Zurich, Switzerland
- 24 ³⁵ NCAS-Climate, Climatic Research Unit, School of Environmental Sciences, University of East Anglia,
- 25 Norwich Research Park, Norwich, NR4 7TJ, UK
- 26 ³⁶ Woodwell Climate Research Center, Falmouth, MA 02540, USA
- 27 ³⁷ Atmosphere and Ocean Department, Japan Meteorological Agency, Minato-Ku, Tokyo 105-8431,
- 28 Japan
- 29 ³⁸ Department of Atmospheric Sciences, University of Illinois, Urbana, IL 61821, USA
- 30 ³⁹ Institute of Applied Energy (IAE), Minato-ku, Tokyo 105-0003, Japan
- 31 ⁴⁰ National Center for Atmospheric Research, Climate and Global Dynamics, Terrestrial Sciences
- 32 Section, Boulder, CO 80305, USA
- 33 ⁴¹ Utrecht University, Faculty of Geosciences, Department IMEW, Copernicus Institute of Sustainable
- 34 Development, Heidelberglaan 2, P.O. Box 80115, 3508 TC, Utrecht, the Netherlands
- 35 ⁴² Hawkesbury Institute for the Environment, Western Sydney University, Penrith, New South Wales,
- 36 Australia
- 37 ⁴³ GEOMAR Helmholtz Centre for Ocean Research Kiel, Düsternbrooker Weg 20, 24105 Kiel,
- 38 Germany
- 39 ⁴⁴ NORCE Norwegian Research Centre, Jahnebakken 5, 5007 Bergen, Norway
- 40 ⁴⁵ LOCEAN/IPSL laboratory, Sorbonne Université, CNRS/IRD/MNHN, Paris, France
- 41 ⁴⁶ Climate and Environmental Physics, Physics Institute and Oeschger Centre for Climate Change
- 42 Research, University of Bern, Bern, Switzerland
- 43 ⁴⁷ Jet Propulsion Laboratory, California Institute of Technology, Pasadena, CA, USA.
- 44 ⁴⁸ Research Institute for Environment, Energy, and Economics, Appalachian State University, Boone,
- 45 North Carolina, USA
- 46 ⁴⁹ Department of Geological and Environmental Sciences, Appalachian State University, Boone,
- 47 North Carolina, USA



- 1 ⁵⁰ Department of Meteorology, Department of Geography & Environmental Science, National Centre
2 for Atmospheric Science, University of Reading, Reading, UK
3 ⁵¹ Climate Research Division, Environment and Climate Change Canada, Victoria, BC, Canada
4 ⁵² Cooperative Institute for Research in Environmental Sciences, University of Colorado, Boulder, CO,
5 80305, USA
6 ⁵³ National Oceanic & Atmospheric Administration/Global Monitoring Laboratory (NOAA/GML),
7 Boulder, CO, 80305, USA
8 ⁵⁴ Max Planck Institute for Biogeochemistry, Jena, Germany
9 ⁵⁵ Earth System Division, National Institute for Environmental Studies, 16-2 Onogawa, Tsukuba,
10 Ibaraki, 305-8506 Japan
11 ⁵⁶ Meteorological Research Institute, 1-1 Nagamine, Tsukuba, Ibaraki, 305-0052 Japan
12 ⁵⁷ Japan Fisheries Research and Education Agency, 2-12-4 Fukuura, Kanazawa-Ku, Yokohama 236-
13 8648, Japan
14 ⁵⁸ National Oceanic & Atmospheric Administration/Atlantic Oceanographic & Meteorological
15 Laboratory (NOAA/AOML), Miami, FL 33149, USA
16 ⁵⁹ NASA Goddard Space Flight Center, Biospheric Sciences Laboratory, Greenbelt, Maryland 20771,
17 USA
18 ⁶⁰ Leibniz Institute for Baltic Sea Research Warnemuende (IOW), Seestrasse 15; 18119 Rostock,
19 Germany
20 ⁶¹ Princeton University, Department of Geosciences and Princeton Environmental Institute,
21 Princeton, NJ, USA
22 ⁶² Met Office Hadley Centre, FitzRoy Road, Exeter EX1 3PB, UK
23 ⁶³ National Oceanic and Atmospheric Administration, Earth System Research Laboratory (NOAA
24 ESRL), Boulder, CO 80305, USA
25 ⁶⁴ School of Forestry and Wildlife Sciences, Auburn University, 602 Duncan Drive, Auburn, AL 36849,
26 USA
27 ⁶⁵ CSIRO Oceans and Atmosphere, PO Box 1538, Hobart Tasmania 7001, Australia
28 ⁶⁶ Australian Antarctic Partnership Program, University of Tasmania, Hobart, Australia
29 ⁶⁷ Statistics Division, Food and Agriculture Organization of the United Nations, Via Terme di
30 Caracalla, Rome 00153, Italy
31 ⁶⁸ Faculty of Earth and Life Sciences, VU University, Amsterdam, The Netherlands
32 ⁶⁹ School of Atmospheric Sciences, Sun Yat-sen University, Zhuhai, Guangdong 510245, China
33 ⁷⁰ School of Environmental Science and Engineering, Nanjing University of Information Science and
34 Technology (NUIST)
35

36 **Correspondence:** Pierre Friedlingstein (p.friedlingstein@exeter.ac.uk)
37
38

39 **Abstract**

40
41 Accurate assessment of anthropogenic carbon dioxide (CO₂) emissions and their
42 redistribution among the atmosphere, ocean, and terrestrial biosphere in a changing
43 climate is critical to better understand the global carbon cycle, support the development of
44 climate policies, and project future climate change. Here we describe and synthesize data
45 sets and methodology to quantify the five major components of the global carbon budget
46 and their uncertainties. Fossil CO₂ emissions (E_{FOS}) are based on energy statistics and



1 cement production data, while emissions from land-use change (E_{LUC}), mainly deforestation,
2 are based on land-use and land-use change data and bookkeeping models. Atmospheric CO_2
3 concentration is measured directly, and its growth rate (G_{ATM}) is computed from the annual
4 changes in concentration. The ocean CO_2 sink (S_{OCEAN}) is estimated with global ocean
5 biogeochemistry models and observation-based data-products. The terrestrial CO_2 sink
6 (S_{LAND}) is estimated with dynamic global vegetation models. The resulting carbon budget
7 imbalance (B_{IM}), the difference between the estimated total emissions and the estimated
8 changes in the atmosphere, ocean, and terrestrial biosphere, is a measure of imperfect data
9 and understanding of the contemporary carbon cycle. All uncertainties are reported as $\pm 1\sigma$.
10 For the first time, an approach is shown to reconcile the difference in our E_{LUC} estimate with
11 the one from national greenhouse gases inventories, supporting the assessment of
12 collective countries' climate progress.

13 For the year 2020, E_{FOS} declined by 5.4% relative to 2019, with fossil emissions at 9.5 ± 0.5
14 $GtC yr^{-1}$ ($9.3 \pm 0.5 GtC yr^{-1}$ when the cement carbonation sink is included), E_{LUC} was 0.9 ± 0.7
15 $GtC yr^{-1}$, for a total anthropogenic CO_2 emission of $10.2 \pm 0.8 GtC yr^{-1}$ ($37.4 \pm 2.9 GtCO_2$).
16 Also, for 2020, G_{ATM} was $5.0 \pm 0.2 GtC yr^{-1}$ ($2.4 \pm 0.1 ppm yr^{-1}$), S_{OCEAN} was $3.0 \pm 0.4 GtC yr^{-1}$
17 and S_{LAND} was $2.9 \pm 1 GtC yr^{-1}$, with a B_{IM} of $-0.8 GtC yr^{-1}$. The global atmospheric CO_2
18 concentration averaged over 2020 reached $412.45 \pm 0.1 ppm$. Preliminary data for 2021,
19 suggest a rebound in E_{FOS} relative to 2020 of +4.9% (4.1% to 5.7%) globally.

20 Overall, the mean and trend in the components of the global carbon budget are consistently
21 estimated over the period 1959-2020, but discrepancies of up to $1 GtC yr^{-1}$ persist for the
22 representation of annual to semi-decadal variability in CO_2 fluxes. Comparison of estimates
23 from multiple approaches and observations shows: (1) a persistent large uncertainty in the
24 estimate of land-use changes emissions, (2) a low agreement between the different
25 methods on the magnitude of the land CO_2 flux in the northern extra-tropics, and (3) a
26 discrepancy between the different methods on the strength of the ocean sink over the last
27 decade. This living data update documents changes in the methods and data sets used in
28 this new global carbon budget and the progress in understanding of the global carbon cycle
29 compared with previous publications of this data set (Friedlingstein et al., 2020;
30 Friedlingstein et al., 2019; Le Quéré et al., 2018b, 2018a, 2016, 2015b, 2015a, 2014, 2013).
31 The data presented in this work are available at <https://doi.org/10.18160/gcp-2021>
32 (Friedlingstein et al., 2021).



1 **Executive Summary**

2 **Global fossil CO₂ emissions (excluding cement carbonation) in 2021 are returning towards**
3 **their 2019 levels after decreasing [5.4%] in 2020.** The 2020 decrease was 0.52 GtC yr⁻¹ (1.9
4 GtCO₂ yr⁻¹), bringing 2020 emissions to 9.5 ± 0.5 GtC yr⁻¹ (34.8 ± 1.8 GtCO₂ yr⁻¹), comparable
5 to the emissions level of 2012. Preliminary estimates based on data available in October
6 2021 and a projection for the rest of the year suggest fossil CO₂ emissions will rebound 4.9%
7 in 2021 (4.1% to 5.7%), bringing emissions at 9.9 GtC yr⁻¹ (36.4 GtCO₂ yr⁻¹), back to about the
8 same level as in 2019 (10.0 ± 0.5 GtC yr⁻¹, 36.7 ± 1.8 GtCO₂ yr⁻¹). Emissions from coal and gas
9 in 2021 are expected to rebound above 2019 levels, while emissions from oil are still below
10 their 2019 level. Emissions in China are expected to be 5.5% higher in 2021 than in 2019,
11 reaching 3.0 GtC (11.1 GtCO₂) and also higher in India with a 4.4% increase in 2021 relative
12 to 2019, reaching 0.75 GtC (2.7 GtCO₂). In contrast, projected 2021 emissions in the United
13 States (1.4 GtC, 5.1 GtCO₂), European Union (0.8 GtC, 2.8 GtCO₂), and the rest of the world
14 (4.0 GtC, 14.8 GtCO₂, in aggregate) remain respectively 3.7%, 4.2%, and 4.2% below their
15 2019 levels. These patterns reflect the stringency of the COVID-19 confinement levels and
16 the background trends in emissions in these countries.

17 **Fossil CO₂ emissions significantly decreased in 23 countries during the decade 2010-2019.**
18 Altogether, these 23 countries contribute to about 2.5 GtC yr⁻¹ fossil fuel CO₂ emissions over
19 the last decade, only about one quarter of world CO₂ fossil emissions.

20 **Global CO₂ emissions from land-use, land-use change, and forestry (LUC) converge based**
21 **on revised data of land-use change and show a small decrease over the past two decades.**
22 Near constant gross emissions estimated at 3.8 ± 0.6 GtC yr⁻¹ in the 2011-2020 decade are
23 only partly offset by growing carbon removals on managed land of 2.7 ± 0.4 GtC yr⁻¹,
24 resulting in the net emissions in managed land of 1.1 ± 0.7 GtC yr⁻¹ (4.1 ± 2.6 GtCO₂ yr⁻¹).
25 These net emissions decreased by 0.2 GtC in 2020 compared to 2019 levels, with large
26 uncertainty. Preliminary estimates for emissions in 2021 suggest a 0.1 GtC decrease for
27 2021, giving net emissions of 0.8 GtC yr⁻¹ (2.9 GtCO₂ yr⁻¹). The convergence of different
28 emission estimates does not reflect the high uncertainty in land-use change datasets, which
29 likely underestimate interannual variability and the (rising) importance of degradation,
30 highlighting the need for accurate land-use data. For the first time, we link the global carbon



1 budget models' estimates to the official country reporting of national greenhouse gases
2 inventories. While the global carbon budget distinguishes anthropogenic from natural
3 drivers of land carbon fluxes, country reporting is area based and attributes part of the
4 natural terrestrial sink on managed land to the land-use sector. Accounting for this
5 redistribution, the two approaches are shown to be consistent with each other.

6 **The remaining carbon budget for a 50% likelihood to limit global warming to 1.5°C, 1.7°C**
7 **and 2°C has shrunk to 120 GtC (420 GtCO₂), 210 GtC (770 GtCO₂) and 350 GtC (1270 GtCO₂)**
8 **respectively, equivalent to 11, 20 and 32 years from the beginning of 2022, assuming 2021**
9 **emissions levels.** Total anthropogenic emissions were 10.4 GtC yr⁻¹ (38.0 GtCO₂ yr⁻¹) in
10 2020, with a preliminary estimate of 10.7 GtC yr⁻¹ (39.4 GtCO₂ yr⁻¹) for 2021. The remaining
11 carbon budget to keep global temperatures below the climate targets of the Paris
12 Agreement has shrunk by 21 GtC (77 GtCO₂) relative to the remaining carbon budget
13 estimate assessed in the IPCC AR6 Working Group 1 assessment. Reaching net zero CO₂
14 emissions by 2050 entails cutting total anthropogenic CO₂ emissions by about 0.4 GtC (1.4
15 GtCO₂) each year on average, comparable to the decrease during 2020, highlighting the
16 scale of the action needed.

17 **The concentration of CO₂ in the atmosphere is set to reach 414.7 ppm in 2021, 49% above**
18 **pre-industrial levels.** The atmospheric CO₂ growth was 5.1 ± 0.02 GtC yr⁻¹ during the decade
19 2011-2020 (47% of total CO₂ emissions) with a preliminary 2021 growth rate estimate of
20 around 4.2 GtC yr⁻¹. The 2020 decrease in total CO₂ emissions of about 0.7 GtC propagated
21 to a reduction of the atmospheric CO₂ growth rate of 0.38GtC (0.18 ppm).

22 **The ocean CO₂ sink resumed a more rapid growth in the past decade after low or no**
23 **growth during the 1991-2002 period.** However, the growth of the ocean CO₂ sink in the
24 past decade has an uncertainty of a factor of three, with estimates based on data products
25 and estimates based on models showing an ocean sink increase of 0.9 GtC yr⁻¹ and 0.3 GtC
26 yr⁻¹ since 2010, respectively. The discrepancy in the trend originates from all latitudes but is
27 largest in the Southern Ocean. The ocean CO₂ sink was 2.8 ± 0.4 GtC yr⁻¹ during the decade
28 2011-2020 (26% of total CO₂ emissions), with a preliminary 2021 estimate of around 2.9 GtC
29 yr⁻¹.



1 **The land CO₂ sink continued to increase during the 2011-2020 period primarily in response**
2 **to increased atmospheric CO₂, albeit with large interannual variability.** The land CO₂ sink
3 was 3.1 ± 0.6 GtC yr⁻¹ during the 2011-2020 decade (29% of total CO₂ emissions), 0.5 GtC yr⁻¹
4 larger than during the previous decade (2000-2009), with a preliminary 2021 estimate of
5 around 3.3 GtC yr⁻¹. Year to year variability in the land sink is about 1 GtC yr⁻¹, making small
6 annual changes in anthropogenic emissions hard to detect in global atmospheric CO₂
7 concentration.



1 1 Introduction

2 The concentration of carbon dioxide (CO₂) in the atmosphere has increased from
3 approximately 277 parts per million (ppm) in 1750 (Joos and Spahni, 2008), the beginning of
4 the Industrial Era, to 412.4 ± 0.1 ppm in 2020 (Dlugokencky and Tans, 2021); Fig. 1). The
5 atmospheric CO₂ increase above pre-industrial levels was, initially, primarily caused by the
6 release of carbon to the atmosphere from deforestation and other land-use change
7 activities (Canadell et al., 2021). While emissions from fossil fuels started before the
8 Industrial Era, they became the dominant source of anthropogenic emissions to the
9 atmosphere from around 1950 and their relative share has continued to increase until
10 present. Anthropogenic emissions occur on top of an active natural carbon cycle that
11 circulates carbon between the reservoirs of the atmosphere, ocean, and terrestrial
12 biosphere on time scales from sub-daily to millennia, while exchanges with geologic
13 reservoirs occur at longer timescales (Archer et al., 2009).

14 The global carbon budget (GCB) presented here refers to the mean, variations, and trends in
15 the perturbation of CO₂ in the environment, referenced to the beginning of the Industrial
16 Era (defined here as 1750). This paper describes the components of the global carbon cycle
17 over the historical period with a stronger focus on the recent period (since 1958, onset of
18 atmospheric CO₂ measurements), the last decade (2011-2020), the last year (2020) and the
19 current year (2021). We quantify the input of CO₂ to the atmosphere by emissions from
20 human activities, the growth rate of atmospheric CO₂ concentration, and the resulting
21 changes in the storage of carbon in the land and ocean reservoirs in response to increasing
22 atmospheric CO₂ levels, climate change and variability, and other anthropogenic and natural
23 changes (Fig. 2). An understanding of this perturbation budget over time and the underlying
24 variability and trends of the natural carbon cycle is necessary to understand the response of
25 natural sinks to changes in climate, CO₂ and land-use change drivers, and to quantify the
26 permissible emissions for a given climate stabilization target.

27 The components of the CO₂ budget that are reported annually in this paper include separate
28 and independent estimates for the CO₂ emissions from (1) fossil fuel combustion and
29 oxidation from all energy and industrial processes; also including cement production and
30 carbonation (E_{FOS}; GtC yr⁻¹) and (2) the emissions resulting from deliberate human activities
31 on land, including those leading to land-use change (E_{LUC}; GtC yr⁻¹); and their partitioning



1 among (3) the growth rate of atmospheric CO₂ concentration (G_{ATM} ; GtC yr⁻¹), and the
2 uptake of CO₂ (the 'CO₂ sinks') in (4) the ocean (S_{OCEAN} ; GtC yr⁻¹) and (5) on land (S_{LAND} ; GtC
3 yr⁻¹). The CO₂ sinks as defined here conceptually include the response of the land (including
4 inland waters and estuaries) and ocean (including coasts and territorial seas) to elevated
5 CO₂ and changes in climate and other environmental conditions, although in practice not all
6 processes are fully accounted for (see Section 2.7). Global emissions and their partitioning
7 among the atmosphere, ocean and land are in reality in balance. Due to the combination of
8 imperfect spatial and/or temporal data coverage, errors in each estimate, and smaller terms
9 not included in our budget estimate (discussed in Section 2.7), the independent estimates
10 (1) to (5) above do not necessarily add up to zero. We therefore (a) additionally assess a set
11 of global atmospheric inverse model results that by design close the global carbon balance
12 (see Section 2.6), and (b) estimate a budget imbalance (B_{IM}), which is a measure of the
13 mismatch between the estimated emissions and the estimated changes in the atmosphere,
14 land and ocean, as follows:

$$15 \quad B_{IM} = E_{FOS} + E_{LUC} - (G_{ATM} + S_{OCEAN} + S_{LAND}) \quad (1)$$

16 G_{ATM} is usually reported in ppm yr⁻¹, which we convert to units of carbon mass per year, GtC
17 yr⁻¹, using 1 ppm = 2.124 GtC (Ballantyne et al., 2012; Table 1). All quantities are presented
18 in units of gigatonnes of carbon (GtC, 10¹⁵ gC), which is the same as petagrams of carbon
19 (PgC; Table 1). Units of gigatonnes of CO₂ (or billion tonnes of CO₂) used in policy are equal
20 to 3.664 multiplied by the value in units of GtC.

21 We also include a quantification of E_{FOS} by country, computed with both territorial and
22 consumption-based accounting (see Section 2), and discuss missing terms from sources
23 other than the combustion of fossil fuels (see Section 2.7).

24 The global CO₂ budget has been assessed by the Intergovernmental Panel on Climate
25 Change (IPCC) in all assessment reports (Prentice et al., 2001; Schimel et al., 1995; Watson
26 et al., 1990; Denman et al., 2007; Ciais et al., 2013; Canadell et al., 2021), and by others (e.g.
27 Ballantyne et al., 2012). The Global Carbon Project (GCP, www.globalcarbonproject.org, last
28 access: 15 October 2021) has coordinated this cooperative community effort for the annual
29 publication of global carbon budgets for the year 2005 (Raupach et al., 2007; including fossil
30 emissions only), year 2006 (Canadell et al., 2007), year 2007 (GCP, 2008), year 2008 (Le
31 Quéré et al., 2009), year 2009 (Friedlingstein et al., 2010), year 2010 (Peters et al., 2012b),



1 year 2012 (Le Quéré et al., 2013; Peters et al., 2013), year 2013 (Le Quéré et al., 2014), year
2 2014 (Le Quéré et al., 2015a; Friedlingstein et al., 2014), year 2015 (Jackson et al., 2016; Le
3 Quéré et al., 2015b), year 2016 (Le Quéré et al., 2016), year 2017 (Le Quéré et al., 2018a;
4 Peters et al., 2017), year 2018 (Le Quéré et al., 2018b; Jackson et al., 2018) year 2019
5 (Friedlingstein et al., 2019; Jackson et al., 2019; Peters et al., 2020) and more recently the
6 year 2020 (Friedlingstein et al., 2020; Le Quéré et al., 2021) . Each of these papers updated
7 previous estimates with the latest available information for the entire time series.

8 We adopt a range of ± 1 standard deviation (σ) to report the uncertainties in our estimates,
9 representing a likelihood of 68% that the true value will be within the provided range if the
10 errors have a Gaussian distribution, and no bias is assumed. This choice reflects the difficulty
11 of characterising the uncertainty in the CO₂ fluxes between the atmosphere and the ocean
12 and land reservoirs individually, particularly on an annual basis, as well as the difficulty of
13 updating the CO₂ emissions from land-use change. A likelihood of 68% provides an
14 indication of our current capability to quantify each term and its uncertainty given the
15 available information. The uncertainties reported here combine statistical analysis of the
16 underlying data, assessments of uncertainties in the generation of the data sets, and expert
17 judgement of the likelihood of results lying outside this range. The limitations of current
18 information are discussed in the paper and have been examined in detail elsewhere
19 (Ballantyne et al., 2015; Zscheischler et al., 2017). We also use a qualitative assessment of
20 confidence level to characterise the annual estimates from each term based on the type,
21 amount, quality, and consistency of the evidence as defined by the IPCC (Stocker et al.,
22 2013).

23 This paper provides a detailed description of the data sets and methodology used to
24 compute the global carbon budget estimates for the industrial period, from 1750 to 2020,
25 and in more detail for the period since 1959. It also provides decadal averages starting in
26 1960 including the most recent decade (2011-2020), results for the year 2020, and a
27 projection for the year 2021. Finally, it provides cumulative emissions from fossil fuels and
28 land-use change since the year 1750, the pre-industrial period; and since the year 1850, the
29 reference year for historical simulations in IPCC AR6 (Eyring et al., 2016). This paper is
30 updated every year using the format of 'living data' to keep a record of budget versions and
31 the changes in new data, revision of data, and changes in methodology that lead to changes



1 in estimates of the carbon budget. Additional materials associated with the release of each
2 new version will be posted at the Global Carbon Project (GCP) website
3 (<http://www.globalcarbonproject.org/carbonbudget>, last access: 15 October 2021), with
4 fossil fuel emissions also available through the Global Carbon Atlas
5 (<http://www.globalcarbonatlas.org>, last access: 15 October 2021). With this approach, we
6 aim to provide the highest transparency and traceability in the reporting of CO₂, the key
7 driver of climate change.

8 **2 Methods**

9 Multiple organizations and research groups around the world generated the original
10 measurements and data used to complete the global carbon budget. The effort presented
11 here is thus mainly one of synthesis, where results from individual groups are collated,
12 analysed, and evaluated for consistency. We facilitate access to original data with the
13 understanding that primary data sets will be referenced in future work (see Table 2 for how
14 to cite the data sets). Descriptions of the measurements, models, and methodologies follow
15 below, and detailed descriptions of each component are provided elsewhere.

16 This is the 16th version of the global carbon budget and the tenth revised version in the
17 format of a living data update in Earth System Science Data. It builds on the latest published
18 global carbon budget of Friedlingstein et al. (2020). The main changes are: the inclusion of
19 (1) data to year 2020 and a projection for the global carbon budget for year 2021; (2) a Kaya
20 analysis to identify the driving factors behind the recent trends in fossil fuel emissions
21 (changes in population, GDP per person, energy use per GDP, and CO₂ emissions per unit
22 energy), (3) an estimate of the ocean sink from models and data-products combined, (4) an
23 assessment of the relative contributions of increased atmospheric CO₂ and climate change
24 in driving the land and ocean sinks, and (5) an assessment of the current trends in
25 anthropogenic emissions and implications for the remaining carbon budget for specific
26 climate targets. The main methodological differences between recent annual carbon
27 budgets (2016–2020) are summarised in Table 3 and previous changes since 2006 are
28 provided in Table A7.



1 **2.1 Fossil CO₂ emissions (E_{FOS})**

2 **2.1.1 Historical period 1850-2020**

3 The estimates of global and national fossil CO₂ emissions (E_{FOS}) include the oxidation of fossil
4 fuels through both combustion (e.g., transport, heating) and chemical oxidation (e.g. carbon
5 anode decomposition in aluminium refining) activities, and the decomposition of carbonates
6 in industrial processes (e.g. the production of cement). We also include CO₂ uptake from the
7 cement carbonation process. Several emissions sources are not estimated or not fully
8 covered: coverage of emissions from lime production are not global, and decomposition of
9 carbonates in glass and ceramic production are included only for UNFCCC Annex 1 countries
10 for lack of activity data. These omissions are considered to be minor. Short-cycle carbon
11 emissions - for example from combustion of biomass - are not included.

12 Our estimates of fossil CO₂ emissions are derived using the standard approach of activity
13 data and emission factors, relying on data collection by many other parties. Our goal is to
14 produce the best estimate of this flux, and we therefore use a prioritisation framework to
15 combine data from different sources that have used different methods, while being careful
16 to avoid double counting and undercounting of emissions sources. The CDIAC-FF emissions
17 dataset, derived largely from UN energy data, forms the foundation, and we extend
18 emissions to year Y-1 using energy growth rates reported by BP. We then proceed to replace
19 estimates using data from what we consider to be superior sources, for example Annex 1
20 countries' official submissions to the UNFCCC. All data points are potentially subject to
21 revision, not just the latest year. For full details see Andrew and Peters (2021).

22 Other estimates of global fossil CO₂ emissions exist, and these are compared by Andrew
23 (2020a). The most common reason for differences in estimates of global fossil CO₂ emissions
24 is a difference in which emissions sources are included in the datasets. Datasets such as
25 those published by BP, the US Energy Information Administration, and the International
26 Energy Agency's 'CO₂ emissions from fuel combustion' are all generally limited to emissions
27 from combustion of fossil fuels. In contrast, datasets such as PRIMAP-hist, CEDS, EDGAR,
28 and GCP's dataset aim to include all sources of fossil CO₂ emissions. See Andrew (2020a) for
29 detailed comparisons and discussion.

30 Cement absorbs CO₂ from the atmosphere over its lifetime, a process known as 'cement
31 carbonation'. We estimate this CO₂ sink as the average of two studies in the literature (Cao



1 et al., 2020; Guo et al., 2021). Both studies use the same model, developed by Xi et al.
2 (2016), with different parameterisations and input data. Since carbonation is a function of
3 both current and previous cement production, we extend these estimates by one year to
4 2020 by using the growth rate derived from the smoothed cement emissions (10-year
5 smoothing) fitted to the carbonation data.
6 We use the Kaya Identity for a simple decomposition of CO₂ emissions into the key drivers
7 (Raupach et al., 2007). While there are variations (Peters et al 2017), we focus here on a
8 decomposition of CO₂ emissions into population, GDP per person, energy use per GDP, and
9 CO₂ emissions per energy. Multiplying these individual components together returns the
10 CO₂ emissions. Using the decomposition, it is possible to attribute the change in CO₂
11 emissions to the change in each of the drivers. This method gives a first order understanding
12 of what causes CO₂ emissions to change each year.

13 **2.1.2 2021 projection**

14 We provide a projection of global CO₂ emissions in 2021 by combining separate projections
15 for China, USA, EU, India, and all other countries combined. The methods are different for
16 each of these. For China we combine monthly fossil fuel production data from the National
17 Bureau of Statistics, import/export data from the Customs Administration, and monthly coal
18 consumption estimates from SX Coal (2021), giving us partial data for the growth rates to
19 date of natural gas, petroleum, and cement, and of the consumption itself for raw coal. We
20 then use a regression model to project full-year emissions based on historical observations.
21 For the USA our projection is taken directly from the Energy Information Administration's
22 (EIA) Short-Term Energy Outlook (EIA, 2021), combined with the year-to-date growth rate of
23 cement production. For the EU we use monthly energy data from Eurostat to derive
24 estimates of monthly CO₂ emissions through July, with coal emissions extended first through
25 September using a statistical relationship with reported electricity generation from coal and
26 other factors, then through December assuming normal seasonal patterns. EU emissions
27 from natural gas - a strongly seasonal cycle - are extended through December using bias-
28 adjusted Holt-Winters exponential smoothing (Chatfield, 1978). EU emissions from oil are
29 derived using the EIA's projection of oil consumption for Europe. EU cement emissions are
30 based on available year-to-date data from two of the largest producers, Germany and
31 Poland. India's projected emissions are derived from estimates through August (September



1 for coal) using the methods of Andrew (2020b) and extrapolated assuming normal seasonal
2 patterns. Emissions for the rest of the world are derived using projected growth in economic
3 production from the IMF (2021) combined with extrapolated changes in emissions intensity
4 of economic production. More details on the E_{FOS} methodology and its 2021 projection can
5 be found in Appendix C.1.

6 **2.2 CO₂ emissions from land-use, land-use change and forestry (E_{LUC})**

7 The net CO₂ flux from land-use, land-use change and forestry (E_{LUC} , called land-use change
8 emissions in the rest of the text) includes CO₂ fluxes from deforestation, afforestation,
9 logging and forest degradation (including harvest activity), shifting cultivation (cycle of
10 cutting forest for agriculture, then abandoning), and regrowth of forests following wood
11 harvest or abandonment of agriculture. Emissions from peat burning and drainage are
12 added from external datasets.

13 Three bookkeeping approaches (updated estimates each of BLUE (Hansis et al., 2015),
14 OSCAR (Gasser et al., 2020), and H&N2017 (Houghton and Nassikas, 2017)) were used to
15 quantify gross sources and sinks and the resulting net E_{LUC} . Uncertainty estimates were
16 derived from the DGVMs ensemble for the time period prior to 1960, using for the recent
17 decades an uncertainty range of ± 0.7 GtC yr⁻¹, which is a semi-quantitative measure for
18 annual and decadal emissions and reflects our best value judgment that there is at least 68%
19 chance ($\pm 1\sigma$) that the true land-use change emission lies within the given range, for the
20 range of processes considered here. This uncertainty range had been increased from 0.5 GtC
21 yr⁻¹ after new bookkeeping models were included that indicated a larger spread than
22 assumed before (Le Quéré et al., 2018). Projections for 2021 are based on fire activity from
23 tropical deforestation and degradation as well as emissions from peat fires and drainage.

24
25 Our E_{LUC} estimates follow the definition of global carbon cycle models of CO₂ fluxes related
26 to land-use and land management and differ from IPCC definitions adopted in national GHG
27 inventories (NGHGI) for reporting under the UNFCCC, which additionally generally include,
28 through adoption of the IPCC so-called managed land proxy approach, the terrestrial fluxes
29 occurring on land defined by countries as managed. This partly includes fluxes due to
30 environmental change (e.g. atmospheric CO₂ increase), which are part of S_{LAND} in our
31 definition. This causes the global emission estimates to be smaller for NGHGI than for the



1 global carbon budget definition (Grassi et al., 2018). The same is the case for FAO estimates
2 of carbon fluxes on forest land, which include, compared to S_{LAND} , both anthropogenic and
3 natural sources on managed land (Tubiello et al., 2021). Using the approach outlined in
4 Grassi et al. (2021), here we map as additional information the two definitions to each
5 other, to provide a comparison of the anthropogenic carbon budget to the official country
6 reporting to the climate convention. More details on the E_{LUC} methodology can be found in
7 Appendix C.2.

8 **2.3 Growth rate in atmospheric CO₂ concentration (G_{ATM})**

9 **2.3.1 Historical period**

10 The rate of growth of the atmospheric CO₂ concentration is provided for years 1959-2020 by
11 the US National Oceanic and Atmospheric Administration Earth System Research Laboratory
12 (NOAA/ESRL; Dlugokencky and Tans, 2021), which is updated from Ballantyne et al. (2012)
13 and includes recent revisions to the calibration scale of atmospheric CO₂ measurements
14 (Hall et al., 2021). For the 1959-1979 period, the global growth rate is based on
15 measurements of atmospheric CO₂ concentration averaged from the Mauna Loa and South
16 Pole stations, as observed by the CO₂ Program at Scripps Institution of Oceanography
17 (Keeling et al., 1976). For the 1980-2020 time period, the global growth rate is based on the
18 average of multiple stations selected from the marine boundary layer sites with well-mixed
19 background air (Ballantyne et al., 2012), after fitting each station with a smoothed curve as
20 a function of time, and averaging by latitude band (Masarie and Tans, 1995). The annual
21 growth rate is estimated by Dlugokencky and Tans (2021) from atmospheric CO₂
22 concentration by taking the average of the most recent December-January months
23 corrected for the average seasonal cycle and subtracting this same average one year earlier.
24 The growth rate in units of ppm yr⁻¹ is converted to units of GtC yr⁻¹ by multiplying by a
25 factor of 2.124 GtC per ppm, assuming instantaneous mixing of CO₂ throughout the
26 atmosphere (Ballantyne et al., 2012).

27 Starting in 2020, NOAA/ESRL now provides estimates of atmospheric CO₂ concentrations
28 with respect to a new calibration scale, referred to as WMO-CO₂-X2019, in line with the
29 recommendation of the World Meteorological Organization (WMO) Global Atmosphere
30 Watch (GAW) community (Hall et al., 2021). The WMO-CO₂-X2019 scale improves upon the



1 earlier WMO-CO₂-X2007 scale by including a broader set of standards, which contain CO₂ in
2 a wider range of concentrations that span the range 250-800 ppm (versus 250–520 ppm for
3 WMO-CO₂-X2007). In addition, NOAA/ESRL made two minor corrections to the analytical
4 procedure used to quantify CO₂ concentrations, fixing an error in the second virial
5 coefficient of CO₂ and accounting for loss of a small amount of CO₂ to materials in the
6 manometer during the measurement process. The difference in concentrations measured
7 using WMO-CO₂-X2019 versus WMO-CO₂-X2007 is $\sim +0.18$ ppm at 400 ppm and the
8 observational record of atmospheric CO₂ concentrations have been revised accordingly. The
9 revisions have been applied retrospectively in all cases where the calibrations were
10 performed by NOAA/ESRL, thus affecting measurements made by members of the WMO-
11 GAW programme and other regionally coordinated programmes (e.g., Integrated Carbon
12 Observing System, ICOS). Changes to the CO₂ concentrations measured across these
13 networks propagate to the global mean CO₂ concentrations. Comparing the estimates of
14 G_{ATM} made by Dlugokencky and Tans (2020), used in the Global Carbon Budget 2020
15 (Friedlingstein et al., 2020), with updated estimates from Dlugokencky and Tans (2021),
16 used here, we find that G_{ATM} reduced on average by -0.06 GtC yr⁻¹ during 2010-2019 and by -
17 0.01 GtC yr⁻¹ during 1959-2019 (well within the uncertainty ranges reported below). Hence
18 the change in analytical procedures made by NOAA/ESRL has a negligible impact on the
19 atmospheric growth rate G_{ATM} .

20 The uncertainty around the atmospheric growth rate is due to four main factors. First, the
21 long-term reproducibility of reference gas standards (around 0.03 ppm for 1σ from the
22 1980s; Dlugokencky and Tans, 2021). Second, small unexplained systematic analytical errors
23 that may have a duration of several months to two years come and go. They have been
24 simulated by randomizing both the duration and the magnitude (determined from the
25 existing evidence) in a Monte Carlo procedure. Third, the network composition of the
26 marine boundary layer with some sites coming or going, gaps in the time series at each site,
27 etc (Dlugokencky and Tans, 2021). The latter uncertainty was estimated by NOAA/ESRL with
28 a Monte Carlo method by constructing 100 "alternative" networks (Masarie and Tans, 1995;
29 NOAA/ESRL, 2019). The second and third uncertainties, summed in quadrature, add up to
30 0.085 ppm on average (Dlugokencky and Tans, 2021). Fourth, the uncertainty associated
31 with using the average CO₂ concentration from a surface network to approximate the true



1 atmospheric average CO₂ concentration (mass-weighted, in 3 dimensions) as needed to
2 assess the total atmospheric CO₂ burden. In reality, CO₂ variations measured at the stations
3 will not exactly track changes in total atmospheric burden, with offsets in magnitude and
4 phasing due to vertical and horizontal mixing. This effect must be very small on decadal and
5 longer time scales, when the atmosphere can be considered well mixed. Preliminary
6 estimates suggest this effect would increase the annual uncertainty, but a full analysis is not
7 yet available. We therefore maintain an uncertainty around the annual growth rate based
8 on the multiple stations data set ranges between 0.11 and 0.72 GtC yr⁻¹, with a mean of 0.61
9 GtC yr⁻¹ for 1959-1979 and 0.17 GtC yr⁻¹ for 1980-2020, when a larger set of stations were
10 available as provided by Dlugokencky and Tans (2021) but recognise further exploration of
11 this uncertainty is required. At this time, we estimate the uncertainty of the decadal
12 averaged growth rate after 1980 at 0.02 GtC yr⁻¹ based on the calibration and the annual
13 growth rate uncertainty but stretched over a 10-year interval. For years prior to 1980, we
14 estimate the decadal averaged uncertainty to be 0.07 GtC yr⁻¹ based on a factor
15 proportional to the annual uncertainty prior and after 1980 (0.02 * [0.61/0.17] GtC yr⁻¹).

16 We assign a high confidence to the annual estimates of G_{ATM} because they are based on
17 direct measurements from multiple and consistent instruments and stations distributed
18 around the world (Ballantyne et al., 2012; Hall et al., 2021).

19 To estimate the total carbon accumulated in the atmosphere since 1750 or 1850, we use an
20 atmospheric CO₂ concentration of 277 ± 3 ppm or 286 ± 3 ppm, respectively, based on a
21 cubic spline fit to ice core data (Joos and Spahni, 2008). For the construction of the
22 cumulative budget shown in Figure 3, we use the fitted estimates of CO₂ concentration from
23 Joos and Spahni (2008) to estimate the annual atmospheric growth rate using the
24 conversion factors shown in Table 1. The uncertainty of ±3 ppm (converted to ±1σ) is taken
25 directly from the IPCC's AR5 assessment (Ciais et al., 2013). Typical uncertainties in the
26 growth rate in atmospheric CO₂ concentration from ice core data are equivalent to ±0.1-
27 0.15 GtC yr⁻¹ as evaluated from the Law Dome data (Etheridge et al., 1996) for individual 20-
28 year intervals over the period from 1850 to 1960 (Bruno and Joos, 1997).



1 **2.3.2 2021 projection**

2 We provide an assessment of G_{ATM} for 2021 based on the monthly calculated global
3 atmospheric CO_2 concentration (GLO) through August (Dlugokencky and Tans, 2021), and
4 bias-adjusted Holt–Winters exponential smoothing with additive seasonality (Chatfield,
5 1978) to project to January 2022. Additional analysis suggests that the first half of the year
6 (the boreal winter-spring-summer transition) shows more interannual variability than the
7 second half of the year (the boreal summer-autumn-winter transition), so that the exact
8 projection method applied to the second half of the year has a relatively smaller impact on
9 the projection of the full year. Uncertainty is estimated from past variability using the
10 standard deviation of the last 5 years' monthly growth rates.

11 **2.4 Ocean CO_2 sink**

12 The reported estimate of the global ocean anthropogenic CO_2 sink S_{OCEAN} is derived as the
13 average of two estimates. The first estimate is derived as the mean over an ensemble of
14 eight global ocean biogeochemistry models (GOBMs, Table 4 and Table A2). The second
15 estimate is obtained as the mean over an ensemble of seven observation-based data-
16 products (Table 4 and Table A3). The GOBMs simulate both the natural and anthropogenic
17 CO_2 cycles in the ocean. They constrain the anthropogenic air-sea CO_2 flux (the dominant
18 component of S_{OCEAN}) by the transport of carbon into the ocean interior, which is also the
19 controlling factor of present-day ocean carbon uptake in the real world. They cover the full
20 globe and all seasons and were recently evaluated against surface ocean carbon
21 observations, suggesting they are suitable to estimate the annual ocean carbon sink (Hauck
22 et al., 2020). The data-products are tightly linked to observations of fCO_2 (fugacity of CO_2 ,
23 which equals pCO_2 corrected for the non-ideal behaviour of the gas; Pfeil et al., 2013), which
24 carry imprints of temporal and spatial variability, but are also sensitive to uncertainties in
25 gas-exchange parameterizations and data-sparsity. Their asset is the assessment of
26 interannual and spatial variability (Hauck et al., 2020). We further use two diagnostic ocean
27 models to estimate S_{OCEAN} over the industrial era (1781-1958).

28 The global fCO_2 -based flux estimates were adjusted to remove the pre-industrial ocean
29 source of CO_2 to the atmosphere of 0.61 GtC yr^{-1} from river input to the ocean (the average
30 of $0.45 \pm 0.18 \text{ GtC yr}^{-1}$ by Jacobson et al. (2007) and $0.78 \pm 0.41 \text{ GtC yr}^{-1}$ by Resplandy et al.,



1 2018), to satisfy our definition of S_{OCEAN} (Hauck et al., 2020). The river flux adjustment was
2 distributed over the latitudinal bands using the regional distribution of Aumont et al. (2001;
3 North: 0.16 GtC yr^{-1} , Tropics: 0.15 GtC yr^{-1} , South: 0.30 GtC yr^{-1}), acknowledging that the
4 boundaries of Aumont et al (2001; namely 20°S and 20°N) are not consistent with the
5 boundaries otherwise used in the GCB (30°S and 30°N). A recent modelling study (Lacroix et
6 al., 2020) suggests that more of the riverine outgassing is located in the tropics than in the
7 Southern Ocean; and hence this regional distribution is associated with a major uncertainty.
8 Anthropogenic perturbations of river carbon and nutrient transport to the ocean are not
9 considered (see section 2.7).

10 We derive S_{OCEAN} from GOBMs by using a simulation (sim A) with historical forcing of climate
11 and atmospheric CO_2 , accounting for model biases and drift from a control simulation (sim
12 B) with constant atmospheric CO_2 and normal year climate forcing. A third simulation (sim
13 C) with historical atmospheric CO_2 increase and normal year climate forcing is used to
14 attribute the ocean sink to CO_2 (sim C minus sim B) and climate (sim A minus sim C) effects.
15 Data-products are adjusted to represent the full ocean area by a simple scaling approach
16 when coverage is below 98%. GOBMs and data-products fall within the observational
17 constraints over the 1990s ($2.2 \pm 0.7 \text{ GtC yr}^{-1}$, Ciais et al., 2013) after applying adjustments .
18 We assign an uncertainty of $\pm 0.4 \text{ GtC yr}^{-1}$ to the ocean sink based on a combination of
19 random (ensemble standard deviation) and systematic uncertainties (GOBMs bias in
20 anthropogenic carbon accumulation, previously reported uncertainties in $f\text{CO}_2$ -based data-
21 products; see section C.3.3). We assess a medium confidence level to the annual ocean CO_2
22 sink and its uncertainty because it is based on multiple lines of evidence, it is consistent with
23 ocean interior carbon estimates (Gruber et al., 2019, see section 3.5.5) and the results are
24 consistent in that the interannual variability in the GOBMs and data-based estimates are all
25 generally small compared to the variability in the growth rate of atmospheric CO_2
26 concentration. We refrain from assigning a high confidence because of the systematic
27 deviation between the GOBM and data-product trends since around 2002. More details on
28 the S_{OCEAN} methodology can be found in Appendix C.3.

29 The ocean CO_2 sink forecast for the year 2021 is based on the annual historical and
30 estimated 2021 atmospheric CO_2 concentration (Dlugokencky and Tans 2021), historical and
31 estimated 2021 annual global fossil fuel emissions from this year's carbon budget, and the
32 spring (March, April, May) Oceanic Niño Index (ONI) index (NCEP, 2021). Using a non-linear



1 regression approach, i.e., a feed-forward neural network, atmospheric CO₂, the ONI index
2 and the fossil fuel emissions are used as training data to best match the annual ocean CO₂
3 sink (i.e. combined S_{OCEAN} estimate from GOBMs and data products) from 1959 through
4 2020 from this year's carbon budget. Using this relationship, the 2021 S_{OCEAN} can then be
5 estimated from the projected 2021 input data using the non-linear relationship established
6 during the network training. To avoid overfitting, the neural network was trained with a
7 variable number of hidden neurons (varying between 2-5) and 20% of the randomly
8 selected training data were withheld for independent internal testing. Based on the best
9 output performance (tested using the 20% withheld input data), the best performing
10 number of neurons was selected. In a second step, we trained the network 10 times using
11 the best number of neurons identified in step 1 and different sets of randomly selected
12 training data. The mean of the 10 trainings is considered our best forecast, whereas the
13 standard deviation of the 10 ensembles provides a first order estimate of the forecast
14 uncertainty. This uncertainty is then combined with the S_{OCEAN} uncertainty (0.4 GtC yr⁻¹) to
15 estimate the overall uncertainty of the 2021 prediction.

16 **2.5 Terrestrial CO₂ sink**

17 The terrestrial land sink (S_{LAND}) is thought to be due to the combined effects of fertilisation
18 by rising atmospheric CO₂ and N inputs on plant growth, as well as the effects of climate
19 change such as the lengthening of the growing season in northern temperate and boreal
20 areas. S_{LAND} does not include land sinks directly resulting from land-use and land-use change
21 (e.g., regrowth of vegetation) as these are part of the land-use flux (E_{LUC}), although system
22 boundaries make it difficult to attribute exactly CO₂ fluxes on land between S_{LAND} and E_{LUC}
23 (Erb et al., 2013).

24 S_{LAND} is estimated from the multi-model mean of 17 DGVMs (Table A1). As described in
25 Appendix C.4, DGVMs simulations include all climate variability and CO₂ effects over land,
26 with 12 DGVMs also including the effect of N inputs. The DGVMs estimate of S_{LAND} does not
27 include the export of carbon to aquatic systems or its historical perturbation, which is
28 discussed in Appendix D3. See Appendix C.4 for DGVMs evaluation and uncertainty
29 assessment for S_{LAND}, using the International Land Model Benchmarking system (ILAMB;
30 Collier et al., 2018). More details on the S_{LAND} methodology can be found in Appendix C.4.



1 Like the ocean forecast, the land CO₂ sink (S_{LAND}) forecast is based on the annual historical
2 and estimated 2021 atmospheric CO₂ concentration (Dlugokencky and Tans 2021), historical
3 and estimated 2021 annual global fossil fuel emissions from this year's carbon budget, and
4 the summer (June, July, August) ONI index (NCEP, 2021). All training data are again used to
5 best match S_{LAND} from 1959 through 2020 from this year's carbon budget using a feed-
6 forward neural network. To avoid overfitting, the neural network was trained with a variable
7 number of hidden neurons (varying between 2-15), larger than for S_{OCEAN} prediction due to
8 the stronger land carbon interannual variability. As done for S_{OCEAN} , a pre-training selects the
9 optimal number of hidden neurons based on 20% withheld input data, and in a second step,
10 an ensemble of 10 forecasts is produced to provide the mean forecast plus uncertainty. This
11 uncertainty is then combined with the S_{LAND} uncertainty for 2020 (1.0 GtC yr⁻¹) to estimate
12 the overall uncertainty of the 2021 prediction.

13 **2.6 The atmospheric perspective**

14 The world-wide network of in-situ atmospheric measurements and satellite derived
15 atmospheric CO₂ column ($x\text{CO}_2$) observations put a strong constraint on changes in the
16 atmospheric abundance of CO₂. This is true globally (hence our large confidence in G_{ATM}),
17 but also regionally in regions with sufficient observational density found mostly in the extra-
18 tropics. This allows atmospheric inversion methods to constrain the magnitude and location
19 of the combined total surface CO₂ fluxes from all sources, including fossil and land-use
20 change emissions and land and ocean CO₂ fluxes. The inversions assume E_{FOS} to be well
21 known, and they solve for the spatial and temporal distribution of land and ocean fluxes
22 from the residual gradients of CO₂ between stations that are not explained by fossil fuel
23 emissions. By design, such systems thus close the carbon balance ($B_{\text{IM}} = 0$) and thus provide
24 an additional perspective on the independent estimates of the ocean and land fluxes.
25 This year's release includes six inversion systems that are described in Table A4. Each system
26 is rooted in Bayesian inversion principles but uses slightly different methodologies. These
27 differences concern the selection of atmospheric CO₂ data and the choice of a-priori fluxes
28 to refine with these data. They also differ in spatial and temporal resolution, assumed
29 correlation structures, and mathematical approach of the models (see references in Table
30 A4 for details). Importantly, the systems use a variety of transport models, which was
31 demonstrated to be a driving factor behind differences in atmospheric inversion-based flux



1 estimates, and specifically their distribution across latitudinal bands (Gaubert et al., 2019;
2 Schuh et al., 2019). Multiple inversion systems (UoE, CTE, and CAMS) were previously tested
3 with satellite xCO₂ retrievals from GOSAT or OCO-2 measurements, but their results at the
4 larger scales (as discussed in this work) did not deviate substantially from their in-situ
5 counterparts and are therefore not separately included. One inversion this year (CMS-Flux)
6 used ACOS-GOSAT v9 retrievals between July 2009 and Dec 2014 and OCO-2 b10 retrievals
7 between Jan 2015 to Dec 2015, in addition to the in-situ observational CO₂ mole fraction
8 records.

9 The original products delivered by the inverse modelers were modified to facilitate the
10 comparison to the other elements of the budget, specifically on 3 accounts: (1) global total
11 fossil fuel emissions, (2) riverine CO₂ transport, and (3) cement carbonation CO₂ uptake.
12 Details are given below. We note that with these adjustments the inverse results no longer
13 represent the net atmosphere-surface exchange over land/ocean areas as sensed by
14 atmospheric observations. Instead for land they become the net loss/uptake of CO₂ by
15 vegetation and soils that is not exported by fluvial systems, similar to the DGVMs estimates.
16 For oceans, they become the net uptake of anthropogenic CO₂, similar to the GOBMs
17 estimates.

18 The inversion systems prescribe global fossil fuel emissions based on the GCP's Gridded
19 Fossil Emissions Dataset version 2021.2 (GCP-GridFEDv2021.2; Jones et al., 2021b), which is
20 an update to 2019 of the first version of GCP-GridFED presented by Jones et al. (2021a).
21 GCP-GridFEDv2021.2 scales gridded estimates of CO₂ emissions from EDGARv4.3.2
22 (Janssens-Maenhout et al., 2019) within national territories to match national emissions
23 estimates provided by the GCB for the years 1959-2020, which were compiled following the
24 methodology described in Section 2.1 with all datasets available on August 14th 2021 (R.
25 Andrew, *pers. comm.*). Small differences between the systems due to for instance regridding
26 to the transport model resolution are corrected for in the latitudinal partitioning we
27 present, to ensure agreement with the estimate of E_{FOS} in this budget. We also note that the
28 ocean fluxes used as prior by 5 out of 6 inversions are part of the suite of the ocean process
29 model or fCO₂ data products suite listed in Section 2.4. Although these fluxes are further
30 adjusted by the atmospheric inversions, it makes the inversion estimates of the ocean fluxes
31 not completely independent of S_{OCEAN} assessed here.



1 To facilitate comparisons to the independent S_{OCEAN} and S_{LAND} , we used the same corrections
2 for transport and outgassing of carbon transported from land to ocean, as done for the
3 observation-based estimates of S_{OCEAN} (see Appendix C.3). Furthermore, the inversions did
4 not include a cement carbonation sink (see section 2.1) and therefore this GCB component
5 is implicitly part of their total land sink estimate. In the numbers presented in this budget,
6 each year's global carbonation sink from cement was subtracted from each year's estimated
7 land sink in each inversion, distributed proportional to fossil fuel emissions per region
8 (North-Tropics-South).

9 The atmospheric inversions are evaluated using vertical profiles of atmospheric CO_2
10 concentrations (Fig. B4). More than 30 aircraft programs over the globe, either regular
11 programs or repeated surveys over at least 9 months, have been used to assess model
12 performance (with space-time observational coverage sparse in the SH and tropics, and
13 denser in NH mid-latitudes; Table A6). The six models are compared to the independent
14 aircraft CO_2 measurements between 2 and 7 km above sea level between 2001 and 2020.
15 Results are shown in Fig. B4 and discussed in Section 3.7.

16 With a relatively small ensemble ($N=6$) of systems that moreover share some a-priori fluxes
17 used with one another, or with the process-based models, it is difficult to justify using their
18 mean and standard deviation as a metric for uncertainty across the ensemble. We therefore
19 report their full range (min-max) without their mean. More details on the atmospheric
20 inversions methodology can be found in Appendix C.5.

21 **2.7 Processes not included in the global carbon budget**

22 The contribution of anthropogenic CO and CH₄ to the global carbon budget is not fully
23 accounted for in Eq. (1) and is described in Appendix D1. The contributions of other
24 carbonates to CO_2 emissions is described in Appendix D2. The contribution of anthropogenic
25 changes in river fluxes is conceptually included in Eq. (1) in S_{OCEAN} and in S_{LAND} , but it is not
26 represented in the process models used to quantify these fluxes. This effect is discussed in
27 Appendix D3. Similarly, the loss of additional sink capacity from reduced forest cover is
28 missing in the combination of approaches used here to estimate both land fluxes (E_{LUC} and
29 S_{LAND}) and its potential effect is discussed and quantified in Appendix D4.

30



1 **3 Results**

2 For each component of the global carbon budget, we present results for three different time
3 periods: the full historical period, from 1850 to 2020, the six decades in which we have
4 atmospheric concentration records from Mauna Loa (1960-2020), a specific focus on last
5 year (2020), and the projection for the current year (2021). Subsequently, we assess the
6 combined constraints from the budget components (often referred to as a bottom-up
7 budget) against the top-down constraints from inverse modeling of atmospheric
8 observations. We do this for the global balance of the last decade, as well as for a regional
9 breakdown of land and ocean sinks by broad latitude bands.

10 **3.1 Fossil CO₂ Emissions**

11 **3.1.1 Historical period 1850-2020**

12 Cumulative fossil CO₂ emissions for 1850-2020 were 455 ± 25 GtC, including the cement
13 carbonation sink (Fig. 3, Table 8) .

14 In this period, 46% of fossil CO₂ emissions came from coal, 35% from oil, 14% from natural
15 gas, 3% from decomposition of carbonates, and 1% from flaring.

16 In 1850, the UK stood for 62% of global fossil CO₂ emissions. In 1891 the combined
17 cumulative emissions of the current members of the European Union reached and
18 subsequently surpassed the level of the UK. Since 1917 US cumulative emissions have been
19 the largest. Over the entire period 1850-2020, US cumulative emissions amount to 110GtC
20 (25% of world total) , the EU's to 80 GtC (18%), and China's to 60 GtC (14%).

21 There are three additional global datasets that include all sources of fossil CO₂ emissions:
22 CDIAC-FF (Gilfillan and Marland, 2021), CEDS version v_2021_04_21 (Hoesly et al., 2018);
23 O'Rourke et al., 2021) and PRIMAP-hist version 2.3.1 (Gütschow et al., 2016, 2021), although
24 these datasets are not independent. CDIAC-FF has the lowest cumulative emissions over
25 1750-2018 at 437 GtC, GCP has 443 GtC, CEDS 445 GtC, PRIMAP-hist TP 453 GtC, and
26 PRIMAP-hist CR 455 GtC. CDIAC-FF excludes emissions from lime production, while both
27 CDIAC-FF and GCP exclude emissions from international bunker fuels prior to 1950. CEDS
28 has higher emissions from international shipping in recent years, while PRIMAP-hist has
29 higher fugitive emissions than the other datasets. However, in general these four datasets
30 are in relative agreement as to total historical global emissions of fossil CO₂.



1 **3.1.2 Recent period 1960-2020**

2 Global fossil CO₂ emissions, E_{FOS} (including the cement carbonation sink), have increased
3 every decade from an average of 3.0 ± 0.2 GtC yr⁻¹ for the decade of the 1960s to an average
4 of 9.5 ± 0.5 GtC yr⁻¹ during 2011-2020 (Table 6, Fig. 2 and Fig. 5). The growth rate in these
5 emissions decreased between the 1960s and the 1990s, from 4.3% yr⁻¹ in the 1960s (1960-
6 1969), 3.2% yr⁻¹ in the 1970s (1970-1979), 1.6% yr⁻¹ in the 1980s (1980-1989), to 0.9% yr⁻¹ in
7 the 1990s (1990-1999). After this period, the growth rate began increasing again in the
8 2000s at an average growth rate of 3.0% yr⁻¹, decreasing to 0.6% yr⁻¹ for the last decade
9 (2011-2020). China's emissions increased by +1.0% yr⁻¹ on average over the last 10 years
10 dominating the global trend, followed by India's emissions increase by +3.9% yr⁻¹, while
11 emissions decreased in EU27 by -1.9% yr⁻¹, and in the USA by -1.1% yr⁻¹. Fig.6 illustrates the
12 spatial distribution of fossil fuel emissions for the 2011-2020 period.

13 E_{FOS} includes the uptake of CO₂ by cement via carbonation which has increased with
14 increasing stocks of cement products, from an average of 20 MtC yr⁻¹ (0.02 GtC yr⁻¹) in the
15 1960s to an average of 200 MtC yr⁻¹ (0.2 GtC yr⁻¹) during 2011-2020 (Fig. 5).

16 **3.1.3 Final year 2020**

17 The estimate of global fossil CO₂ emissions for 2020 is 5.4% lower than in 2019, declining 0.5
18 GtC to reach 9.5 ± 0.5 GtC (9.3 ± 0.5 GtC when including the cement carbonation sink) in
19 2020 (Fig. 5), distributed among coal (40%), oil (32%), natural gas (21%), cement (5%) and
20 others (2%). Compared to the previous year, 2020 emissions from coal, oil and gas declined
21 by 4.4%, 9.7% and 2.3% respectively, while emissions from cement increased by 0.8%. All
22 growth rates presented are adjusted for the leap year, unless stated otherwise.

23 In 2020, the largest absolute contributions to global fossil CO₂ emissions were from China
24 (31%), the USA (14%), the EU27 (7%), and India (7%). These four regions account for 59% of
25 global CO₂ emissions, while the rest of the world contributed 41%, including international
26 aviation and marine bunker fuels (2.9% of the total). Growth rates for these countries from
27 2019 to 2020 were +1.4% (China), -10.6% (USA), -10.9% (EU27), and -7.3% (India), with -
28 7.0% for the rest of the world. The per-capita fossil CO₂ emissions in 2020 were 1.2 tC
29 person⁻¹ yr⁻¹ for the globe, and were 3.9 (USA), 2.0 (China), 1.6 (EU27) and 0.5 (India) tC
30 person⁻¹ yr⁻¹ for the four highest emitting countries (Fig. 5).



1 The decline in emissions of -5.4% in 2020 is close to the projected decline of -6.7%, which
2 was the median of four approaches, published in Friedlingstein et al. (2020). Of the four
3 approaches, the 'GCP' method was closest at -5.8%. That method was based on national
4 emissions projections for China, the USA, the EU27, and India using reported monthly
5 activity data when available and projections of gross domestic product corrected for trends
6 in fossil fuel intensity (I_{FOS}) for the rest of the world. Of the regions, the projection for the
7 EU27 was least accurate, and the reasons for this are discussed by Andrew (2021).

8 **3.1.4 Year 2021 Projection**

9 Globally, we estimate that global fossil CO₂ emissions will rebound 4.9% in 2021 (4.1% to
10 5.7%) to 9.9 GtC (36.4 GtCO₂), returning near their 2019 emission levels of 10.0 GtC (36.7
11 GtCO₂). Global increase in 2021 emissions per fuel types are +5.7% (range 4.5% to 6.8%) for
12 coal, +4.4% (range 3.0% to 5.8%) for oil, +4.3% (range 3.2% to 5.4%) for natural gas, and
13 +6.5% (range 4.8% to 8.3%) for cement.

14 For China, projected fossil emissions in 2021 are expected to increase by 4.0% (range 2.1%
15 to 5.8%) compared with 2020 emissions, bringing 2021 emissions for China around 3.0 GtC
16 yr⁻¹ (11.1 GtCO₂ yr⁻¹). Chinese emissions appear to have risen in both 2020 and 2021 despite
17 the economic disruptions of COVID-19. Increases in fuel specific projections for China are
18 +2.5% for coal, +6.0% for oil, +15.3% natural gas, and +6.4% for cement.

19 For the USA, the Energy Information Administration (EIA) emissions projection for 2021
20 combined with cement clinker data from USGS gives an increase of 7.6% (range 5.3% to
21 10.0%) compared to 2020, bringing USA 2021 emissions around 1.4 GtC yr⁻¹ (5.1 GtCO₂ yr⁻¹).
22 This is based on separate projections for coal +20.4%, oil +9.1%, natural gas -0.4%, and
23 cement +0.7%.

24 For the European Union, our projection for 2021 is for an increase of 7.6% (range 5.6% to
25 9.5%) over 2020, with 2021 emissions around 0.8 GtC yr⁻¹ (2.8 GtCO₂ yr⁻¹). This is based on
26 separate projections for coal of +15.4%, oil +4.3%, natural gas +7.6%, and cement -0.2%.

27 For India, our projection for 2021 is an increase of 12.6% (range of 10.7% to 13.6%) over
28 2020, with 2021 emissions around 0.7 GtC yr⁻¹ (2.7 GtCO₂ yr⁻¹). This is based on separate
29 projections for coal of +14.8%, oil +6.7%, natural gas +4.7%, and cement +21.4%.



1 For the rest of the world, the expected growth rate for 2021 is 2.9% (range 1.8% to 4.1%).
2 This is computed using the GDP projection for the world (excluding China, the USA, the EU,
3 and India) of 4.4% made by the IMF (2021) and a decrease in I_{FOS} of $-1.7\%yr^{-1}$, which is the
4 average over 2011-2020. The uncertainty range is based on the standard deviation of the
5 interannual variability in I_{FOS} during 2011–2020 of $0.6\%yr^{-1}$ and our estimates of uncertainty
6 in the IMF's GDP forecast of 0.6%. The methodology allows independent projections for
7 coal, oil, natural gas, cement, and other components, which add to the total emissions in
8 the rest of the world. The fuel specific projected 2021 growth rates for the rest of the world
9 are: +3.0% (range 0.5% to 5.6%) for coal, +2.1% (-0.5% to +4.7%) for oil, +3.9% (2.4% to
10 5.5%) for natural gas, +4.6% (+2.5% to +6.7%) for cement.

11 Independently, the IEA has published two forecasts of global fossil energy CO₂ emissions
12 (i.e., a subset of fossil CO₂ emissions), first in April (4.8%; IEA, 2021a) and so revised in
13 October at 4% (IEA, 2021b). Carbon Monitor produces estimates of global emissions with
14 low temporal lag, and their estimates suggest that emissions in the first eight months of
15 2021 were 7.0% higher than in the same period in 2020 (Carbon Monitor, 2021).

16 **3.2 Emissions from Land Use Changes**

17 **3.2.1 Historical period 1850-2020**

18 Cumulative CO₂ emissions from land-use changes (E_{LUC}) for 1850-2020 were 200 ± 65 GtC
19 (Table 8; Fig. 3; Fig. 13). The cumulative emissions from E_{LUC} are particularly uncertain, with
20 large spread among individual estimates of 140 GtC (updated H&N2017), 270 GtC (BLUE),
21 and 195 GtC (OSCAR) for the three bookkeeping models and a similar wide estimate of $190 \pm$
22 60 GtC for the DGVMs (all cumulative numbers are rounded to the nearest 5GtC). These
23 estimates are broadly consistent with indirect constraints from vegetation biomass
24 observations, giving a cumulative source of 155 ± 50 GtC over the 1901-2012 period (Li et
25 al., 2017). However, given the large spread a best estimate is difficult to ascertain.

26 **3.2.2 Recent period 1960-2020**

27 In contrast to growing fossil emissions, CO₂ emissions from land-use, land-use change and
28 forestry have remained relatively constant, at around 1.3 ± 0.7 GtC yr^{-1} over the 1970-1999
29 period, and even show a slight decrease over the last 20 years (Table 6) but with large
30 spread across estimates (Table 5, Fig. 7). Emissions are relatively constant in the DGVMs



1 ensemble of models since the 1970s, with similar mean values until the 1990s as the
2 bookkeeping mean and large model spread (Table 5, Fig. 7). The DGVMs average grows
3 larger than the bookkeeping average in the recent decades and shows no sign of decreasing
4 emissions, which is, however, expected as DGVM-based estimates include the loss of
5 additional sink capacity, which grows with time, while the bookkeeping estimates do not
6 (Appendix D4).

7 E_{LUC} is a net term of various gross fluxes, which comprise emissions and removals. Gross
8 emissions are on average 2-4 times larger than the net E_{LUC} emissions, and remained largely
9 constant over the last 60 years, with a moderate increase from an average of 3.4 ± 0.9 GtC
10 yr^{-1} for the decade of the 1960s to an average of 3.8 ± 0.6 GtC yr^{-1} during 2011-2020 (Fig. 7,
11 Table 5), showing the relevance of land management such as harvesting or rotational
12 agriculture. Increases in gross removals, from 1.9 ± 0.4 GtC yr^{-1} for the 1960s to 2.7 ± 0.4 GtC
13 yr^{-1} for 2011-2020, were larger than the increase in gross emissions. Since the processes
14 behind gross removals, foremost forest regrowth and soil recovery, are all slow, while gross
15 emissions include a large instantaneous component, short-term changes in land-use
16 dynamics, such as a temporary decrease in deforestation, influences gross emissions
17 dynamics more than gross removals dynamics. It is these relative changes to each other that
18 explain the decrease in net E_{LUC} emissions over the last two decades and the last few years.
19 Gross fluxes differ more across the three bookkeeping estimates than net fluxes, which is
20 expected due to different process representation; in particular, treatment of shifting
21 cultivation, which increases both gross emissions and removals, differs across models.

22 There is a decrease in net CO_2 emissions from land-use change over the last decade (Fig. 7,
23 Table 6), in contrast to earlier estimates of no clear trend across E_{LUC} estimates
24 (Friedlingstein et al., 2020, Hong et al., 2021). The trend in the last decade is now about -4%
25 per year, compared to the +1.8% per year reported by Friedlingstein et al. (2020). This
26 decrease is principally attributable to changes in E_{LUC} estimates from BLUE and OSCAR,
27 which relate to changes in the underlying land-use forcing, LUH2 (Chini et al. 2021, Hurtt et
28 al. 2020) based on HYDE3.3 (Klein Goldewijk et al., 2017a, b). HYDE3.3 now incorporates
29 updated estimates of agricultural areas by the FAO (see Appendix C.2.2) and uses multi-
30 annual land cover maps from satellite remote sensing (ESA CCI Land Cover) to constrain
31 contemporary land cover patterns. These changes lead to lower global E_{LUC} estimates in the



1 last two decades compared to earlier versions of the global carbon budget due most notably
2 to lower emissions from cropland expansion, particularly in the tropical regions. Rosan et al.
3 (2021) showed that for Brazil, the new HYDE3.3 version is closer to independent, regional
4 estimates of land-use and land cover change (MapBiomas, 2021) with respect to spatial
5 patterns, but it shows less land-use and land cover changes than these independent
6 estimates, while HYDE3.2-based estimates had shown higher changes. The update in land-
7 use forcing leads to a decrease in estimated emissions in Brazil across several models after
8 the documented deforestation peak of 2003-2004 that preceded policies and monitoring
9 systems decreasing deforestation rates. However, estimated emissions based on the new
10 land-use forcing do not reflect the rise in Brazilian deforestation in the recent few years
11 (Silva Junior, 2021), and associated increasing emissions from deforestation would have
12 been missed here. The update in FAO agricultural areas in Brazil also implied that substantial
13 interannual variability reported to earlier FAO assessment and captured by the HYDE3.2
14 version since 2000 was removed. Due to the asymmetry of (fast) decay (like clearing by fire)
15 and (slower) regrowth, such reduced variability is expected to decrease annual emissions.
16 Also, the approach by Houghton and Nassikas (2017) smooths land use area changes before
17 calculating carbon fluxes by a 5-year running mean, hence the three emission estimates are
18 in better agreement than in previous GCB estimates. However, differences still exist, which
19 highlight the need for accurate knowledge of land-use transitions and their spatial and
20 temporal variability. A further caveat is that global land-use change data for model input
21 does not capture forest degradation, which often occurs on small scale or without forest
22 cover changes easily detectable from remote sensing and poses a growing threat to forest
23 area and carbon stocks that may surpass deforestation effects (e.g., Matricardi et al., 2020,
24 Qin et al., 2021).

25 Highest land-use emissions occur in the tropical regions of all three continents, including the
26 Arc of Deforestation in the Amazon basin (Fig. 6b). This is related to massive expansion of
27 cropland, particularly in the last few decades in Latin America, Southeast Asia, and sub-
28 Saharan Africa Emissions (Hong et al., 2021), to a substantial part for export (Pendrill et al.,
29 2019). Emission intensity is high in many tropical countries, particularly of Southeast Asia,
30 due to high rates of land conversion in regions of carbon-dense and often still pristine,
31 undegraded natural forests (Hong et al., 2021). Emissions are further increased by peat fires



1 in equatorial Asia (GFED4s, van der Werf et al., 2017). Uptake due to land-use change
2 occurs, particularly in Europe, partly related to expanding forest area as a consequence of
3 the forest transition in the 19th and 20th century and subsequent regrowth of forest (Fig. 6b)
4 (Mather 2001; McGrath et al., 2015).

5 National GHG inventory data (NGHGI) under the LULUCF sector or data submitted by
6 countries to FAOSTAT differ from the global models' definition of E_{LUC} we adopt here in that
7 in the NGHGI reporting, the natural fluxes (S_{LAND}) are counted towards E_{LUC} when they occur
8 on managed land (Grassi et al., 2018). In order to compare our results to the NGHGI
9 approach, we perform a re-mapping of our E_{LUC} estimate by including the S_{LAND} over
10 managed forest from the DGVMs simulations (following Grassi et al., 2021) to the
11 bookkeeping E_{LUC} estimate (see Appendix C.2.3). For the 2010-2019 period, we estimate
12 that 1.5 GtC yr^{-1} of S_{LAND} occurred on managed forests and is then reallocated to E_{LUC} here, as
13 done in the NGHGI method. Doing so, our mean estimate of E_{LUC} is reduced from a source of
14 1.2 GtC to a sink of -0.4 GtC , very similar to the NGHGI estimate of -0.3 GtC (Table A.8).

15 Though estimates between GHGI, FAOSTAT, individual process-based models and the
16 mapped budget estimates still differ in value and need further analysis, the approach taken
17 here provides a possibility to relate the global models' and NGHGI approach to each other
18 routinely and thus link the anthropogenic carbon budget estimates of land CO_2 fluxes
19 directly to the Global Stocktake, as part of UNFCCC Paris Agreement.

20 **3.2.3 Final year 2020**

21 The global CO_2 emissions from land-use change are estimated as $0.9 \pm 0.7 \text{ GtC}$ in 2020, 0.2
22 GtC lower than 2019, which had featured particularly large peat and tropical
23 deforestation/degradation fires. The surge in deforestation fires in the Amazon, causing
24 about 30% higher emissions from deforestation and degradation fires in 2019 over the
25 previous decade, continued into 2020 (GFED4.1s, van der Werf et al., 2017). However, the
26 unusually dry conditions for a non-El Niño year that occurred in Indonesia in 2019 and led to
27 fire emissions from peat burning, deforestation and degradation in equatorial Asia to be
28 about twice as large as the average over the previous decade (GFED4.1s, van der Werf et al.,
29 2017) ceased in 2020. However, confidence in the annual change remains low.



1 Land-use change and related emissions may have been affected by the COVID-19 pandemic
2 (e.g. Poulter et al., 2021). Although emissions from tropical deforestation and degradation
3 fires have been decreasing from 2019 to 2020 on the global scale, they increased in Latin
4 America (GFED4s; van der Werf et al., 2017). During the period of the pandemic,
5 environmental protection policies and their implementation may have been weakened in
6 Brazil (Vale et al., 2021). In other countries, too, monitoring capacities and legal
7 enforcement of measures to reduce tropical deforestation have been reduced due to
8 budget restrictions of environmental agencies or impairments to ground-based monitoring
9 that prevents land grabs and tenure conflicts (Brancalion et al., 2020, Amador-Jiménez et
10 al., 2020). Effects of the pandemic on trends in fire activity or forest cover changes are hard
11 to separate from those of general political developments and environmental changes and
12 the long-term consequences of disruptions in agricultural and forestry economic activities
13 (e.g., Gruère and Brooks, 2020; Golar et al., 2020; Beckman and Countryman, 2021) remain
14 to be seen.

15 **3.2.4 Year 2021 Projection**

16 With wet conditions in Indonesia and a below-average fire season in South America our
17 preliminary estimate of E_{LUC} for 2021 is substantially lower than the 2011-2020 average. By
18 the end of September 2021 emissions from tropical deforestation and degradation fires
19 were estimated to be 192 TgC, down from 347 TgC in 2019 and 288 in 2020 (315 TgC 1997-
20 2020 average). Peat fire emissions in Equatorial Asia were estimated to be 1 TgC, down from
21 117 TgC in 2019 and 2 TgC in 2020 (74 TgC 1997-2020 average) (GFED4.1s, van der Werf et
22 al., 2017). Based on the fire emissions until the end of September, we expect E_{LUC} emissions
23 of around 0.8 GtC in 2021. Note that although our extrapolation is based on tropical
24 deforestation and degradation fires, degradation attributable to selective logging, edge-
25 effects or fragmentation will not be captured.

26 **3.3 Total anthropogenic emissions**

27 Cumulative anthropogenic CO₂ emissions for 1850-2020 totalled 660 ± 65 GtC (2420 ± 240
28 GtCO₂), of which almost 70% (455 GtC) occurred since 1960 and more than 30% (205 GtC)
29 since 2000 (Table 6 and 8). Total anthropogenic emissions more than doubled over the last



1 60 years, from 4.6 ± 0.7 GtC yr⁻¹ for the decade of the 1960s to an average of 10.6 ± 0.8 GtC
2 yr⁻¹ during 2011-2020.
3 The total anthropogenic CO₂ emissions from fossil plus land-use change amounted to $10.2 \pm$
4 0.8 GtC (37.2 ± 2.9 GtCO₂) in 2020, while for 2021, we project global total anthropogenic
5 CO₂ emissions from fossil and land use changes to be around 10.5 GtC (38.5 GtCO₂).
6 During the historical period 1850-2020, 30% of historical emissions were from land use
7 change and 70% from fossil emissions. However, fossil emissions have grown significantly
8 since 1960 while land use changes have not, and consequently the contributions of land use
9 change to total anthropogenic emissions were smaller during recent periods (17% during
10 the period 1960-2020 and 10% during 2011-2020).

11 **3.4 Atmospheric CO₂**

12 **3.4.1 Historical period 1850-2020**

13 Atmospheric CO₂ concentration was approximately 277 parts per million (ppm) in 1750
14 (Joos and Spahni, 2008), reaching 300ppm in the 1910s, 350ppm in the late 1980s, and
15 reaching 412.44 ± 0.1 ppm in 2020 (Dlugokencky and Tans, 2021); Fig. 1). The mass of
16 carbon in the atmosphere increased by 48% from 590 GtC in 1750 to 876 GtC in 2020.
17 Current CO₂ concentrations in the atmosphere are unprecedented in the last 2 million years
18 and the current rate of atmospheric CO₂ increase is at least 10 times faster than at any other
19 time during the last 800,000 years (Canadell et al., 2021).

20 **3.4.2 Recent period 1960-2020**

21 The growth rate in atmospheric CO₂ level increased from 1.7 ± 0.07 GtC yr⁻¹ in the 1960s to
22 5.1 ± 0.02 GtC yr⁻¹ during 2011-2020 with important decadal variations (Table 6, Fig. 3 and
23 Fig 4).

24 During the last decade (2011-2020), the growth rate in atmospheric CO₂ concentration
25 continued to increase, albeit with large interannual variability (Fig. 4).

26 The airborne fraction (AF), defined as the ratio of atmospheric CO₂ growth rate to total
27 anthropogenic emissions:

$$28 \quad AF = G_{ATM} / (E_{FOS} + E_{LUC}) \quad (2)$$



1 provides a diagnostic of the relative strength of the land and ocean carbon sinks in removing
2 part of the anthropogenic CO₂ perturbation. The evolution of AF over the last 60 years
3 shows no significant trend, remaining nearly at around 45%, albeit showing a large
4 interannual variability driven by the year-to-year variability in G_{ATM} (Fig. 8). The observed
5 stability of the airborne fraction over the 1960-2020 period indicates that the ocean and
6 land CO₂ sinks have been removing on average about 55% of the anthropogenic emissions
7 (see sections 3.5 and 3.6).

8 **3.4.3 Final year 2020**

9 The growth rate in atmospheric CO₂ concentration was 5.0 ± 0.2 GtC (2.37 ± 0.08 ppm) in
10 2020 (Fig. 4; Dlugokencky and Tans, 2021), very close to the 2011-2020 average. The 2020
11 decrease in E_{FOS} and E_{LUC} of about 0.7 GtC propagated to an atmospheric CO₂ growth rate
12 reduction of 0.38 GtC (0.18 ppm), given the significant interannual variability of the land
13 carbon sink.

14 **3.4.4 Year 2021 Projection**

15 The 2021 growth in atmospheric CO₂ concentration (G_{ATM}) is projected to be about 4.2 GtC
16 (1.98 ppm) based on GLO observations until the end of July 2021, bringing the atmospheric
17 CO₂ concentration to an expected level of 414.7 ppm averaged over the year, 49% over the
18 pre-industrial level.

19 **3.5 Ocean Sink**

20 **3.5.1 Historical period 1850-2020**

21 Cumulated since 1850, the ocean sink adds up to 170 ± 35 GtC, with two thirds of this
22 amount being taken up by the global ocean since 1960. Over the historical period, the ocean
23 sink increased in pace with the anthropogenic emissions exponential increase (Fig. 3b).
24 Since 1850, the ocean has removed 26% of total anthropogenic emissions.

25 **3.5.2 Recent period 1960-2020**

26 The ocean CO₂ sink increased from 1.1 ± 0.4 GtC yr⁻¹ in the 1960s to 2.8 ± 0.4 GtC yr⁻¹ during
27 2011-2020 (Table 6), with interannual variations of the order of a few tenths of GtC yr⁻¹ (Fig.
28 9). The ocean-borne fraction ($S_{\text{OCEAN}}/(E_{\text{FOS}}+E_{\text{LUC}})$) has been remarkably constant around 25%



1 on average (Fig. 8). Variations around this mean illustrate decadal variability of the ocean
2 carbon sink. So far, there is no indication of a decrease in the ocean-borne fraction from
3 1960 to 2020. The increase of the ocean sink is primarily driven by the increased
4 atmospheric CO₂ concentration, with the strongest CO₂ induced signal in the North Atlantic
5 and the Southern Ocean (Fig. 10a). The effect of climate change is much weaker, reducing
6 the ocean sink globally by 0.12 ± 0.07 GtC yr⁻¹ or 5% (2011-2020, range -0.8 to -7.4%), and
7 does not show clear spatial patterns across the GOBMs ensemble (Fig. 10b). This is the
8 combined effect of change and variability in all atmospheric forcing fields, previously
9 attributed to wind and temperature changes in one model (LeQuéré et al., 2010).

10 The global net air-sea CO₂ flux is a residual of large natural and anthropogenic CO₂ fluxes
11 into and out of the ocean with distinct regional and seasonal variations (Fig. 6 and B1).
12 Natural fluxes dominate on regional scales, but largely cancel out when integrated globally
13 (Gruber et al., 2009). Mid-latitudes in all basins and the high-latitude North Atlantic
14 dominate the ocean CO₂ uptake where low temperatures and high wind speeds facilitate
15 CO₂ uptake at the surface (Takahashi et al., 2009). In these regions, formation of mode,
16 intermediate and deep-water masses transport anthropogenic carbon into the ocean
17 interior, thus allowing for continued CO₂ uptake at the surface. Outgassing of natural CO₂
18 occurs mostly in the tropics, especially in the equatorial upwelling region, and to a lesser
19 extent in the North Pacific and polar Southern Ocean, mirroring a well-established
20 understanding of regional patterns of air-sea CO₂ exchange (e.g., Takahashi et al., 2009,
21 Gruber et al., 2009). These patterns are also noticeable in the Surface Ocean CO₂ Atlas
22 (SOCAT) dataset, where an ocean fCO₂ value above the atmospheric level indicates
23 outgassing (Fig. B1). This map further illustrates the data-sparsity in the Indian Ocean and
24 the southern hemisphere in general.

25 Interannual variability of the ocean carbon sink is driven by climate variability with a first-
26 order effect from a stronger ocean sink during large El Niño events (e.g., 1997-1998) (Fig. 9;
27 Rödenbeck et al., 2014, Hauck et al., 2020). The GOBMs show the same patterns of decadal
28 variability as the mean of the fCO₂-based data products, with a stagnation of the ocean sink
29 in the 1990s and a strengthening since the early 2000s (Fig. 9, Le Quéré et al., 2007;
30 Landschützer et al., 2015, 2016; DeVries et al., 2017; Hauck et al., 2020; McKinley et al.,
31 2020). Different explanations have been proposed for this decadal variability, ranging from



1 the ocean's response to changes in atmospheric wind and pressure systems (e.g., Le Qué
2 et al., 2007, Keppler and Landschützer, 2019), including variations in upper ocean
3 overturning circulation (DeVries et al., 2017) to the eruption of Mount Pinatubo and its
4 effects on sea surface temperature and slowed atmospheric CO₂ growth rate in the 1990s
5 (McKinley et al., 2020). The main origin of the decadal variability is a matter of debate with a
6 number of studies initially pointing to the Southern Ocean (see review in Canadell et al.,
7 2021), but also contributions from the North Atlantic and North Pacific (Landschützer et al.,
8 2016, DeVries et al., 2019), or a global signal (McKinley et al., 2020) were proposed.

9 Although all individual GOBMs and data-products fall within the observational constraint,
10 the ensemble means of GOBMs, and data-products adjusted for the riverine flux diverge
11 over time with a mean offset increasing from 0.24 GtC yr⁻¹ in the 1990s to 0.66 GtC yr⁻¹
12 in the decade 2011-2020 and reaching 1.1 GtC yr⁻¹ in 2020. The S_{OCEAN} trend diverges with a
13 factor two difference since 2002 (GOBMs: 0.3 ± 0.1 GtC yr⁻¹ per decade, data-products: 0.7 ±
14 0.2 GtC yr⁻¹ per decade, best estimate: 0.5 GtC yr⁻¹ per decade) and with a factor of three
15 since 2010 (GOBMs: 0.3 ± 0.1 GtC yr⁻¹ per decade, data-products: 0.9 ± 0.3 GtC yr⁻¹ per
16 decade, best estimate: 0.6 GtC yr⁻¹ per decade). The GOBMs estimate is lower than in the
17 previous global carbon budget (Friedlingstein et al., 2020), because one high-sink model was
18 not available. The effect of two models (CNRM, MOM6-COBALT) revising their estimates
19 downwards was largely balanced by two models revising their estimate upwards (FESOM-
20 REcoM, PlankTOM).

21 The discrepancy between the two types of estimates stems mostly from a larger Southern
22 Ocean sink in the data-products prior to 2001, and from a larger S_{OCEAN} trend in the northern
23 and southern extra-tropics since then (Fig. 12). Possible explanations for the discrepancy in
24 the Southern Ocean could be missing winter observations and data sparsity in general
25 (Bushinsky et al., 2019, Gloege et al., 2021), model biases (as indicated by the large model
26 spread in the South, Figure 12, and the larger model-data mismatch, Figure B2), or
27 uncertainties in the regional river flux adjustment (Hauck et al., 2020, Lacroix et al., 2020).

28 During 2010-2016, the ocean CO₂ sink appears to have intensified in line with the expected
29 increase from atmospheric CO₂ (McKinley et al., 2020). This effect is stronger in the fCO₂-
30 based data products (Fig. 9, GOBMs: +0.43 GtC yr⁻¹, data-products: +0.56 GtC yr⁻¹). The
31 reduction of -0.09 GtC yr⁻¹ (range: -0.30 to +0.12 GtC yr⁻¹) in the ocean CO₂ sink in 2017 is



1 consistent with the return to normal conditions after the El Niño in 2015/16, which caused
2 an enhanced sink in previous years. After 2017, the GOBMs ensemble mean suggests the
3 ocean sink levelling off at about 2.5 GtC yr^{-1} , whereas the data-products' estimate increases
4 by 0.3 GtC yr^{-1} over the same period.

5 **3.5.3 Final year 2020**

6 The estimated ocean CO_2 sink was $3.0 \pm 0.4 \text{ GtC}$ in 2020. This is the average of GOBMs and
7 data-products, and is a small increase of 0.02 GtC compared to 2019, in line with the
8 competing effects from an expected sink strengthening from atmospheric CO_2 growth and
9 expected sink weakening from La Nina conditions. There is, however, a substantial
10 difference between GOBMs and $f\text{CO}_2$ -based data-products in their mean 2020 S_{OCEAN}
11 estimate (GOBMs: 2.5 GtC , data-products: 3.5 GtC). While the GOBMs simulate a stagnation
12 of the sink from 2019 to 2020 ($-0.02 \pm 0.11 \text{ GtCGtC}$), the data-products suggest an increase
13 by 0.06 GtC , although not significant at the 1σ level ($\pm 0.13 \text{ GtC}$). Four models and four data
14 products show an increase of S_{OCEAN} (GOBMs up to $+0.18 \text{ GtC}$, data-product up to $+0.21$
15 GtC), while four models and three data products show no change or a decrease of S_{OCEAN}
16 (GOBMs down to -0.12 GtC , data-products down to -0.13 GtC ; Fig. 9). The data-products
17 have a larger uncertainty at the tails of the reconstructed time series (e.g., Watson et al.,
18 2020). Specifically, the data-products' estimate of the last year is regularly adjusted in the
19 following release owing to the tail effect and an incrementally increasing data availability
20 with 1-5 years lag (Figure 9 bottom).

21 **3.5.4 Year 2021 Projection**

22 Using a feed-forward neural network method (see section 2.4) we project an ocean sink of
23 2.9 GtC for 2021. This is a reduction of the sink by 0.1 GtC relative to the 2020 value which
24 we attribute to La Niña conditions in January to May 2021 and projections of a re-
25 emergence of La Niña later in the year.

26 **3.5.5 Model Evaluation**

27 The evaluation of the ocean estimates (Fig. B2) shows an RMSE from annually detrended
28 data of 1.3 to $2.8 \mu\text{atm}$ for the seven $f\text{CO}_2$ -based data products over the globe, relative to
29 the $f\text{CO}_2$ observations from the SOCAT v2021 dataset for the period 1990-2020. The GOBMs



1 RMSEs are larger and range from 3.3 to 5.9 μatm . The RMSEs are generally larger at high
2 latitudes compared to the tropics, for both the data products and the GOBMs. The data
3 products have RMSEs of 1.3 to 3.6 μatm in the tropics, 1.3 to 2.7 μatm in the north, and 2.2
4 to 6.1 μatm in the south. Note that the data products are based on the SOCAT v2021
5 database, hence the latter are not independent dataset for the evaluation of the data
6 products. The GOBMs RMSEs are more spread across regions, ranging from 2.7 to 4.3 μatm
7 in the tropics, 2.9 to 6.9 μatm in the North, and 6.4 to 9.8 μatm in the South. The higher
8 RMSEs occur in regions with stronger climate variability, such as the northern and southern
9 high latitudes (poleward of the subtropical gyres). The upper-range of the model RMSEs
10 have decreased somewhat relative to Friedlingstein et al. (2020), owing to one model with
11 upper-end RMSE not being represented this year, and the reduction of RMSE in one model
12 (MPIOM-HAMOCC6), presumably related to the inclusion of riverine carbon fluxes.
13 The additional simulation C allows to separate the steady-state anthropogenic carbon
14 component (sim C - sim B) and to compare the model flux and DIC inventory change directly
15 to the interior ocean estimate of Gruber et al (2019) without further assumptions. The
16 GOBMs ensemble average of steady-state anthropogenic carbon inventory change 1994-
17 2007 amounts to 2.1 GtC yr^{-1} , and is significantly lower than the $2.6 \pm 0.3 \text{ GtC yr}^{-1}$ estimated
18 by Gruber et al (2019). Only the three models with the highest sink estimate fall within the
19 range reported by Gruber et al. (2019). This suggests that most of the models
20 underestimates anthropogenic carbon uptake by the ocean likely due to biases in ocean
21 carbon transport and mixing from the surface mixed layer to the ocean interior.
22 The reported S_{OCEAN} estimate from GOBMs and data-products is $2.1 \pm 0.4 \text{ GtC yr}^{-1}$ over the
23 period 1994 to 2007, which is in agreement with the ocean interior estimate of $2.2 \pm 0.4 \text{ GtC}$
24 yr^{-1} when accounting for the climate effect on the natural CO_2 flux of $-0.4 \pm 0.24 \text{ GtC yr}^{-1}$
25 (Gruber et al., 2019) to match the definition of S_{OCEAN} used here (Hauck et al., 2020). This
26 comparison depends critically on the estimate of the climate effect on the natural CO_2 flux,
27 which is smaller from the GOBMs (section 3.5.2) than in Gruber et al. (2019).



1 **3.6 Land Sink**

2 **3.6.1 Historical period 1850-2020**

3 Cumulated since 1850, the terrestrial CO₂ sink amounts to 195 ± 45 GtC, 30% of total
4 anthropogenic emissions. Over the historical period, the sink increased in pace with the
5 anthropogenic emissions exponential increase (Fig. 3b).

6 **3.6.2 Recent period 1960-2020**

7 The terrestrial CO₂ sink increased from 1.2 ± 0.5 GtC yr⁻¹ in the 1960s to 3.1 ± 0.6 GtC yr⁻¹
8 during 2010-2019, with important interannual variations of up to 2 GtC yr⁻¹ generally
9 showing a decreased land sink during El Niño events (Fig. 7), responsible for the
10 corresponding enhanced growth rate in atmospheric CO₂ concentration. The larger land CO₂
11 sink during 2010-2019 compared to the 1960s is reproduced by all the DGVMs in response
12 to the combined atmospheric CO₂ increase and the changes in climate, and consistent with
13 constraints from the other budget terms (Table 5).

14 Over the period 1960 to present the increase in the global terrestrial CO₂ sink is largely
15 attributed to the CO₂ fertilization effect in the models (Prentice et al., 2001, Piao et al.,
16 2009), directly stimulating plant photosynthesis and increased plant water use in water
17 limited systems, with a small negative contribution of climate change (Fig. 10). There is a
18 range of evidence to support a positive terrestrial carbon sink in response to increasing
19 atmospheric CO₂, albeit with uncertain magnitude (Walker et al., 2021). As expected from
20 theory the greatest CO₂ effect is simulated in the tropical forest regions, associated with
21 warm temperatures and long growing seasons (Hickler et al., 2008) (Fig. 10a). However,
22 evidence from tropical intact forest plots indicate an overall decline in the land sink across
23 Amazonia (1985-2011), attributed to enhanced mortality offsetting productivity gains
24 (Brienen et al., 2005, Hubau et al., 2020). During 2011-2020 the land sink is positive in all
25 regions (Fig. 6) with the exception of central and eastern Brazil, Southwest USA and
26 northern Mexico, Southeast Europe and Central Asia, South Africa, and eastern Australia,
27 where the negative effects of climate variability and change (i.e. reduced rainfall)
28 counterbalance CO₂ effects. This is clearly visible on Figure 10 where the effects of CO₂ (Fig.
29 10a) and climate (Fig. 10b) as simulated by the DGVMs are isolated. The negative effect of
30 climate is the strongest in most of South America, Central America, Southwest US and



1 Central Europe (Fig. 10b). Globally, climate change reduces the land sink by 0.45 ± 0.39 GtC
2 yr^{-1} (2011-2020).

3 In the past years several regions experienced record-setting fire events. While global burned
4 area has declined over the past decades mostly due to declining fire activity in savannas
5 (Andela et al., 2017), forest fire emissions are rising and have the potential to counter the
6 negative fire trend in savannas (Zheng et al., 2021). Noteworthy events include the 2019-
7 2020 Black Summer event in Australia (emissions of roughly 0.2 GtC; van der Velde et al.,
8 2021) and Siberia in 2021 where emissions approached 0.4 GtC or three times the 1997-
9 2020 average according to GFED4s. While other regions, including Western US and
10 Mediterranean Europe, also experienced intense fire seasons in 2021 their emissions are
11 substantially lower.

12 Despite these regional negative effects of climate change on S_{LAND} , the efficiency of land to
13 remove anthropogenic CO_2 emissions has remained broadly constant over the last six
14 decades, with a land-borne fraction ($S_{\text{LAND}}/(E_{\text{FOS}}+E_{\text{LUC}})$) of $\sim 30\%$ (Fig 8).

15 **3.6.3 Final year 2020**

16 The terrestrial CO_2 sink from the DGVMs ensemble was 2.9 ± 1.0 GtC in 2020, slightly below
17 the decadal average of 3.1 GtC yr^{-1} (Fig. 4, Table 6). We note that the DGVMs estimate for
18 2020 is significantly larger than the 2.1 ± 0.9 GtC yr^{-1} estimate from the residual sink from
19 the global budget ($E_{\text{FOS}}+E_{\text{LUC}}-G_{\text{ATM}}-S_{\text{OCEAN}}$) (Table 5).

20 **3.6.4 Year 2021 Projection**

21 Using a feed-forward neural network method (see section 2.5) we project a land sink of 3.3
22 GtC for 2021. This is an increase of the land sink by 0.3 GtC relative to the 2020 value which
23 we attribute to La Niña conditions in 2021.

24 **3.6.5 Model Evaluation**

25 The evaluation of the DGVMs (Fig. B3) shows generally high skill scores across models for
26 runoff, and to a lesser extent for vegetation biomass, GPP, and ecosystem respiration (Fig.
27 B3, left panel). Skill score was lowest for leaf area index and net ecosystem exchange, with a
28 widest disparity among models for soil carbon. Further analysis of the results will be



1 provided separately, focusing on the strengths and weaknesses in the DGVMs ensemble and
2 its validity for use in the global carbon budget.

3 **3.7 Partitioning the carbon sinks**

4 **3.7.1 Global sinks and spread of estimates**

5 In the period 2011-2020, the bottom-up view of total global carbon sinks provided by the
6 GCB ($S_{\text{OCEAN}} + S_{\text{LAND}} - E_{\text{LUC}}$) agrees closely with the top-down budget delivered by the
7 atmospheric inversions. Figure 11 shows both total sink estimates of the last decade split by
8 land and ocean, which match the difference between G_{ATM} and E_{FOS} to within 0.06–0.17 GtC
9 yr^{-1} for inverse models, and to 0.3 GtC yr^{-1} for the GCB mean. The latter represents the B_{IM}
10 discussed in Section 3.8, which by design is minimal for the inverse models.

11 The distributions based on the individual models and data products reveal substantial
12 spread but converge near the decadal means quoted in Tables 5 and 6. Sink estimates for
13 S_{OCEAN} and from inverse models are mostly non-Gaussian, while the ensemble of DGVMs
14 appears more normally distributed justifying the use of a multi-model mean and standard
15 deviation for their errors in the budget. Noteworthy is that the tails of the distributions
16 provided by the land and ocean bottom-up estimates would not agree with the global
17 constraint provided by the fossil fuel emissions and the observed atmospheric CO_2 growth
18 rate ($E_{\text{FOS}} - G_{\text{ATM}}$). This illustrates the power of the atmospheric joint constraint from G_{ATM}
19 and the global CO_2 observation network it derives from.

20 **3.7.2 Total atmosphere-to-land fluxes**

21 The total atmosphere-to-land fluxes ($S_{\text{LAND}} - E_{\text{LUC}}$), calculated here as the difference between
22 S_{LAND} from the DGVMs and E_{LUC} from the bookkeeping models, amounts to a 1.9 ± 0.9 GtC yr^{-1}
23 sink during 2011-2020 (Table 5). Estimates of total atmosphere-to-land fluxes ($S_{\text{LAND}} - E_{\text{LUC}}$)
24 from the DGVMs alone (1.6 ± 0.6 GtC yr^{-1}) are consistent with this estimate and also with
25 the global carbon budget constraint ($E_{\text{FOS}} - G_{\text{ATM}} - S_{\text{OCEAN}}$, 1.7 ± 0.8 GtC yr^{-1} Table 5).

26 Consistent with the bookkeeping models estimates, the DGVM-based E_{LUC} is substantially
27 lower than in Friedlingstein et al., (2020) due to the improved land cover forcing (see
28 section 3.2.2), increasing their total atmosphere-to-land fluxes and hence the consistency
29 with the budget constraint. For the last decade (2011-2020), the inversions estimate the net



1 atmosphere-to-land uptake to lie within a range of 1.3 to 2.0 GtC yr⁻¹, consistent with the
2 GCB and DGVMs estimates of $S_{\text{LAND}} - E_{\text{LUC}}$ (Figure 11, Figure 12 top row).

3 **3.7.3 Total atmosphere-to-ocean fluxes**

4 For the 2011-2020 period, the GOBMs (2.5 ± 0.6 GtC yr⁻¹) produce a lower estimate for the
5 ocean sink than the fCO₂-based data products (3.1 ± 0.5 GtC yr⁻¹), which shows up in Figure
6 11 as a separate peak in the distribution from the GOBMs (triangle symbols pointing right)
7 and from the fCO₂-based products (triangle symbols pointing left). Atmospheric inversions
8 (2.6 to 3.1 GtC yr⁻¹) also suggest higher ocean uptake in the recent decade (Figure 11, Figure
9 12 top row). In interpreting these differences, we caution that the riverine transport of
10 carbon taken up on land and outgassing from the ocean is a substantial (0.6 GtC yr⁻¹) and
11 uncertain term that separates the various methods. A recent estimate of decadal ocean
12 uptake from observed O₂/N₂ ratios (Tohjima et al., 2019) also points towards a larger ocean
13 sink, albeit with large uncertainty (2012-2016: 3.1 ± 1.5 GtC yr⁻¹).

14 **3.7.4 Regional breakdown and interannual variability**

15 Figure 12 also shows the latitudinal partitioning of the total atmosphere-to-surface fluxes
16 excluding fossil CO₂ emissions ($S_{\text{OCEAN}} + S_{\text{LAND}} - E_{\text{LUC}}$) according to the multi-model average
17 estimates from GOBMs and ocean fCO₂-based products (S_{OCEAN}) and DGVMs ($S_{\text{LAND}} - E_{\text{LUC}}$),
18 and from atmospheric inversions (S_{OCEAN} and $S_{\text{LAND}} - E_{\text{LUC}}$).

19 **3.7.4.1 North**

20 Despite being one of the most densely observed and studied regions of our globe, annual
21 mean carbon sink estimates in the northern extra-tropics (north of 30°N) continue to differ
22 by about 0.5 GtC yr⁻¹. The atmospheric inversions suggest an atmosphere-to-surface sink
23 ($S_{\text{OCEAN}} + S_{\text{LAND}} - E_{\text{LUC}}$) for 2011-2020 of 2.0 to 3.4 GtC yr⁻¹, which is higher than the process
24 models' estimate of 2.1 ± 0.5 GtC yr⁻¹ (Fig. 12). The GOBMs (1.1 ± 0.2 GtC yr⁻¹), fCO₂-based
25 data products (1.3 ± 0.1 GtC yr⁻¹), and inversion models (0.9 to 1.5 GtC yr⁻¹) produce
26 consistent estimates of the ocean sink. Thus, the difference mainly arises from the total land
27 flux ($S_{\text{LAND}} - E_{\text{LUC}}$) estimate, which is 1.0 ± 0.4 GtC yr⁻¹ in the DGVMs compared to 0.7 to 2.4
28 GtC yr⁻¹ in the atmospheric inversions (Figure 12, second row).

29 Discrepancies in the northern land fluxes conforms with persistent issues surrounding the
30 quantification of the drivers of the global net land CO₂ flux (Arneeth et al., 2017; Huntzinger



1 et al., 2017) and the distribution of atmosphere-to-land fluxes between the tropics and high
2 northern latitudes (Baccini et al., 2017; Schimel et al., 2015; Stephens et al., 2007; Ciais et al.
3 2019; Gaubert et al., 2019).

4 In the northern extratropics, the process models, inversions, and fCO₂-based data products
5 consistently suggest that most of the variability stems from the land (Fig. 12). Inversions
6 generally estimate similar interannual variations (IAV) over land to DGVMs (0.28 – 0.47 vs
7 0.20 – 0.73 GtC yr⁻¹, averaged over 1990-2020), and they have higher IAV in ocean fluxes
8 (0.03 – 0.19 GtC yr⁻¹) relative to GOBMs (0.03 – 0.05 GtC yr⁻¹, Fig. B2), and fCO₂-based data
9 products (0.03 – 0.09 GtC yr⁻¹).

10 **3.7.4.2 Tropics**

11 In the tropics (30°S-30°N), both the atmospheric inversions and process models estimate a
12 total carbon balance ($S_{\text{OCEAN}}+S_{\text{LAND-ELUC}}$) that is close to neutral over the past decade. The
13 GOBMs (0.0 ± 0.3 GtC yr⁻¹), fCO₂-based data products (0.03 ± 0.2 GtC yr⁻¹), and inversion
14 models (-0.2 to 0.2 GtC yr⁻¹) all indicate an approximately neutral tropical ocean flux (see
15 Fig. B1 for spatial patterns). DGVMs indicate a net land sink ($S_{\text{LAND-ELUC}}$) of 0.6 ± 0.3 GtC yr⁻¹,
16 whereas the inversion models indicate a net land flux between -0.7 and 0.9 GtC yr⁻¹, though
17 with high uncertainty (Figure 12, third row).

18 The tropical lands are the origin of most of the atmospheric CO₂ interannual variability
19 (Ahlström et al., 2015), consistently among the process models and inversions (Fig. 12). The
20 interannual variability in the tropics is similar among the ocean data products (0.07 – 0.15
21 GtC yr⁻¹) and the models (0.07 – 0.15 GtC yr⁻¹, Fig. B2), which is the highest ocean sink
22 variability of all regions. The DGVMs and inversions indicate that atmosphere-to-land CO₂
23 fluxes are more variable than atmosphere-to-ocean CO₂ fluxes in the tropics, with
24 interannual variability of 0.4 to 1.2 and 0.6 to 1.1 GtC yr⁻¹ respectively.

25 **3.7.4.3 South**

26 In the southern extra-tropics (south of 30°S), the atmospheric inversions suggest a total
27 atmosphere-to-surface sink ($S_{\text{OCEAN}}+S_{\text{LAND-ELUC}}$) for 2011-2020 of 1.6 to 1.9 GtC yr⁻¹, slightly
28 higher than the process models' estimate of 1.4 ± 0.3 GtC yr⁻¹ (Fig. 12). An approximately
29 neutral total land flux ($S_{\text{LAND-ELUC}}$) for the southern extra-tropics is estimated by both the
30 DGVMs (0.02 ± 0.05 GtC yr⁻¹) and the inversion models (sink of -0.1 to 0.2 GtC yr⁻¹). This



1 means nearly all carbon uptake is due to oceanic sinks south of 30°S. The southern ocean
2 flux in the fCO₂-based data products ($1.7 \pm 0.1 \text{ GtC yr}^{-1}$) and inversion estimates (1.4 to 1.8
3 GtCyr-1) is higher than in the GOBMs ($1.4 \pm 0.3 \text{ GtC yr}^{-1}$) (Figure 12, bottom row). This might
4 be explained by the data-products potentially underestimating the winter CO₂ outgassing
5 south of the Polar Front (Bushinsky et al., 2019), by model biases, or by the uncertainty in
6 the regional distribution of the river flux adjustment (Aumont et al., 2001, Lacroix et al.,
7 2020) applied to fCO₂-based data products and inverse models to isolate the anthropogenic
8 S_{OCEAN} flux. CO₂ fluxes from this region are more sparsely sampled by all methods, especially
9 in wintertime (Fig. B1).

10 The interannual variability in the southern extra-tropics is low because of the dominance of
11 ocean area with low variability compared to land areas. The split between land (S_{LAND-ELUC})
12 and ocean (S_{OCEAN}) shows a substantial contribution to variability in the south coming from
13 the land, with no consistency between the DGVMs and the inversions or among inversions.
14 This is expected due to the difficulty of separating exactly the land and oceanic fluxes when
15 viewed from atmospheric observations alone. The S_{OCEAN} interannual variability was found to
16 be higher in the fCO₂-based data products (0.09 to 0.14 GtC yr⁻¹) compared to GOBMs (0.04
17 to 0.06 GtC yr⁻¹) in 1990-2020 (Fig. B2). Model subsampling experiments recently
18 illustrated that observation-based products may overestimate decadal variability in the
19 Southern Ocean carbon sink by 30% due to data sparsity, based on one data product with
20 the highest decadal variability (Gloege et al., 2021).

21 **3.7.4.4 Tropical vs northern land uptake**

22 A continuing conundrum is the partitioning of the global atmosphere-land flux between the
23 northern hemisphere land, and the tropical land (Stephens et al., 2017; Pan et al., 2011;
24 Gaubert et al., 2019). It is of importance because each region has its own history of land-use
25 change, climate drivers, and impact of increasing atmospheric CO₂ and nitrogen deposition.
26 Quantifying the magnitude of each sink is a prerequisite to understanding how each
27 individual driver impacts the tropical and mid/high-latitude carbon balance.

28 We define the North-South (N-S) difference as net atmosphere-land flux north of 30N
29 minus the net atmosphere-land flux south of 30°N. For the inversions, the N-S difference
30 ranges from -0.1 GtC yr⁻¹ to 2.9 GtC yr⁻¹ across this year's inversion ensemble with an equal



1 preference across models for either a small Northern land sink and a tropical land sink
2 (small N-S difference), a medium Northern land sink and a neutral tropical land flux
3 (medium N-S difference), or a large Northern land sink and a tropical land source (large N-S
4 difference).

5 In the ensemble of DGVMs the N-S difference is 0.5 ± 0.5 GtC yr⁻¹, a much narrower range
6 than the one from inversions. Only three DGVMs have a N-S difference larger than 1.0 GtC
7 yr⁻¹. The larger agreement across DGVMs than across inversions is to be expected as there is
8 no correlation between Northern and Tropical land sinks in the DGVMs as opposed to the
9 inversions where the sum of the two regions being well-constrained leads to an anti-
10 correlation between these two regions. The much smaller spread in the N-S difference
11 between the DGVMs could help to scrutinize the inverse models further. For example, a
12 large northern land sink and a tropical land source in an inversion would suggest a large
13 sensitivity to CO₂ fertilization (the dominant factor driving the land sinks) for Northern
14 ecosystems, which would be not mirrored by tropical ecosystems. Such a combination could
15 be hard to reconcile with the process understanding gained from the DGVMs ensembles and
16 independent measurements (e.g., FACE experiments). Such investigations will be further
17 pursued in the upcoming assessment from REgional Carbon Cycle Assessment and Processes
18 (RECCAP2; Ciais et al., 2020).

19 **3.8 Closing the Global Carbon Cycle**

20 **3.8.1 Partitioning of Cumulative Emissions and Sink Fluxes**

21 The global carbon budget over the historical period (1850-2020) is shown in Fig. 3.
22 Emissions during the period 1850-2020 amounted to 660 ± 65 GtC and were partitioned
23 among the atmosphere (270 ± 5 GtC; 41%), ocean (170 ± 35 GtC; 26%), and the land ($195 \pm$
24 45 GtC; 30%). The cumulative land sink is almost equal to the cumulative land-use emissions
25 (200 ± 65 GtC), making the global land nearly neutral over the whole 1850-2020 period.
26 The use of nearly independent estimates for the individual terms shows a cumulative
27 budget imbalance of 25 GtC (4%) during 1850-2020 (Fig. 3, Table 8), which, if correct,
28 suggests that emissions are slightly too high by the same proportion (4%) or that the
29 combined land and ocean sinks are slightly underestimated (by about 7%). The bulk of the
30 imbalance could originate from the estimation of large E_{LUC} between the mid 1920s and the



1 mid 1960s which is unmatched by a growth in atmospheric CO₂ concentration as recorded in
2 ice cores (Fig. 3). However, the known loss of additional sink capacity of 30-40 GtC (over the
3 1850-2020 period) due to reduced forest cover has not been accounted for in our method
4 and would further exacerbate the budget imbalance (Section 2.7.4).

5 For the more recent 1960-2020 period where direct atmospheric CO₂ measurements are
6 available, 375 ± 20 GtC (82%) of the total emissions (E_{FOS} + E_{LUC}) were caused by fossil CO₂
7 emissions, and 80 ± 45 GtC (18%) by land-use change (Table 8). The total emissions were
8 partitioned among the atmosphere (205 ± 5 GtC; 47%), ocean (115 ± 25 GtC; 25%), and the
9 land (135 ± 25 GtC; 30%), with a near zero unattributed budget imbalance. All components
10 except land-use change emissions have significantly grown since 1960, with important
11 interannual variability in the growth rate in atmospheric CO₂ concentration and in the land
12 CO₂ sink (Fig. 4), and some decadal variability in all terms (Table 6). Differences with
13 previous budget releases are documented in Fig. B5.

14 The global carbon budget averaged over the last decade (2011-2020) is shown in Fig. 2, Fig.
15 13 (right panel) and Table 6. For this time period, 90% of the total emissions (E_{FOS} + E_{LUC})
16 were from fossil CO₂ emissions (E_{FOS}), and 10% from land-use change (E_{LUC}). The total
17 emissions were partitioned among the atmosphere (47%), ocean (26%) and land (29%), with
18 a near-zero unattributed budget imbalance (~3%). For single years, the budget imbalance
19 can be larger (Figure 4). For 2020, the combination of our sources and sinks estimates leads
20 to a B_{IM} of -0.8 GtC, suggesting an underestimation of the anthropogenic sources
21 (potentially E_{LUC}), and/or an overestimation of the combined land and ocean sinks

22 3.8.2 Carbon Budget Imbalance

23 The carbon budget imbalance (B_{IM}; Eq. 1, Fig.4) quantifies the mismatch between the
24 estimated total emissions and the estimated changes in the atmosphere, land, and ocean
25 reservoirs. The mean budget imbalance from 1960 to 2020 is very small (average of 0.03 GtC
26 yr⁻¹) and shows no trend over the full time series. The process models (GOBMs and DGVMs)
27 and data-products have been selected to match observational constraints in the 1990s, but
28 no further constraints have been applied to their representation of trend and variability.
29 Therefore, the near-zero mean and trend in the budget imbalance is seen as evidence of a
30 coherent community understanding of the emissions and their partitioning on those time



1 scales (Fig. 4). However, the budget imbalance shows substantial variability of the order of
2 $\pm 1 \text{ GtC yr}^{-1}$, particularly over semi-decadal time scales, although most of the variability is
3 within the uncertainty of the estimates. The positive carbon imbalance during the 1960s,
4 and early 1990s, indicates that either the emissions were overestimated, or the sinks were
5 underestimated during these periods. The reverse is true for the 1970s, 1980s, and for the
6 2011-2020 period (Fig. 4, Table 6).

7 We cannot attribute the cause of the variability in the budget imbalance with our analysis,
8 we only note that the budget imbalance is unlikely to be explained by errors or biases in the
9 emissions alone because of its large semi-decadal variability component, a variability that is
10 untypical of emissions and has not changed in the past 60 years despite a near tripling in
11 emissions (Fig. 4). Errors in S_{LAND} and S_{OCEAN} are more likely to be the main cause for the
12 budget imbalance. For example, underestimation of the S_{LAND} by DGVMs has been reported
13 following the eruption of Mount Pinatubo in 1991 possibly due to missing responses to
14 changes in diffuse radiation (Mercado et al., 2009). Although in GCB2021 we have for the
15 first time accounted for aerosol effects on solar radiation quantity and quality (diffuse vs
16 direct), most DGVMs only used the former as input (i.e., total solar radiation). Thus, the
17 ensemble mean may not capture the full effects of volcanic eruptions, i.e. associated with
18 high light scattering sulphate aerosols, on the land carbon sink (O'Sullivan et al., 2021).

19 DGVMs are suspected to overestimate the land sink in response to the wet decade of the
20 1970s (Sitch et al., 2008). Quasi-decadal variability in the ocean sink has also been reported,
21 with all methods agreeing on a smaller than expected ocean CO_2 sink in the 1990s and a
22 larger than expected sink in the 2000s (Fig. 9; Landschützer et al., 2016, DeVries et al., 2019,
23 Hauck et al., 2020, McKinley et al., 2020). Errors in sink estimates could also be driven by
24 errors in the climatic forcing data, particularly precipitation for S_{LAND} and wind for S_{OCEAN} .

25 The budget imbalance (B_{IM}) was negative (-0.3 GtC yr^{-1}) on average over 2011-2020,
26 although the B_{IM} uncertainty is large (1.1 GtC yr^{-1} over the decade). Also, the B_{IM} shows
27 substantial departure from zero on yearly time scales (Fig. 4), highlighting unresolved
28 variability of the carbon cycle, likely in the land sink (S_{LAND}), given its large year to year
29 variability (Fig. 4e and 7).

30 Both the budget imbalance (B_{IM} , Table 6) and the residual land sink from the global budget
31 ($E_{\text{FOS}} + E_{\text{LUC}} - G_{\text{ATM}} - S_{\text{OCEAN}}$, Table 5) include an error term due to the inconsistencies that arises



1 from using E_{LUC} from bookkeeping models, and S_{LAND} from DGVMs, most notably the loss of
2 additional sink capacity (see section 2.7). Other differences include a better accounting of
3 land use changes practices and processes in bookkeeping models than in DGVMs, or the
4 bookkeeping models error of having present-day observed carbon densities fixed in the
5 past. That the budget imbalance shows no clear trend towards larger values over time is an
6 indication that these inconsistencies probably play a minor role compared to other errors in
7 S_{LAND} or S_{OCEAN} .

8 Although the budget imbalance is near zero for the recent decades, it could be due to
9 compensation of errors. We cannot exclude an overestimation of CO_2 emissions, particularly
10 from land-use change, given their large uncertainty, as has been suggested elsewhere (Piao
11 et al., 2018), combined with an underestimate of the sinks. A larger S_{LAND} would reconcile
12 model results with inversion estimates for fluxes in the total land during the past decade
13 (Fig. 12; Table 5). Likewise, a larger S_{OCEAN} is also possible given the higher estimates from
14 the data-products (see section 3.1.2, Fig. 9 and Fig. 12) and the recently suggested upward
15 correction of the ocean carbon sink (Watson et al., 2020, Fig. 9). If S_{OCEAN} were to be based
16 on data-products alone, with all data-products including the Watson et al. (2020)
17 adjustment, this would result in a 2011-2020 S_{OCEAN} of nearly 4 GtC yr^{-1} , outside of the range
18 supported by the atmospheric inversions, with a negative B_{IM} of more than 1 GtC yr^{-1}
19 indicating that a closure of the budget could only be achieved with either anthropogenic
20 emissions being larger and/or the net land sink being substantially smaller than estimated
21 here. More integrated use of observations in the Global Carbon Budget, either on their own
22 or for further constraining model results, should help resolve some of the budget imbalance
23 (Peters et al., 2017).

24 **4 Tracking progress towards mitigation targets**

25 Fossil CO_2 emissions growth peaked at 3% per year during the 2000s, driven by the rapid
26 growth in Chinese emissions. In the last decade, however, the growth rate for the preceding
27 10 years has slowly declined, reaching a low 0.4% per year from 2012-2021 (including the
28 2020 global decline and the expected 2021 emissions rebound). While this slowdown in
29 global fossil CO_2 emissions growth is welcome, it is far from what is needed to be consistent
30 with the temperature goals of the Paris Agreement.



1 Since the 1990s, the average growth rate of fossil CO₂ emissions has continuously declined
2 across the group of developed countries of the Organisation for Economic Co-operation and
3 Development (OECD), with emissions peaking in around 2005 and now declining at around
4 1% yr⁻¹ (Le Quéré et al., 2021). In the decade 2010-2019, territorial fossil CO₂ emissions
5 decreased significantly (at the 95% confidence level) in 23 countries whose economies grew
6 significantly (also at the 95% confidence level): Barbados, Belgium, Croatia, Czech Republic,
7 Denmark, Finland, France, Germany, Israel, Japan, Luxembourg, North Macedonia, Malta,
8 Mexico, Netherlands, Slovakia, Slovenia, Solomon Islands, Sweden, Switzerland, Tuvalu,
9 United Kingdom and the USA (updated from Le Quéré et al., 2019). Altogether, these 23
10 countries contribute to 2.5 GtC yr⁻¹ over the last decade, about one quarter of world CO₂
11 fossil emissions. Consumption-based emissions are also falling significantly in 15 of these
12 countries (Belgium, Croatia, Czech Republic, Denmark, Finland, France, Germany, Israel,
13 Japan, Mexico, Netherlands, Slovenia, Sweden, United Kingdom, and the USA). Figure 14
14 shows that the emission declines in the USA and the EU27 are primarily driven by increased
15 decarbonisation (CO₂ emissions per unit energy) in the last decade compared to the
16 previous, with smaller contributions in the EU27 from slightly weaker economic growth and
17 slightly larger declines in energy per GDP. These countries have stable or declining energy
18 use and so decarbonisation policies replace existing fossil fuel infrastructure (Le Quéré et al.
19 2019).

20 In contrast, fossil CO₂ emissions continue to grow in non-OECD countries, although the
21 growth rate has slowed from over 5% yr⁻¹ during the 2000s to around 2% yr⁻¹ in the last
22 decade. A large part of this slowdown in non-OECD countries is due to China, which has
23 seen emissions growth declining from nearly 10% yr⁻¹ in the 2000s to 2% yr⁻¹ in the last
24 decade. Excluding China, non-OECD emissions grew at 3% yr⁻¹ in the 2000s compared to 2%
25 yr⁻¹ in the last decade. Figure 14 shows that compared to the previous decade, China has
26 had weaker economic growth in the last decade and a larger decarbonisation rate, with
27 more rapid declines in energy per GDP which are now back to levels during the 1990s. India
28 and the rest of the world have strong economic growth that is not compensated by
29 decarbonisation or declines in energy per GDP, implying fossil CO₂ emissions continue to
30 grow. Despite the high deployment of renewables in some countries (e.g., India), fossil
31 energy sources continue to grow to meet growing energy demand (Le Quéré et al. 2019).



1 Globally, fossil CO₂ emissions growth is slowing, and this is primarily due to the emergence
2 of climate policy and emission declines in OECD countries (Eskander and Fankhauser 2020).
3 At the aggregated global level, decarbonisation shows a strong and growing signal in the last
4 decade, with smaller contributions from lower economic growth and declines in energy per
5 GDP. Despite the slowing growth in global fossil CO₂ emissions, emissions are still growing,
6 far from the reductions needed to meet the ambitious climate goals of the UNFCCC Paris
7 agreement.

8 We update the remaining carbon budget assessed by the IPCC AR6 (Canadell et al., 2021),
9 accounting for the 2020 and estimated 2021 emissions from fossil fuel combustion (E_{FOS})
10 and land use changes (E_{LUC}). From January 2022, the remaining carbon (50% likelihood) for
11 limiting global warming to 1.5°C, 1.7°C and 2°C is estimated to amount to 120, 210, and 350
12 GtC (420, 770, 1270 GtCO₂). These numbers include an uncertainty based on model spread
13 (as in IPCC AR6), which is reflected through the percent likelihood of exceeding the given
14 temperature threshold. These remaining amounts correspond to respectively about 11, 20
15 and 32 years from beginning of 2020, at the 2021 level of total CO₂ emissions. Reaching net
16 zero CO₂ emissions by 2050 entails cutting total anthropogenic CO₂ emissions by about 0.4
17 GtC (1.4 GtCO₂) each year on average, comparable to the decrease during 2020.

18 **5 Discussion**

19 Each year when the global carbon budget is published, each flux component is updated for
20 all previous years to consider corrections that are the result of further scrutiny and
21 verification of the underlying data in the primary input data sets. Annual estimates may be
22 updated with improvements in data quality and timeliness (e.g., to eliminate the need for
23 extrapolation of forcing data such as land-use). Of all terms in the global budget, only the
24 fossil CO₂ emissions and the growth rate in atmospheric CO₂ concentration are based
25 primarily on empirical inputs supporting annual estimates in this carbon budget. The carbon
26 budget imbalance, yet an imperfect measure, provides a strong indication of the limitations
27 in observations in understanding and representing processes in models, and/or in the
28 integration of the carbon budget components.

29 The persistent unexplained variability in the carbon budget imbalance limits our ability to
30 verify reported emissions (Peters et al., 2017) and suggests we do not yet have a complete



1 understanding of the underlying carbon cycle dynamics on annual to decadal timescales.
2 Resolving most of this unexplained variability should be possible through different and
3 complementary approaches. First, as intended with our annual updates, the imbalance as an
4 error term is reduced by improvements of individual components of the global carbon
5 budget that follow from improving the underlying data and statistics and by improving the
6 models through the resolution of some of the key uncertainties detailed in Table 9. Second,
7 additional clues to the origin and processes responsible for the variability in the budget
8 imbalance could be obtained through a closer scrutiny of carbon variability in light of other
9 Earth system data (e.g., heat balance, water balance), and the use of a wider range of
10 biogeochemical observations to better understand the land-ocean partitioning of the carbon
11 imbalance (e.g. oxygen, carbon isotopes). Finally, additional information could also be
12 obtained through higher resolution and process knowledge at the regional level, and
13 through the introduction of inferred fluxes such as those based on satellite CO₂ retrievals.
14 The limit of the resolution of the carbon budget imbalance is yet unclear, but most certainly
15 not yet reached given the possibilities for improvements that lie ahead.

16 Estimates of global fossil CO₂ emissions from different datasets are in relatively good
17 agreement when the different system boundaries of these datasets are considered
18 (Andrew, 2020a). But while estimates of E_{FOS} are derived from reported activity data
19 requiring much fewer complex transformations than some other components of the budget,
20 uncertainties remain, and one reason for the apparently low variation between datasets is
21 precisely the reliance on the same underlying reported energy data. The budget excludes
22 some sources of fossil CO₂ emissions, which available evidence suggests are relatively small
23 (<1%). We have added emissions from lime production in China and the US, but these are
24 still absent in most other non-Annex I countries, and before 1990 in other Annex I countries.
25 Further changes to E_{FOS} this year are documented by Andrew and Peters (2021).

26 Estimates of E_{LUC} suffer from a range of intertwined issues, including the poor quality of
27 historical land-cover and land-use change maps, the rudimentary representation of
28 management processes in most models, and the confusion in methodologies and boundary
29 conditions used across methods (e.g., Arneeth et al., 2017; Pongratz et al., 2014, see also
30 Section 2.7.4 on the loss of sink capacity; Bastos et al., 2021). Uncertainties in current and
31 historical carbon stocks in soils and vegetation also add uncertainty in the E_{LUC} estimates.



1 Unless a major effort to resolve these issues is made, little progress is expected in the
2 resolution of E_{LUC} . This is particularly concerning given the growing importance of E_{LUC} for
3 climate mitigation strategies, and the large issues in the quantification of the cumulative
4 emissions over the historical period that arise from large uncertainties in E_{LUC} .

5 By adding the DGVMs estimates of CO_2 fluxes due to environmental change from countries'
6 managed forest areas (part of S_{LAND} in this budget) to the budget E_{LUC} estimate, we
7 successfully reconciled the large gap between our E_{LUC} estimate and the land use flux from
8 NGHGs using the approach described in Grassi et al. (2021). This latter estimate has been
9 used in the recent UNFCCC's Synthesis Report on Nationally Determined Contribution
10 (UNFCCC, 2021b) to enable the total national emission estimates to be comparable with
11 those of the IPCC. However, while Grassi et al. (2021) used only one DGVM, here 17 DGVMs
12 are used, thus providing a more robust value to be used as potential adjustment in the
13 policy context, e.g., to help assessing the collective countries' progress towards the goal of
14 the Paris Agreement and avoiding double-accounting for the sink in managed forests. In the
15 absence of this adjustment, collective progress would hence appear better than it is (Grassi
16 et al. 2021).

17 The comparison of GOBMs, data products and inversions highlights substantial discrepancy
18 in the Southern Ocean (Fig. 12, Hauck et al., 2020). The long-standing sparse data coverage
19 of fCO_2 observations in the Southern compared to the Northern Hemisphere (e.g., Takahashi
20 et al., 2009) continues to exist (Bakker et al., 2016, 2021, Fig. B1) and to lead to substantially
21 higher uncertainty in the S_{OCEAN} estimate for the Southern Hemisphere (Watson et al., 2020,
22 Gloor et al., 2021). This discrepancy, which also hampers model improvement, points to
23 the need for increased high-quality fCO_2 observations especially in the Southern Ocean. At
24 the same time, model uncertainty is illustrated by the large spread of individual GOBM
25 estimates (indicated by shading in Fig. 12) and highlights the need for model improvement.
26 Further uncertainty stems from the regional distribution of the river flux adjustment term
27 being based on one model study yielding the largest riverine outgassing flux south of $20^\circ S$
28 (Aumont et al., 2001), with a recent study questioning this distribution (Lacroix et al., 2020).
29 The diverging trends in S_{OCEAN} from different methods is a matter of concern, which is
30 unresolved. The assessment of the net land-atmosphere exchange from DGVMs and
31 atmospheric inversions also shows substantial discrepancy, particularly for the estimate of



1 the total land flux over the northern extra-tropic. This discrepancy highlights the difficulty to
2 quantify complex processes (CO₂ fertilisation, nitrogen deposition and fertilisers, climate
3 change and variability, land management, etc.) that collectively determine the net land CO₂
4 flux. Resolving the differences in the Northern Hemisphere land sink will require the
5 consideration and inclusion of larger volumes of observations.

6 We provide metrics for the evaluation of the ocean and land models and the atmospheric
7 inversions (Figs. B2 to B4). These metrics expand the use of observations in the global
8 carbon budget, helping 1) to support improvements in the ocean and land carbon models
9 that produce the sink estimates, and 2) to constrain the representation of key underlying
10 processes in the models and to allocate the regional partitioning of the CO₂ fluxes. However,
11 GOBMs skills have changed little since the introduction of the ocean model evaluation. An
12 additional simulation this year allows for direct comparison with interior ocean
13 anthropogenic carbon estimates and suggests that the models underestimate
14 anthropogenic carbon uptake and storage. This is an initial step towards the introduction of
15 a broader range of observations that we hope will support continued improvements in the
16 annual estimates of the global carbon budget.

17 We assessed before that a sustained decrease of –1% in global emissions could be detected
18 at the 66% likelihood level after a decade only (Peters et al., 2017). Similarly, a change in
19 behaviour of the land and/or ocean carbon sink would take as long to detect, and much
20 longer if it emerges more slowly. To continue reducing the carbon imbalance on annual to
21 decadal time scales, regionalising the carbon budget, and integrating multiple variables are
22 powerful ways to shorten the detection limit and ensure the research community can
23 rapidly identify issues of concern in the evolution of the global carbon cycle under the
24 current rapid and unprecedented changing environmental conditions.

25 **6 Conclusions**

26 The estimation of global CO₂ emissions and sinks is a major effort by the carbon cycle
27 research community that requires a careful compilation and synthesis of measurements,
28 statistical estimates, and model results. The delivery of an annual carbon budget serves two
29 purposes. First, there is a large demand for up-to-date information on the state of the
30 anthropogenic perturbation of the climate system and its underpinning causes. A broad



1 stakeholder community relies on the data sets associated with the annual carbon budget
2 including scientists, policy makers, businesses, journalists, and non-governmental
3 organizations engaged in adapting to and mitigating human-driven climate change. Second,
4 over the last decades we have seen unprecedented changes in the human and biophysical
5 environments (e.g., changes in the growth of fossil fuel emissions, impact of COVID-19
6 pandemic, Earth’s warming, and strength of the carbon sinks), which call for frequent
7 assessments of the state of the planet, a better quantification of the causes of changes in
8 the contemporary global carbon cycle, and an improved capacity to anticipate its evolution
9 in the future. Building this scientific understanding to meet the extraordinary climate
10 mitigation challenge requires frequent, robust, transparent, and traceable data sets and
11 methods that can be scrutinized and replicated. This paper via ‘living data’ helps to keep
12 track of new budget updates.

13 **7 Data availability**

14 The data presented here are made available in the belief that their wide dissemination will
15 lead to greater understanding and new scientific insights of how the carbon cycle works,
16 how humans are altering it, and how we can mitigate the resulting human-driven climate
17 change. The free availability of these data does not constitute permission for publication of
18 the data. For research projects, if the data are essential to the work, or if an important
19 result or conclusion depends on the data, co-authorship may need to be considered for the
20 relevant data providers. Full contact details and information on how to cite the data shown
21 here are given at the top of each page in the accompanying database and summarised in
22 Table 2.

23 The accompanying database includes two Excel files organised in the following
24 spreadsheets:

25 File `Global_Carbon_Budget_2021v1.0.xlsx` includes the following:

- 26 1. Summary
- 27 2. The global carbon budget (1959-2020);
- 28 3. The historical global carbon budget (1750-2020);
- 29 4. Global CO₂ emissions from fossil fuels and cement production by fuel type, and the per-
30 capita emissions (1959-2020);



- 1 5. CO₂ emissions from land-use change from the individual methods and models (1959-
- 2 2020);
- 3 6. Ocean CO₂ sink from the individual ocean models and fCO₂-based products (1959-
- 4 2020);
- 5 7. Terrestrial CO₂ sink from the DGVMs (1959-2020).

6

7 File `National_Carbon_Emissions_2021v1.0.xlsx` includes the following:

- 8 1. Summary
- 9 2. Territorial country CO₂ emissions from fossil CO₂ emissions (1959-2020);
- 10 3. Consumption country CO₂ emissions from fossil CO₂ emissions and emissions transfer
- 11 from the international trade of goods and services (1990-2019) using CDIAC/UNFCCC
- 12 data as reference;
- 13 4. Emissions transfers (Consumption minus territorial emissions; 1990-2019);
- 14 5. Country definitions;
- 15 6. Details of disaggregated countries;
- 16 7. Details of aggregated countries.

17 Both spreadsheets are published by the Integrated Carbon Observation System (ICOS)

18 Carbon Portal and are available at <https://doi.org/10.18160/gcp-2021> (Friedlingstein et al.,

19 2021). National emissions data are also available from the Global Carbon Atlas

20 (<http://www.globalcarbonatlas.org/>, last access: 21 October 2021) and from Our World in

21 Data (<https://ourworldindata.org/co2-emissions>, last access: 21 October 2021).

22

23 **Author contributions**

24 PF, MWJ, MOS, CLQ, RMA, DCEB, JH, GPP, WP, JP and SS designed the study, conducted the

25 analysis, and wrote the paper with input from JGC, PC and RBJ. RMA, GPP and JIK produced

26 the fossil fuel emissions and their uncertainties and analysed the emissions data. DG and

27 GM provided fossil fuel emission data. JP, TG, CS and RAH provided the bookkeeping land-

28 use change emissions. JH, LB, OG, NG, TI, LR, JS, RS and DW provided an update of the global



1 ocean biogeochemical models. SRA, TTTC, LD, LG, YI, PL, CR, AJW and JZ provided an update
2 of the ocean fCO₂ data products, with synthesis by JH. MB, NRB, KIC, MC, WE, RAF, SRA, TG,
3 AK, NL, SKL, DRM, CIS, CoS, SN, CW, TO, DP, GR, AJS, BT, TT, CW, and RW provided ocean
4 fCO₂ measurements for the year 2020, with synthesis by DCEB and SDJ. PA, BD, AKJ, DK, EK,
5 JK, SL, PCM, JRM, JEMSN, BP, HT, NV, AJW, WY, XY and SZ provided an update of the
6 Dynamic Global Vegetation Models, with synthesis by SS. WP, FC, LF, ITL, JL, YN and CR
7 provided an updated atmospheric inversion, developed the protocol and produced the
8 evaluation, with synthesis by WP. RMA provided predictions of the 2021 emissions and
9 atmospheric CO₂ growth rate. PL provided the predictions of the 2021 ocean and land sinks.
10 LPC, GCH, KKG, TMS and GRvdW provided forcing data for land-use change. GG, FT, and CY
11 provided data for the land-use change NGHGI mapping. PPT provided key atmospheric CO₂
12 data. MWJ produced the historical record of atmospheric CO₂ concentration and growth
13 rate, including the atmospheric CO₂ forcing. MOS and NB produced the aerosol diffuse
14 radiative forcing for the DGVMs. IH provided the climate forcing data for the DGVMs. ER
15 provided the evaluation of the DGVMs. MWJ provided the emissions prior for use in the
16 inversion models. XD provided seasonal emissions data for years 2019-2020 for the emission
17 prior. MWJ and MOS developed a new data management pipeline which automates many
18 aspects of the data collation, analysis, plotting and synthesis. PF, MWJ, and MOS revised all
19 figures, tables, text and/or numbers to ensure the update is clear from the 2020 edition and
20 in phase with the globalcarbonatlas.org.

21

22 **Competing interests.** The authors declare that they have no conflict of interest.



1 **Acknowledgements**

2 We thank all people and institutions who provided the data used in this global carbon budget
3 2021 and the Global Carbon Project members for their input throughout the development of
4 this publication. We thank Nigel Hawtin for producing Figure 2 and Figure 13. We thank Omar
5 Jamil and Freddy Wordingham for technical support. We thank Ed Dlugokencky for providing
6 atmospheric CO₂ measurements. We thank Vivek Arora, Ian G.C. Ashton, Erik Buitenhuis,
7 Fatemeh Cheginig, Christian Ethé, Marion Gehlen, Lonneke Goddijn-Murphy, T. Holding,
8 Fabrice Lacroix, Enhui Liao, Pedro M.S. Monteiro, Naiqing Pan, Tristan Quaife, Shijie Shu,
9 Jamie D. Shutler, Jade Skye, Anthony Walker, and David K. Woolf for their involvement in the
10 development, use and analysis of the models and data-products used here. We thank Markus
11 Ritschel, Carmen Rodriguez, Claire Lo Monaco, Nicolas Metzler, Vassilis Kitidis, Sören Gutekunst,
12 Anne Willstrand Wranne, Tobias Steinhoff, Jessica N. Cross, Natalie M. Monacci, Alice Benoit-
13 Cattin, Sólveig R. Ólafsdóttir, Joe Salisbury, Doug Vandemark and Christopher W. Hunt, who
14 contributed to the provision of surface ocean CO₂ observations for the year 2020 (see Table
15 A5). We also thank Benjamin Pfeil, Rocío Castaño-Primo, Camilla Landa and Maren Karlsen of
16 the Ocean Thematic Centre of the EU Integrated Carbon Observation System (ICOS) Research
17 Infrastructure, Kevin O'Brien and Eugene Burger of NOAA's Pacific Marine Environmental
18 Laboratory and Alex Kozyr of NOAA's National Centers for Environmental Information, for
19 their contribution to surface ocean CO₂ data and metadata management. We thank the
20 scientists, institutions, and funding agencies responsible for the collection and quality control
21 of the data in SOCAT as well as the International Ocean Carbon Coordination Project (IOCCP),
22 the Surface Ocean Lower Atmosphere Study (SOLAS) and the Integrated Marine Biosphere
23 Research (IMBeR) program for their support. We thank data providers ObsPack



1 GLOBALVIEWplus v6.1 and NRT v6.1.1 for atmospheric CO₂ observations. We thank the
2 individuals and institutions that provided the databases used for the models evaluations used
3 here. We thank Fortunat Joos, Samar Khatiwala and Timothy DeVries for providing historical
4 data. NV thanks the whole ORCHIDEE group. YN thanks CSIRO, EC, EMPA, FMI, IPEN, JMA,
5 LSCE, NCAR, NIES, NILU, NIWA, NOAA, SIO, and TU/NIPR for providing data for NISMON-CO₂.
6 JL thanks the Jet Propulsion Laboratory, California Institute of Technology. This is PMEL
7 contribution 5317. SDJ thanks the data management team at the Bjerknes Climate Data
8 Centre. WE thanks the Tula Foundation for funding support. Australian ocean CO₂ data were
9 sourced from Australia's Integrated Marine Observing System (IMOS); IMOS is enabled by the
10 National Collaborative Research Infrastructure Strategy (NCRIS). MC thanks Anthony English,
11 Clynt Gregory and Gordon Furey (P&O Maritime Services) and Tobias Steinhoff for support.
12 NL thanks the crew of the Cap San Lorenzo and the US IMAGO of IRD Brest for technical
13 support. GR is grateful for the skillful technical support of M. Glockzin and B. Sadkowiak. MWJ
14 thanks Anthony J. De-Gol for his technical and conceptual assistance with the development
15 of GCP-GridFED. FAOSTAT is funded by FAO member states through their contributions to the
16 FAO Regular Programme, data contributions by national experts are greatly acknowledged.
17 The views expressed in this paper are the authors' only and do not necessarily reflect those
18 of FAO. Finally, we thank all funders who have supported the individual and joint
19 contributions to this work (see Table A9), as well as the reviewers of this manuscript and
20 previous versions, and the many researchers who have provided feedback.



1 **References**

- 2 Ahlström, A., Raupach, M. R., Schurgers, G., Smith, B., Arneth, A., Jung, M., Reichstein, M.,
- 3 Canadell, J. G., Friedlingstein, P., Jain, A. K., Kato, E., Poulter, B., Sitch, S., Stocker, B. D.,
- 4 Viovy, N., Wang, Y. P., Wiltshire, A., Zaehle, S., and Zeng, N.: The dominant role of semi-arid
- 5 ecosystems in the trend and variability of the land CO₂ sink, 348, 895–899,
- 6 <https://doi.org/10.1126/science.aaa1668>, 2015.

- 7 Ahlström, A., Raupach, M. R., Schurgers, G., Smith, B., Arneth, A., Jung, M., Reichstein, M.,
- 8 Canadell, J. G., Friedlingstein, P., Jain, A. K., Kato, E., Poulter, B., Sitch, S., Stocker, B. D.,
- 9 Viovy, N., Wang, Y. P., Wiltshire, A., Zaehle, S., and Zeng, N.: The dominant role of semi-arid
- 10 ecosystems in the trend and variability of the land CO₂ sink, 348, 895–899,
- 11 <https://doi.org/10.1126/science.aaa1668>, 2015.

- 12 Amador-Jiménez, M., Millner, N., Palmer, C., Pennington, R. T., and Sileci, L.: The
- 13 Unintended Impact of Colombia’s Covid-19 Lockdown on Forest Fires, *Environ Resource*
- 14 *Econ*, 76, 1081–1105, <https://doi.org/10.1007/s10640-020-00501-5>, 2020.

- 15 Amante, C. and Eakins, B. W.: ETOPO1 Global Relief Model converted to PanMap layer
- 16 format, <https://doi.org/10.1594/PANGAEA.769615>, 2009.

- 17 Andela, N., Morton, D. C., Giglio, L., Chen, Y., van der Werf, G. R., Kasibhatla, P. S., DeFries,
- 18 R. S., Collatz, G. J., Hantson, S., Kloster, S., Bachelet, D., Forrest, M., Lasslop, G., Li, F.,
- 19 Mangeon, S., Melton, J. R., Yue, C., and Randerson, J. T.: A human-driven decline in global
- 20 burned area, *Science*, 356, 1356–1362, <https://doi.org/10.1126/science.aal4108>, 2017.

- 21 Andres, R. J., Boden, T. A., Bréon, F.-M., Ciais, P., Davis, S., Erickson, D., Gregg, J. S.,
- 22 Jacobson, A., Marland, G., Miller, J., Oda, T., Olivier, J. G. J., Raupach, M. R., Rayner, P., and
- 23 Treanton, K.: A synthesis of carbon dioxide emissions from fossil-fuel combustion,
- 24 *Biogeosciences*, 9, 1845–1871, <https://doi.org/10.5194/bg-9-1845-2012>, 2012.

- 25 Andres, R. J., Boden, T. A., and Higdson, D.: A new evaluation of the uncertainty associated
- 26 with CDIAC estimates of fossil fuel carbon dioxide emission, *Tellus B: Chemical and Physical*
- 27 *Meteorology*, 66, 23616, <https://doi.org/10.3402/tellusb.v66.23616>, 2014.

- 28 Andrew, R. M.: A comparison of estimates of global carbon dioxide emissions from fossil



- 1 carbon sources, *Earth Syst. Sci. Data*, 12, 1437–1465, [https://doi.org/10.5194/essd-12-1437-](https://doi.org/10.5194/essd-12-1437-2020)
2 2020, 2020a.
- 3 Andrew, R. M.: Timely estimates of India’s annual and monthly fossil CO₂ emissions, *Earth*
4 *Syst. Sci. Data*, 12, 2411–2421, <https://doi.org/10.5194/essd-12-2411-2020>, 2020b.
- 5 Andrew, R. M.: Towards near real-time, monthly fossil CO₂ emissions estimates for the
6 European Union with current-year projections, *Atmospheric Pollution Research*, 101229,
7 <https://doi.org/10.1016/j.apr.2021.101229>, 2021.
- 8 Andrew, R. M. and Peters, G. P.: A MULTI-REGION INPUT–OUTPUT TABLE BASED ON THE
9 GLOBAL TRADE ANALYSIS PROJECT DATABASE (GTAP-MRIO), *Economic Systems Research*,
10 25, 99–121, <https://doi.org/10.1080/09535314.2012.761953>, 2013.
- 11 Andrew, R. M. and Peters, G. P.: The Global Carbon Project’s fossil CO₂ emissions dataset
12 (2021v34), <https://doi.org/10.5281/ZENODO.5569235>, 2021.
- 13 Aragão, L. E. O. C., Anderson, L. O., Fonseca, M. G., Rosan, T. M., Vedovato, L. B., Wagner, F.
14 H., Silva, C. V. J., Silva Junior, C. H. L., Arai, E., Aguiar, A. P., Barlow, J., Berenguer, E., Deeter,
15 M. N., Domingues, L. G., Gatti, L., Gloor, M., Malhi, Y., Marengo, J. A., Miller, J. B., Phillips, O.
16 L., and Saatchi, S.: 21st Century drought-related fires counteract the decline of Amazon
17 deforestation carbon emissions, *Nat Commun*, 9, 536, [https://doi.org/10.1038/s41467-017-](https://doi.org/10.1038/s41467-017-02771-y)
18 02771-y, 2018.
- 19 Archer, D., Eby, M., Brovkin, V., Ridgwell, A., Cao, L., Mikolajewicz, U., Caldeira, K.,
20 Matsumoto, K., Munhoven, G., Montenegro, A., and Tokos, K.: Atmospheric Lifetime of
21 Fossil Fuel Carbon Dioxide, *Annu. Rev. Earth Planet. Sci.*, 37, 117–134,
22 <https://doi.org/10.1146/annurev.earth.031208.100206>, 2009.
- 23 Arneth, A., Sitch, S., Pongratz, J., Stocker, B. D., Ciais, P., Poulter, B., Bayer, A. D., Bondeau,
24 A., Calle, L., Chini, L. P., Gasser, T., Fader, M., Friedlingstein, P., Kato, E., Li, W., Lindeskog,
25 M., Nabel, J. E. M. S., Pugh, T. A. M., Robertson, E., Viovy, N., Yue, C., and Zaehle, S.:
26 Historical carbon dioxide emissions caused by land-use changes are possibly larger than
27 assumed, *Nature Geosci*, 10, 79–84, <https://doi.org/10.1038/ngeo2882>, 2017.
- 28 Arora, V. K., Boer, G. J., Christian, J. R., Curry, C. L., Denman, K. L., Zahariev, K., Flato, G. M.,



- 1 Scinocca, J. F., Merryfield, W. J., and Lee, W. G.: The Effect of Terrestrial Photosynthesis
- 2 Down Regulation on the Twentieth-Century Carbon Budget Simulated with the CCCma Earth
- 3 System Model, 22, 6066–6088, <https://doi.org/10.1175/2009JCLI3037.1>, 2009.
- 4 Asaadi, A., Arora, V. K., Melton, J. R., and Bartlett, P.: An improved parameterization of leaf
- 5 area index (LAI) seasonality in the Canadian Land Surface Scheme (CLASS) and Canadian
- 6 Terrestrial Ecosystem Model (CTEM) modelling framework, 15, 6885–6907,
- 7 <https://doi.org/10.5194/bg-15-6885-2018>, 2018.
- 8 Aumont, O., Orr, J. C., Monfray, P., Ludwig, W., Amiotte-Suchet, P., and Probst, J.-L.:
- 9 Riverine-driven interhemispheric transport of carbon, *Global Biogeochem. Cycles*, 15, 393–
- 10 405, <https://doi.org/10.1029/1999GB001238>, 2001.
- 11 Aumont, O., Ethé, C., Tagliabue, A., Bopp, L., and Gehlen, M.: PISCES-v2: an ocean
- 12 biogeochemical model for carbon and ecosystem studies, 8, 2465–2513,
- 13 <https://doi.org/10.5194/gmd-8-2465-2015>, 2015.
- 14 Avitabile, V., Herold, M., Heuvelink, G. B. M., Lewis, S. L., Phillips, O. L., Asner, G. P.,
- 15 Armston, J., Ashton, P. S., Banin, L., Bayol, N., Berry, N. J., Boeckx, P., de Jong, B. H. J.,
- 16 DeVries, B., Girardin, C. A. J., Kearsley, E., Lindsell, J. A., Lopez-Gonzalez, G., Lucas, R., Malhi,
- 17 Y., Morel, A., Mitchard, E. T. A., Nagy, L., Qie, L., Quinones, M. J., Ryan, C. M., Ferry, S. J. W.,
- 18 Sunderland, T., Laurin, G. V., Gatti, R. C., Valentini, R., Verbeeck, H., Wijaya, A., and Willcock,
- 19 S.: An integrated pan-tropical biomass map using multiple reference datasets, *Glob Change*
- 20 *Biol*, 22, 1406–1420, <https://doi.org/10.1111/gcb.13139>, 2016.
- 21 Baccini, A., Walker, W., Carvalho, L., Farina, M., Sulla-Menashe, D., and Houghton, R. A.:
- 22 Tropical forests are a net carbon source based on aboveground measurements of gain and
- 23 loss, *Science*, 358, 230–234, <https://doi.org/10.1126/science.aam5962>, 2017.
- 24 Bakker, D. C. E., Pfeil, B., Landa, C. S., Metzler, N., O'Brien, K. M., Olsen, A., Smith, K., Cosca, C.,
- 25 Harasawa, S., Jones, S. D., Nakaoka, S., Nojiri, Y., Schuster, U., Steinhoff, T., Sweeney, C.,
- 26 Takahashi, T., Tilbrook, B., Wada, C., Wanninkhof, R., Alin, S. R., Balestrini, C. F., Barbero, L.,
- 27 Bates, N. R., Bianchi, A. A., Bonou, F., Boutin, J., Bozec, Y., Burger, E. F., Cai, W.-J., Castle, R.
- 28 D., Chen, L., Chierici, M., Currie, K., Evans, W., Featherstone, C., Feely, R. A., Fransson, A.,
- 29 Goyet, C., Greenwood, N., Gregor, L., Hankin, S., Hardman-Mountford, N. J., Harlay, J.,



- 1 Hauck, J., Hoppema, M., Humphreys, M. P., Hunt, C. W., Huss, B., Ibáñez, J. S. P.,
2 Johannessen, T., Keeling, R., Kitidis, V., Körtzinger, A., Kozyr, A., Krasakopoulou, E., Kuwata,
3 A., Landschützer, P., Lauvset, S. K., Lefèvre, N., Lo Monaco, C., Manke, A., Mathis, J. T.,
4 Merlivat, L., Millero, F. J., Monteiro, P. M. S., Munro, D. R., Murata, A., Newberger, T., Omar,
5 A. M., Ono, T., Paterson, K., Pearce, D., Pierrot, D., Robbins, L. L., Saito, S., Salisbury, J.,
6 Schlitzer, R., Schneider, B., Schweitzer, R., Sieger, R., Skjelvan, I., Sullivan, K. F., Sutherland,
7 S. C., Sutton, A. J., Tadokoro, K., Telszewski, M., Tuma, M., van Heuven, S. M. A. C.,
8 Vandemark, D., Ward, B., Watson, A. J., and Xu, S.: A multi-decade record of high-quality
9 CO₂ data in version 3 of the Surface Ocean CO₂ Atlas (SOCAT), *Earth Syst. Sci. Data*, 8, 383–
10 413, <https://doi.org/10.5194/essd-8-383-2016>, 2016.
- 11 Bakker, D. C. E., Alin, S. R., Castaño-Primo, R., Cronin, M., Gkritzalis, T., Kozyr, A., Lauvset, S.
12 K., Metzl, N., Munro, D. R., Nakaoka, S.-I., O'Brien, K. M., Olsen, A., Omar, A. M., Pfeil, B.,
13 Pierrot, D., Rodriguez, C., Steinhoff, T., Sutton, A. J., Tilbrook, B., Wanninkhof, R., Willstrand
14 Wranne, A., Ahmed, M., Andersson, A., Apelthun, L. B., Bates, N., Battisti, R., Beaumont, L.,
15 Becker, M., Benoit-Cattin, A., Berghoff, C. F., Boutin, J., Burger, E. F., Burgers, T. M., Cantoni,
16 C., Catrijsse, A., Chierici, M., Cross, J. N., Coppola, L., Cosca, C. E., Currie, K. I., De Carlo, E.
17 H., Else, B., Enright, M. P., Ericson, Y., Evans, W., Feely, R. A., Fiedler, B., Fransson, A., García-
18 Ibáñez, M. I., Gehrung, M., Glockzin, M., González Dávila, M., Gutekunst, S., Hermes, R.,
19 Humphreys, M. P., Hunt, C. W., Ibáñez, J. S. P., Jones, S. D., Kitidis, V., Körtzinger, A.,
20 Kosugi, N., Landa, C. S., Landschützer, P., Lefèvre, N., Lo Monaco, C., Luchetta, A., Lutz, V. A.,
21 Macovei, V. A., Manke, A. B., Merlivat, L., Millero, F. J., Monacci, N. M., Negri, R. M.,
22 Newberger, T., Newton, J., Nickford, S. E., Nojiri, Y., Ohman, M., Ólafsdóttir, S. R., Sweeney,
23 C., Ono, T., Palter, J. B., Papakyriakou, T., Peterson, W. T., Plueddemann, A. J., Qi, D.,
24 Rehder, G., Ritschel, M., Rutgersson, A., Sabine, C. L., Salisbury, J. E., Santana-Casiano, J. M.,
25 Schlitzer, R., Send, U., Skjelvan, I., Smith, K., Sparnocchia, S., Sullivan, K. F., Sutherland, S. C.,
26 et al.: Surface Ocean CO₂ Atlas Database Version 2021 (SOCATv2021) (NCEI Accession
27 0235360), <https://doi.org/10.25921/YG69-JD96>, 2021.
- 28 Ballantyne, A. P., Alden, C. B., Miller, J. B., Tans, P. P., and White, J. W. C.: Increase in
29 observed net carbon dioxide uptake by land and oceans during the past 50 years, *Nature*,
30 488, 70–72, <https://doi.org/10.1038/nature11299>, 2012.



- 1 Ballantyne, A. P., Andres, R., Houghton, R., Stocker, B. D., Wanninkhof, R., Anderegg, W.,
- 2 Cooper, L. A., DeGrandpre, M., Tans, P. P., Miller, J. B., Alden, C., and White, J. W. C.: Audit
- 3 of the global carbon budget: estimate errors and their impact on uptake uncertainty,
- 4 *Biogeosciences*, 12, 2565–2584, <https://doi.org/10.5194/bg-12-2565-2015>, 2015.
- 5 Bastos, A., O’Sullivan, M., Ciais, P., Makowski, D., Sitch, S., Friedlingstein, P., Chevallier, F.,
- 6 Rödenbeck, C., Pongratz, J., Luijkx, I. T., Patra, P. K., Peylin, P., Canadell, J. G., Lauerwald, R.,
- 7 Li, W., Smith, N. E., Peters, W., Goll, D. S., Jain, A. K., Kato, E., Lienert, S., Lombardozzi, D. L.,
- 8 Haverd, V., Nabel, J. E. M. S., Poulter, B., Tian, H., Walker, A. P., and Zaehle, S.: Sources of
- 9 Uncertainty in Regional and Global Terrestrial CO₂ Exchange Estimates, *Global Biogeochem.*
- 10 *Cycles*, 34, <https://doi.org/10.1029/2019GB006393>, 2020.
- 11 Bastos, A., Hartung, K., Nützel, T. B., Nabel, J. E. M. S., Houghton, R. A., and Pongratz, J.:
12 Comparison of uncertainties in land-use change fluxes from bookkeeping model
13 parameterisation, 12, 745–762, <https://doi.org/10.5194/esd-12-745-2021>, 2021.
- 14 Basu, S., Baker, D. F., Chevallier, F., Patra, P. K., Liu, J., and Miller, J. B.: The impact of
15 transport model differences on CO₂ surface flux estimates from OCO-2 retrievals of column
16 average CO₂, *Atmos. Chem. Phys.*, 18, 7189–7215, [https://doi.org/10.5194/acp-18-7189-](https://doi.org/10.5194/acp-18-7189-2018)
17 2018, 2018.
- 18 Bauer, J. E., Cai, W.-J., Raymond, P. A., Bianchi, T. S., Hopkinson, C. S., and Regnier, P. A. G.:
19 The changing carbon cycle of the coastal ocean, *Nature*, 504, 61–70,
20 <https://doi.org/10.1038/nature12857>, 2013.
- 21 Beckman, J. and Countryman, A. M.: The Importance of Agriculture in the Economy: Impacts
22 from COVID-19, 103, 1595–1611, <https://doi.org/10.1111/ajae.12212>, 2021.
- 23 Bellouin, N., Rae, J., Jones, A., Johnson, C., Haywood, J., and Boucher, O.: Aerosol forcing in
24 the Climate Model Intercomparison Project (CMIP5) simulations by HadGEM2-ES and the
25 role of ammonium nitrate, 116, <https://doi.org/10.1029/2011JD016074>, 2011.
- 26 Berthet, S., Séférian, R., Bricaud, C., Chevallier, M., Voldoire, A., and Ethé, C.: Evaluation of
27 an Online Grid-Coarsening Algorithm in a Global Eddy-Admitting Ocean Biogeochemical
28 Model, 11, 1759–1783, <https://doi.org/10.1029/2019MS001644>, 2019.



- 1 Brancalion, P. H. S., Broadbent, E. N., de-Miguel, S., Cardil, A., Rosa, M. R., Almeida, C. T.,
- 2 Almeida, D. R. A., Chakravarty, S., Zhou, M., Gamarra, J. G. P., Liang, J., Crouzeilles, R.,
- 3 Hérault, B., Aragão, L. E. O. C., Silva, C. A., and Almeyda-Zambrano, A. M.: Emerging threats
- 4 linking tropical deforestation and the COVID-19 pandemic, *Perspectives in Ecology and*
- 5 *Conservation*, 18, 243–246, <https://doi.org/10.1016/j.pecon.2020.09.006>, 2020.

- 6 Brienen, R. J. W., Phillips, O. L., Feldpausch, T. R., Gloor, E., Baker, T. R., Lloyd, J., Lopez-
- 7 Gonzalez, G., Monteagudo-Mendoza, A., Malhi, Y., Lewis, S. L., Vásquez Martinez, R.,
- 8 Alexiades, M., Álvarez Dávila, E., Alvarez-Loayza, P., Andrade, A., Aragão, L. E. O. C., Araujo-
- 9 Murakami, A., Arets, E. J. M. M., Arroyo, L., Aymard C., G. A., Bánki, O. S., Baraloto, C.,
- 10 Barroso, J., Bonal, D., Boot, R. G. A., Camargo, J. L. C., Castilho, C. V., Chama, V., Chao, K. J.,
- 11 Chave, J., Comiskey, J. A., Cornejo Valverde, F., da Costa, L., de Oliveira, E. A., Di Fiore, A.,
- 12 Erwin, T. L., Fauset, S., Forsthofer, M., Galbraith, D. R., Grahame, E. S., Groot, N., Hérault, B.,
- 13 Higuchi, N., Honorio Coronado, E. N., Keeling, H., Killeen, T. J., Laurance, W. F., Laurance, S.,
- 14 Licona, J., Magnussen, W. E., Marimon, B. S., Marimon-Junior, B. H., Mendoza, C., Neill, D.
- 15 A., Nogueira, E. M., Núñez, P., Pallqui Camacho, N. C., Parada, A., Pardo-Molina, G., Peacock,
- 16 J., Peña-Claros, M., Pickavance, G. C., Pitman, N. C. A., Poorter, L., Prieto, A., Quesada, C. A.,
- 17 Ramírez, F., Ramírez-Angulo, H., Restrepo, Z., Roopsind, A., Rudas, A., Salomão, R. P.,
- 18 Schwarz, M., Silva, N., Silva-Espejo, J. E., Silveira, M., Stropp, J., Talbot, J., ter Steege, H.,
- 19 Teran-Aguilar, J., Terborgh, J., Thomas-Caesar, R., Toledo, M., Torello-Raventos, M., Umetsu,
- 20 R. K., van der Heijden, G. M. F., van der Hout, P., Guimarães Vieira, I. C., Vieira, S. A.,
- 21 Vilanova, E., Vos, V. A., and Zagt, R. J.: Long-term decline of the Amazon carbon sink, 519,
- 22 344–348, <https://doi.org/10.1038/nature14283>, 2015.

- 23 Broecker, W. S.: Ocean chemistry during glacial time, *Geochimica et Cosmochimica Acta*, 46,
- 24 1689–1705, [https://doi.org/10.1016/0016-7037\(82\)90110-7](https://doi.org/10.1016/0016-7037(82)90110-7), 1982.

- 25 Bruno, M. and Joos, F.: Terrestrial carbon storage during the past 200 years: A Monte Carlo
- 26 Analysis of CO₂ data from ice core and atmospheric measurements, *Global Biogeochem.*
- 27 *Cycles*, 11, 111–124, <https://doi.org/10.1029/96GB03611>, 1997.

- 28 Buitenhuis, E. T., Hashioka, T., and Quéré, C. L.: Combined constraints on global ocean
- 29 primary production using observations and models: OCEAN PRIMARY PRODUCTION, *Global*
- 30 *Biogeochem. Cycles*, 27, 847–858, <https://doi.org/10.1002/gbc.20074>, 2013.



- 1 Burton, C., Betts, R., Cardoso, M., Feldpausch, T. R., Harper, A., Jones, C. D., Kelley, D. I.,
- 2 Robertson, E., and Wiltshire, A.: Representation of fire, land-use change and vegetation
- 3 dynamics in the Joint UK Land Environment Simulator vn4.9 (JULES), *Geosci. Model Dev.*, 12,
- 4 179–193, <https://doi.org/10.5194/gmd-12-179-2019>, 2019.

- 5 Bushinsky, S. M., Landschützer, P., Rödenbeck, C., Gray, A. R., Baker, D., Mazloff, M. R.,
- 6 Resplandy, L., Johnson, K. S., and Sarmiento, J. L.: Reassessing Southern Ocean Air-Sea CO₂
- 7 Flux Estimates With the Addition of Biogeochemical Float Observations, *Global Biogeochem.*
- 8 *Cycles*, 33, 1370–1388, <https://doi.org/10.1029/2019GB006176>, 2019.

- 9 Canadell, J. G., Le Quere, C., Raupach, M. R., Field, C. B., Buitenhuis, E. T., Ciais, P., Conway,
- 10 T. J., Gillett, N. P., Houghton, R. A., and Marland, G.: Contributions to accelerating
- 11 atmospheric CO₂ growth from economic activity, carbon intensity, and efficiency of natural
- 12 sinks, *Proceedings of the National Academy of Sciences*, 104, 18866–18870,
- 13 <https://doi.org/10.1073/pnas.0702737104>, 2007.

- 14 Canadell, J. G., Monteiro, P. M. S., Costa, M. H., Cotrim da Cunha, L., Cox, P. M., Eliseev, A.
- 15 V., Henson, S., Ishii, M., Jaccard, S., Koven, C., Lohila, A., Patra, P. K., Piao, S., Rogelj, J.,
- 16 Syampungani, S., Zaehle, S., and Zickfeld, K.: Global Carbon and other Biogeochemical Cycles
- 17 and Feedbacks. In: *Climate Change 2021: The Physical Science Basis. Contribution of*
- 18 *Working Group I to the Sixth Assessment Report of the Intergovernmental Panel on Climate*
- 19 *Change* [Masson-Delmotte, V., P. Zhai, A. Pirani, S. L. Connors, C. Péan, S. Berger, N. Caud, Y.
- 20 Chen, L. Goldfarb, M. I. Gomis, M. Huang, K. Leitzell, E. Lonnoy, J.B.R. Matthews, T. K.
- 21 Maycock, T. Waterfield, O. Yelekçi, R. Yu and B. Zhou (eds.)]. Cambridge University Press. In
- 22 Press., 2021.

- 23 Cao, Z., Myers, R. J., Lupton, R. C., Duan, H., Sacchi, R., Zhou, N., Reed Miller, T., Cullen, J.
- 24 M., Ge, Q., and Liu, G.: The sponge effect and carbon emission mitigation potentials of the
- 25 global cement cycle, *Nat Commun*, 11, 3777, <https://doi.org/10.1038/s41467-020-17583-w>,
- 26 2020.

- 27 Carbon Monitor: CO₂ Emissions Variation, available at: <https://carbonmonitor.org/>, last
- 28 access: 25 October 2021., 2021.

- 29 Chatfield, C.: The Holt-Winters Forecasting Procedure, 27, 264–279,



- 1 <https://doi.org/10.2307/2347162>, 1978.
- 2 Chau, T. T. T., Gehlen, M., and Chevallier, F.: QUALITY INFORMATION DOCUMENT for Global
3 Ocean Surface Carbon Product MULTIOBS_GLO_BIO_CARBON_SURFACE_REP_015_008, Le
4 Laboratoire des Sciences du Climat et de l'Environnement, 2020.
- 5 Chau, T. T. T., Gehlen, M., and Chevallier, F.: A seamless ensemble-based reconstruction of
6 surface ocean pCO₂ and air-sea CO₂ fluxes over the global coastal and open oceans, 1–30,
7 <https://doi.org/10.5194/bg-2021-207>, 2021.
- 8 Chevallier, F.: On the parallelization of atmospheric inversions of CO₂ surface fluxes within a
9 variational framework, 6, 783–790, <https://doi.org/10.5194/gmd-6-783-2013>, 2013.
- 10 Chevallier, F., Fisher, M., Peylin, P., Serrar, S., Bousquet, P., Bréon, F.-M., Chédin, A., and
11 Ciais, P.: Inferring CO₂ sources and sinks from satellite observations: Method and
12 application to TOVS data, *J. Geophys. Res.*, 110, D24309,
13 <https://doi.org/10.1029/2005JD006390>, 2005.
- 14 Chevallier, F., Remaud, M., O'Dell, C. W., Baker, D., Peylin, P., and Cozic, A.: Objective
15 evaluation of surface- and satellite-driven carbon dioxide atmospheric inversions, *Atmos.*
16 *Chem. Phys.*, 19, 14233–14251, <https://doi.org/10.5194/acp-19-14233-2019>, 2019.
- 17 Chini, L., Hurtt, G., Sahajpal, R., Frohling, S., Klein Goldewijk, K., Sitch, S., Ganzenmüller, R.,
18 Ma, L., Ott, L., Pongratz, J., and Poulter, B.: Land-use harmonization datasets for annual
19 global carbon budgets, 13, 4175–4189, <https://doi.org/10.5194/essd-13-4175-2021>, 2021.
- 20 Ciais, P., Sabine, C., Bala, G., Bopp, L., Brovkin, V., Canadell, J. G., Chhabra, A., DeFries, R.,
21 Galloway, J., Heimann, M., Jones, C., Le Quéré, C., Myneni, R., Piao, S., Thornton, P., Willem,
22 J., Friedlingstein, P., and Munhoven, G.: Carbon and Other Biogeochemical Cycles, in *Climate*
23 *Change 2013: The Physical Science Basis, Contribution of Working Group I to the Fifth*
24 *Assessment Report of the Intergovernmental Panel on Climate Change*, edited by:
25 Intergovernmental Panel on Climate Change, Cambridge University Press, Cambridge, UK,
26 465–570, 2013.
- 27 Ciais, P., Tan, J., Wang, X., Roedenbeck, C., Chevallier, F., Piao, S.-L., Moriarty, R., Broquet,
28 G., Le Quéré, C., Canadell, J. G., Peng, S., Poulter, B., Liu, Z., and Tans, P.: Five decades of



- 1 northern land carbon uptake revealed by the interhemispheric CO₂ gradient, *Nature*, 568,
2 221–225, <https://doi.org/10.1038/s41586-019-1078-6>, 2019.
- 3 Ciais, P., Bastos, A., Chevallier, F., Lauerwald, R., Poulter, B., Canadell, P., Hugelius, G.,
4 Jackson, R. B., Jain, A., Jones, M., Kondo, M., Lujikx, I., Patra, P. K., Peters, W., Pongratz, J.,
5 Petrescu, A. M. R., Piao, S., Qiu, C., Von Randow, C., Regnier, P., Saunois, M., Scholes, R.,
6 Shvidenko, A., Tian, H., Yang, H., Wang, X., and Zheng, B.: Definitions and methods to
7 estimate regional land carbon fluxes for the second phase of the REgional Carbon Cycle
8 Assessment and Processes Project (RECCAP-2), 1–46, [https://doi.org/10.5194/gmd-2020-](https://doi.org/10.5194/gmd-2020-259)
9 259, 2020.
- 10 Collier, N., Hoffman, F. M., Lawrence, D. M., Keppel-Aleks, G., Koven, C. D., Riley, W. J., Mu,
11 M., and Randerson, J. T.: The International Land Model Benchmarking (ILAMB) System:
12 Design, Theory, and Implementation, *J. Adv. Model. Earth Syst.*, 10, 2731–2754,
13 <https://doi.org/10.1029/2018MS001354>, 2018.
- 14 Conchedda, G. and Tubiello, F. N.: Drainage of organic soils and GHG emissions: Validation
15 with country data, *Biosphere – Biogeosciences*, <https://doi.org/10.5194/essd-2020-202>,
16 2020.
- 17 Cooper, D. J., Watson, A. J., and Ling, R. D.: Variation of pCO₂ along a North Atlantic shipping
18 route (U.K. to the Caribbean): A year of automated observations, *Marine Chemistry*, 60,
19 147–164, [https://doi.org/10.1016/S0304-4203\(97\)00082-0](https://doi.org/10.1016/S0304-4203(97)00082-0), 1998.
- 20 Cox, A., Vermeulen, A., Manning, A., Beyersdorf, A., Zahn, A., Manning, A., Watson, A.,
21 Karion, A., Hensen, A., Arlyn Andrews, Frumau, A., Colomb, A., Scheeren, B., Law, B., Baier,
22 B., Munger, B., Paplawsky, B., Viner, B., Stephens, B., Daube, B., Labuschagne, C., Myhre, C.
23 L., Hanson, C., Miller, C. E., Plass-Duelmer, C., Plass-Duelmer, C., Gerbig, C., Sloop, C. D.,
24 Sweeney, C., Kubistin, D., Goto, D., Jaffe, D., Say, D., Van Dinter, D., Bowling, D., Lam, D. H.
25 Y., Dickon Young, Worthy, D., Dlugokencky, E., Kozlova, E., Gloor, E., Cuevas, E., Reyes-
26 Sanchez, E., Hintsa, E., Kort, E., Morgan, E., Obersteiner, F., Apadula, F., Francois Gheusi,
27 Meinhardt, F., Moore, F., Vitkova, G., Chen, G., Bentz, G., Manca, G., Brailsford, G., Forster,
28 G., Boenisch, H., Riris, H., Meijer, H., Timas, H., Matsueda, H., Huilin Chen, Levin, I., Lehner,
29 I., Mammarella, I., Bartyzel, J., Abshire, J. B., Elkins, J. W., Levula, J., Jaroslaw Necki, Pichon,



- 1 J. M., Peischl, J., Müller-Williams, J., Turnbull, J., Miller, J. B., Lee, J., Lin, J., Josep-Anton
- 2 Morgui, DiGangi, J. P., Hatakka, J., Coletta, J. D., Worsey, J., Holst, J., Kominkova, K., McKain,
- 3 K., Saito, K., Aikin, K., Davis, K., Thoning, K., Tørseth, K., Haszpra, L., Mitchell, L., Gatti, L. V.,
- 4 Emmenegger, L., Lukasz Chmura, Merchant, L., Sha, M. K., Delmotte, M., et al.: Multi-
- 5 laboratory compilation of atmospheric carbon dioxide data for the period 1957-2019;
- 6 obspack_co2_1_GLOBALVIEWplus_v6.1_2021-03-01, <https://doi.org/10.25925/20201204>,
- 7 2021.

- 8 Cox, P. M., Pearson, D., Booth, B. B., Friedlingstein, P., Huntingford, C., Jones, C. D., and
- 9 Luke, C. M.: Sensitivity of tropical carbon to climate change constrained by carbon dioxide
- 10 variability, *Nature*, 494, 341–344, <https://doi.org/10.1038/nature11882>, 2013.

- 11 Crippa, M., Janssens-Maenhout, G., Guizzardi, D., Van Dingenen, R., and Dentener, F.:
- 12 Contribution and uncertainty of sectorial and regional emissions to regional and global
- 13 PM2.5 health impacts, 19, 5165–5186, <https://doi.org/10.5194/acp-19-5165-2019>, 2019.

- 14 Dai, A. and Trenberth, K. E.: Estimates of Freshwater Discharge from Continents: Latitudinal
- 15 and Seasonal Variations, 3, 660–687, [https://doi.org/10.1175/1525-](https://doi.org/10.1175/1525-7541(2002)003<0660:EOFDFC>2.0.CO;2)
- 16 [7541\(2002\)003<0660:EOFDFC>2.0.CO;2](https://doi.org/10.1175/1525-7541(2002)003<0660:EOFDFC>2.0.CO;2), 2002.

- 17 Davis, S. J. and Caldeira, K.: Consumption-based accounting of CO2 emissions, *Proceedings*
- 18 *of the National Academy of Sciences*, 107, 5687–5692,
- 19 <https://doi.org/10.1073/pnas.0906974107>, 2010.

- 20 De Kauwe, M. G., Disney, M. I., Quaife, T., Lewis, P., and Williams, M.: An assessment of the
- 21 MODIS collection 5 leaf area index product for a region of mixed coniferous forest, *Remote*
- 22 *Sensing of Environment*, 115, 767–780, <https://doi.org/10.1016/j.rse.2010.11.004>, 2011.

- 23 Decharme, B., Delire, C., Minvielle, M., Colin, J., Vergnes, J.-P., Alias, A., Saint-Martin, D.,
- 24 Séférian, R., Sénési, S., and Voldoire, A.: Recent Changes in the ISBA-CTRIP Land Surface
- 25 System for Use in the CNRM-CM6 Climate Model and in Global Off-Line Hydrological
- 26 Applications, 11, 1207–1252, <https://doi.org/10.1029/2018MS001545>, 2019.

- 27 Delire, C., Séférian, R., Decharme, B., Alkama, R., Calvet, J.-C., Carrer, D., Gibelin, A.-L.,
- 28 Joetzer, E., Morel, X., Rocher, M., and Tzanos, D.: The Global Land Carbon Cycle Simulated



- 1 With ISBA-CTrip: Improvements Over the Last Decade, 12, e2019MS001886,
- 2 <https://doi.org/10.1029/2019MS001886>, 2020.

- 3 Denman, K. L., Brasseur, G., Chidthaisong, A., Ciais, P., Cox, P. M., Dickinson, R. E.,
- 4 Hauglustaine, D., Heinze, C., Holland, E., Jacob, D., Lohmann, U., Ramachandran, S., Leite da
- 5 Silva Dias, P., Wofsy, S. C., and Zhang, X.: Couplings Between Changes in the Climate System
- 6 and Biogeochemistry, in: Climate Change 2007: The Physical Science Basis. Contribution of
- 7 Working Group I to the Fourth Assessment Report of the Intergovernmental Panel on
- 8 Climate Change, edited by: Solomon, S., Qin, D., Manning, M., Marquis, M., Averyt, K.,
- 9 Tignor, M. M. B., Miller, H. L., and Chen, Z. L., Cambridge University Press, Cambridge, UK
- 10 and New York, USA, 499–587, 2007.

- 11 Denning, A. S., Fung, I. Y., and Randall, D.: Latitudinal gradient of atmospheric CO₂ due to
- 12 seasonal exchange with land biota, *Nature*, 376, 240–243,
- 13 <https://doi.org/10.1038/376240a0>, 1995.

- 14 Denvil-Sommer, A., Gehlen, M., Vrac, M., and Mejia, C.: LSCE-FFNN-v1: a two-step neural
- 15 network model for the reconstruction of surface ocean pCO₂ over the global ocean, 12,
- 16 2091–2105, <https://doi.org/10.5194/gmd-12-2091-2019>, 2019.

- 17 DeVries, T.: The oceanic anthropogenic CO₂ sink: Storage, air-sea fluxes, and transports
- 18 over the industrial era, *Global Biogeochem. Cycles*, 28, 631–647,
- 19 <https://doi.org/10.1002/2013GB004739>, 2014.

- 20 DeVries, T., Holzer, M., and Primeau, F.: Recent increase in oceanic carbon uptake driven by
- 21 weaker upper-ocean overturning, *Nature*, 542, 215–218,
- 22 <https://doi.org/10.1038/nature21068>, 2017.

- 23 DeVries, T., Quéré, C. L., Andrews, O., Berthet, S., Hauck, J., Ilyina, T., Landschützer, P.,
- 24 Lenton, A., Lima, I. D., Nowicki, M., Schwinger, J., and Séférian, R.: Decadal trends in the
- 25 ocean carbon sink, *PNAS*, 116, 11646–11651, <https://doi.org/10.1073/pnas.1900371116>,
- 26 2019.

- 27 Di Sarra, A. G., Karion, A., Arlyn Andrews, Colomb, A., Scheeren, B., Viner, B., Myhre, C. L.,
- 28 Miller, C. E., Plass-Duelmer, C., Plass-Duelmer, C., Sloop, C. D., Sweeney, C., Kubistin, D.,



- 1 Jaffe, D., Dlugokencky, E., Vitkova, G., Manca, G., Huilin Chen, Lehner, I., Mammarella, I.,
- 2 Pichon, J. M., Müller-Williams, J., Miller, J. B., Lee, J., Hatakka, J., Holst, J., Kominkova, K.,
- 3 McKain, K., Thoning, K., Tørseth, K., Emmenegger, L., Sha, M. K., Delmotte, M., Fischer, M.
- 4 L., Schumacher, M., Leuenberger, M., Steinbacher, M., De Mazière, M., Lindauer, M.,
- 5 Mölder, M., Heliasz, M., Marek, M. V., Ramonet, M., Lopez, M., Laurent, O., Hermanssen, O.,
- 6 Trisolino, P., Cristofanelli, P., Smith, P., Bakwin, P., Bergamaschi, P., Keronen, P., Tans, P.,
- 7 Piacentino, S., Biraud, S. C., Conil, S., De Wekker, S., Biermann, T., Laurila, T., Aalto, T., and
- 8 Kazan, V.: Multi-laboratory compilation of atmospheric carbon dioxide data for the years
- 9 2020-2021; obspack_co2_1_NRT_v6.1.1_2021-05-17, <https://doi.org/10.25925/20210517>,
- 10 2021.
- 11 Dickson, A. G., Sabine, C. L., and Christian, J. R.: Guide to best practices for ocean CO₂
- 12 measurement. Sidney, British Columbia, North Pacific Marine Science Organization, 191pp.
- 13 (PICES Special Publication 3; IOCCP Report 8). DOI: <https://doi.org/10.25607/OBP-1342>,
- 14 2007.
- 15 Dlugokencky, E. and Tans, P.: Trends in atmospheric carbon dioxide, National Oceanic and
- 16 Atmospheric Administration, Earth System Research Laboratory (NOAA/ESRL), available at:
- 17 <http://www.esrl.noaa.gov/gmd/ccgg/trends/global.html>, accessed: 16 November 2020.,
- 18 2020.
- 19 Dlugokencky, E. and Tans, P.: Trends in atmospheric carbon dioxide, National Oceanic and
- 20 Atmospheric Administration, Earth System Research Laboratory (NOAA/ESRL), available at:
- 21 <http://www.esrl.noaa.gov/gmd/ccgg/trends/global.html>, last access: 25 October 2021.,
- 22 2021.
- 23 Doney, S. C., Lima, I., Feely, R. A., Glover, D. M., Lindsay, K., Mahowald, N., Moore, J. K., and
- 24 Wanninkhof, R.: Mechanisms governing interannual variability in upper-ocean inorganic
- 25 carbon system and air–sea CO₂ fluxes: Physical climate and atmospheric dust, Deep Sea
- 26 Research Part II: Topical Studies in Oceanography, 56, 640–655,
- 27 <https://doi.org/10.1016/j.dsr2.2008.12.006>, 2009.
- 28 Duce, R. A., LaRoche, J., Altieri, K., Arrigo, K. R., Baker, A. R., Capone, D. G., Cornell, S.,
- 29 Dentener, F., Galloway, J., Ganeshram, R. S., Geider, R. J., Jickells, T., Kuypers, M. M.,



- 1 Langlois, R., Liss, P. S., Liu, S. M., Middelburg, J. J., Moore, C. M., Nickovic, S., Oschlies, A.,
- 2 Pedersen, T., Prospero, J., Schlitzer, R., Seitzinger, S., Sorensen, L. L., Uematsu, M., Ulloa, O.,
- 3 Voss, M., Ward, B., and Zamora, L.: Impacts of Atmospheric Anthropogenic Nitrogen on the
- 4 Open Ocean, *Science*, 320, 893–897, <https://doi.org/10.1126/science.1150369>, 2008.
- 5 Dufour, C. O., Sommer, J. L., Gehlen, M., Orr, J. C., Molines, J., Simeon, J., and Barnier, B.:
- 6 Eddy compensation and controls of the enhanced sea-to-air CO₂ flux during positive phases
- 7 of the Southern Annular Mode, *Global Biogeochem. Cycles*, 27, 950–961,
- 8 <https://doi.org/10.1002/gbc.20090>, 2013.
- 9 Eakins, B. W. and Sharman, G. F.: National Geophysical Data Center: Volumes of the World’s
- 10 Oceans from ETOPO1, available at:
- 11 https://www.ngdc.noaa.gov/mgg/global/etopo1_ocean_volumes.html, last access: 25
- 12 October 2021, U.S. Department of Commerce, 2010.
- 13 Eggleston, H. S., Buendia, L., Miwa, K., Ngara, T., and Tanabe, K.: Volume 4: Agriculture,
- 14 forestry and land use. in: 2006 IPCC guidelines for national greenhouse gas inventories.,
- 15 2006.
- 16 EIA: U.S. Energy Information Administration: Short-Term Energy Outlook, available at:
- 17 <http://www.eia.gov/forecasts/steo/outlook>, last access: 25 October 2021., 2021.
- 18 Erb, K.-H., Kastner, T., Luyssaert, S., Houghton, R. A., Kuemmerle, T., Olofsson, P., and
- 19 Haberl, H.: Bias in the attribution of forest carbon sinks, *Nature Clim Change*, 3, 854–856,
- 20 <https://doi.org/10.1038/nclimate2004>, 2013.
- 21 Erb, K.-H., Kastner, T., Plutzer, C., Bais, A. L. S., Carvalhais, N., Fetzel, T., Gingrich, S., Haberl,
- 22 H., Lauk, C., Niedertscheider, M., Pongratz, J., Thurner, M., and Luyssaert, S.: Unexpectedly
- 23 large impact of forest management and grazing on global vegetation biomass, *Nature*, 553,
- 24 73–76, <https://doi.org/10.1038/nature25138>, 2018.
- 25 Eskander, S. M. S. U. and Fankhauser, S.: Reduction in greenhouse gas emissions from
- 26 national climate legislation, *Nat. Clim. Chang.*, 10, 750–756,
- 27 <https://doi.org/10.1038/s41558-020-0831-z>, 2020.
- 28 Etheridge, D. M., Steele, L. P., Langenfelds, R. L., Francey, R. J., Barnola, J.-M., and Morgan,



- 1 V. I.: Natural and anthropogenic changes in atmospheric CO₂ over the last 1000 years from
- 2 air in Antarctic ice and firn, *J. Geophys. Res.*, 101, 4115–4128,
- 3 <https://doi.org/10.1029/95JD03410>, 1996.
- 4 Eyring, V., Bony, S., Meehl, G. A., Senior, C. A., Stevens, B., Stouffer, R. J., and Taylor, K. E.:
- 5 Overview of the Coupled Model Intercomparison Project Phase 6 (CMIP6) experimental
- 6 design and organization, *Geosci. Model Dev.*, 9, 1937–1958, [https://doi.org/10.5194/gmd-9-](https://doi.org/10.5194/gmd-9-1937-2016)
- 7 1937-2016, 2016.
- 8 FAO: Global Forest Resources Assessment 2020: Main report, FAO, Rome, Italy, 184 pp.,
- 9 <https://doi.org/10.4060/ca9825en>, 2020.
- 10 FAO: FAO: FAOSTAT Statistical Database, domains Climate Change, available at:
- 11 <http://www.fao.org/faostat/en/#data/GT>, last accessed: 25 October 2021, 2021.
- 12 FAOSTAT: FAOSTAT: Food and Agriculture Organization Statistics Division, available at:
- 13 <http://faostat.fao.org/>, last access: 25 October 2021), 2021.
- 14 FAO/UNEP: Food and Agriculture Organisation / United Nations Environment Programme:
- 15 The state of food and agriculture 1981, available at:
- 16 <https://www.fao.org/3/ap661e/ap661e.pdf>, last access: 25 October 2021, 1981.
- 17 Fay, A. R. and McKinley, G. A.: Global open-ocean biomes: mean and temporal variability, 6,
- 18 273–284, <https://doi.org/10.5194/essd-6-273-2014>, 2014.
- 19 Fay, A. R., Gregor, L., Landschützer, P., McKinley, G. A., Gruber, N., Gehlen, M., Iida, Y.,
- 20 Laruelle, G. G., Rödenbeck, C., and Zeng, J.: Harmonization of global surface ocean pCO₂
- 21 mapped products and their flux calculations; an improved estimate of the ocean carbon
- 22 sink, 1–32, <https://doi.org/10.5194/essd-2021-16>, 2021a.
- 23 Fay, A. R., Gregor, L., Landschützer, P., McKinley, G. A., Gruber, N., Gehlen, M., Iida, Y.,
- 24 Laruelle, G. G., Rödenbeck, C., Roobaert, A., and Zeng, J.: SeaFlux: harmonization of air–sea
- 25 CO₂ fluxes from surface pCO₂ data products using a standardized approach, 13, 4693–4710,
- 26 <https://doi.org/10.5194/essd-13-4693-2021>, 2021b.
- 27 Feng, L., Palmer, P. I., Bosch, H., and Dance, S.: Estimating surface CO₂ fluxes from space-



- 1 borne CO₂ dry air mole fraction observations using an ensemble Kalman Filter, 15, 2009.
- 2 Feng, L., Palmer, P. I., Parker, R. J., Deutscher, N. M., Feist, D. G., Kivi, R., Morino, I., and
3 Sussmann, R.: Estimates of European uptake of CO₂ inferred from GOSAT XCO₂ retrievals:
4 sensitivity to measurement bias inside and outside Europe, *Atmos. Chem. Phys.*, 16, 1289–
5 1302, <https://doi.org/10.5194/acp-16-1289-2016>, 2016.
- 6 Friedlingstein, P., Houghton, R. A., Marland, G., Hackler, J., Boden, T. A., Conway, T. J.,
7 Canadell, J. G., Raupach, M. R., Ciais, P., and Le Quéré, C.: Update on CO₂ emissions, *Nature*
8 *Geosci*, 3, 811–812, <https://doi.org/10.1038/ngeo1022>, 2010.
- 9 Friedlingstein, P., Andrew, R. M., Rogelj, J., Peters, G. P., Canadell, J. G., Knutti, R., Luderer,
10 G., Raupach, M. R., Schaeffer, M., van Vuuren, D. P., and Le Quéré, C.: Persistent growth of
11 CO₂ emissions and implications for reaching climate targets, *Nature Geosci*, 7, 709–715,
12 <https://doi.org/10.1038/ngeo2248>, 2014.
- 13 Friedlingstein, P., Jones, M. W., O’Sullivan, M., Andrew, R. M., Hauck, J., Peters, G. P., Peters,
14 W., Pongratz, J., Sitch, S., Le Quéré, C., Bakker, D. C. E., Canadell, J. G., Ciais, P., Jackson, R.
15 B., Anthoni, P., Barbero, L., Bastos, A., Bastrikov, V., Becker, M., Bopp, L., Buitenhuis, E.,
16 Chandra, N., Chevallier, F., Chini, L. P., Currie, K. I., Feely, R. A., Gehlen, M., Gilfillan, D.,
17 Gkritzalis, T., Goll, D. S., Gruber, N., Gutekunst, S., Harris, I., Haverd, V., Houghton, R. A.,
18 Hurtt, G., Ilyina, T., Jain, A. K., Joetzjer, E., Kaplan, J. O., Kato, E., Klein Goldewijk, K.,
19 Korsbakken, J. I., Landschützer, P., Lauvset, S. K., Lefèvre, N., Lenton, A., Lienert, S.,
20 Lombardozzi, D., Marland, G., McGuire, P. C., Melton, J. R., Metzl, N., Munro, D. R., Nabel, J.
21 E. M. S., Nakaoka, S.-I., Neill, C., Omar, A. M., Ono, T., Peregón, A., Pierrot, D., Poulter, B.,
22 Rehder, G., Resplandy, L., Robertson, E., Rödenbeck, C., Séférian, R., Schwinger, J., Smith, N.,
23 Tans, P. P., Tian, H., Tilbrook, B., Tubiello, F. N., van der Werf, G. R., Wiltshire, A. J., and
24 Zaehle, S.: Global Carbon Budget 2019, *Earth Syst. Sci. Data*, 11, 1783–1838,
25 <https://doi.org/10.5194/essd-11-1783-2019>, 2019.
- 26 Friedlingstein, P., O’Sullivan, M., Jones, M. W., Andrew, R. M., Hauck, J., Olsen, A., Peters, G.
27 P., Peters, W., Pongratz, J., Sitch, S., Le Quéré, C., Canadell, J. G., Ciais, P., Jackson, R. B., Alin,
28 S., Aragão, L. E. O. C., Arneeth, A., Arora, V., Bates, N. R., Becker, M., Benoit-Cattin, A., Bittig,
29 H. C., Bopp, L., Bultan, S., Chandra, N., Chevallier, F., Chini, L. P., Evans, W., Florentie, L.,



- 1 Forster, P. M., Gasser, T., Gehlen, M., Gilfillan, D., Gkritzalis, T., Gregor, L., Gruber, N., Harris,
2 I., Hartung, K., Haverd, V., Houghton, R. A., Ilyina, T., Jain, A. K., Joetzjer, E., Kadono, K., Kato,
3 E., Kitidis, V., Korsbakken, J. I., Landschützer, P., Lefèvre, N., Lenton, A., Lienert, S., Liu, Z.,
4 Lombardozi, D., Marland, G., Metzli, N., Munro, D. R., Nabel, J. E. M. S., Nakaoka, S.-I., Niwa,
5 Y., O'Brien, K., Ono, T., Palmer, P. I., Pierrot, D., Poulter, B., Resplandy, L., Robertson, E.,
6 Rödenbeck, C., Schwinger, J., Séférian, R., Skjelvan, I., Smith, A. J. P., Sutton, A. J., Tanhua, T.,
7 Tans, P. P., Tian, H., Tilbrook, B., van der Werf, G., Vuichard, N., Walker, A. P., Wanninkhof,
8 R., Watson, A. J., Willis, D., Wiltshire, A. J., Yuan, W., Yue, X., and Zaehle, S.: Global Carbon
9 Budget 2020, *Earth Syst. Sci. Data*, 12, 3269–3340, [https://doi.org/10.5194/essd-12-3269-](https://doi.org/10.5194/essd-12-3269-2020)
10 2020, 2020.
- 11 Friedlingstein, P., Jones, M. W., O'Sullivan, M., Andrew, R. M., Bakker, D. C. E., Hauck, J., Le
12 Quéré, C., Peters, G. P., Peters, W., Pongratz, J., Sitch, S., Canadell, J. G., Ciais, P., Jackson, R.
13 B., Anthoni, P., Bates, N. R., Becker, M., Bopp, L., Tuyen, T., Chau, T., Chevallier, F., Chini, L.
14 P., Cronin, M., Currie, K. I., Decharme, B., Djeutchouang, L. M., Dou, X., Evans, W., Feely, R.
15 A., Feng, L., Gasser, T., Gilfillan, D., Gkritzalis, T., Grassi, G., Gregor, L., Gruber, N., Gürses, Ö.,
16 Harris, I., Houghton, R. A., Hurtt, G. C., Iida, Y., Ilyina, T., Luijkx, I. T., Jain, A. K., Jones, S. D.,
17 Kato, E., Kennedy, D., Klein Goldewijk, K., Knauer, J., Korsbakken, J. I., Körtzinger, A.,
18 Landschützer, P., Lauvset, S. K., Lefèvre, N., Lienert, S., Liu, J., Marland, G., McGuire, P. C.,
19 Melton, J. R., Munro, D. R., Nabel, J. E. M. S., Nakaoka, S.-I., Niwa, Y., Ono, T., Pierrot, D.,
20 Poulter, B., Rehder, G., Resplandy, L., Robertson, E., Rödenbeck, C., Schwinger, J.,
21 Schwingshackl, C., Séférian, R., Sutton, A. J., Tanhua, T., Tans, P., Tian, H., Tilbrook, B.,
22 Tubiello, F., van der Werf, G. R., Vuichard, N., Wanninkhof, R., Watson, A. J., Willis, D.,
23 Wiltshire, A. J., Wenping Yuan, Yue, C., Yue, X., Zaehle, S., and Zeng, J.: Supplemental data of
24 the Global Carbon Budget 2021, ICOS-ERIC Carbon Portal, [https://doi.org/10.18160/gcp-](https://doi.org/10.18160/gcp-2021)
25 2021, 2021.
- 26 Gasser, T. and Ciais, P.: A theoretical framework for the net land-to-atmosphere CO₂ flux
27 and its implications in the definition of "emissions from land-use change", *Earth Syst.*
28 *Dynam.*, 4, 171–186, <https://doi.org/10.5194/esd-4-171-2013>, 2013.
- 29 Gasser, T., Crepin, L., Quilcaille, Y., Houghton, R. A., Ciais, P., and Obersteiner, M.: Historical
30 CO₂ emissions from land use and land cover change and their uncertainty, *Biogeosciences*,



- 1 17, 4075–4101, <https://doi.org/10.5194/bg-17-4075-2020>, 2020.
- 2 Gaubert, B., Stephens, B. B., Basu, S., Chevallier, F., Deng, F., Kort, E. A., Patra, P. K., Peters,
3 W., Rödenbeck, C., Saeki, T., Schimel, D., Van der Laan-Luijkx, I., Wofsy, S., and Yin, Y.: Global
4 atmospheric CO₂ inverse models converging on neutral tropical land exchange, but
5 disagreeing on fossil fuel and atmospheric growth rate, *Biogeosciences*, 16, 117–134,
6 <https://doi.org/10.5194/bg-16-117-2019>, 2019.
- 7 Gaubert, B., Emmons, L. K., Raeder, K., Tilmes, S., Miyazaki, K., Arellano Jr., A. F., Elguindi, N.,
8 Granier, C., Tang, W., Barré, J., Worden, H. M., Buchholz, R. R., Edwards, D. P., Franke, P.,
9 Anderson, J. L., Saunois, M., Schroeder, J., Woo, J.-H., Simpson, I. J., Blake, D. R., Meinardi,
10 S., Wennberg, P. O., Crouse, J., Teng, A., Kim, M., Dickerson, R. R., He, H., Ren, X., Pusede,
11 S. E., and Diskin, G. S.: Correcting model biases of CO in East Asia: impact on oxidant
12 distributions during KORUS-AQ, 20, 14617–14647, [https://doi.org/10.5194/acp-20-14617-](https://doi.org/10.5194/acp-20-14617-2020)
13 2020, 2020.
- 14 General Administration of Customs of the People’s Republic of China: Monthly statistical
15 reports, available at:
16 [http://www.customs.gov.cn/customs/302249/zfxxgk/2799825/302274/302277/3512606/in-](http://www.customs.gov.cn/customs/302249/zfxxgk/2799825/302274/302277/3512606/index.html)
17 dex.html, last access: 25 October 2021, 2021.
- 18 Giglio, L., Schroeder, W., and Justice, C. O.: The collection 6 MODIS active fire detection
19 algorithm and fire products, *Remote Sensing of Environment*, 178, 31–41,
20 <https://doi.org/10.1016/j.rse.2016.02.054>, 2016.
- 21 Gilfillan, D. and Marland, G.: CDIAC-FF: global and national CO₂ emissions from fossil fuel
22 combustion and cement manufacture: 1751–2017, 13, 1667–1680,
23 <https://doi.org/10.5194/essd-13-1667-2021>, 2021.
- 24 Gloege, L., McKinley, G. A., Landschützer, P., Fay, A. R., Frölicher, T. L., Fyfe, J. C., Ilyina, T.,
25 Jones, S., Lovenduski, N. S., Rodgers, K. B., Schlunegger, S., and Takano, Y.: Quantifying
26 Errors in Observationally Based Estimates of Ocean Carbon Sink Variability, 35,
27 e2020GB006788, <https://doi.org/10.1029/2020GB006788>, 2021.
- 28 Goddijn-Murphy, L. M., Woolf, D. K., Land, P. E., Shutler, J. D., and Donlon, C.: The OceanFlux



- 1 Greenhouse Gases methodology for deriving a sea surface climatology of CO₂ fugacity in
2 support of air–sea gas flux studies, 11, 519–541, <https://doi.org/10.5194/os-11-519-2015>,
3 2015.
- 4 Golar, G., Malik, A., Muis, H., Herman, A., Nurudin, N., and Lukman, L.: The social-economic
5 impact of COVID-19 pandemic: implications for potential forest degradation, *Heliyon*, 6,
6 e05354, <https://doi.org/10.1016/j.heliyon.2020.e05354>, 2020.
- 7 Grassi, G., House, J., Kurz, W. A., Cescatti, A., Houghton, R. A., Peters, G. P., Sanz, M. J.,
8 Viñas, R. A., Alkama, R., Arneth, A., Bondeau, A., Dentener, F., Fader, M., Federici, S.,
9 Friedlingstein, P., Jain, A. K., Kato, E., Koven, C. D., Lee, D., Nabel, J. E. M. S., Nassikas, A. A.,
10 Perugini, L., Rossi, S., Sitch, S., Viovy, N., Wiltshire, A., and Zaehle, S.: Reconciling global-
11 model estimates and country reporting of anthropogenic forest CO₂ sinks, *Nature Clim*
12 *Change*, 8, 914–920, <https://doi.org/10.1038/s41558-018-0283-x>, 2018.
- 13 Grassi, G., Stehfest, E., Rogelj, J., van Vuuren, D., Cescatti, A., House, J., Nabuurs, G.-J., Rossi,
14 S., Alkama, R., Viñas, R. A., Calvin, K., Ceccherini, G., Federici, S., Fujimori, S., Gusti, M.,
15 Hasegawa, T., Havlik, P., Humpenöder, F., Korosuo, A., Perugini, L., Tubiello, F. N., and Popp,
16 A.: Critical adjustment of land mitigation pathways for assessing countries’ climate progress,
17 *Nat. Clim. Chang.*, 11, 425–434, <https://doi.org/10.1038/s41558-021-01033-6>, 2021.
- 18 Gregg, J. S., Andres, R. J., and Marland, G.: China: Emissions pattern of the world leader in
19 CO₂ emissions from fossil fuel consumption and cement production, *Geophys. Res. Lett.*,
20 35, L08806, <https://doi.org/10.1029/2007GL032887>, 2008.
- 21 Gregor, L. and Gruber, N.: OceanSODA-ETHZ: a global gridded data set of the surface ocean
22 carbonate system for seasonal to decadal studies of ocean acidification, 13, 777–808,
23 <https://doi.org/10.5194/essd-13-777-2021>, 2021.
- 24 Gregor, L., Lebehot, A. D., Kok, S., and Scheel Monteiro, P. M.: A comparative assessment of
25 the uncertainties of global surface ocean CO₂ estimates using a machine-learning ensemble
26 (CSIR-ML6 version 2019a) – have we hit the wall?, 12, 5113–5136,
27 <https://doi.org/10.5194/gmd-12-5113-2019>, 2019.
- 28 Gruber, N., Gloor, M., Mikaloff Fletcher, S. E., Doney, S. C., Dutkiewicz, S., Follows, M. J.,



- 1 Gerber, M., Jacobson, A. R., Joos, F., Lindsay, K., Menemenlis, D., Mouchet, A., Müller, S. A.,
- 2 Sarmiento, J. L., and Takahashi, T.: Oceanic sources, sinks, and transport of atmospheric
- 3 CO₂, 23, <https://doi.org/10.1029/2008GB003349>, 2009.

- 4 Gruber, N., Clement, D., Carter, B. R., Feely, R. A., van Heuven, S., Hoppema, M., Ishii, M.,
- 5 Key, R. M., Kozyr, A., Lauvset, S. K., Lo Monaco, C., Mathis, J. T., Murata, A., Olsen, A., Perez,
- 6 F. F., Sabine, C. L., Tanhua, T., and Wanninkhof, R.: The oceanic sink for anthropogenic CO₂
- 7 from 1994 to 2007, 363, 1193–1199, <https://doi.org/10.1126/science.aau5153>, 2019.

- 8 Gruère, G. and Brooks, J.: Viewpoint: Characterising early agricultural and food policy
- 9 responses to the outbreak of COVID-19, *Food Policy*, 100, 102017,
- 10 <https://doi.org/10.1016/j.foodpol.2020.102017>, 2021.

- 11 Guan, D., Liu, Z., Geng, Y., Lindner, S., and Hubacek, K.: The gigatonne gap in China's carbon
- 12 dioxide inventories, *Nature Clim Change*, 2, 672–675,
- 13 <https://doi.org/10.1038/nclimate1560>, 2012.

- 14 Guo, R., Wang, J., Bing, L., Tong, D., Ciais, P., Davis, S. J., Andrew, R. M., Xi, F., and Liu, Z.:
15 Global CO₂ uptake by cement from 1930 to 2019, 13, 1791–1805,
16 <https://doi.org/10.5194/essd-13-1791-2021>, 2021.

- 17 Gütschow, J., Jeffery, M. L., Gieseke, R., Gebel, R., Stevens, D., Krapp, M., and Rocha, M.:
18 The PRIMAP-hist national historical emissions time series, 8, 571–603,
19 <https://doi.org/10.5194/essd-8-571-2016>, 2016.

- 20 Gütschow, J., Günther, A., and Pflüger, M.: The PRIMAP-hist national historical emissions
21 time series (1750-2019) v2.3.1, <https://doi.org/10.5281/zenodo.5494497>, 2021.

- 22 Hall, B. D., Crotwell, A. M., Kitzis, D. R., Mefford, T., Miller, B. R., Schibig, M. F., and Tans, P.
23 P.: Revision of the World Meteorological Organization Global Atmosphere Watch
24 (WMO/GAW) CO₂ calibration scale, 14, 3015–3032, [https://doi.org/10.5194/amt-14-3015-](https://doi.org/10.5194/amt-14-3015-2021)
25 2021, 2021.

- 26 Hansen, M. C., Potapov, P. V., Moore, R., Hancher, M., Turubanova, S. A., Tyukavina, A.,
27 Thau, D., Stehman, S. V., Goetz, S. J., Loveland, T. R., Kommareddy, A., Egorov, A., Chini, L.,
28 Justice, C. O., and Townshend, J. R. G.: High-Resolution Global Maps of 21st-Century Forest



- 1 Cover Change, *Science*, 342, 850–853, <https://doi.org/10.1126/science.1244693>, 2013.
- 2 Hansis, E., Davis, S. J., and Pongratz, J.: Relevance of methodological choices for accounting
3 of land use change carbon fluxes, *Global Biogeochem. Cycles*, 29, 1230–1246,
4 <https://doi.org/10.1002/2014GB004997>, 2015.
- 5 Harris, I., Jones, P. D., Osborn, T. J., and Lister, D. H.: Updated high-resolution grids of
6 monthly climatic observations - the CRU TS3.10 Dataset: UPDATED HIGH-RESOLUTION
7 GRIDS OF MONTHLY CLIMATIC OBSERVATIONS, *Int. J. Climatol.*, 34, 623–642,
8 <https://doi.org/10.1002/joc.3711>, 2014.
- 9 Harris, I., Osborn, T. J., Jones, P., and Lister, D.: Version 4 of the CRU TS monthly high-
10 resolution gridded multivariate climate dataset, *Sci Data*, 7, 109,
11 <https://doi.org/10.1038/s41597-020-0453-3>, 2020.
- 12 Hauck, J., Zeising, M., Le Quéré, C., Gruber, N., Bakker, D. C. E., Bopp, L., Chau, T. T. T.,
13 Gürses, Ö., Ilyina, T., Landschützer, P., Lenton, A., Resplandy, L., Rödenbeck, C., Schwinger,
14 J., and Séférian, R.: Consistency and Challenges in the Ocean Carbon Sink Estimate for the
15 Global Carbon Budget, *Front. Mar. Sci.*, 7, 571720,
16 <https://doi.org/10.3389/fmars.2020.571720>, 2020.
- 17 Haverd, V., Smith, B., Nieradzik, L., Briggs, P. R., Woodgate, W., Trudinger, C. M., Canadell, J.
18 G., and Cuntz, M.: A new version of the CABLE land surface model (Subversion revision
19 r4601) incorporating land use and land cover change, woody vegetation demography, and a
20 novel optimisation-based approach to plant coordination of photosynthesis, *Geosci. Model
21 Dev.*, 11, 2995–3026, <https://doi.org/10.5194/gmd-11-2995-2018>, 2018.
- 22 Heinimann, A., Mertz, O., Froking, S., Christensen, A. E., Hurni, K., Sedano, F., Chini, L. P.,
23 Sahajpal, R., Hansen, M., and Hurtt, G.: A global view of shifting cultivation: Recent, current,
24 and future extent, *PLOS ONE*, 12, e0184479, <https://doi.org/10.1371/journal.pone.0184479>,
25 2017.
- 26 Hertwich, E. G. and Peters, G. P.: Carbon Footprint of Nations: A Global, Trade-Linked
27 Analysis, *Environ. Sci. Technol.*, 43, 6414–6420, <https://doi.org/10.1021/es803496a>, 2009.
- 28 Hickler, T., Smith, B., Prentice, I. C., Mjöfors, K., Miller, P., Arneth, A., and Sykes, M. T.: CO2



- 1 fertilization in temperate FACE experiments not representative of boreal and tropical
- 2 forests, 14, 1531–1542, <https://doi.org/10.1111/j.1365-2486.2008.01598.x>, 2008.
- 3 Ho, D. T., Wanninkhof, R., Schlosser, P., Ullman, D. S., Hebert, D., and Sullivan, K. F.: Toward
- 4 a universal relationship between wind speed and gas exchange: Gas transfer velocities
- 5 measured with $^3\text{He}/\text{SF}_6$ during the Southern Ocean Gas Exchange Experiment, 116,
- 6 <https://doi.org/10.1029/2010JC006854>, 2011.
- 7 Hoesly, R. M., Smith, S. J., Feng, L., Klimont, Z., Janssens-Maenhout, G., Pitkanen, T., Seibert,
- 8 J. J., Vu, L., Andres, R. J., Bolt, R. M., Bond, T. C., Dawidowski, L., Kholod, N., Kurokawa, J., Li,
- 9 M., Liu, L., Lu, Z., Moura, M. C. P., O'Rourke, P. R., and Zhang, Q.: Historical (1750–2014)
- 10 anthropogenic emissions of reactive gases and aerosols from the Community Emissions Data
- 11 System (CEDS), *Geosci. Model Dev.*, 11, 369–408, [https://doi.org/10.5194/gmd-11-369-](https://doi.org/10.5194/gmd-11-369-2018)
- 12 2018, 2018.
- 13 Hong, C., Burney, J. A., Pongratz, J., Nabel, J. E. M. S., Mueller, N. D., Jackson, R. B., and
- 14 Davis, S. J.: Global and regional drivers of land-use emissions in 1961–2017, 589, 554–561,
- 15 <https://doi.org/10.1038/s41586-020-03138-y>, 2021.
- 16 Hooijer, A., Page, S., Canadell, J. G., Silvius, M., Kwadijk, J., Wösten, H., and Jauhiainen, J.:
- 17 Current and future CO₂ emissions from drained peatlands in Southeast Asia,
- 18 *Biogeosciences*, 7, 1505–1514, <https://doi.org/10.5194/bg-7-1505-2010>, 2010.
- 19 Houghton, R. A.: Why are estimates of the terrestrial carbon balance so different?, 9, 500–
- 20 509, <https://doi.org/10.1046/j.1365-2486.2003.00620.x>, 2003.
- 21 Houghton, R. A. and Nassikas, A. A.: Global and regional fluxes of carbon from land use and
- 22 land cover change 1850-2015: Carbon Emissions From Land Use, *Global Biogeochem. Cycles*,
- 23 31, 456–472, <https://doi.org/10.1002/2016GB005546>, 2017.
- 24 Houghton, R. A., House, J. I., Pongratz, J., van der Werf, G. R., DeFries, R. S., Hansen, M. C.,
- 25 Le Quéré, C., and Ramankutty, N.: Carbon emissions from land use and land-cover change,
- 26 *Biogeosciences*, 9, 5125–5142, <https://doi.org/10.5194/bg-9-5125-2012>, 2012.
- 27 Hubau, W., Lewis, S. L., Phillips, O. L., Affum-Baffoe, K., Beeckman, H., Cuní-Sánchez, A.,
- 28 Daniels, A. K., Ewango, C. E. N., Fauset, S., Mukinzi, J. M., Sheil, D., Sonké, B., Sullivan, M. J.



- 1 P., Sunderland, T. C. H., Taedoumg, H., Thomas, S. C., White, L. J. T., Abernethy, K. A., Adu-
2 Bredu, S., Amani, C. A., Baker, T. R., Banin, L. F., Baya, F., Begne, S. K., Bennett, A. C.,
3 Benedet, F., Bitariho, R., Bocko, Y. E., Boeckx, P., Boundja, P., Brienen, R. J. W., Brncic, T.,
4 Chezeaux, E., Chuyong, G. B., Clark, C. J., Collins, M., Comiskey, J. A., Coomes, D. A., Dargie,
5 G. C., de Haulleville, T., Kamdem, M. N. D., Doucet, J.-L., Esquivel-Muelbert, A., Feldpausch,
6 T. R., Fofanah, A., Foli, E. G., Gilpin, M., Gloor, E., Gonmadje, C., Gourlet-Fleury, S., Hall, J. S.,
7 Hamilton, A. C., Harris, D. J., Hart, T. B., Hockemba, M. B. N., Hladik, A., Ifo, S. A., Jeffery, K.
8 J., Jucker, T., Yakusu, E. K., Kearsley, E., Kenfack, D., Koch, A., Leal, M. E., Levesley, A.,
9 Lindsell, J. A., Lisingo, J., Lopez-Gonzalez, G., Lovett, J. C., Makana, J.-R., Malhi, Y., Marshall,
10 A. R., Martin, J., Martin, E. H., Mbayu, F. M., Medjibe, V. P., Mihindou, V., Mitchard, E. T. A.,
11 Moore, S., Munishi, P. K. T., Bengone, N. N., Ojo, L., Ondo, F. E., Peh, K. S.-H., Pickavance, G.
12 C., Poulsen, A. D., Poulsen, J. R., Qie, L., Reitsma, J., Rovero, F., Swaine, M. D., Talbot, J.,
13 Taplin, J., Taylor, D. M., Thomas, D. W., Toirambe, B., Mukendi, J. T., Tuagben, D., Umunay,
14 P. M., et al.: Asynchronous carbon sink saturation in African and Amazonian tropical forests,
15 579, 80–87, <https://doi.org/10.1038/s41586-020-2035-0>, 2020.
- 16 Hugelius, G., Bockheim, J. G., Camill, P., Elberling, B., Grosse, G., Harden, J. W., Johnson, K.,
17 Jorgenson, T., Koven, C. D., Kuhry, P., Michaelson, G., Mishra, U., Palmtag, J., Ping, C.-L.,
18 O'Donnell, J., Schirmer, L., Schuur, E. A. G., Sheng, Y., Smith, L. C., Strauss, J., and Yu, Z.:
19 A new data set for estimating organic carbon storage to 3 m depth in soils of the northern
20 circumpolar permafrost region, *Earth Syst. Sci. Data*, 5, 393–402,
21 <https://doi.org/10.5194/essd-5-393-2013>, 2013.
- 22 Humphrey, V., Zscheischler, J., Ciais, P., Gudmundsson, L., Sitch, S., and Seneviratne, S. I.:
23 Sensitivity of atmospheric CO₂ growth rate to observed changes in terrestrial water storage,
24 560, 628–631, <https://doi.org/10.1038/s41586-018-0424-4>, 2018.
- 25 Humphrey, V., Berg, A., Ciais, P., Gentine, P., Jung, M., Reichstein, M., Seneviratne, S. I., and
26 Frankenberg, C.: Soil moisture–atmosphere feedback dominates land carbon uptake
27 variability, 592, 65–69, <https://doi.org/10.1038/s41586-021-03325-5>, 2021.
- 28 Huntzinger, D. N., Michalak, A. M., Schwalm, C., Ciais, P., King, A. W., Fang, Y., Schaefer, K.,
29 Wei, Y., Cook, R. B., Fisher, J. B., Hayes, D., Huang, M., Ito, A., Jain, A. K., Lei, H., Lu, C.,
30 Maignan, F., Mao, J., Parazoo, N., Peng, S., Poulter, B., Ricciuto, D., Shi, X., Tian, H., Wang,



- 1 W., Zeng, N., and Zhao, F.: Uncertainty in the response of terrestrial carbon sink to
2 environmental drivers undermines carbon-climate feedback predictions, *Sci Rep*, 7, 4765,
3 <https://doi.org/10.1038/s41598-017-03818-2>, 2017.
- 4 Hurtt, G., Chini, L., Sahajpal, R., Frohling, S., Bodirsky, B. L., Calvin, K., Doelman, J., Fisk, J.,
5 Fujimori, S., Goldewijk, K. K., Hasegawa, T., Havlik, P., Heinemann, A., Humpeöder, F.,
6 Jungclaus, J., Kaplan, J., Krisztin, T., Lawrence, D., Lawrence, P., Mertz, O., Pongratz, J., Popp,
7 A., Riahi, K., Shevliakova, E., Stehfest, E., Thornton, P., van Vuuren, D., and Zhang, X.:
8 input4MIPs.CMIP6.CMIP.UofMD.UofMD-landState-2-1-h,
9 <https://doi.org/10.22033/ESGF/input4MIPs.1127>, 2017.
- 10 Hurtt, G. C., Chini, L. P., Frohling, S., Betts, R. A., Feddema, J., Fischer, G., Fisk, J. P., Hibbard,
11 K., Houghton, R. A., Janetos, A., Jones, C. D., Kindermann, G., Kinoshita, T., Klein Goldewijk,
12 K., Riahi, K., Shevliakova, E., Smith, S., Stehfest, E., Thomson, A., Thornton, P., van Vuuren, D.
13 P., and Wang, Y. P.: Harmonization of land-use scenarios for the period 1500–2100: 600
14 years of global gridded annual land-use transitions, wood harvest, and resulting secondary
15 lands, *Climatic Change*, 109, 117–161, <https://doi.org/10.1007/s10584-011-0153-2>, 2011.
- 16 Hurtt, G. C., Chini, L., Sahajpal, R., Frohling, S., Bodirsky, B. L., Calvin, K., Doelman, J. C., Fisk,
17 J., Fujimori, S., Klein Goldewijk, K., Hasegawa, T., Havlik, P., Heinemann, A., Humpeöder, F.,
18 Jungclaus, J., Kaplan, J. O., Kennedy, J., Krisztin, T., Lawrence, D., Lawrence, P., Ma, L., Mertz,
19 O., Pongratz, J., Popp, A., Poulter, B., Riahi, K., Shevliakova, E., Stehfest, E., Thornton, P.,
20 Tubiello, F. N., van Vuuren, D. P., and Zhang, X.: Harmonization of global land use change
21 and management for the period 850–2100 (LUH2) for CMIP6, *Geosci. Model Dev.*, 13, 5425–
22 5464, <https://doi.org/10.5194/gmd-13-5425-2020>, 2020.
- 23 IEA: International Energy Agency: Global Energy Review, available at:
24 <https://www.iea.org/reports/global-energy-review-2021>, last access: 25 October 2021.,
25 2021a.
- 26 IEA: International Energy Agency: World Energy Outlook, available at:
27 <https://www.iea.org/reports/world-energy-outlook-2021>, last access: 25 October 2021.,
28 2021b.
- 29 IEA/OECD: International Energy Agency/Organisation for Economic Cooperation and



- 1 Development: CO2 emissions from fuel combustion, available at:
- 2 <https://webstore.iea.org/co2-emissions-from-fuel-combustion-2019-highlights>, last access:
- 3 25 October 2021, 2019.

- 4 Iida, Y., Kojima, A., Takatani, Y., Nakano, T., Sugimoto, H., Midorikawa, T., and Ishii, M.:
5 Trends in pCO₂ and sea–air CO₂ flux over the global open oceans for the last two decades, *J*
6 *Oceanogr*, 71, 637–661, <https://doi.org/10.1007/s10872-015-0306-4>, 2015.

- 7 Iida, Y., Takatani, Y., Kojima, A., and Ishii, M.: Global trends of ocean CO₂ sink and ocean
8 acidification: an observation-based reconstruction of surface ocean inorganic carbon
9 variables, *J Oceanogr*, 77, 323–358, <https://doi.org/10.1007/s10872-020-00571-5>, 2021.

- 10 Ilyina, T., Six, K. D., Segschneider, J., Maier-Reimer, E., Li, H., and Núñez-Riboni, I.: Global
11 ocean biogeochemistry model HAMOCC: Model architecture and performance as
12 component of the MPI-Earth system model in different CMIP5 experimental realizations:
13 The Model Hamocc within Mpi-Esm in Cmp5, *J. Adv. Model. Earth Syst.*, 5, 287–315,
14 <https://doi.org/10.1029/2012MS000178>, 2013.

- 15 IMF: International Monetary Fund: World Economic Outlook, available at:
16 <http://www.imf.org>, last access: 25 October 2021., 2021.

- 17 Inness, A., Ades, M., Agustí-Panareda, A., Barré, J., Benedictow, A., Blechschmidt, A.-M.,
18 Dominguez, J. J., Engelen, R., Eskes, H., Flemming, J., Huijnen, V., Jones, L., Kipling, Z.,
19 Massart, S., Parrington, M., Peuch, V.-H., Razinger, M., Remy, S., Schulz, M., and Suttie, M.:
20 The CAMS reanalysis of atmospheric composition, 19, 3515–3556,
21 <https://doi.org/10.5194/acp-19-3515-2019>, 2019.

- 22 IPCC: Summary for Policymakers. In: *Climate Change 2021: The Physical Science Basis*.
23 Contribution of Working Group I to the Sixth Assessment Report of the Intergovernmental
24 Panel on Climate Change [Masson-Delmotte, V., P. Zhai, A. Pirani, S.L. Connors, C. Péan, S.
25 Berger, N. Caud, Y. Chen, L. Goldfarb, M.I. Gomis, M. Huang, K. Leitzell, E. Lonnoy, J.B.R.
26 Matthews, T.K. Maycock, T. Waterfield, O. Yelekçi, R. Yu, and B. Zhou (eds.)]. Cambridge
27 University Press. In Press., 2021.

- 28 Ito, A. and Inatomi, M.: Use of a process-based model for assessing the methane budgets of



- 1 global terrestrial ecosystems and evaluation of uncertainty, 9, 759–773,
- 2 <https://doi.org/10.5194/bg-9-759-2012>, 2012.
- 3 Jackson, R. B., Canadell, J. G., Le Quéré, C., Andrew, R. M., Korsbakken, J. I., Peters, G. P.,
- 4 and Nakicenovic, N.: Reaching peak emissions, *Nature Clim Change*, 6, 7–10,
- 5 <https://doi.org/10.1038/nclimate2892>, 2016.
- 6 Jackson, R. B., Le Quéré, C., Andrew, R. M., Canadell, J. G., Korsbakken, J. I., Liu, Z., Peters, G.
- 7 P., and Zheng, B.: Global energy growth is outpacing decarbonization, *Environ. Res. Lett.*, 13,
- 8 120401, <https://doi.org/10.1088/1748-9326/aaf303>, 2018.
- 9 Jackson, R. B., Friedlingstein, P., Andrew, R. M., Canadell, J. G., Le Quéré, C., and Peters, G.
- 10 P.: Persistent fossil fuel growth threatens the Paris Agreement and planetary health,
- 11 *Environ. Res. Lett.*, 14, 121001, <https://doi.org/10.1088/1748-9326/ab57b3>, 2019.
- 12 Jacobson, A. R., Mikaloff Fletcher, S. E., Gruber, N., Sarmiento, J. L., and Gloor, M.: A joint
- 13 atmosphere-ocean inversion for surface fluxes of carbon dioxide: 1. Methods and global-
- 14 scale fluxes: JOINT INVERSION-METHODS AND GLOBAL FLUXES, *Global Biogeochem. Cycles*,
- 15 21, <https://doi.org/10.1029/2005GB002556>, 2007.
- 16 Jain, A. K., Meiyappan, P., Song, Y., and House, J. I.: CO₂ emissions from land-use change
- 17 affected more by nitrogen cycle, than by the choice of land-cover data, 19, 2893–2906,
- 18 <https://doi.org/10.1111/gcb.12207>, 2013.
- 19 Janssens-Maenhout, G., Crippa, M., Guizzardi, D., Muntean, M., Schaaf, E., Dentener, F.,
- 20 Bergamaschi, P., Pagliari, V., Olivier, J. G. J., Peters, J. A. H. W., van Aardenne, J. A., Monni,
- 21 S., Doering, U., Petrescu, A. M. R., Solazzo, E., and Oreggioni, G. D.: EDGAR v4.3.2 Global
- 22 Atlas of the three major greenhouse gas emissions for the period 1970–2012, *Earth Syst. Sci.*
- 23 *Data*, 11, 959–1002, <https://doi.org/10.5194/essd-11-959-2019>, 2019.
- 24 JODI: Joint Organisations Data Initiative, available at: <https://www.jodidata.org>, last access:
- 25 25 October 2021, 2021.
- 26 Jones, M. W., Andrew, R. M., Peters, G. P., Janssens-Maenhout, G., De-Gol, A. J., Ciais, P.,
- 27 Patra, P. K., Chevallier, F., and Le Quéré, C.: Gridded fossil CO₂ emissions and related O₂
- 28 combustion consistent with national inventories 1959–2018, *Sci Data*, 8, 2,



- 1 <https://doi.org/10.1038/s41597-020-00779-6>, 2021a.
- 2 Jones, M. W., Andrew, R. M., Peters, G. P., Janssens-Maenhout, G., De-Gol, A. J., Dou, X., Liu,
3 Z., Ciais, P., Patra, P. K., Chevallier, F., and Le Quéré, C.: Gridded fossil CO₂ emissions and
4 related O₂ combustion consistent with national inventories 1959-2020,
5 <https://doi.org/10.5281/zenodo.5565199>, 2021b.
- 6 Joos, F. and Spahni, R.: Rates of change in natural and anthropogenic radiative forcing over
7 the past 20,000 years, *Proceedings of the National Academy of Sciences*, 105, 1425–1430,
8 <https://doi.org/10.1073/pnas.0707386105>, 2008.
- 9 Jung, M., Reichstein, M., Ciais, P., Seneviratne, S. I., Sheffield, J., Goulden, M. L., Bonan, G.,
10 Cescatti, A., Chen, J., de Jeu, R., Dolman, A. J., Eugster, W., Gerten, D., Gianelle, D., Gobron,
11 N., Heinke, J., Kimball, J., Law, B. E., Montagnani, L., Mu, Q., Mueller, B., Oleson, K., Papale,
12 D., Richardson, A. D., Rouspard, O., Running, S., Tomelleri, E., Viovy, N., Weber, U., Williams,
13 C., Wood, E., Zaehle, S., and Zhang, K.: Recent decline in the global land evapotranspiration
14 trend due to limited moisture supply, *Nature*, 467, 951–954,
15 <https://doi.org/10.1038/nature09396>, 2010.
- 16 Jung, M., Reichstein, M., Schwalm, C. R., Huntingford, C., Sitch, S., Ahlström, A., Arneth, A.,
17 Camps-Valls, G., Ciais, P., Friedlingstein, P., Gans, F., Ichii, K., Jain, A. K., Kato, E., Papale, D.,
18 Poulter, B., Raduly, B., Rödenbeck, C., Tramontana, G., Viovy, N., Wang, Y.-P., Weber, U.,
19 Zaehle, S., and Zeng, N.: Compensatory water effects link yearly global land CO₂ sink
20 changes to temperature, *Nature*, 541, 516–520, <https://doi.org/10.1038/nature20780>,
21 2017.
- 22 Kalnay, E., Kanamitsu, M., Kistler, R., Collins, W., Deaven, D., Gandin, L., Iredell, M., Saha, S.,
23 White, G., Woollen, J., Zhu, Y., Chelliah, M., Ebisuzaki, W., Higgins, W., Janowiak, J., Mo, K.
24 C., Ropelewski, C., Wang, J., Leetmaa, A., Reynolds, R., Jenne, R., and Joseph, D.: The
25 NCEP/NCAR 40-Year Reanalysis Project, 77, 437–472, [https://doi.org/10.1175/1520-0477\(1996\)077<0437:TNYRP>2.0.CO;2](https://doi.org/10.1175/1520-0477(1996)077<0437:TNYRP>2.0.CO;2), 1996.
- 27 Kato, E., Kinoshita, T., Ito, A., Kawamiya, M., and Yamagata, Y.: Evaluation of spatially
28 explicit emission scenario of land-use change and biomass burning using a process-based
29 biogeochemical model, 8, 104–122, <https://doi.org/10.1080/1747423X.2011.628705>, 2013.



- 1 Keeling, C. D., Bacastow, R. B., Bainbridge, A. E., Ekdahl, C. A., Guenther, P. R., Waterman, L.
- 2 S., and Chin, J. F. S.: Atmospheric carbon dioxide variations at Mauna Loa Observatory,
- 3 Hawaii, 28, 538–551, <https://doi.org/10.1111/j.2153-3490.1976.tb00701.x>, 1976.
- 4 Keeling, R. F. and Manning, A. C.: 5.15 - Studies of Recent Changes in Atmospheric O₂
- 5 Content, in: *Treatise on Geochemistry (Second Edition)*, edited by: Holland, H. D. and
- 6 Turekian, K. K., Elsevier, Oxford, 385–404, [https://doi.org/10.1016/B978-0-08-095975-](https://doi.org/10.1016/B978-0-08-095975-7.00420-4)
- 7 [7.00420-4](https://doi.org/10.1016/B978-0-08-095975-7.00420-4), 2014.
- 8 Keppler, L. and Landschützer, P.: Regional Wind Variability Modulates the Southern Ocean
- 9 Carbon Sink, *Sci Rep*, 9, 7384, <https://doi.org/10.1038/s41598-019-43826-y>, 2019.
- 10 Khatiwala, S., Primeau, F., and Hall, T.: Reconstruction of the history of anthropogenic CO₂
- 11 concentrations in the ocean, *Nature*, 462, 346–349, <https://doi.org/10.1038/nature08526>,
- 12 2009.
- 13 Khatiwala, S., Tanhua, T., Mikaloff Fletcher, S., Gerber, M., Doney, S. C., Graven, H. D.,
- 14 Gruber, N., McKinley, G. A., Murata, A., Ríos, A. F., and Sabine, C. L.: Global ocean storage of
- 15 anthropogenic carbon, *Biogeosciences*, 10, 2169–2191, [https://doi.org/10.5194/bg-10-](https://doi.org/10.5194/bg-10-2169-2013)
- 16 [2169-2013](https://doi.org/10.5194/bg-10-2169-2013), 2013.
- 17 Klein Goldewijk, K., Beusen, A., Doelman, J., and Stehfest, E.: Anthropogenic land use
- 18 estimates for the Holocene – HYDE 3.2, *Earth Syst. Sci. Data*, 9, 927–953,
- 19 <https://doi.org/10.5194/essd-9-927-2017>, 2017a.
- 20 Klein Goldewijk, K., Dekker, S. C., and van Zanden, J. L.: Per-capita estimations of long-term
- 21 historical land use and the consequences for global change research, *Journal of Land Use*
- 22 *Science*, 1747423X.2017.1354938, <https://doi.org/10.1080/1747423X.2017.1354938>,
- 23 2017b.
- 24 Kobayashi, S., Ota, Y., Harada, Y., Ebata, A., Moriya, M., Onoda, H., Onogi, K., Kamahori, H.,
- 25 Kobayashi, C., Endo, H., Miyaoka, K., and Takahashi, K.: The JRA-55 Reanalysis: General
- 26 Specifications and Basic Characteristics, *Journal of the Meteorological Society of Japan*, 93,
- 27 5–48, <https://doi.org/10.2151/jmsj.2015-001>, 2015.
- 28 Korsbakken, J. I., Peters, G. P., and Andrew, R. M.: Uncertainties around reductions in



- 1 China's coal use and CO₂ emissions, *Nature Clim Change*, 6, 687–690,
- 2 <https://doi.org/10.1038/nclimate2963>, 2016.
- 3 Krinner, G., Viovy, N., de Noblet-Ducoudré, N., Ogée, J., Polcher, J., Friedlingstein, P., Ciais,
- 4 P., Sitch, S., and Prentice, I. C.: A dynamic global vegetation model for studies of the coupled
- 5 atmosphere-biosphere system: DVGM FOR COUPLED CLIMATE STUDIES, *Global*
- 6 *Biogeochem. Cycles*, 19, <https://doi.org/10.1029/2003GB002199>, 2005.
- 7 Lacroix, F., Ilyina, T., and Hartmann, J.: Oceanic CO₂ outgassing and biological production
- 8 hotspots induced by pre-industrial river loads of nutrients and carbon in a global modeling
- 9 approach, *Biogeosciences*, 17, 55–88, <https://doi.org/10.5194/bg-17-55-2020>, 2020.
- 10 Lacroix, F., Ilyina, T., Mathis, M., Laruelle, G. G., and Regnier, P.: Historical increases in land-
- 11 derived nutrient inputs may alleviate effects of a changing physical climate on the oceanic
- 12 carbon cycle, *Glob Change Biol*, 27, 5491–5513, <https://doi.org/10.1111/gcb.15822>, 2021.
- 13 Landschützer, P., Gruber, N., Bakker, D. C. E., Schuster, U., Nakaoka, S., Payne, M. R., Sasse,
- 14 T. P., and Zeng, J.: A neural network-based estimate of the seasonal to inter-annual
- 15 variability of the Atlantic Ocean carbon sink, *Biogeosciences*, 10, 7793–7815,
- 16 <https://doi.org/10.5194/bg-10-7793-2013>, 2013.
- 17 Landschützer, P., Gruber, N., Bakker, D. C. E., and Schuster, U.: Recent variability of the
- 18 global ocean carbon sink, *Global Biogeochem. Cycles*, 28, 927–949,
- 19 <https://doi.org/10.1002/2014GB004853>, 2014.
- 20 Landschützer, P., Gruber, N., Haumann, F. A., Rödenbeck, C., Bakker, D. C. E., van Heuven, S.,
- 21 Hoppema, M., Metzl, N., Sweeney, C., Takahashi, T., Tilbrook, B., and Wanninkhof, R.: The
- 22 reinvigoration of the Southern Ocean carbon sink, *Science*, 349, 1221–1224,
- 23 <https://doi.org/10.1126/science.aab2620>, 2015.
- 24 Landschützer, P., Gruber, N., and Bakker, D. C. E.: Decadal variations and trends of the global
- 25 ocean carbon sink: DECADEAL AIR-SEA CO₂ FLUX VARIABILITY, *Global Biogeochem. Cycles*,
- 26 30, 1396–1417, <https://doi.org/10.1002/2015GB005359>, 2016.
- 27 Landschützer, P., Laruelle, G. G., Roobaert, A., and Regnier, P.: A uniform pCO₂ climatology
- 28 combining open and coastal oceans, 12, 2537–2553, <https://doi.org/10.5194/essd-12-2537->



- 1 2020, 2020.
- 2 Lang, F., Ackermann, L., Huang, Y., Truong, S. C. H., Siems, S. T., and Manton, M. J.: A
3 climatology of open and closed mesoscale cellular convection over the Southern Ocean
4 derived from Himawari-8 observations, 1–27, <https://doi.org/10.5194/acp-2021-681>, 2021.
- 5 Lasslop, G., Reichstein, M., Papale, D., Richardson, A. D., Arneeth, A., Barr, A., Stoy, P., and
6 Wohlfahrt, G.: Separation of net ecosystem exchange into assimilation and respiration using
7 a light response curve approach: critical issues and global evaluation: Separation of NEE into
8 GPP and RECO, 16, 187–208, <https://doi.org/10.1111/j.1365-2486.2009.02041.x>, 2010.
- 9 Lawrence, D. M., Fisher, R. A., Koven, C. D., Oleson, K. W., Swenson, S. C., Bonan, G., Collier,
10 N., Ghimire, B., van Kampenhout, L., Kennedy, D., Kluzek, E., Lawrence, P. J., Li, F., Li, H.,
11 Lombardozzi, D., Riley, W. J., Sacks, W. J., Shi, M., Vertenstein, M., Wieder, W. R., Xu, C., Ali,
12 A. A., Badger, A. M., Bisht, G., van den Broeke, M., Brunke, M. A., Burns, S. P., Buzan, J.,
13 Clark, M., Craig, A., Dahlin, K., Drewniak, B., Fisher, J. B., Flanner, M., Fox, A. M., Gentine, P.,
14 Hoffman, F., Keppel-Aleks, G., Knox, R., Kumar, S., Lenaerts, J., Leung, L. R., Lipscomb, W. H.,
15 Lu, Y., Pandey, A., Pelletier, J. D., Perket, J., Randerson, J. T., Ricciuto, D. M., Sanderson, B.
16 M., Slater, A., Subin, Z. M., Tang, J., Thomas, R. Q., Val Martin, M., and Zeng, X.: The
17 Community Land Model Version 5: Description of New Features, Benchmarking, and Impact
18 of Forcing Uncertainty, 11, 4245–4287, <https://doi.org/10.1029/2018MS001583>, 2019.
- 19 Le Quéré, C., Rödenbeck, C., Buitenhuis, E. T., Conway, T. J., Langenfelds, R., Gomez, A.,
20 Labuschagne, C., Ramonet, M., Nakazawa, T., Metzl, N., Gillett, N., and Heimann, M.:
21 Saturation of the Southern Ocean CO₂ Sink Due to Recent Climate Change, 316, 1735–1738,
22 <https://doi.org/10.1126/science.1136188>, 2007.
- 23 Le Quéré, C., Raupach, M. R., Canadell, J. G., Marland, G., Bopp, L., Ciais, P., Conway, T. J.,
24 Doney, S. C., Feely, R. A., Foster, P., Friedlingstein, P., Gurney, K., Houghton, R. A., House, J.
25 I., Huntingford, C., Levy, P. E., Lomas, M. R., Majkut, J., Metzl, N., Ometto, J. P., Peters, G. P.,
26 Prentice, I. C., Randerson, J. T., Running, S. W., Sarmiento, J. L., Schuster, U., Sitch, S.,
27 Takahashi, T., Viovy, N., van der Werf, G. R., and Woodward, F. I.: Trends in the sources and
28 sinks of carbon dioxide, *Nature Geosci*, 2, 831–836, <https://doi.org/10.1038/ngeo689>, 2009.
- 29 Le Quéré, C., Andres, R. J., Boden, T., Conway, T., Houghton, R. A., House, J. I., Marland, G.,



- 1 Peters, G. P., van der Werf, G. R., Ahlström, A., Andrew, R. M., Bopp, L., Canadell, J. G., Ciais,
- 2 P., Doney, S. C., Enright, C., Friedlingstein, P., Huntingford, C., Jain, A. K., Jourdain, C., Kato,
- 3 E., Keeling, R. F., Klein Goldewijk, K., Levis, S., Levy, P., Lomas, M., Poulter, B., Raupach, M.
- 4 R., Schwinger, J., Sitch, S., Stocker, B. D., Viovy, N., Zaehle, S., and Zeng, N.: The global
- 5 carbon budget 1959–2011, *Earth Syst. Sci. Data*, 5, 165–185, [https://doi.org/10.5194/essd-](https://doi.org/10.5194/essd-5-165-2013)
- 6 5-165-2013, 2013.

- 7 Le Quéré, C., Peters, G. P., Andres, R. J., Andrew, R. M., Boden, T. A., Ciais, P., Friedlingstein,
- 8 P., Houghton, R. A., Marland, G., Moriarty, R., Sitch, S., Tans, P., Arneeth, A., Arvanitis, A.,
- 9 Bakker, D. C. E., Bopp, L., Canadell, J. G., Chini, L. P., Doney, S. C., Harper, A., Harris, I.,
- 10 House, J. I., Jain, A. K., Jones, S. D., Kato, E., Keeling, R. F., Klein Goldewijk, K., Körtzinger, A.,
- 11 Koven, C., Lefèvre, N., Maignan, F., Omar, A., Ono, T., Park, G.-H., Pfeil, B., Poulter, B.,
- 12 Raupach, M. R., Regnier, P., Rödenbeck, C., Saito, S., Schwinger, J., Segschneider, J., Stocker,
- 13 B. D., Takahashi, T., Tilbrook, B., van Heuven, S., Viovy, N., Wanninkhof, R., Wiltshire, A., and
- 14 Zaehle, S.: Global carbon budget 2013, *Earth Syst. Sci. Data*, 6, 235–263,
- 15 <https://doi.org/10.5194/essd-6-235-2014>, 2014.

- 16 Le Quéré, C., Moriarty, R., Andrew, R. M., Peters, G. P., Ciais, P., Friedlingstein, P., Jones, S.
- 17 D., Sitch, S., Tans, P., Arneeth, A., Boden, T. A., Bopp, L., Bozec, Y., Canadell, J. G., Chini, L. P.,
- 18 Chevallier, F., Cosca, C. E., Harris, I., Hoppema, M., Houghton, R. A., House, J. I., Jain, A. K.,
- 19 Johannessen, T., Kato, E., Keeling, R. F., Kitidis, V., Klein Goldewijk, K., Koven, C., Landa, C. S.,
- 20 Landschützer, P., Lenton, A., Lima, I. D., Marland, G., Mathis, J. T., Metzl, N., Nojiri, Y., Olsen,
- 21 A., Ono, T., Peng, S., Peters, W., Pfeil, B., Poulter, B., Raupach, M. R., Regnier, P., Rödenbeck,
- 22 C., Saito, S., Salisbury, J. E., Schuster, U., Schwinger, J., Séférian, R., Segschneider, J.,
- 23 Steinhoff, T., Stocker, B. D., Sutton, A. J., Takahashi, T., Tilbrook, B., van der Werf, G. R.,
- 24 Viovy, N., Wang, Y.-P., Wanninkhof, R., Wiltshire, A., and Zeng, N.: Global carbon budget
- 25 2014, *Earth Syst. Sci. Data*, 7, 47–85, <https://doi.org/10.5194/essd-7-47-2015>, 2015a.

- 26 Le Quéré, C., Moriarty, R., Andrew, R. M., Canadell, J. G., Sitch, S., Korsbakken, J. I.,
- 27 Friedlingstein, P., Peters, G. P., Andres, R. J., Boden, T. A., Houghton, R. A., House, J. I.,
- 28 Keeling, R. F., Tans, P., Arneeth, A., Bakker, D. C. E., Barbero, L., Bopp, L., Chang, J., Chevallier,
- 29 F., Chini, L. P., Ciais, P., Fader, M., Feely, R. A., Gkritzalis, T., Harris, I., Hauck, J., Ilyina, T.,
- 30 Jain, A. K., Kato, E., Kitidis, V., Klein Goldewijk, K., Koven, C., Landschützer, P., Lauvset, S. K.,



- 1 Lefèvre, N., Lenton, A., Lima, I. D., Metzl, N., Millero, F., Munro, D. R., Murata, A., Nabel, J. E.
- 2 M. S., Nakaoka, S., Nojiri, Y., O'Brien, K., Olsen, A., Ono, T., Pérez, F. F., Pfeil, B., Pierrot, D.,
- 3 Poulter, B., Rehder, G., Rödenbeck, C., Saito, S., Schuster, U., Schwinger, J., Séférian, R.,
- 4 Steinhoff, T., Stocker, B. D., Sutton, A. J., Takahashi, T., Tilbrook, B., van der Laan-Luijkx, I. T.,
- 5 van der Werf, G. R., van Heuven, S., Vandemark, D., Viovy, N., Wiltshire, A., Zaehle, S., and
- 6 Zeng, N.: Global Carbon Budget 2015, *Earth Syst. Sci. Data*, 7, 349–396,
- 7 <https://doi.org/10.5194/essd-7-349-2015>, 2015b.

- 8 Le Quéré, C., Andrew, R. M., Canadell, J. G., Sitch, S., Korsbakken, J. I., Peters, G. P.,
- 9 Manning, A. C., Boden, T. A., Tans, P. P., Houghton, R. A., Keeling, R. F., Alin, S., Andrews, O.
- 10 D., Anthoni, P., Barbero, L., Bopp, L., Chevallier, F., Chini, L. P., Ciais, P., Currie, K., Delire, C.,
- 11 Doney, S. C., Friedlingstein, P., Gkritzalis, T., Harris, I., Hauck, J., Haverd, V., Hoppema, M.,
- 12 Klein Goldewijk, K., Jain, A. K., Kato, E., Körtzinger, A., Landschützer, P., Lefèvre, N., Lenton,
- 13 A., Lienert, S., Lombardozi, D., Melton, J. R., Metzl, N., Millero, F., Monteiro, P. M. S.,
- 14 Munro, D. R., Nabel, J. E. M. S., Nakaoka, S., O'Brien, K., Olsen, A., Omar, A. M., Ono, T.,
- 15 Pierrot, D., Poulter, B., Rödenbeck, C., Salisbury, J., Schuster, U., Schwinger, J., Séférian, R.,
- 16 Skjelvan, I., Stocker, B. D., Sutton, A. J., Takahashi, T., Tian, H., Tilbrook, B., van der Laan-
- 17 Luijkx, I. T., van der Werf, G. R., Viovy, N., Walker, A. P., Wiltshire, A. J., and Zaehle, S.:
- 18 Global Carbon Budget 2016, *Earth Syst. Sci. Data*, 8, 605–649, [https://doi.org/10.5194/essd-](https://doi.org/10.5194/essd-8-605-2016)
- 19 [8-605-2016](https://doi.org/10.5194/essd-8-605-2016), 2016.

- 20 Le Quéré, C., Andrew, R. M., Friedlingstein, P., Sitch, S., Pongratz, J., Manning, A. C.,
- 21 Korsbakken, J. I., Peters, G. P., Canadell, J. G., Jackson, R. B., Boden, T. A., Tans, P. P.,
- 22 Andrews, O. D., Arora, V. K., Bakker, D. C. E., Barbero, L., Becker, M., Betts, R. A., Bopp, L.,
- 23 Chevallier, F., Chini, L. P., Ciais, P., Cosca, C. E., Cross, J., Currie, K., Gasser, T., Harris, I.,
- 24 Hauck, J., Haverd, V., Houghton, R. A., Hunt, C. W., Hurtt, G., Ilyina, T., Jain, A. K., Kato, E.,
- 25 Kautz, M., Keeling, R. F., Klein Goldewijk, K., Körtzinger, A., Landschützer, P., Lefèvre, N.,
- 26 Lenton, A., Lienert, S., Lima, I., Lombardozi, D., Metzl, N., Millero, F., Monteiro, P. M. S.,
- 27 Munro, D. R., Nabel, J. E. M. S., Nakaoka, S., Nojiri, Y., Padin, X. A., Pregon, A., Pfeil, B.,
- 28 Pierrot, D., Poulter, B., Rehder, G., Reimer, J., Rödenbeck, C., Schwinger, J., Séférian, R.,
- 29 Skjelvan, I., Stocker, B. D., Tian, H., Tilbrook, B., Tubiello, F. N., van der Laan-Luijkx, I. T., van
- 30 der Werf, G. R., van Heuven, S., Viovy, N., Vuichard, N., Walker, A. P., Watson, A. J.,
- 31 Wiltshire, A. J., Zaehle, S., and Zhu, D.: Global Carbon Budget 2017, *Earth Syst. Sci. Data*, 10,



- 1 405–448, <https://doi.org/10.5194/essd-10-405-2018>, 2018a.
- 2 Le Quéré, C., Andrew, R. M., Friedlingstein, P., Sitch, S., Hauck, J., Pongratz, J., Pickers, P. A.,
3 Korsbakken, J. I., Peters, G. P., Canadell, J. G., Arneeth, A., Arora, V. K., Barbero, L., Bastos, A.,
4 Bopp, L., Chevallier, F., Chini, L. P., Ciais, P., Doney, S. C., Gkritzalis, T., Goll, D. S., Harris, I.,
5 Haverd, V., Hoffman, F. M., Hoppema, M., Houghton, R. A., Hurtt, G., Ilyina, T., Jain, A. K.,
6 Johannessen, T., Jones, C. D., Kato, E., Keeling, R. F., Goldewijk, K. K., Landschützer, P.,
7 Lefèvre, N., Lienert, S., Liu, Z., Lombardozzi, D., Metzl, N., Munro, D. R., Nabel, J. E. M. S.,
8 Nakaoka, S., Neill, C., Olsen, A., Ono, T., Patra, P., Peregón, A., Peters, W., Peylin, P., Pfeil, B.,
9 Pierrot, D., Poulter, B., Rehder, G., Resplandy, L., Robertson, E., Rocher, M., Rödenbeck, C.,
10 Schuster, U., Schwinger, J., Séférian, R., Skjelvan, I., Steinhoff, T., Sutton, A., Tans, P. P., Tian,
11 H., Tilbrook, B., Tubiello, F. N., van der Laan-Luijkx, I. T., van der Werf, G. R., Viovy, N.,
12 Walker, A. P., Wiltshire, A. J., Wright, R., Zaehle, S., and Zheng, B.: Global Carbon Budget
13 2018, *Earth Syst. Sci. Data*, 10, 2141–2194, <https://doi.org/10.5194/essd-10-2141-2018>,
14 2018b.
- 15 Le Quéré, C., Korsbakken, J. I., Wilson, C., Tosun, J., Andrew, R., Andres, R. J., Canadell, J. G.,
16 Jordan, A., Peters, G. P., and van Vuuren, D. P.: Drivers of declining CO₂ emissions in 18
17 developed economies, *Nat. Clim. Chang.*, 9, 213–217, [https://doi.org/10.1038/s41558-019-](https://doi.org/10.1038/s41558-019-0419-7)
18 0419-7, 2019.
- 19 Le Quéré, C., Peters, G. P., Friedlingstein, P., Andrew, R. M., Canadell, J. G., Davis, S. J.,
20 Jackson, R. B., and Jones, M. W.: Fossil CO₂ emissions in the post-COVID-19 era, *Nat. Clim.*
21 *Chang.*, 11, 197–199, <https://doi.org/10.1038/s41558-021-01001-0>, 2021.
- 22 Li, H. and Ilyina, T.: Current and Future Decadal Trends in the Oceanic Carbon Uptake Are
23 Dominated by Internal Variability, *Geophys. Res. Lett.*, 45, 916–925,
24 <https://doi.org/10.1002/2017GL075370>, 2018.
- 25 Li, W., Ciais, P., Peng, S., Yue, C., Wang, Y., Thurner, M., Saatchi, S. S., Arneeth, A., Avitabile,
26 V., Carvalhais, N., Harper, A. B., Kato, E., Koven, C., Liu, Y. Y., Nabel, J. E. M. S., Pan, Y.,
27 Pongratz, J., Poulter, B., Pugh, T. A. M., Santoro, M., Sitch, S., Stocker, B. D., Viovy, N.,
28 Wiltshire, A., Yousefpour, R., and Zaehle, S.: Land-use and land-cover change carbon
29 emissions between 1901 and 2012 constrained by biomass observations, *Biogeosciences*,



- 1 14, 5053–5067, <https://doi.org/10.5194/bg-14-5053-2017>, 2017.
- 2 Liao, E., Resplandy, L., Liu, J., and Bowman, K. W.: Amplification of the Ocean Carbon Sink
3 During El Niños: Role of Poleward Ekman Transport and Influence on Atmospheric CO₂, 34,
4 e2020GB006574, <https://doi.org/10.1029/2020GB006574>, 2020.
- 5 Lienert, S. and Joos, F.: A Bayesian ensemble data assimilation to constrain model
6 parameters and land-use carbon emissions, *Biogeosciences*, 15, 2909–2930,
7 <https://doi.org/10.5194/bg-15-2909-2018>, 2018.
- 8 Liu, J., Baskaran, L., Bowman, K., Schimel, D., Bloom, A. A., Parazoo, N. C., Oda, T., Carroll, D.,
9 Menemenlis, D., Joiner, J., Commane, R., Daube, B., Gatti, L. V., McKain, K., Miller, J.,
10 Stephens, B. B., Sweeney, C., and Wofsy, S.: Carbon Monitoring System Flux Net Biosphere
11 Exchange 2020 (CMS-Flux NBE 2020), 13, 299–330, [https://doi.org/10.5194/essd-13-299-](https://doi.org/10.5194/essd-13-299-2021)
12 [2021](https://doi.org/10.5194/essd-13-299-2021), 2021.
- 13 Liu, Z., Guan, D., Wei, W., Davis, S. J., Ciais, P., Bai, J., Peng, S., Zhang, Q., Hubacek, K.,
14 Marland, G., Andres, R. J., Crawford-Brown, D., Lin, J., Zhao, H., Hong, C., Boden, T. A., Feng,
15 K., Peters, G. P., Xi, F., Liu, J., Li, Y., Zhao, Y., Zeng, N., and He, K.: Reduced carbon emission
16 estimates from fossil fuel combustion and cement production in China, *Nature*, 524, 335–
17 338, <https://doi.org/10.1038/nature14677>, 2015.
- 18 Liu, Z., Ciais, P., Deng, Z., Davis, S. J., Zheng, B., Wang, Y., Cui, D., Zhu, B., Dou, X., Ke, P., Sun,
19 T., Guo, R., Zhong, H., Boucher, O., Bréon, F.-M., Lu, C., Guo, R., Xue, J., Boucher, E., Tanaka,
20 K., and Chevallier, F.: Carbon Monitor, a near-real-time daily dataset of global CO₂ emission
21 from fossil fuel and cement production, *Sci Data*, 7, 392, [https://doi.org/10.1038/s41597-](https://doi.org/10.1038/s41597-020-00708-7)
22 [020-00708-7](https://doi.org/10.1038/s41597-020-00708-7), 2020a.
- 23 Liu, Z., Ciais, P., Deng, Z., Lei, R., Davis, S. J., Feng, S., Zheng, B., Cui, D., Dou, X., Zhu, B., Guo,
24 R., Ke, P., Sun, T., Lu, C., He, P., Wang, Y., Yue, X., Wang, Y., Lei, Y., Zhou, H., Cai, Z., Wu, Y.,
25 Guo, R., Han, T., Xue, J., Boucher, O., Boucher, E., Chevallier, F., Tanaka, K., Wei, Y., Zhong,
26 H., Kang, C., Zhang, N., Chen, B., Xi, F., Liu, M., Bréon, F.-M., Lu, Y., Zhang, Q., Guan, D.,
27 Gong, P., Kammen, D. M., He, K., and Schellhuber, H. J.: Near-real-time monitoring of
28 global CO₂ emissions reveals the effects of the COVID-19 pandemic, *Nat Commun*, 11, 5172,
29 <https://doi.org/10.1038/s41467-020-18922-7>, 2020b.



- 1 Ma, L., Hurtt, G. C., Chini, L. P., Sahajpal, R., Pongratz, J., Frohking, S., Stehfest, E., Klein
- 2 Goldewijk, K., O'Leary, D., and Doelman, J. C.: Global rules for translating land-use change
- 3 (LUH2) to land-cover change for CMIP6 using GLM2, *Geosci. Model Dev.*, 13, 3203–3220,
- 4 <https://doi.org/10.5194/gmd-13-3203-2020>, 2020.
- 5 Maki, T., Ikegami, M., Fujita, T., Hirahara, T., Yamada, K., Mori, K., Takeuchi, A., Tsutsumi, Y.,
- 6 Suda, K., and Conway, T. J.: New technique to analyse global distributions of CO₂
- 7 concentrations and fluxes from non-processed observational data, 62, 797–809,
- 8 <https://doi.org/10.1111/j.1600-0889.2010.00488.x>, 2010.
- 9 MapBiomass: MapBiomass Collection 5, available at:
- 10 <https://plataforma.brasil.mapbiomas.org/>, last access: 21 October 2021, 2021.
- 11 Marland, G.: Uncertainties in Accounting for CO₂ From Fossil Fuels, 12, 136–139,
- 12 <https://doi.org/10.1111/j.1530-9290.2008.00014.x>, 2008.
- 13 Marland, G., Hamal, K., and Jonas, M.: How Uncertain Are Estimates of CO₂ Emissions?, 13,
- 14 4–7, <https://doi.org/10.1111/j.1530-9290.2009.00108.x>, 2009.
- 15 Masarie, K. A. and Tans, P. P.: Extension and integration of atmospheric carbon dioxide data
- 16 into a globally consistent measurement record, *J. Geophys. Res.*, 100, 11593,
- 17 <https://doi.org/10.1029/95JD00859>, 1995.
- 18 Mather, A.: The transition from deforestation to reforestation in Europe., 35–52, 2001.
- 19 Matricardi, E. A. T., Skole, D. L., Costa, O. B., Pedlowski, M. A., Samek, J. H., and Miguel, E. P.:
- 20 Long-term forest degradation surpasses deforestation in the Brazilian Amazon, 369, 1378–
- 21 1382, <https://doi.org/10.1126/science.abb3021>, 2020.
- 22 Mauritsen, T., Bader, J., Becker, T., Behrens, J., Bittner, M., Brokopf, R., Brovkin, V.,
- 23 Claussen, M., Crueger, T., Esch, M., Fast, I., Fiedler, S., Fläschner, D., Gayler, V., Giorgetta,
- 24 M., Goll, D. S., Haak, H., Hagemann, S., Hedemann, C., Hohenegger, C., Ilyina, T., Jahns, T.,
- 25 Jimenez-de-la-Cuesta, D., Jungclaus, J., Kleinen, T., Kloster, S., Kracher, D., Kinne, S., Kleberg,
- 26 D., Lasslop, G., Kornblueh, L., Marotzke, J., Matei, D., Meraner, K., Mikolajewicz, U., Modali,
- 27 K., Möbis, B., Müller, W. A., Nabel, J. E. M. S., Nam, C. C. W., Notz, D., Nyawira, S.-S.,
- 28 Paulsen, H., Peters, K., Pincus, R., Pohlmann, H., Pongratz, J., Popp, M., Raddatz, T. J., Rast,



- 1 S., Redler, R., Reick, C. H., Rohrschneider, T., Schemann, V., Schmidt, H., Schnur, R.,
2 Schulzweida, U., Six, K. D., Stein, L., Stemmler, I., Stevens, B., von Storch, J.-S., Tian, F., Voigt,
3 A., Vrese, P., Wieners, K.-H., Wilkenskjaeld, S., Winkler, A., and Roeckner, E.: Developments in
4 the MPI-M Earth System Model version 1.2 (MPI-ESM1.2) and Its Response to Increasing
5 CO₂, 11, 998–1038, <https://doi.org/10.1029/2018MS001400>, 2019.
- 6 McGrath, M. J., Luyssaert, S., Meyfroidt, P., Kaplan, J. O., Bürgi, M., Chen, Y., Erb, K., Gimmi,
7 U., McInerney, D., Naudts, K., Otto, J., Pasztor, F., Ryder, J., Schelhaas, M.-J., and Valade, A.:
8 Reconstructing European forest management from 1600 to 2010, 12, 4291–4316,
9 <https://doi.org/10.5194/bg-12-4291-2015>, 2015.
- 10 McKinley, G. A., Pilcher, D. J., Fay, A. R., Lindsay, K., Long, M. C., and Lovenduski, N. S.:
11 Timescales for detection of trends in the ocean carbon sink, *Nature*, 530, 469–472,
12 <https://doi.org/10.1038/nature16958>, 2016.
- 13 McKinley, G. A., Fay, A. R., Eddebbar, Y. A., Gloege, L., and Lovenduski, N. S.: External
14 Forcing Explains Recent Decadal Variability of the Ocean Carbon Sink, *AGU Advances*, 1,
15 <https://doi.org/10.1029/2019AV000149>, 2020.
- 16 McNeil, B. I.: Anthropogenic CO₂ Uptake by the Ocean Based on the Global
17 Chlorofluorocarbon Data Set, 299, 235–239, <https://doi.org/10.1126/science.1077429>,
18 2003.
- 19 Meiyappan, P., Jain, A. K., and House, J. I.: Increased influence of nitrogen limitation on CO₂
20 emissions from future land use and land use change, *Global Biogeochem. Cycles*, 29, 1524–
21 1548, <https://doi.org/10.1002/2015GB005086>, 2015.
- 22 Melton, J. R., Arora, V. K., Wisernig-Cojoc, E., Seiler, C., Fortier, M., Chan, E., and Teckentrup,
23 L.: CLASSIC v1.0: the open-source community successor to the Canadian Land Surface
24 Scheme (CLASS) and the Canadian Terrestrial Ecosystem Model (CTEM) – Part 1: Model
25 framework and site-level performance, *Geosci. Model Dev.*, 13, 2825–2850,
26 <https://doi.org/10.5194/gmd-13-2825-2020>, 2020.
- 27 Mercado, L. M., Bellouin, N., Sitch, S., Boucher, O., Huntingford, C., Wild, M., and Cox, P. M.:
28 Impact of changes in diffuse radiation on the global land carbon sink, *Nature*, 458, 1014–



- 1 1017, <https://doi.org/10.1038/nature07949>, 2009.
- 2 Mikaloff Fletcher, S. E., Gruber, N., Jacobson, A. R., Doney, S. C., Dutkiewicz, S., Gerber, M.,
3 Follows, M., Joos, F., Lindsay, K., Menemenlis, D., Mouchet, A., Müller, S. A., and Sarmiento,
4 J. L.: Inverse estimates of anthropogenic CO₂ uptake, transport, and storage by the ocean:
5 AIR-SEA EXCHANGE OF ANTHROPOGENIC CARBON, *Global Biogeochem. Cycles*, 20,
6 <https://doi.org/10.1029/2005GB002530>, 2006.
- 7 Myneni, R. B., Ramakrishna, R., Nemani, R., and Running, S. W.: Estimation of global leaf
8 area index and absorbed par using radiative transfer models, *IEEE Trans. Geosci. Remote*
9 *Sensing*, 35, 1380–1393, <https://doi.org/10.1109/36.649788>, 1997.
- 10 Naegler, T.: Reconciliation of excess 14C-constrained global CO₂ piston velocity estimates,
11 61, 372–384, <https://doi.org/10.1111/j.1600-0889.2008.00408.x>, 2009.
- 12 Nakamura, T., Yamazaki, K., Iwamoto, K., Honda, M., Miyoshi, Y., Ogawa, Y., and Ukita, J.: A
13 negative phase shift of the winter AO/NAO due to the recent Arctic sea-ice reduction in late
14 autumn, 120, 3209–3227, <https://doi.org/10.1002/2014JD022848>, 2015.
- 15 Narayanan, B., Aguiar, A., and McDougall, R.: Global Trade, Assistance, and Production: The
16 GTAP 9 Data Base, *Cent. Glob. Trade Anal. Purdue Univ.*, 2015 September, available at:
17 <https://www.gtap.agecon.purdue.edu/databases/v9/default.asp>, last access: 25 October
18 2021, 2021.
- 19 NBS: National Bureau of Statistics (NBS): National Data (online database), National Bureau
20 of Statistics, available at: <http://data.stats.gov.cn/>, last access: 25 October 2021, 2021.
- 21 NCEP: National Centers for Environmental Prediction. ONI Index. Cold & Warm Episodes by
22 Season, available at:
23 https://origin.cpc.ncep.noaa.gov/products/analysis_monitoring/ensostuff/ONI_v5.php, last
24 access: 25 October 2021, 2021.
- 25 Nightingale, P. D., Liss, P. S., and Schlosser, P.: Measurements of air-sea gas transfer during
26 an open ocean algal bloom, 27, 2117–2120, <https://doi.org/10.1029/2000GL011541>, 2000.
- 27 Niwa, Y., Fujii, Y., Sawa, Y., Iida, Y., Ito, A., Satoh, M., Imasu, R., Tsuboi, K., Matsueda, H., and



- 1 Saigusa, N.: A 4D-Var inversion system based on the icosahedral grid model (NICAM-TM 4D-
2 Var v1.0) – Part 2: Optimization scheme and identical twin experiment of atmospheric CO₂
3 inversion, *Geosci. Model Dev.*, 10, 2201–2219, <https://doi.org/10.5194/gmd-10-2201-2017>,
4 2017.
- 5 Niwa, Y., Langenfelds, R., Krummel, P., Loh, Zoe, Worthy, Doug, Hatakka, Juha, Aalto, Tuula,
6 Ramonet, Michel, Delmotte, Marc, Schmidt, Martina, Gheusi, Francois, Mihalopoulos, N.,
7 Morgui, J.A., Andrews, Arlyn, Dlugokencky, Ed, Lee, John, Sweeney, Colm, Thoning, Kirk,
8 Tans, Pieter, De Wekker, Stephan, Fischer, Marc L., Jaffe, Dan, McKain, Kathryn, Viner, Brian,
9 Miller, John B., Karion, Anna, Miller, Charles, Sloop, Christopher D., Saito, Kazuyuki, Aoki,
10 Shuji, Morimoto, Shinji, Goto, Daisuke, Steinbacher, Martin, Myhre, Cathrine Lund,
11 Hermanssen, Ove, Stephens, Britton, Keeling, Ralph, Afshar, Sara, Paplawsky, Bill, Cox,
12 Adam, Walker, Stephen, Schuldt, Kenneth, Mukai, Hitoshi, Machida, Toshinobu, Sasakawa,
13 Motoki, Nomura, Shohei, Ito, Akihiko, Iida, Yosuke, and Jones, Matthew W.: Long-term
14 global CO₂ fluxes estimated by NICAM-based Inverse Simulation for Monitoring CO₂
15 (NISMON-CO₂) (ver.2020.1), <https://doi.org/10.17595/20201127.001>, 2020.
- 16 Obermeier, W. A., Nabel, J. E. M. S., Loughran, T., Hartung, K., Bastos, A., Havermann, F.,
17 Anthoni, P., Arneth, A., Goll, D. S., Lienert, S., Lombardozzi, D., Luyssaert, S., McGuire, P. C.,
18 Melton, J. R., Poulter, B., Sitch, S., Sullivan, M. O., Tian, H., Walker, A. P., Wiltshire, A. J.,
19 Zaehle, S., and Pongratz, J.: Modelled land use and land cover change emissions – a spatio-
20 temporal comparison of different approaches, 12, 635–670, [https://doi.org/10.5194/esd-](https://doi.org/10.5194/esd-12-635-2021)
21 12-635-2021, 2021.
- 22 O’Rourke, P. R., Smith, S. J., Mott, A., Ahsan, H., McDuffie, E. E., Crippa, M., Klimont, Z.,
23 McDonald, B., Wang, S., Nicholson, M. B., Feng, L., and Hoesly, R. M.: CEDS v_2021_04_21
24 Release Emission Data, <https://doi.org/10.5281/zenodo.4741285>, 2021.
- 25 Orr, J. C., Najjar, R. G., Aumont, O., Bopp, L., Bullister, J. L., Danabasoglu, G., Doney, S. C.,
26 Dunne, J. P., Dutay, J.-C., Graven, H., Griffies, S. M., John, J. G., Joos, F., Levin, I., Lindsay, K.,
27 Matear, R. J., McKinley, G. A., Mouchet, A., Oschlies, A., Romanou, A., Schlitzer, R.,
28 Tagliabue, A., Tanhua, T., and Yool, A.: Biogeochemical protocols and diagnostics for the
29 CMIP6 Ocean Model Intercomparison Project (OMIP), 10, 2169–2199,
30 <https://doi.org/10.5194/gmd-10-2169-2017>, 2017.



- 1 O’Sullivan, M., Zhang, Y., Bellouin, N., Harris, I., Mercado, L. M., Sitch, S., Ciais, P., and
- 2 Friedlingstein, P.: (under review) Aerosol-light interactions reduce the carbon budget
- 3 imbalance, *Environmental Research Letters*, 2021.
- 4 Palmer, P. I., Feng, L., Baker, D., Chevallier, F., Bösch, H., and Somkuti, P.: Net carbon
- 5 emissions from African biosphere dominate pan-tropical atmospheric CO₂ signal, *Nat*
- 6 *Commun*, 10, 3344, <https://doi.org/10.1038/s41467-019-11097-w>, 2019.
- 7 Pan, Y., Birdsey, R. A., Fang, J., Houghton, R., Kauppi, P. E., Kurz, W. A., Phillips, O. L.,
- 8 Shvidenko, A., Lewis, S. L., Canadell, J. G., Ciais, P., Jackson, R. B., Pacala, S. W., McGuire, A.
- 9 D., Piao, S., Rautiainen, A., Sitch, S., and Hayes, D.: A Large and Persistent Carbon Sink in the
- 10 World’s Forests, *Science*, 333, 988–993, <https://doi.org/10.1126/science.1201609>, 2011.
- 11 Patra, P. K., Takigawa, M., Watanabe, S., Chandra, N., Ishijima, K., and Yamashita, Y.:
- 12 Improved Chemical Tracer Simulation by MIROC4.0-based Atmospheric Chemistry-Transport
- 13 Model (MIROC4-ACTM), *SOLA*, 14, 91–96, <https://doi.org/10.2151/sola.2018-016>, 2018.
- 14 Pendrill, F., Persson, U. M., Godar, J., Kastner, T., Moran, D., Schmidt, S., and Wood, R.:
- 15 Agricultural and forestry trade drives large share of tropical deforestation emissions, *Global*
- 16 *Environmental Change*, 56, 1–10, <https://doi.org/10.1016/j.gloenvcha.2019.03.002>, 2019.
- 17 Peters, G. P., Andrew, R., and Lennox, J.: Constructing an environmentally-extended multi-
- 18 regional input–output table using the GTAP database, *Economic Systems Research*, 23, 131–
- 19 152, <https://doi.org/10.1080/09535314.2011.563234>, 2011a.
- 20 Peters, G. P., Minx, J. C., Weber, C. L., and Edenhofer, O.: Growth in emission transfers via
- 21 international trade from 1990 to 2008, *Proceedings of the National Academy of Sciences*,
- 22 108, 8903–8908, <https://doi.org/10.1073/pnas.1006388108>, 2011b.
- 23 Peters, G. P., Davis, S. J., and Andrew, R.: A synthesis of carbon in international trade,
- 24 *Biogeosciences*, 9, 3247–3276, <https://doi.org/10.5194/bg-9-3247-2012>, 2012a.
- 25 Peters, G. P., Marland, G., Le Quéré, C., Boden, T., Canadell, J. G., and Raupach, M. R.: Rapid
- 26 growth in CO₂ emissions after the 2008–2009 global financial crisis, *Nature Clim Change*, 2,
- 27 2–4, <https://doi.org/10.1038/nclimate1332>, 2012b.



- 1 Peters, G. P., Andrew, R. M., Boden, T., Canadell, J. G., Ciais, P., Le Quéré, C., Marland, G.,
- 2 Raupach, M. R., and Wilson, C.: The challenge to keep global warming below 2 °C, *Nature*
- 3 *Clim Change*, 3, 4–6, <https://doi.org/10.1038/nclimate1783>, 2013.
- 4 Peters, G. P., Le Quéré, C., Andrew, R. M., Canadell, J. G., Friedlingstein, P., Ilyina, T.,
- 5 Jackson, R. B., Joos, F., Korsbakken, J. I., McKinley, G. A., Sitch, S., and Tans, P.: Towards real-
- 6 time verification of CO₂ emissions, *Nature Clim Change*, 7, 848–850,
- 7 <https://doi.org/10.1038/s41558-017-0013-9>, 2017.
- 8 Peters, G. P., Andrew, R. M., Canadell, J. G., Friedlingstein, P., Jackson, R. B., Korsbakken, J.
- 9 I., Le Quéré, C., and Pregon, A.: Carbon dioxide emissions continue to grow amidst slowly
- 10 emerging climate policies, *Nat. Clim. Chang.*, 10, 3–6, [https://doi.org/10.1038/s41558-019-](https://doi.org/10.1038/s41558-019-0659-6)
- 11 [0659-6](https://doi.org/10.1038/s41558-019-0659-6), 2020.
- 12 Petrescu, A. M. R., Peters, G. P., Janssens-Maenhout, G., Ciais, P., Tubiello, F. N., Grassi, G.,
- 13 Nabuurs, G.-J., Leip, A., Carmona-Garcia, G., Winiwarter, W., Höglund-Isaksson, L., Günther,
- 14 D., Solazzo, E., Kiesow, A., Bastos, A., Pongratz, J., Nabel, J. E. M. S., Conchedda, G., Pilli, R.,
- 15 Andrew, R. M., Schelhaas, M.-J., and Dolman, A. J.: European anthropogenic AFOLU
- 16 greenhouse gas emissions: a review and benchmark data, *Earth Syst. Sci. Data*, 12, 961–
- 17 [1001](https://doi.org/10.5194/essd-12-961-2020), <https://doi.org/10.5194/essd-12-961-2020>, 2020.
- 18 Pfeil, B., Olsen, A., Bakker, D. C. E., Hankin, S., Koyuk, H., Kozyr, A., Malczyk, J., Manke, A.,
- 19 Metzl, N., Sabine, C. L., Akl, J., Alin, S. R., Bates, N., Bellerby, R. G. J., Borges, A., Boutin, J.,
- 20 Brown, P. J., Cai, W.-J., Chavez, F. P., Chen, A., Cosca, C., Fassbender, A. J., Feely, R. A.,
- 21 González-Dávila, M., Goyet, C., Hales, B., Hardman-Mountford, N., Heinze, C., Hood, M.,
- 22 Hoppema, M., Hunt, C. W., Hydes, D., Ishii, M., Johannessen, T., Jones, S. D., Key, R. M.,
- 23 Körtzinger, A., Landschützer, P., Lauvset, S. K., Lefèvre, N., Lenton, A., Lourantou, A.,
- 24 Merlivat, L., Midorikawa, T., Mintrop, L., Miyazaki, C., Murata, A., Nakadate, A., Nakano, Y.,
- 25 Nakaoka, S., Nojiri, Y., Omar, A. M., Padin, X. A., Park, G.-H., Paterson, K., Perez, F. F.,
- 26 Pierrot, D., Poisson, A., Ríos, A. F., Santana-Casiano, J. M., Salisbury, J., Sarma, V. V. S. S.,
- 27 Schlitzer, R., Schneider, B., Schuster, U., Sieger, R., Skjelvan, I., Steinhoff, T., Suzuki, T.,
- 28 Takahashi, T., Tedesco, K., Telszewski, M., Thomas, H., Tilbrook, B., Tjiputra, J., Vandemark,
- 29 D., Veness, T., Wanninkhof, R., Watson, A. J., Weiss, R., Wong, C. S., and Yoshikawa-Inoue,
- 30 H.: A uniform, quality controlled Surface Ocean CO₂ Atlas (SOCAT), *Earth Syst. Sci. Data*, 5,



- 1 125–143, <https://doi.org/10.5194/essd-5-125-2013>, 2013.
- 2 Piao, S., Ciais, P., Friedlingstein, P., de Noblet-Ducoudré, N., Cadule, P., Viovy, N., and Wang,
3 T.: Spatiotemporal patterns of terrestrial carbon cycle during the 20th century, 23,
4 <https://doi.org/10.1029/2008GB003339>, 2009.
- 5 Piao, S., Huang, M., Liu, Z., Wang, X., Ciais, P., Canadell, J. G., Wang, K., Bastos, A.,
6 Friedlingstein, P., Houghton, R. A., Le Quéré, C., Liu, Y., Myneni, R. B., Peng, S., Pongratz, J.,
7 Sitch, S., Yan, T., Wang, Y., Zhu, Z., Wu, D., and Wang, T.: Lower land-use emissions
8 responsible for increased net land carbon sink during the slow warming period, *Nature*
9 *Geosci*, 11, 739–743, <https://doi.org/10.1038/s41561-018-0204-7>, 2018.
- 10 Pongratz, J., Reick, C. H., Houghton, R. A., and House, J. I.: Terminology as a key uncertainty
11 in net land use and land cover change carbon flux estimates, *Earth Syst. Dynam.*, 5, 177–
12 195, <https://doi.org/10.5194/esd-5-177-2014>, 2014.
- 13 Potapov, P., Hansen, M. C., Laestadius, L., Turubanova, S., Yaroshenko, A., Thies, C., Smith,
14 W., Zhuravleva, I., Komarova, A., Minnemeyer, S., and Esipova, E.: The last frontiers of
15 wilderness: Tracking loss of intact forest landscapes from 2000 to 2013, 3, e1600821,
16 <https://doi.org/10.1126/sciadv.1600821>, 2017.
- 17 Poulter, B., Frank, D. C., Hodson, E. L., and Zimmermann, N. E.: Impacts of land cover and
18 climate data selection on understanding terrestrial carbon dynamics and the CO₂ airborne
19 fraction, *Biogeosciences*, 8, 2027–2036, <https://doi.org/10.5194/bg-8-2027-2011>, 2011.
- 20 Poulter, B., Freeborn, P. H., Jolly, W. M., and Varner, J. M.: COVID-19 lockdowns drive
21 decline in active fires in southeastern United States, *PNAS*, 118,
22 <https://doi.org/10.1073/pnas.2105666118>, 2021.
- 23 Prather, M.: Interactive comment on “Carbon dioxide and climate impulse response
24 functions for the computation of greenhouse gas metrics: a multi-model analysis” by F. Joos
25 et al., 6, 2012.
- 26 Prentice, I. C., Farquhar, G. D., Fasham, M. J. R., Goulden, M. L., Heimann, M., Jaramillo, V.
27 J., Khashgi, H. S., Le Quéré, C., Scholes, R. J., and Wallace, D. W. R.: The Carbon Cycle and
28 Atmospheric Carbon Dioxide, in *Climate Change 2001: The Scientific Basis. Contribution of*



- 1 Working Group I to the Third Assessment Report of the Intergovernmental Panel on Climate
- 2 Change, edited by: Houghton, J. T., Ding, Y., Griggs, D. J., Noguer, M., van der Linden, P. J.,
- 3 Dai, X., Maskell, K., and Johnson, C. A., Cambridge University Press, Cambridge, United
- 4 Kingdom and New York, NY, USA, 183–237, 2001.

- 5 Price, J. T. and Warren, R.: Literature Review of the Potential of “Blue Carbon” Activities to
- 6 Reduce Emissions, available at: [https://avoid-net-uk.cc.ic.ac.uk/wp-](https://avoid-net-uk.cc.ic.ac.uk/wp-content/uploads/delightful-downloads/2016/03/Literature-review-of-the-potential-of-blue-carbon-activities-to-reduce-emissions-AVOID2-WPE2.pdf)
- 7 [content/uploads/delightful-downloads/2016/03/Literature-review-of-the-potential-of-blue-](https://avoid-net-uk.cc.ic.ac.uk/wp-content/uploads/delightful-downloads/2016/03/Literature-review-of-the-potential-of-blue-carbon-activities-to-reduce-emissions-AVOID2-WPE2.pdf)
- 8 [carbon-activities-to-reduce-emissions-AVOID2-WPE2.pdf](https://avoid-net-uk.cc.ic.ac.uk/wp-content/uploads/delightful-downloads/2016/03/Literature-review-of-the-potential-of-blue-carbon-activities-to-reduce-emissions-AVOID2-WPE2.pdf), last access: 25 October 2021,
- 9 2016.

- 10 Qin, Y., Xiao, X., Wigneron, J.-P., Ciais, P., Brandt, M., Fan, L., Li, X., Crowell, S., Wu, X.,
- 11 Doughty, R., Zhang, Y., Liu, F., Sitch, S., and Moore, B.: Carbon loss from forest degradation
- 12 exceeds that from deforestation in the Brazilian Amazon, *Nat. Clim. Chang.*, **11**, 442–448,
- 13 <https://doi.org/10.1038/s41558-021-01026-5>, 2021.

- 14 Qiu, C., Ciais, P., Zhu, D., Guenet, B., Peng, S., Petrescu, A. M. R., Lauerwald, R., Makowski,
- 15 D., Gallego-Sala, A. V., Charman, D. J., and Brewer, S. C.: Large historical carbon emissions
- 16 from cultivated northern peatlands, *7*, eabf1332, <https://doi.org/10.1126/sciadv.abf1332>,
- 17 2021.

- 18 Raupach, M. R., Marland, G., Ciais, P., Le Quere, C., Canadell, J. G., Klepper, G., and Field, C.
- 19 B.: Global and regional drivers of accelerating CO₂ emissions, *Proceedings of the National*
- 20 *Academy of Sciences*, **104**, 10288–10293, <https://doi.org/10.1073/pnas.0700609104>, 2007.

- 21 Regnier, P., Friedlingstein, P., Ciais, P., Mackenzie, F. T., Gruber, N., Janssens, I. A., Laruelle,
- 22 G. G., Lauerwald, R., Luysaert, S., Andersson, A. J., Arndt, S., Arnosti, C., Borges, A. V., Dale,
- 23 A. W., Gallego-Sala, A., Godd ris, Y., Goossens, N., Hartmann, J., Heinze, C., Ilyina, T., Joos,
- 24 F., LaRowe, D. E., Leifeld, J., Meysman, F. J. R., Munhoven, G., Raymond, P. A., Spahni, R.,
- 25 Suntharalingam, P., and Thullner, M.: Anthropogenic perturbation of the carbon fluxes from
- 26 land to ocean, *Nature Geosci*, **6**, 597–607, <https://doi.org/10.1038/ngeo1830>, 2013.

- 27 Reick, C. H., Gayler, V., Goll, D., Hagemann, S., Heidkamp, M., Nabel, J. E. M. S., Raddatz, T.,
- 28 Roeckner, E., Schnur, R., and Wilkenskjeld, S.: JSBACH 3 - The land component of the MPI
- 29 Earth System Model: documentation of version 3.2, <https://doi.org/10.17617/2.3279802>,



- 1 2021.
- 2 Remaud, M., Chevallier, F., Cozic, A., Lin, X., and Bousquet, P.: On the impact of recent
3 developments of the LMDz atmospheric general circulation model on the simulation of CO₂
4 transport, *11*, 4489, <https://doi.org/10.5194/gmd-11-4489-2018>, 2018.
- 5 Resplandy, L., Keeling, R. F., Rödenbeck, C., Stephens, B. B., Khatiwala, S., Rodgers, K. B.,
6 Long, M. C., Bopp, L., and Tans, P. P.: Revision of global carbon fluxes based on a
7 reassessment of oceanic and riverine carbon transport, *Nature Geosci*, *11*, 504–509,
8 <https://doi.org/10.1038/s41561-018-0151-3>, 2018.
- 9 Rhein, M., Rintoul, S. R., Aoki, S., Campos, E., Chambers, D., Feely, R. A., Gulev, S., Johnson,
10 G. C., Josey, S. A., Kostianoy, A., Mauritzen, C., Roemmich, D., and Talley, L. D.:
11 Observations: Ocean, edited by: Stocker, T. F., Qin, D., Plattner, G.-K., Tignor, M., Allen, S. K.,
12 Boschung, J., Nauels, A., Xia, Y., Bex, V., and Midgley, P. M., Cambridge University Press,
13 255–316, 2013.
- 14 Rodenbeck, C., Houweling, S., Gloor, M., and Heimann, M.: CO₂ flux history 1982–2001
15 inferred from atmospheric data using a global inversion of atmospheric transport, *46*, 2003.
- 16 Rödenbeck, C., Keeling, R. F., Bakker, D. C. E., Metzl, N., Olsen, A., Sabine, C., and Heimann,
17 M.: Global surface-ocean pCO₂ and sea–air CO₂ flux variability from an observation-driven
18 ocean mixed-layer scheme, *9*, 193–216, <https://doi.org/10.5194/os-9-193-2013>, 2013.
- 19 Rödenbeck, C., Bakker, D. C. E., Metzl, N., Olsen, A., Sabine, C., Cassar, N., Reum, F., Keeling,
20 R. F., and Heimann, M.: Interannual sea–air CO₂ flux variability from an observation-driven
21 ocean mixed-layer scheme, *11*, 4599–4613, <https://doi.org/10.5194/bg-11-4599-2014>,
22 2014.
- 23 Rödenbeck, C., Bakker, D. C. E., Gruber, N., Iida, Y., Jacobson, A. R., Jones, S., Landschützer,
24 P., Metzl, N., Nakaoka, S., Olsen, A., Park, G.-H., Peylin, P., Rodgers, K. B., Sasse, T. P.,
25 Schuster, U., Shutler, J. D., Valsala, V., Wanninkhof, R., and Zeng, J.: Data-based estimates of
26 the ocean carbon sink variability – first results of the Surface Ocean CO₂ Mapping
27 intercomparison (SOCOM), *Biogeosciences*, *12*, 7251–7278, [https://doi.org/10.5194/bg-12-](https://doi.org/10.5194/bg-12-7251-2015)
28 7251-2015, 2015.



- 1 Rödenbeck, C., Zaehle, S., Keeling, R., and Heimann, M.: History of El Niño impacts on the
- 2 global carbon cycle 1957–2017: a quantification from atmospheric CO₂ data, 373,
- 3 20170303, <https://doi.org/10.1098/rstb.2017.0303>, 2018.
- 4 Roobaert, A., Laruelle, G. G., Landschützer, P., and Regnier, P.: Uncertainty in the global
- 5 oceanic CO₂ uptake induced by wind forcing: quantification and spatial analysis, 15, 1701–
- 6 1720, <https://doi.org/10.5194/bg-15-1701-2018>, 2018.
- 7 Rosan, T. M., Goldewijk, K. K., Ganzenmüller, R., O’Sullivan, M., Pongratz, J., Mercado, L. M.,
- 8 Aragao, L. E. O. C., Heinrich, V., Randow, C. V., Wiltshire, A., Tubiello, F. N., Bastos, A.,
- 9 Friedlingstein, P., and Sitch, S.: A multi-data assessment of land use and land cover
- 10 emissions from Brazil during 2000–2019, *Environ. Res. Lett.*, 16, 074004,
- 11 <https://doi.org/10.1088/1748-9326/ac08c3>, 2021.
- 12 Rypdal, K., Paciorek, N., Eggleston, S., Goodwin, J., Irving, W., Penman, J., and Woodfield,
- 13 M.: Volume 1: Introduction to the 2006 Guidelines in: 2006 IPCC guidelines for national
- 14 greenhouse gas inventories., 2006.
- 15 Saatchi, S. S., Harris, N. L., Brown, S., Lefsky, M., Mitchard, E. T. A., Salas, W., Zutta, B. R.,
- 16 Buermann, W., Lewis, S. L., Hagen, S., Petrova, S., White, L., Silman, M., and Morel, A.:
- 17 Benchmark map of forest carbon stocks in tropical regions across three continents,
- 18 *Proceedings of the National Academy of Sciences*, 108, 9899–9904,
- 19 <https://doi.org/10.1073/pnas.1019576108>, 2011.
- 20 Sabine, C. L., Feely, R. A., Gruber, N., Key, R. M., Lee, K., Bullister, J. L., Wanninkhof, R.,
- 21 Wong, C. S., Wallace, D. W. R., Tilbrook, B., Millero, F. J., Peng, T.-H., Kozyr, A., Ono, T., and
- 22 Rios, A. F.: The Oceanic Sink for Anthropogenic CO₂, 305, 367–371,
- 23 <https://doi.org/10.1126/science.1097403>, 2004.
- 24 Sarmiento, J. L., Orr, J. C., and Siegenthaler, U.: A perturbation simulation of CO₂ uptake in
- 25 an ocean general circulation model, 97, 3621–3645, <https://doi.org/10.1029/91JC02849>,
- 26 1992.
- 27 Sato, M., Hansen, J. E., McCormick, M. P., and Pollack, J. B.: Stratospheric aerosol optical
- 28 depths, 1850–1990, 98, 22987–22994, <https://doi.org/10.1029/93JD02553>, 1993.



- 1 Saunois, M., Stavert, A. R., Poulter, B., Bousquet, P., Canadell, J. G., Jackson, R. B., Raymond,
2 P. A., Dlugokencky, E. J., Houweling, S., Patra, P. K., Ciais, P., Arora, V. K., Bastviken, D.,
3 Bergamaschi, P., Blake, D. R., Brailsford, G., Bruhwiler, L., Carlson, K. M., Carrol, M., Castaldi,
4 S., Chandra, N., Crevoisier, C., Crill, P. M., Covey, K., Curry, C. L., Etiope, G., Frankenberg, C.,
5 Gedney, N., Hegglin, M. I., Höglund-Isaksson, L., Hugelius, G., Ishizawa, M., Ito, A., Janssens-
6 Maenhout, G., Jensen, K. M., Joos, F., Kleinen, T., Krummel, P. B., Langenfelds, R. L., Laruelle,
7 G. G., Liu, L., Machida, T., Maksyutov, S., McDonald, K. C., McNorton, J., Miller, P. A.,
8 Melton, J. R., Morino, I., Müller, J., Murguia-Flores, F., Naik, V., Niwa, Y., Noce, S., O'Doherty,
9 S., Parker, R. J., Peng, C., Peng, S., Peters, G. P., Prigent, C., Prinn, R., Ramonet, M., Regnier,
10 P., Riley, W. J., Rosentreter, J. A., Segers, A., Simpson, I. J., Shi, H., Smith, S. J., Steele, L. P.,
11 Thornton, B. F., Tian, H., Tohjima, Y., Tubiello, F. N., Tsuruta, A., Viovy, N., Voulgarakis, A.,
12 Weber, T. S., van Weele, M., van der Werf, G. R., Weiss, R. F., Worthy, D., Wunch, D., Yin, Y.,
13 Yoshida, Y., Zhang, W., Zhang, Z., Zhao, Y., Zheng, B., Zhu, Q., Zhu, Q., and Zhuang, Q.: The
14 Global Methane Budget 2000–2017, *Earth Syst. Sci. Data*, 12, 1561–1623,
15 <https://doi.org/10.5194/essd-12-1561-2020>, 2020.
- 16 Schimel, D., Alves, D., Enting, I. G., Heimann, M., Joos, F., Raynaud, D., Wigley, T., Prater, M.,
17 Derwent, R., Ehhalt, D., Fraser, P., Sanhueza, E., Zhou, X., Jonas, P., Charlson, R., Rodhe, H.,
18 Sadasivan, S., Shine, K. P., Fouquart, Y., Ramaswamy, V., Solomon, S., Srinivasan, J.,
19 Albritton, D., Derwent, R., Isaksen, I., Lal, M., and Wuebbles, D.: Radiative Forcing of Climate
20 Change, in: *Climate Change 1995 The Science of Climate Change, Contribution of Working*
21 *Group I to the Second Assessment Report of the Intergovernmental Panel on Climate*
22 *Change*, edited by: Houghton, J. T., Meira Rillo, L. G., Callander, B. A., Harris, N., Kattenberg,
23 A., and Maskell, K., Cambridge University Press, Cambridge, United Kingdom and New York,
24 NY, USA, 1995.
- 25 Schimel, D., Stephens, B. B., and Fisher, J. B.: Effect of increasing CO₂ on the terrestrial
26 carbon cycle, *Proc Natl Acad Sci USA*, 112, 436–441,
27 <https://doi.org/10.1073/pnas.1407302112>, 2015.
- 28 Schourup-Kristensen, V., Sidorenko, D., Wolf-Gladrow, D. A., and Völker, C.: A skill
29 assessment of the biogeochemical model REcoM2 coupled to the Finite Element Sea Ice–
30 Ocean Model (FESOM 1.3), *Geosci. Model Dev.*, 7, 2769–2802,



- 1 <https://doi.org/10.5194/gmd-7-2769-2014>, 2014.
- 2 Schuh, A. E., Jacobson, A. R., Basu, S., Weir, B., Baker, D., Bowman, K., Chevallier, F., Crowell,
3 S., Davis, K. J., Deng, F., Denning, S., Feng, L., Jones, D., Liu, J., and Palmer, P. I.: Quantifying
4 the Impact of Atmospheric Transport Uncertainty on CO₂ Surface Flux Estimates, *Global*
5 *Biogeochem. Cycles*, 33, 484–500, <https://doi.org/10.1029/2018GB006086>, 2019.
- 6 Schwinger, J., Goris, N., Tjiputra, J. F., Kriest, I., Bentsen, M., Bethke, I., Ilicak, M., Assmann,
7 K. M., and Heinze, C.: Evaluation of NorESM-OC (versions 1 and 1.2), the ocean carbon-cycle
8 stand-alone configuration of the Norwegian Earth System Model (NorESM1), *Geosci. Model*
9 *Dev.*, 9, 2589–2622, <https://doi.org/10.5194/gmd-9-2589-2016>, 2016.
- 10 Séférian, R., Nabat, P., Michou, M., Saint-Martin, D., Voltaire, A., Colin, J., Decharme, B.,
11 Delire, C., Berthet, S., Chevallier, M., Sénési, S., Franchisteguy, L., Vial, J., Mallet, M.,
12 Joetzjer, E., Geoffroy, O., Guérémy, J.-F., Moine, M.-P., Msadek, R., Ribes, A., Rocher, M.,
13 Roehrig, R., Salas-y-Méla, D., Sanchez, E., Terray, L., Valcke, S., Waldman, R., Aumont, O.,
14 Bopp, L., Deshayes, J., Éthé, C., and Madec, G.: Evaluation of CNRM Earth System Model,
15 CNRM-ESM2-1: Role of Earth System Processes in Present-Day and Future Climate, 11,
16 4182–4227, <https://doi.org/10.1029/2019MS001791>, 2019.
- 17 Sellar, A. A., Jones, C. G., Mulcahy, J. P., Tang, Y., Yool, A., Wiltshire, A., O’Connor, F. M.,
18 Stringer, M., Hill, R., Palmieri, J., Woodward, S., Mora, L., Kuhlbrodt, T., Rumbold, S. T.,
19 Kelley, D. I., Ellis, R., Johnson, C. E., Walton, J., Abraham, N. L., Andrews, M. B., Andrews, T.,
20 Archibald, A. T., Berthou, S., Burke, E., Blockley, E., Carslaw, K., Dalvi, M., Edwards, J.,
21 Folberth, G. A., Gedney, N., Griffiths, P. T., Harper, A. B., Hendry, M. A., Hewitt, A. J.,
22 Johnson, B., Jones, A., Jones, C. D., Keeble, J., Liddicoat, S., Morgenstern, O., Parker, R. J.,
23 Predoi, V., Robertson, E., Siahann, A., Smith, R. S., Swaminathan, R., Woodhouse, M. T.,
24 Zeng, G., and Zerroukat, M.: UKESM1: Description and Evaluation of the U.K. Earth System
25 Model, *J. Adv. Model. Earth Syst.*, 11, 4513–4558, <https://doi.org/10.1029/2019MS001739>,
26 2019.
- 27 Shu, S., Jain, A. K., Koven, C. D., and Mishra, U.: Estimation of Permafrost SOC Stock and
28 Turnover Time Using a Land Surface Model With Vertical Heterogeneity of Permafrost Soils,
29 34, e2020GB006585, <https://doi.org/10.1029/2020GB006585>, 2020.



- 1 Silva Junior, C. H. L., Pessôa, A. C. M., Carvalho, N. S., Reis, J. B. C., Anderson, L. O., and
- 2 Aragão, L. E. O. C.: The Brazilian Amazon deforestation rate in 2020 is the greatest of the
- 3 decade, *Nat Ecol Evol*, 5, 144–145, <https://doi.org/10.1038/s41559-020-01368-x>, 2021.
- 4 Sitch, S., Huntingford, C., Gedney, N., Levy, P. E., Lomas, M., Piao, S. L., Betts, R., Ciais, P.,
- 5 Cox, P., Friedlingstein, P., Jones, C. D., Prentice, I. C., and Woodward, F. I.: Evaluation of the
- 6 terrestrial carbon cycle, future plant geography and climate-carbon cycle feedbacks using
- 7 five Dynamic Global Vegetation Models (DGVMs): Uncertainty In Land Carbon Cycle
- 8 Feedbacks, 14, 2015–2039, <https://doi.org/10.1111/j.1365-2486.2008.01626.x>, 2008.
- 9 Smith, B., Wårlind, D., Arneth, A., Hickler, T., Leadley, P., Siltberg, J., and Zaehle, S.:
- 10 Implications of incorporating N cycling and N limitations on primary production in an
- 11 individual-based dynamic vegetation model, *Biogeosciences*, 11, 2027–2054,
- 12 <https://doi.org/10.5194/bg-11-2027-2014>, 2014.
- 13 Stephens, B. B., Gurney, K. R., Tans, P. P., Sweeney, C., Peters, W., Bruhwiler, L., Ciais, P.,
- 14 Ramonet, M., Bousquet, P., Nakazawa, T., Aoki, S., Machida, T., Inoue, G., Vinnichenko, N.,
- 15 Lloyd, J., Jordan, A., Heimann, M., Shibistova, O., Langenfelds, R. L., Steele, L. P., Francey, R.
- 16 J., and Denning, A. S.: Weak Northern and Strong Tropical Land Carbon Uptake from Vertical
- 17 Profiles of Atmospheric CO₂, *Science*, 316, 1732–1735,
- 18 <https://doi.org/10.1126/science.1137004>, 2007.
- 19 Stocker, T., Qin, D., and Plattner, G.-K.: *Climate Change 2013: The Physical Science Basis.*
- 20 *Contribution of Working Group I to the Fifth Assessment Report of the Intergovernmental*
- 21 *Panel on Climate Change*, edited by: Intergovernmental Panel on Climate Change,
- 22 Cambridge University Press, Cambridge, 2013.
- 23 Sweeney, C., Gloor, E., Jacobson, A. R., Key, R. M., McKinley, G., Sarmiento, J. L., and
- 24 Wanninkhof, R.: Constraining global air-sea gas exchange for CO₂ with recent bomb 14C
- 25 measurements, 21, <https://doi.org/10.1029/2006GB002784>, 2007.
- 26 SX Coal: Monthly coal consumption estimates, available at: <http://www.sxcoal.com/>, last
- 27 access: 25 October 2021, 2021.
- 28 Takahashi, T., Sutherland, S. C., Wanninkhof, R., Sweeney, C., Feely, R. A., Chipman, D. W.,



- 1 Hales, B., Friederich, G., Chavez, F., Sabine, C., Watson, A., Bakker, D. C. E., Schuster, U.,
- 2 Metzl, N., Yoshikawa-Inoue, H., Ishii, M., Midorikawa, T., Nojiri, Y., Körtzinger, A., Steinhoff,
- 3 T., Hoppema, M., Olafsson, J., Arnarson, T. S., Tilbrook, B., Johannessen, T., Olsen, A.,
- 4 Bellerby, R., Wong, C. S., Delille, B., Bates, N. R., and de Baar, H. J. W.: Climatological mean
- 5 and decadal change in surface ocean pCO₂, and net sea–air CO₂ flux over the global oceans,
- 6 *Deep Sea Research Part II: Topical Studies in Oceanography*, 56, 554–577,
- 7 <https://doi.org/10.1016/j.dsr2.2008.12.009>, 2009.
- 8 Thomason, L. W., Ernest, N., Millán, L., Rieger, L., Bourassa, A., Vernier, J.-P., Manney, G.,
- 9 Luo, B., Arfeuille, F., and Peter, T.: A global space-based stratospheric aerosol climatology:
- 10 1979–2016, 10, 469–492, <https://doi.org/10.5194/essd-10-469-2018>, 2018.
- 11 Tian, H., Xu, X., Lu, C., Liu, M., Ren, W., Chen, G., Melillo, J., and Liu, J.: Net exchanges of
- 12 CO₂, CH₄, and N₂O between China’s terrestrial ecosystems and the atmosphere and their
- 13 contributions to global climate warming, 116, <https://doi.org/10.1029/2010JG001393>, 2011.
- 14 Tian, H., Chen, G., Lu, C., Xu, X., Hayes, D. J., Ren, W., Pan, S., Huntzinger, D. N., and Wofsy,
- 15 S. C.: North American terrestrial CO₂ uptake largely offset by CH₄ and N₂O emissions:
- 16 toward a full accounting of the greenhouse gas budget, *Climatic Change*, 129, 413–426,
- 17 <https://doi.org/10.1007/s10584-014-1072-9>, 2015.
- 18 Todd-Brown, K. E. O., Randerson, J. T., Post, W. M., Hoffman, F. M., Tarnocai, C., Schuur, E.
- 19 A. G., and Allison, S. D.: Causes of variation in soil carbon simulations from CMIP5 Earth
- 20 system models and comparison with observations, *Biogeosciences*, 10, 1717–1736,
- 21 <https://doi.org/10.5194/bg-10-1717-2013>, 2013.
- 22 Tohjima, Y., Mukai, H., Machida, T., Hoshina, Y., and Nakaoka, S.-I.: Global carbon budgets
- 23 estimated from atmospheric O₂/N₂ and CO₂ observations in the western Pacific region over
- 24 a 15-year period, 19, 9269–9285, <https://doi.org/10.5194/acp-19-9269-2019>, 2019.
- 25 Tubiello, F. N., Conchedda, G., Wanner, N., Federici, S., Rossi, S., and Grassi, G.: Carbon
- 26 emissions and removals from forests: new estimates, 1990–2020, 13, 1681–1691,
- 27 <https://doi.org/10.5194/essd-13-1681-2021>, 2021.
- 28 UN: United Nations Statistics Division: National Accounts Main Aggregates Database,



- 1 available at: <http://unstats.un.org/unsd/snaama/Introduction.asp>, last access: 25 October
2 2021, 2021.
- 3 UNFCCC: National Inventory Submissions, available at: [https://unfccc.int/ghg-inventories-
4 annex-i-parties/2021](https://unfccc.int/ghg-inventories-annex-i-parties/2021), last access: 25 October 2021., 2021a.
- 5 UNFCCC: Nationally determined contributions under the Paris Agreement. Synthesis report
6 by the secretariat, available at: <https://unfccc.int/documents/306848>, last access: 25
7 October 2021, 2021b.
- 8 Vale, M. M., Berenguer, E., Argollo de Menezes, M., Viveiros de Castro, E. B., Pugliese de
9 Siqueira, L., and Portela, R. de C. Q.: The COVID-19 pandemic as an opportunity to weaken
10 environmental protection in Brazil, *Biological Conservation*, 255, 108994,
11 <https://doi.org/10.1016/j.biocon.2021.108994>, 2021.
- 12 van der Laan-Luijkx, I. T., van der Velde, I. R., van der Veen, E., Tsuruta, A., Stanislawski, K.,
13 Babenhauserheide, A., Zhang, H. F., Liu, Y., He, W., Chen, H., Masarie, K. A., Krol, M. C., and
14 Peters, W.: The CarbonTracker Data Assimilation Shell (CTDAS) v1.0: implementation and
15 global carbon balance 2001–2015, *Geosci. Model Dev.*, 10, 2785–2800,
16 <https://doi.org/10.5194/gmd-10-2785-2017>, 2017.
- 17 van der Velde, I. R., Miller, J. B., Schaefer, K., van der Werf, G. R., Krol, M. C., and Peters, W.:
18 Terrestrial cycling of ^{13}C by photosynthesis, respiration, and biomass burning in SiBCASA,
19 11, 6553–6571, <https://doi.org/10.5194/bg-11-6553-2014>, 2014.
- 20 van der Velde, I. R., van der Werf, G. R., Houweling, S., Maasackers, J. D., Borsdorff, T.,
21 Landgraf, J., Tol, P., van Kempen, T. A., van Hees, R., Hoogeveen, R., Veefkind, J. P., and
22 Aben, I.: Vast CO_2 release from Australian fires in 2019–2020 constrained by satellite, 597,
23 366–369, <https://doi.org/10.1038/s41586-021-03712-y>, 2021.
- 24 van der Werf, G. R., Randerson, J. T., Giglio, L., Collatz, G. J., Mu, M., Kasibhatla, P. S.,
25 Morton, D. C., DeFries, R. S., Jin, Y., and van Leeuwen, T. T.: Global fire emissions and the
26 contribution of deforestation, savanna, forest, agricultural, and peat fires (1997–2009),
27 *Atmos. Chem. Phys.*, 10, 11707–11735, <https://doi.org/10.5194/acp-10-11707-2010>, 2010.
- 28 van der Werf, G. R., Randerson, J. T., Giglio, L., van Leeuwen, T. T., Chen, Y., Rogers, B. M.,



- 1 Mu, M., van Marle, M. J. E., Morton, D. C., Collatz, G. J., Yokelson, R. J., and Kasibhatla, P. S.:
- 2 Global fire emissions estimates during 1997–2016, *Earth Syst. Sci. Data*, 9, 697–720,
- 3 <https://doi.org/10.5194/essd-9-697-2017>, 2017.
- 4 Viovy, N.: CRUNCEP data set, available at:
- 5 ftp://nacp.ornl.gov/synthesis/2009/frescati/temp/land_use_change/original/readme.htm,
- 6 last access: 25 October 2021, 2016.
- 7 Vuichard, N., Messina, P., Luyssaert, S., Guenet, B., Zaehle, S., Ghattas, J., Bastrikov, V., and
- 8 Peylin, P.: Accounting for carbon and nitrogen interactions in the global terrestrial
- 9 ecosystem model ORCHIDEE (trunk version, rev 4999): multi-scale evaluation of gross
- 10 primary production, *Geosci. Model Dev.*, 12, 4751–4779, [https://doi.org/10.5194/gmd-12-](https://doi.org/10.5194/gmd-12-4751-2019)
- 11 [4751-2019](https://doi.org/10.5194/gmd-12-4751-2019), 2019.
- 12 Walker, A. P., Quaife, T., Bodegom, P. M., De Kauwe, M. G., Keenan, T. F., Joiner, J., Lomas,
- 13 M. R., MacBean, N., Xu, C., Yang, X., and Woodward, F. I.: The impact of alternative trait-
- 14 scaling hypotheses for the maximum photosynthetic carboxylation rate (V_{cmax}) on global
- 15 gross primary production, *New Phytol.*, 215, 1370–1386,
- 16 <https://doi.org/10.1111/nph.14623>, 2017.
- 17 Walker, A. P., De Kauwe, M. G., Bastos, A., Belmecheri, S., Georgiou, K., Keeling, R. F.,
- 18 McMahon, S. M., Medlyn, B. E., Moore, D. J. P., Norby, R. J., Zaehle, S., Anderson-Teixeira, K.
- 19 J., Battipaglia, G., Brienen, R. J. W., Cabugao, K. G., Cailleret, M., Campbell, E., Canadell, J. G.,
- 20 Ciais, P., Craig, M. E., Ellsworth, D. S., Farquhar, G. D., Fatichi, S., Fisher, J. B., Frank, D. C.,
- 21 Graven, H., Gu, L., Haverd, V., Heilman, K., Heimann, M., Hungate, B. A., Iversen, C. M., Joos,
- 22 F., Jiang, M., Keenan, T. F., Knauer, J., Körner, C., Leshyk, V. O., Leuzinger, S., Liu, Y.,
- 23 MacBean, N., Malhi, Y., McVicar, T. R., Penuelas, J., Pongratz, J., Powell, A. S., Riutta, T.,
- 24 Sabot, M. E. B., Schleucher, J., Sitch, S., Smith, W. K., Sulman, B., Taylor, B., Terrer, C., Torn,
- 25 M. S., Treseder, K. K., Trugman, A. T., Trumbore, S. E., van Mantgem, P. J., Voelker, S. L.,
- 26 Whelan, M. E., and Zuidema, P. A.: Integrating the evidence for a terrestrial carbon sink
- 27 caused by increasing atmospheric CO₂, 229, 2413–2445,
- 28 <https://doi.org/10.1111/nph.16866>, 2021.
- 29 Wanninkhof, R.: Relationship between wind speed and gas exchange over the ocean, 97,



- 1 7373–7382, <https://doi.org/10.1029/92JC00188>, 1992.
- 2 Wanninkhof, R.: Relationship between wind speed and gas exchange over the ocean
3 revisited, *12*, 351–362, <https://doi.org/10.4319/lom.2014.12.351>, 2014.
- 4 Wanninkhof, R., Park, G.-H., Takahashi, T., Sweeney, C., Feely, R., Nojiri, Y., Gruber, N.,
5 Doney, S. C., McKinley, G. A., Lenton, A., Le Quéré, C., Heinze, C., Schwinger, J., Graven, H.,
6 and Khatiwala, S.: Global ocean carbon uptake: magnitude, variability and trends,
7 *Biogeosciences*, *10*, 1983–2000, <https://doi.org/10.5194/bg-10-1983-2013>, 2013.
- 8 Watson, A. J., Schuster, U., Shutler, J. D., Holding, T., Ashton, I. G. C., Landschützer, P.,
9 Woolf, D. K., and Goddijn-Murphy, L.: Revised estimates of ocean-atmosphere CO₂ flux are
10 consistent with ocean carbon inventory, *Nat Commun*, *11*, 4422,
11 <https://doi.org/10.1038/s41467-020-18203-3>, 2020.
- 12 Watson, R. T., Rohde, H., Oeschger, H., and Siegenthaler, U.: Greenhouse Gases and
13 Aerosols, in: *Climate Change: The IPCC Scientific Assessment*. Intergovernmental Panel on
14 Climate Change (IPCC), edited by: Houghton, J. T., Jenkins, G. J., and Ephraums, J. J.,
15 Cambridge University Press, Cambridge, 140, 1990.
- 16 Weiss, R. F. and Price, B. A.: Nitrous oxide solubility in water and seawater, *Marine*
17 *Chemistry*, *8*, 347–359, [https://doi.org/10.1016/0304-4203\(80\)90024-9](https://doi.org/10.1016/0304-4203(80)90024-9), 1980.
- 18 Wenzel, S., Cox, P. M., Eyring, V., and Friedlingstein, P.: Projected land photosynthesis
19 constrained by changes in the seasonal cycle of atmospheric CO₂, *Nature*, *538*, 499–501,
20 <https://doi.org/10.1038/nature19772>, 2016.
- 21 Wilkenskjaeld, S., Kloster, S., Pongratz, J., Raddatz, T., and Reick, C. H.: Comparing the
22 influence of net and gross anthropogenic land-use and land-cover changes on the carbon
23 cycle in the MPI-ESM, *Biogeosciences*, *11*, 4817–4828, [https://doi.org/10.5194/bg-11-4817-](https://doi.org/10.5194/bg-11-4817-2014)
24 2014, 2014.
- 25 Wiltshire, A. J., Burke, E. J., Chadburn, S. E., Jones, C. D., Cox, P. M., Davies-Barnard, T.,
26 Friedlingstein, P., Harper, A. B., Liddicoat, S., Sitch, S., and Zaehle, S.: JULES-CN: a coupled
27 terrestrial carbon–nitrogen scheme (JULES vn5.1), *14*, 2161–2186,
28 <https://doi.org/10.5194/gmd-14-2161-2021>, 2021.



- 1 Woodward, F. I. and Lomas, M. R.: Vegetation dynamics – simulating responses to climatic
- 2 change, *Biol. Rev.*, 79, 643–670, <https://doi.org/10.1017/S1464793103006419>, 2004.
- 3 Wright, R. M., Le Quéré, C., Buitenhuis, E., Pitois, S., and Gibbons, M. J.: Role of jellyfish in
- 4 the plankton ecosystem revealed using a global ocean biogeochemical model, 18, 1291–
- 5 1320, <https://doi.org/10.5194/bg-18-1291-2021>, 2021.
- 6 Xi, F., Davis, S. J., Ciais, P., Crawford-Brown, D., Guan, D., Pade, C., Shi, T., Syddall, M., Lv, J.,
- 7 Ji, L., Bing, L., Wang, J., Wei, W., Yang, K.-H., Lagerblad, B., Galan, I., Andrade, C., Zhang, Y.,
- 8 and Liu, Z.: Substantial global carbon uptake by cement carbonation, *Nature Geosci*, 9, 880–
- 9 883, <https://doi.org/10.1038/ngeo2840>, 2016.
- 10 Xia, J., Chen, Y., Liang, S., Liu, D., and Yuan, W.: Global simulations of carbon allocation
- 11 coefficients for deciduous vegetation types, 67, 28016,
- 12 <https://doi.org/10.3402/tellusb.v67.28016>, 2015.
- 13 Yin, X.: Responses of leaf nitrogen concentration and specific leaf area to atmospheric CO₂
- 14 enrichment: a retrospective synthesis across 62 species: Leaf response to atmospheric co₂
- 15 enrichment, 8, 631–642, <https://doi.org/10.1046/j.1365-2486.2002.00497.x>, 2002.
- 16 Yuan, W., Liu, D., Dong, W., Liu, S., Zhou, G., Yu, G., Zhao, T., Feng, J., Ma, Z., Chen, J., Chen,
- 17 Y., Chen, S., Han, S., Huang, J., Li, L., Liu, H., Liu, S., Ma, M., Wang, Y., Xia, J., Xu, W., Zhang,
- 18 Q., Zhao, X., and Zhao, L.: Multiyear precipitation reduction strongly decreases carbon
- 19 uptake over northern China, 119, 881–896, <https://doi.org/10.1002/2014JG002608>, 2014.
- 20 Yue, C., Ciais, P., Luyssaert, S., Li, W., McGrath, M. J., Chang, J., and Peng, S.: Representing
- 21 anthropogenic gross land use change, wood harvest, and forest age dynamics in a global
- 22 vegetation model ORCHIDEE-MICT v8.4.2, 11, 409–428, [https://doi.org/10.5194/gmd-11-](https://doi.org/10.5194/gmd-11-409-2018)
- 23 409-2018, 2018.
- 24 Yue, X. and Unger, N.: The Yale Interactive terrestrial Biosphere model version 1.0:
- 25 description, evaluation and implementation into NASA GISS ModelE2, *Geosci. Model Dev.*, 8,
- 26 2399–2417, <https://doi.org/10.5194/gmd-8-2399-2015>, 2015.
- 27 Zaehle, S. and Friend, A. D.: Carbon and nitrogen cycle dynamics in the O-CN land surface
- 28 model: 1. Model description, site-scale evaluation, and sensitivity to parameter estimates:



- 1 Site-scale evaluation of a C-N model, *Global Biogeochem. Cycles*, 24,
- 2 <https://doi.org/10.1029/2009GB003521>, 2010.

- 3 Zaehle, S., Ciais, P., Friend, A. D., and Prieur, V.: Carbon benefits of anthropogenic reactive
- 4 nitrogen offset by nitrous oxide emissions, *Nature Geosci*, 4, 601–605,
- 5 <https://doi.org/10.1038/ngeo1207>, 2011.

- 6 Zeng, J., Nojiri, Y., Landschützer, P., Telszewski, M., and Nakaoka, S.: A Global Surface Ocean
- 7 fCO₂ Climatology Based on a Feed-Forward Neural Network, 31, 1838–1849,
- 8 <https://doi.org/10.1175/JTECH-D-13-00137.1>, 2014.

- 9 Zheng, B., Chevallier, F., Yin, Y., Ciais, P., Fortems-Cheiney, A., Deeter, M. N., Parker, R. J.,
- 10 Wang, Y., Worden, H. M., and Zhao, Y.: Global atmospheric carbon monoxide budget 2000–
- 11 2017 inferred from multi-species atmospheric inversions, 26, 2019.

- 12 Zheng, B., Ciais, P., Chevallier, F., Chuvieco, E., Chen, Y., and Yang, H.: Increasing forest fire
- 13 emissions despite the decline in global burned area, 7, eabh2646,
- 14 <https://doi.org/10.1126/sciadv.abh2646>, 2021.

- 15 Zscheischler, J., Mahecha, M. D., Avitabile, V., Calle, L., Carvalhais, N., Ciais, P., Gans, F.,
- 16 Gruber, N., Hartmann, J., Herold, M., Ichii, K., Jung, M., Landschützer, P., Laruelle, G. G.,
- 17 Lauerwald, R., Papale, D., Peylin, P., Poulter, B., Ray, D., Regnier, P., Rödenbeck, C., Roman-
- 18 Cuesta, R. M., Schwalm, C., Tramontana, G., Tyukavina, A., Valentini, R., van der Werf, G.,
- 19 West, T. O., Wolf, J. E., and Reichstein, M.: Reviews and syntheses: An empirical
- 20 spatiotemporal description of the global surface–atmosphere carbon fluxes: opportunities
- 21 and data limitations, *Biogeosciences*, 14, 3685–3703, [https://doi.org/10.5194/bg-14-3685-](https://doi.org/10.5194/bg-14-3685-2017)
- 22 2017, 2017.

- 23
- 24
- 25
- 26
- 27



1 Tables

Table 1. Factors used to convert carbon in various units (by convention, Unit 1 = Unit 2 × conversion).			
Unit 1	Unit 2	Conversion	Source
GtC (gigatonnes of carbon)	ppm (parts per million) (a)	2.124 (b)	Ballantyne et al. (2012)
GtC (gigatonnes of carbon)	PgC (petagrams of carbon)		1 SI unit conversion
GtCO ₂ (gigatonnes of carbon dioxide)	GtC (gigatonnes of carbon)		3.664 44.01/12.011 in mass equivalent
GtC (gigatonnes of carbon)	MtC (megatonnes of carbon)		1000 SI unit conversion
(a) Measurements of atmospheric CO ₂ concentration have units of dry-air mole fraction. ‘ppm’ is an abbreviation for micromole/mol, dry air.			
(b) The use of a factor of 2.124 assumes that all the atmosphere is well mixed within one year. In reality, only the troposphere is well mixed and the growth rate of CO ₂ concentration in the less well-mixed stratosphere is not measured by sites from the NOAA network. Using a factor of 2.124 makes the approximation that the growth rate of CO ₂ concentration in the stratosphere equals that of the troposphere on a yearly basis.			

2



1

Table 2. How to cite the individual components of the global carbon budget presented here.	
Component	Primary reference
Global fossil CO ₂ emissions (EFOS), total and by fuel type	Andrew and Peters (2021)
National territorial fossil CO ₂ emissions (EFOS)	Gilfillan and Marland (2021), UNFCCC (2021a)
National consumption-based fossil CO ₂ emissions (EFOS) by country (consumption)	Peters et al. (2011b) updated as described in this paper
Net land-use change flux (ELUC)	This paper (see Table 4 for individual model references).
Growth rate in atmospheric CO ₂ concentration (GATM)	Dlugokencky and Tans (2021)
Ocean and land CO ₂ sinks (SOCEAN and SLAND)	This paper (see Table 4 for individual model references).

2



1

Table 3. Main methodological changes in the global carbon budget since 2017. Methodological changes introduced in one year are kept for the following years unless noted. Empty cells mean there were no methodological changes introduced that year. Table A7 lists methodological changes from the first global carbon budget publication up to 2016.

Publication year	Fossil fuel emissions		LUC emissions	Reservoirs			Uncertainty & other changes
	Global	Country (territorial)		Atmosphere	Ocean	Land	
2017	Projection includes India-specific data		Average of two bookkeeping models; use of 12 DGVMs		Based on eight models that match the observed sink for the 1990s; no longer normalised	Based on 15 models that meet observation-based criteria (see Sect. 2.5)	Land multi-model average now used in main carbon budget, with the carbon imbalance presented separately; new table of key uncertainties
Le Quéré et al. (2018a) GCB2017							
2018	Revision in cement emissions; Projection includes EU-specific data	Aggregation of overseas territories into governing nations for total of 213 countries a	Average of two bookkeeping models; use of 16 DGVMs	Use of four atmospheric inversions	Based on seven models	Based on 16 models; revised atmospheric forcing from CRUNCEP to CRU-JRA-55	Introduction of metrics for evaluation of individual models using observations
Le Quéré et al. (2018b) GCB2018							
2019	Global emissions calculated as sum of all countries plus bunkers, rather than taken directly from CDIAC.		Average of two bookkeeping models; use of 15 DGVMs	Use of three atmospheric inversions	Based on nine models	Based on 16 models	
Friedlingstein et al. (2019) GCB2019							
2020	Cement carbonation now included in the EFOS estimate, reducing EFOS by about 0.2GtC yr ⁻¹ for the last decade	India's emissions from Andrew (2020: India); Corrections to Netherland Antilles and Aruba and Soviet emissions before 1950 as per Andrew (2020: CO ₂);	Average of three bookkeeping models; use of 17 DGVMs. Estimate of gross land use sources and sinks provided	Use of six atmospheric inversions	Based on nine models. River flux revised and partitioned NH, Tropics, SH	Based on 17 models	
Friedlingstein et al. (2020) GCB2020							



		China's coal emissions in 2019 derived from official statistics, emissions now shown for EU27 instead of EU28. Projection for 2020 based on assessment of four approaches.					
2021	Projections are no longer an assessment of four approaches.	Official data included for a number of additional countries, new estimates for South Korea, added emissions from lime production in China.	ELUC estimate compared to the estimates adopted in national GHG inventories (NGHGI)		Average of means of eight models and means of seven data-products. Current year prediction of SOCEAN using a feed-forward neural network method	Current year prediction of SLAND using a feed-forward neural network method	
Friedlingstein et al. (2021) GCB2021 (This study)							

1



1

Table 4. References for the process models, fCO₂-based ocean data products, and atmospheric inversions. All models and products are updated with new data to end of year 2020, and the atmospheric forcing for the DGVMs has been updated as described in Section 2.2.2.

Model/data name	Reference	Change from Global Carbon Budget 2020 (Friedlingstein et al., 2020)
<i>Bookkeeping models for land-use change emissions</i>		
BLUE	Hansis et al. (2015)	No change to model, but simulations performed with updated LUH2 forcing.
updated H&N2017	Houghton and Nassikas (2017)	Adjustment to treatment of harvested wood products. Update to FRA2020 and 2021 FAOSTAT for forest cover and land-use areas. Forest loss in excess of increases in cropland and pastures represented an increase in shifting cultivation. Extratropical peatland drainage emissions added (based on Qiu et al., 2021).
OSCAR	Gasser et al. (2020)	Update to OSCAR3.1.2, which provides finer resolution (96 countries/regions). LUH2-TRENDYv8 input data replaced by LUH2-TRENDYv10. FRA2015 (Houghton & Nassikas, 2017) still used as a second driving dataset, with emissions from FRA2015 extended to 2020. Constraining based on this year's budget data.
<i>Dynamic global vegetation models</i>		
CABLE-POP	Haverd et al. (2018)	changes in parameterisation, minor bug fixes
CLASSIC	Melton et al. (2020) (a)	Non-structural carbohydrates are now explicitly simulated.
CLM5.0	Lawrence et al. (2019)	No Change.
DLEM	Tian et al. (2015) (b)	Updated algorithms for land use change processes.
IBIS	Yuan et al. (2014) (c)	Several changes in parameterisation; Dynamic carbon allocation scheme.
ISAM	Meiyappan et al. (2015) (d)	ISAM now accounting for vertically-resolved soil biogeochemistry (carbon and nitrogen) module (Shu et al., 2020)
ISBA-CTRIP	Delire et al. (2020) (e)	Updated spinup protocol + model name updated (SURFEXv8 in GCB2017) + inclusion of crop harvesting module
JSBACH	Reick et al. (2021) (f)	Wood product pools per plant functional type.
JULES-ES	Wiltshire et al. (2021) (g)	Version 1.1 Inclusion of interactive fire Burton et al., (2019)
LPJ-GUESS	Smith et al. (2014) (h)	No code change. Using updated LUH2 and climate forcings.
LPJ	Poulter et al. (2011) (i)	Updated soil data from FAO to HWSD v2.0



LPX-Bern	Lienert and Joos (2018)	No Change.
OCN	Zaehle and Friend (2010) (j)	No change (uses r294).
ORCHIDEEv3	Vuichard et al. (2019) (k)	Updated growth respiration scheme (revision 7267)
SDGVM	Walker et al. (2017) (l)	No changes from version used in Friedlingstein et al. (2019), except for properly switching from grasslands to pasture in the blending of the ESA data with LUH2; this change affects mostly the semi-arid lands.
VISIT	Kato et al. (2013) (m)	Minor bug fix on CH4 emissions of recent few years.
YIBs	Yue and Unger (2015)	Inclusion of nutrient limit with down regulation approach of Arora et al. (2009)
<i>Global ocean biogeochemistry models</i>		
NEMO-PlankTOM12	Wright et al. (2021) (n)	Updated biochemical model to include 12 functional types. Change to spin-up, now using a looped 1990.
MICOM-HAMOCC (NorESM-OCv1.2)	Schwinger et al. (2016)	No change
MPIOM-HAMOCC6	Lacroix et al. (2021)	Added riverine fluxes; cmip6 model version including modifications and bug-fixes in HAMOCC and MPIOM
NEMO3.6-PISCESv2-gas (CNRM)	Berthet et al. (2019) (o)	small bug fixes; updated model-spin-up (new forcings); atm forcing is now JRA55-Do including 2020 year and varying riverine freshwater inputs
FESOM-2.1-REcoM2	Hauck et al. (2020) (p)	Updated physical model version FESOM2.1, and including 2nd zooplankton and 2nd detritus group. Used new atmospheric CO2 time series provided by GCB
MOM6-COBALT (Princeton)	Liao et al. (2020)	Adjustment of the piston velocity prefactor (0.337 cph/m ² /s ² to 0.251 cph/m ² /s ²). MOM6 update from GitHub version b748b1b (2018-10-03) to version 69a096b (2021-02-24). Updated model spin-up and simulation using JRA55-do v1.5. Used new atmospheric CO2 time series provided by GCB.
CESM-ETHZ	Doney et al. (2009)	No change in the model. Used new atmospheric CO2 time series provided by GCB
NEMO-PISCES (IPSL)	Aumont et al. (2015)	No change
<i>ocean fCO2-based data products</i>		
Landschützer (MPI-SOMFFN)	Landschützer et al. (2016)	update to SOCATv2021 measurements and time period 1982-2020; The estimate now covers the full open ocean and coastal domain as well as the Arctic Ocean extension described in Landschützer et al. (2020)
Rödenbeck (Jena-MLS)	Rödenbeck et al. (2014)	update to SOCATv2021 measurements, time period extended to 1957-2020, involvement of a multi-linear regression for extrapolation (combined with an explicitly interannual correction), use of OCIM (deVries, 2014) as decadal prior, carbonate chemistry parameterization now time-dependent, grid resolution increased to 2.5*2 degrees, adjustable degrees



		of freedom now also covering shallow areas and Arctic, some numerical revisions
CMEMS-LSCE-FFNNv2	Chau et al. (2021)	Update to SOCATv2021 measurements and time period 1985-2020. The CMEMS-LSCE-FFNNv2 product now covers both the open ocean and coastal regions (see in Chau et al. 2021 for model description and evaluation).
CSIR-ML6	Gregor et al. (2019)	Updated to SOCATv2021. Reconstruction now spans the period 1985 - 2020 and includes updates using the SeaFlux protocols (Fay et al., 2021b)
Watson et al	Watson et al. (2020)	Updated to SOCAT v2021. A monthly climatology of the skin temperature deviation as calculated for years 2003-2011 is now used in place of a single global average figure. SOM calculation updated to treat the Arctic as a separate biome.
NIES-NN	Zeng et al. (2014)	New this year
JMA-MLR	Iida et al. (2021)	New this year
OS-ETHZ-GRaCER	Gregor and Gruber (2021)	New this year
<i>Atmospheric inversions</i>		
CAMS	Chevallier et al. (2005) (q)	No change.
CarbonTracker Europe (CTE)	van der Laan-Luijkx et al. (2017)	No change.
Jena CarboScope	Rödenbeck et al. (2018) (r)	No change.
UoE in-situ	Feng et al., (2016) (s)	Fossil fuels now from GCP-GridFEDv2021.2
NISMON-CO2	Niwa et al., (2017) (t)	Some inversion parameters were changed.
CMS-Flux	Liu et al., (2021)	New this year
(a) see also Asaadi et al. (2018).		
(b) see also Tian et al. (2011)		
(c) the dynamic carbon allocation scheme was presented by Xia et al. (2015)		
(d) see also Jain et al. (2013). Soil biogeochemistry is updated based on Shu et al. (2020)		
(e) see also Decharme et al. (2019) and Seferian et al. (2019)		
(f) Mauritsen et al. (2019)		
(g) see also Sellar et al. (2019) and Burton et al., (2019). JULES-ES is the Earth System configuration of the Joint UK Land Environment Simulator as used in the UK Earth System Model (UKESM).		
(h) to account for the differences between the derivation of shortwave radiation from CRU cloudiness and DSWRF from CRUJRA, the photosynthesis scaling parameter α was modified (-15%) to yield similar results.		



(i) compared to published version, decreased LPJ wood harvest efficiency so that 50 % of biomass was removed off-site compared to 85 % used in the 2012 budget. Residue management of managed grasslands increased so that 100 % of harvested grass enters the litter pool.
(j) see also Zaehle et al. (2011).
(k) see also Zaehle and Friend (2010) and Krinner et al. (2005)
(l) see also Woodward and Lomas (2004)
(m) see also Ito and Inatomi (2012).
(n) see also Buitenhuis et al. (2013)
(o) see also Séférian et al. (2019)
(p) see also Schourup-Kristensen et al (2014)
(q) see also Remaud (2018)
(r) see also Rödenbeck et al. (2003)
(s) see also Feng et al. (2009) and Palmer et al. (2019)
(t) see also Niwa et al. (2020)



1
2
3
4
5
6

Table 5. Comparison of results from the bookkeeping method and budget residuals with results from the DGVMs and inverse estimates for different periods, the last decade, and the last year available. All values are in GtCyr⁻¹. The DGVM uncertainties represent $\pm 1\sigma$ of the decadal or annual (for 2020 only) estimates from the individual DGVMs: for the inverse models the range of available results is given. All values are rounded to the nearest 0.1 GtC and therefore columns do not necessarily add to zero.

	Mean (GtC/yr)						
	1960s	1970s	1980s	1990s	2000s	2011-2020	2020
Land-use change emissions (ELUC)							
Bookkeeping methods - net flux (1a)	1.6±0.7	1.3±0.7	1.2±0.7	1.3±0.7	1.2±0.7	1.1±0.7	0.9±0.7
Bookkeeping methods - source	3.4±0.9	3.3±0.8	3.4±0.8	3.6±0.6	3.7±0.6	3.8±0.6	3.6±0.6
Bookkeeping methods - sink	-1.9±0.4	-2±0.4	-2.1±0.3	-2.3±0.4	-2.5±0.4	-2.7±0.4	-2.8±0.4
DGVMs-net flux (1b)	1.6±0.5	1.3±0.4	1.4±0.5	1.4±0.5	1.4±0.5	1.5±0.5	1.4±0.7
Terrestrial sink (SLAND)							
Residual sink from global budget (EFOS+ELUC-GATM-SOCEAN) (2a)	1.8±0.8	1.9±0.8	1.6±0.9	2.5±0.9	2.7±0.9	2.8±0.9	2.1±0.9
DGVMs (2b)	1.2±0.5	2±0.5	1.8±0.5	2.3±0.4	2.6±0.5	3.1±0.6	2.9±1
Total land fluxes (SLAND-ELUC)							
GCB2021 Budget (2b-1a)	-0.4±0.8	0.8±0.8	0.5±0.9	1±0.8	1.4±0.9	1.9±0.9	2±1.2
Budget constraint (2a-1a)	0.2±0.4	0.6±0.5	0.3±0.5	1.2±0.5	1.5±0.6	1.7±0.6	1.3±0.6
DGVMs-net (2b-1b)	-0.4±0.6	0.7±0.4	0.3±0.4	0.9±0.4	1.2±0.4	1.6±0.6	1.5±0.8
Inversions*	---	---	0.5-0.6 (2)	0.9-1.2 (3)	1.3-1.8 (3)	1.3-2 (6)	-0.1-1.3 (6)

* Estimates are adjusted for the pre-industrial influence of river fluxes, for the cement carbonation sink, and adjusted to common EFOS (Sect. 2.6). The ranges given include varying numbers (in parentheses) of inversions in each decade (Table A4)

7



1
 2 **Table 6. Decadal mean in the five components of the anthropogenic CO₂ budget for different periods, and**
 3 **last year available. All values are in GtC yr⁻¹, and uncertainties are reported as ±1σ. Fossil CO₂ emissions**
 4 **include cement carbonation. The table also shows the budget imbalance (B_{IM}), which provides a measure of**
 5 **the discrepancies among the nearly independent estimates and has an uncertainty exceeding ± 1 GtC yr⁻¹. A**
 6 **positive imbalance means the emissions are overestimated and/or the sinks are too small. All values are**
 7 **rounded to the nearest 0.1 GtC and therefore columns do not necessarily add to zero.**

	Mean (GtC/yr)							
	1960s	1970s	1980s	1990s	2000s	2011-2020	2020	2021 (Projection)
Total emissions (EFOS + ELUC)								
Fossil CO ₂ emissions (EFOS)*	3±0.2	4.7±0.2	5.5±0.3	6.3±0.3	7.7±0.4	9.5±0.5	9.3±0.5	9.7±0.5
Land-use change emissions (ELUC)	1.6±0.7	1.3±0.7	1.2±0.7	1.3±0.7	1.2±0.7	1.1±0.7	0.9±0.7	0.8±0.7
Total emissions	4.6±0.7	5.9±0.7	6.7±0.8	7.7±0.8	9±0.8	10.6±0.8	10.2±0.8	10.5±0.9
Partitioning								
Growth rate in atmos CO ₂ (GATM)	1.7±0.07	2.8±0.07	3.4±0.02	3.1±0.02	4±0.02	5.1±0.02	5±0.2	4.2±0.4
Ocean sink (SOCEAN)	1.1±0.4	1.3±0.4	1.8±0.4	2±0.4	2.2±0.4	2.8±0.4	3±0.4	2.9±0.4
Terrestrial sink (SLAND)	1.2±0.5	2±0.5	1.8±0.5	2.3±0.4	2.6±0.5	3.1±0.6	2.9±1	3.3±1
Budget Imbalance								
BIM=EFOS+ELUC-(GATM+SOCEAN+SLAND)	0.6	-0.2	-0.2	0.2	0.1	-0.3	-0.8	0.1

* Fossil emissions excluding the cement carbonation sink amount to 3.1±0.2 GtC/yr, 4.7±0.2 GtC/yr, 5.5±0.3 GtC/yr, 6.4±0.3 GtC/yr, 7.9±0.4 GtC/yr, and 9.7±0.5 GtC/yr for the decades 1960s to 2010s respectively and to 9.5±0.5 GtC/yr for 2020.

8



1

Table 7. Comparison of the projection with realised fossil CO₂ emissions (EFOS). The ‘Actual’ values are first the estimate available using actual data, and the ‘Projected’ values refers to estimates made before the end of the year for each publication. Projections based on a different method from that described here during 2008-2014 are available in Le Quéré et al., (2016). All values are adjusted for leap years.

	World		China		USA		EU28 (h)		India		Rest of World	
	Project ed	Actual	Projec ted	Actual	Projec ted	Actual	Projec ted	Actual	Projec ted	Actual	Projec ted	Actual
2015 (a)	-0.6%	0.06%	-3.9%	-0.7%	-1.5%	-2.5%	-	-	-	-	1.2%	1.2%
	(-1.6 to 0.5)		(-4.6 to -1.1)		(-5.5 to 0.3)						(-0.2 to 2.6)	
2016 (b)	-0.2%	0.20%	-0.5%	-0.3%	-1.7%	-2.1%	-	-	-	-	1.0%	1.3%
	(-1.0 to +1.8)		(-3.8 to +1.3)		(-4.0 to +0.6)						(-0.4 to +2.5)	
2017 (c)	2.0%	1.6%	3.5%	1.5%	-0.4%	-0.5%	-	-	2.00%	3.9%	1.6%	1.9%
	(+0.8 to +3.0)		(+0.7 to +5.4)		(-2.7 to +1.0)				(+0.2 to +3.8)		(0.0 to +3.2)	
2018 (d)	2.7%	2.1%	4.7%	2.3%	2.5%	2.8%	-0.7%	-2.1%	6.3%	8.0%	1.8%	1.7%
	(+1.8 to +3.7)		(+2.0 to +7.4)		(+0.5 to +4.5)		(-2.6 to +1.3)		(+4.3 to +8.3)		(+0.5 to +3.0)	
2019 (e)	0.5%	0.1%	2.6%	2.2%	-2.4%	-2.6%	-1.7%	-4.3%	1.8%	1.0%	0.5%	0.5%
	(-0.3 to +1.4)		(+0.7 to +4.4)		(-4.7 to -0.1)		(-5.1% to +1.8%)		(-0.7 to +3.7)		(-0.8 to +1.8)	
2020 (f)	-6.7%	-5.4%	-1.7%	1.4%	-12.2%	-10.6%	-11.3%	-10.9%	-9.1%	-7.3%	-7.4%	-7.0%
2021 (g)	4.9%		4.0%		7.6%		7.6%		12.6%		2.9%	
	(4.1% to 5.7%)		(2.1% to 5.8%)		(5.3% to 10.0%)		(5.6% to 9.5%)		(10.7% to 13.6%)		(1.8% to 4.1%)	

(a) Jackson et al. (2016) and Le Quéré et al. (2015a). (b) Le Quéré et al. (2016). (c) Le Quéré et al. (2018a). (d) Le Quéré et al. (2018b). (e) Friedlingstein et al., (2019), (f) Friedlingstein et al., (2020), (g) This study (median of four reported estimates, Section 3.4.1.2)

(h) EU28 until 2019, EU27 from 2020

2



1
 2 **Table 8. Cumulative CO₂ for different time periods in gigatonnes of carbon (GtC). All uncertainties are reported as**
 3 **±1σ. Fossil CO₂ emissions include cement carbonation. The budget imbalance (B_{IM}) provides a measure of the**
 4 **discrepancies among the nearly independent estimates. All values are rounded to the nearest 5 GtC and therefore**
 5 **columns do not necessarily add to zero.**

	1750-2020	1850-2014	1850-2020	1960-2020	1850-2021
Emissions					
Fossil CO ₂ emissions (EFOS)	460±25	400±20	455±25	375±20	465±25
Land-use change emissions (ELUC)	235±75	195±60	200±65	80±45	205±65
Total emissions	690±80	595±65	660±65	455±45	670±65
Partitioning					
Growth rate in atmos CO ₂ (GATM)	290±5	235±5	270±5	205±5	270±5
Ocean sink (SOCEAN)	180±35	150±30	170±35	115±25	170±35
Terrestrial sink (SLAND)	215±50	180±40	195±45	135±25	200±45
Budget imbalance					
BIM=EFOS+ELUC-(GATM+SOCEAN+SLAND)	10	30	25	0	25

6



1

Table 9. Major known sources of uncertainties in each component of the Global Carbon Budget, defined as input data or processes that have a demonstrated effect of at least ± 0.3 GtC yr⁻¹.

Source of uncertainty	Time scale (years)	Location	Status	Evidence
Fossil CO₂ emissions (EFOS; Section 2.1)				
energy statistics	annual to decadal	global, but mainly China & major developing countries	see Sect. 2.1	(Korsbakken et al., 2016, Guan et al., 2012)
carbon content of coal	annual to decadal	global, but mainly China & major developing countries	see Sect. 2.1	(Liu et al., 2015)
system boundary	annual to decadal	all countries	see Sect. 2.1	(Andrew, 2020)
Net land-use change flux (ELUC; section 2.2)				
land-cover and land-use change statistics	continuous	global; in particular tropics	see Sect. 2.2	(Houghton et al., 2012; Gasser et al., 2020)
sub-grid-scale transitions	annual to decadal	global	see Table A1	(Wilenskield et al., 2014)
vegetation biomass	annual to decadal	global; in particular tropics	see Table A1	(Houghton et al., 2012)
forest degradation (fire, selective logging)	annual to decadal	tropics		(Aragão et al., 2018; Qin et al., 2020)
wood and crop harvest	annual to decadal	global; SE Asia	see Table A1	(Arneth et al., 2017, Erb et al., 2018)
peat burning (a)	multi-decadal trend	global	see Table A1	(van der Werf et al., 2010, 2017)
loss of additional sink capacity	multi-decadal trend	global	not included; see Appendix D1.4	(Pongratz et al, 2014, Gasser et al, 2020; Obermeier et al., 2021)
Atmospheric growth rate (GATM; section 2.3) no demonstrated uncertainties larger than ± 0.3 GtC yr⁻¹ (b)				
Ocean sink (SOCEAN; section 2.4)				

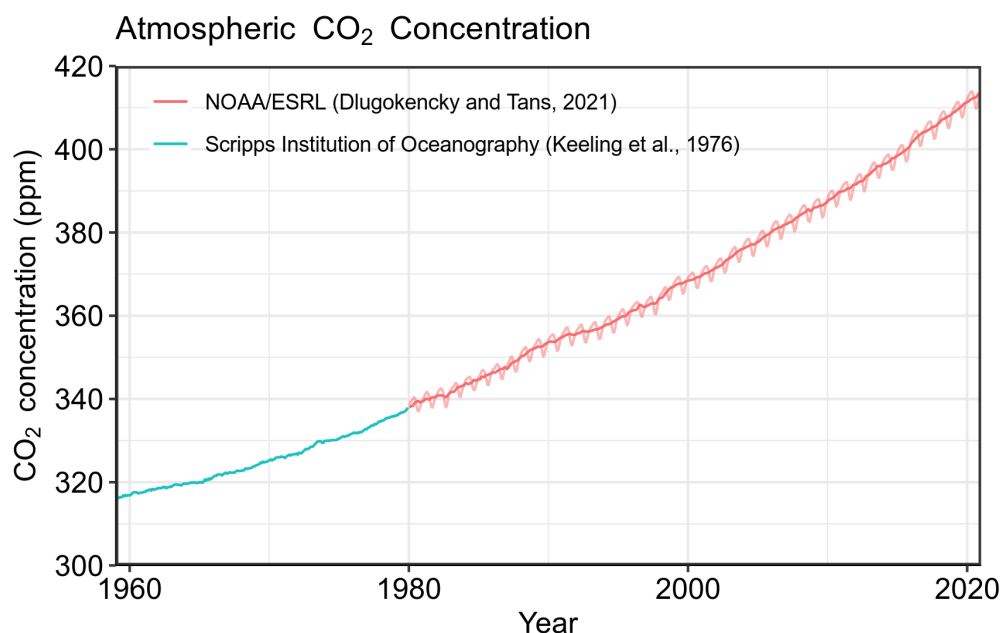


sparsity in surface fCO ₂ observations	mean, decadal variability and trend	global, in particular southern hemisphere	see Sect 3.5.2	(Gloege et al., 2021, Denvil-Sommer et al., 2021, Bushinsky et al., 2019)
riverine carbon outgassing and its anthropogenic perturbation	annual to decadal	global, in particular partitioning between Tropics and South	see Sect. 2.4 (anthropogenic perturbations not included)	(Aumont et al., 2001, Resplandy et al., 2018, Lacroix et al., 2020)
interior ocean anthropogenic carbon storage	annual to decadal	global	see Sect 3.5.5	(Gruber et al., 2019)
near-surface temperature and salinity gradients	mean on all time-scales	global	see Sect. 3.8.2	(Watson et al., 2020)
Land sink (SLAND; section 2.5)				
strength of CO ₂ fertilisation	multi-decadal trend	global	see Sect. 2.5	(Wenzel et al., 2016; Walker et al., 2021)
response to variability in temperature and rainfall	annual to decadal	global; in particular tropics	see Sect. 2.5	(Cox et al., 2013; Jung et al., 2017; Humphrey et al., 2018; 2021)
nutrient limitation and supply				
tree mortality	annual	global in particular tropics	see Sect. 2.5	(Hubau et al., 2021; Brienen et al., 2020)
response to diffuse radiation	annual	global	see Sect. 2.5	(Mercado et al., 2009; O'Sullivan et al., 2021)
a As result of interactions between land-use and climate				
b The uncertainties in GATM have been estimated as ± 0.2 GtC yr ⁻¹ , although the conversion of the growth rate into a global annual flux assuming instantaneous mixing throughout the atmosphere introduces additional errors that have not yet been quantified.				

1



1 Figures and Captions



2

3 **Figure 1.** Surface average atmospheric CO₂ concentration (ppm). Since 1980, monthly data are
4 from NOAA/ESRL (Dlugokencky and Tans, 2021) and are based on an average of direct
5 atmospheric CO₂ measurements from multiple stations in the marine boundary layer (Masarie and
6 Tans, 1995). The 1958-1979 monthly data are from the Scripps Institution of Oceanography, based
7 on an average of direct atmospheric CO₂ measurements from the Mauna Loa and South Pole
8 stations (Keeling et al., 1976). To account for the difference of mean CO₂ and seasonality between
9 the NOAA/ESRL and the Scripps station networks used here, the Scripps surface average (from two
10 stations) was de-seasonalised and adjusted to match the NOAA/ESRL surface average (from
11 multiple stations) by adding the mean difference of 0.667 ppm, calculated here from overlapping
12 data during 1980-2012.

13

14

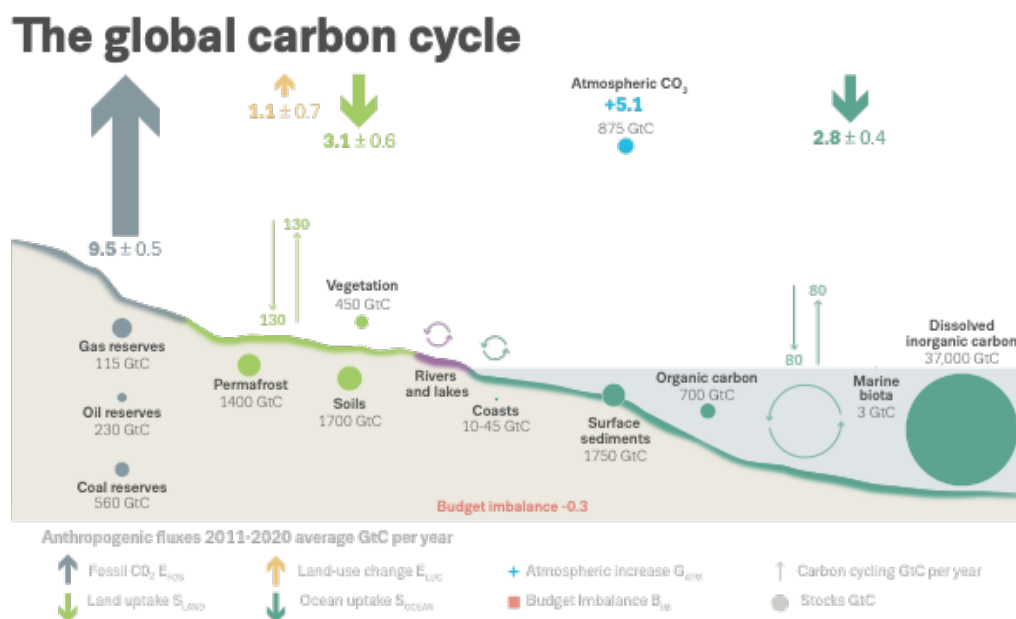
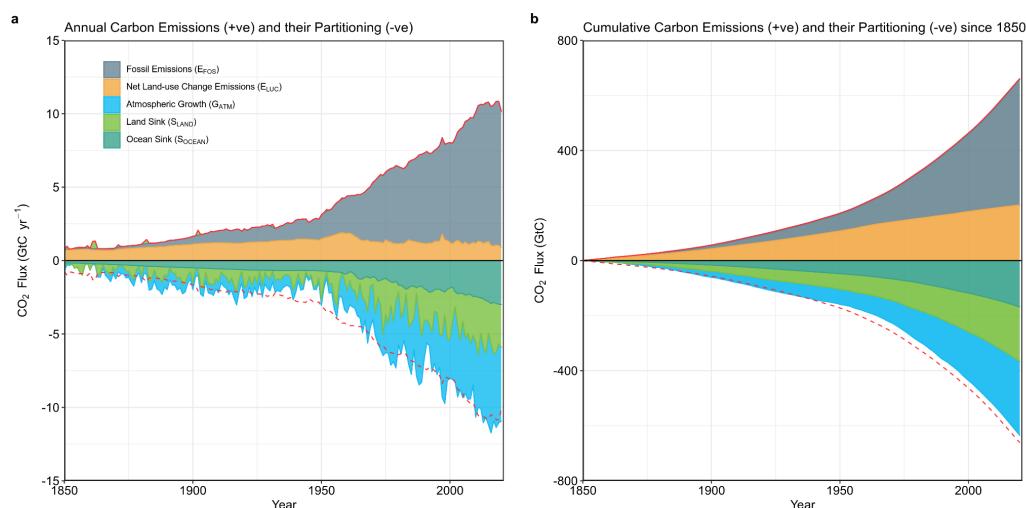
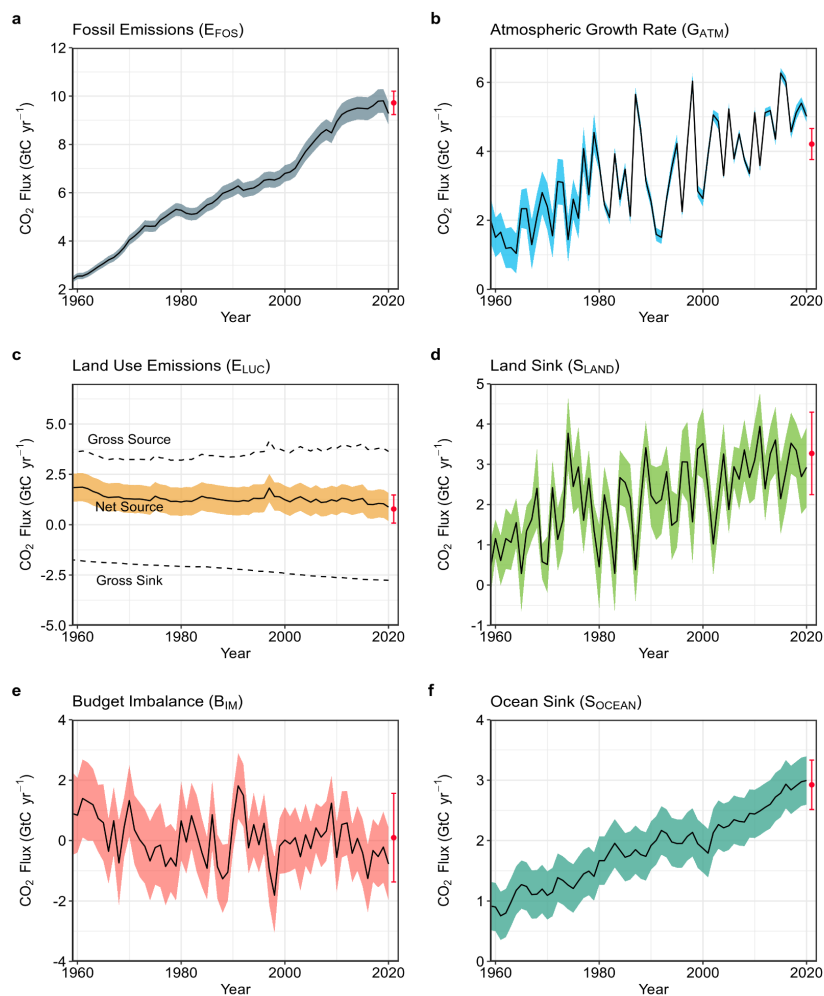


Figure 2. Schematic representation of the overall perturbation of the global carbon cycle caused by anthropogenic activities, averaged globally for the decade 2011-2020. See legends for the corresponding arrows and units. The uncertainty in the atmospheric CO₂ growth rate is very small (± 0.02 GtC yr⁻¹) and is neglected for the figure. The anthropogenic perturbation occurs on top of an active carbon cycle, with fluxes and stocks represented in the background and taken from Canadell et al. (2021) for all numbers, except for the carbon stocks in coasts which is from a literature review of coastal marine sediments (Price and Warren, 2016).



1

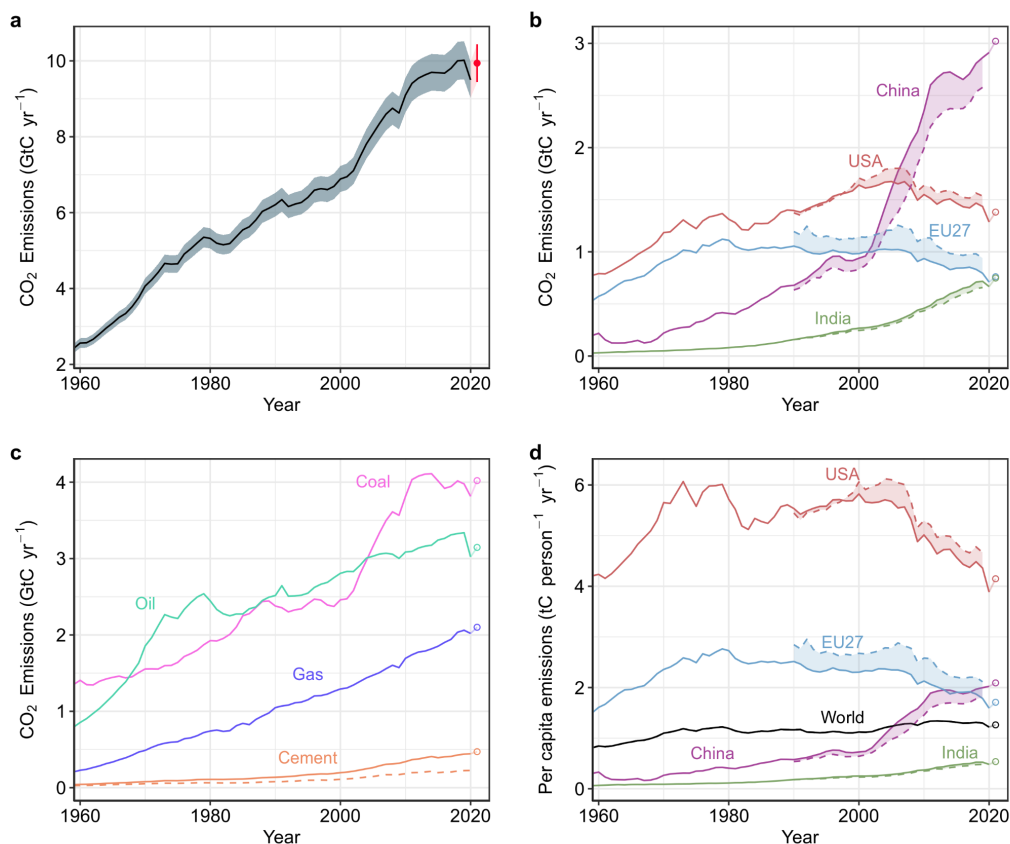
2 **Figure 3.** Combined components of the global carbon budget illustrated in Fig. 2 as a function of
3 time, for fossil CO₂ emissions (E_{FOS} , including a small sink from cement carbonation; grey) and
4 emissions from land-use change (E_{LUC} ; brown), as well as their partitioning among the atmosphere
5 (G_{ATM} ; cyan), ocean (S_{OCEAN} ; blue), and land (S_{LAND} ; green). Panel (a) shows annual estimates of
6 each flux and panel (b) the cumulative flux (the sum of all prior annual fluxes) since the year 1850.
7 The partitioning is based on nearly independent estimates from observations (for G_{ATM}) and from
8 process model ensembles constrained by data (for S_{OCEAN} and S_{LAND}) and does not exactly add up
9 to the sum of the emissions, resulting in a budget imbalance (BI_M) which is represented by the
10 difference between the bottom red line (mirroring total emissions) and the sum of carbon fluxes
11 in the ocean, land, and atmosphere reservoirs. All data are in $GtC\ yr^{-1}$ (panel a) and GtC (panel b).
12 The E_{FOS} estimates are primarily from (Gilfillan and Marland, 2021), with uncertainty of about $\pm 5\%$
13 ($\pm 1\sigma$). The E_{LUC} estimates are from three bookkeeping models (Table 4) with uncertainties of about
14 $\pm 0.7\ GtC\ yr^{-1}$. The G_{ATM} estimates prior to 1959 are from Joos and Spahni (2008) with uncertainties
15 equivalent to about $\pm 0.1\text{--}0.15\ GtC\ yr^{-1}$ and from Dlugokencky and Tans (2021) since 1959 with
16 uncertainties of about $\pm 0.07\ GtC\ yr^{-1}$ during 1959–1979 and $\pm 0.02\ GtC\ yr^{-1}$ since 1980. The S_{OCEAN}
17 estimate is the average from Khatiwala et al. (2013) and DeVries (2014) with uncertainty of about
18 $\pm 30\%$ prior to 1959, and the average of an ensemble of models and an ensemble of fCO_2 data
19 products (Table 4) with uncertainties of about $\pm 0.4\ GtC\ yr^{-1}$ since 1959. The S_{LAND} estimate is the
20 average of an ensemble of models (Table 4) with uncertainties of about $\pm 1\ GtC\ yr^{-1}$. See the text
21 for more details of each component and their uncertainties.



1
2

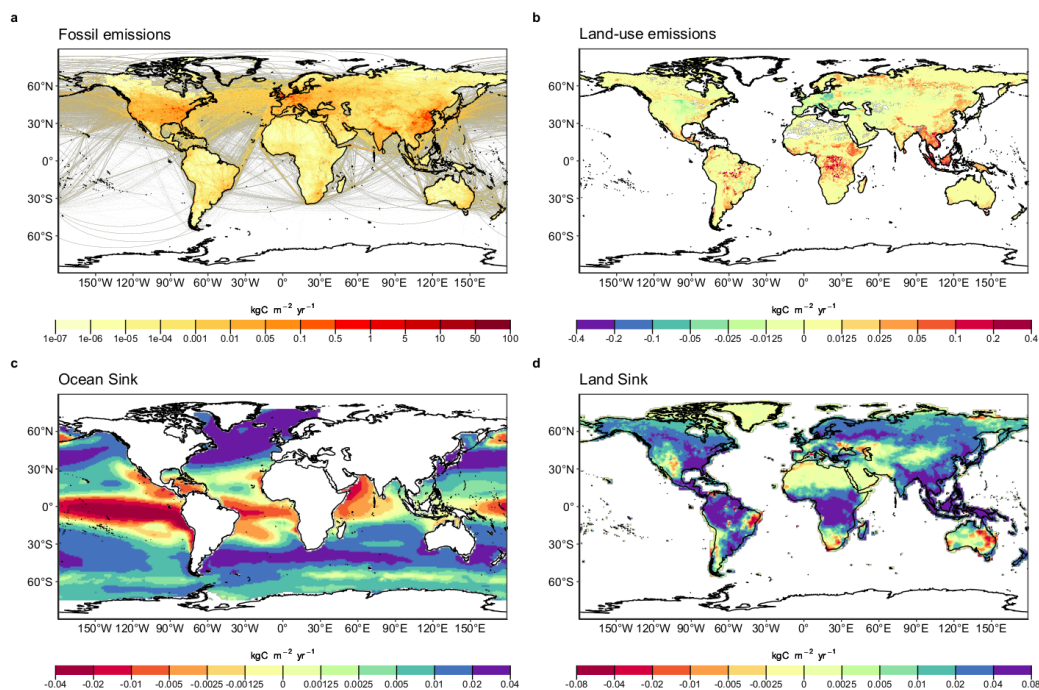
3 **Figure 4.** Components of the global carbon budget and their uncertainties as a function of time,
4 presented individually for (a) fossil CO₂ emissions (E_{FOS}), (b) growth rate in atmospheric CO₂
5 concentration (G_{ATM}), (c) emissions from land-use change (E_{LUC}), (d) the land CO₂ sink (S_{LAND}), (e)
6 the ocean CO₂ sink (S_{OCEAN}), (f) the budget imbalance that is not accounted for by the other terms.
7 Positive values of S_{LAND} and S_{OCEAN} represent a flux from the atmosphere to land or the ocean. All
8 data are in GtC yr⁻¹ with the uncertainty bounds representing ± 1 standard deviation in shaded
9 colour. Data sources are as in Fig. 3. The red dots indicate our projections for the year 2021 and
10 the red error bars the uncertainty in the projections (see methods).

11



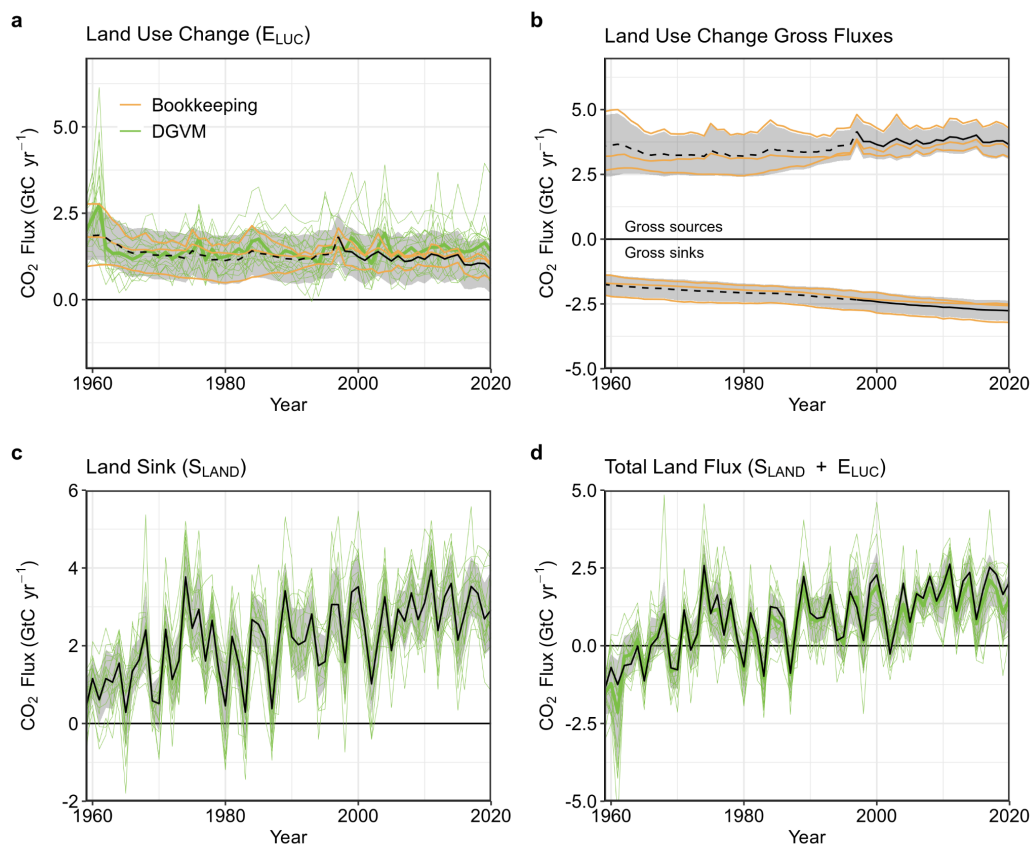
1
2
3
4
5
6
7
8
9
10
11
12

Figure 5. Fossil CO₂ emissions for (a) the globe, including an uncertainty of $\pm 5\%$ (grey shading) and a projection through the year 2021 (red dot and uncertainty range), (b) territorial (solid lines) and consumption (dashed lines) emissions for the top three country emitters (USA, China, India) and for the European Union (EU27), (c) global emissions by fuel type, including coal, oil, gas, and cement, and cement minus cement carbonation (dashed), and (d) per-capita emissions the world and for the large emitters as in panel (b). Territorial emissions are primarily from Gilfillan and Marland (2021) except national data for the USA and EU27 for 1990-2018, which are reported by the countries to the UNFCCC as detailed in the text; consumption-based emissions are updated from Peters et al. (2011b). See Section 2.1 and Appendix C.1 for details of the calculations and data sources.



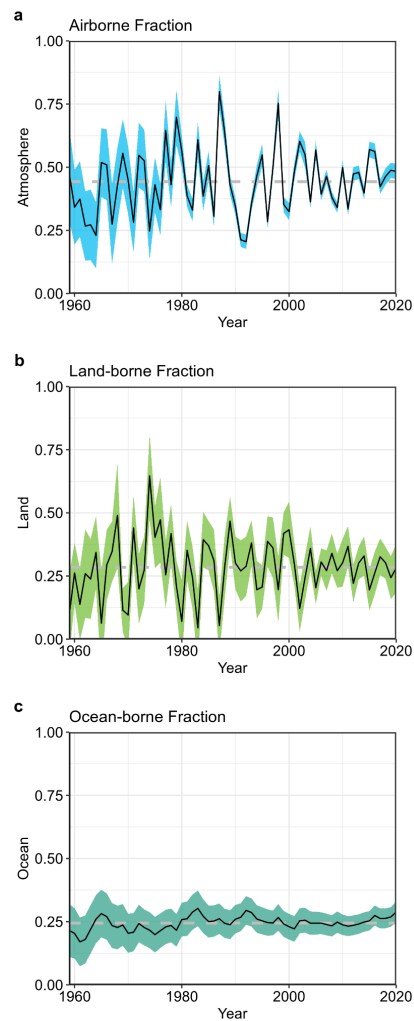
1

2 **Figure 6.** The 2011–2020 decadal mean components of the global carbon budget, presented for (a)
3 fossil CO₂ emissions (E_{FOS}), (b) land-use change emissions (E_{LUC}), (c) the ocean CO₂ sink (S_{OCEAN}), and
4 (d) the land CO₂ sink (S_{LAND}). Positive values for E_{FOS} and E_{LUC} represent a flux to the atmosphere,
5 whereas positive values of S_{OCEAN} and S_{LAND} represent a flux from the atmosphere to the ocean or
6 the land. In all panels, yellow/red (green/blue) colours represent a flux from (into) the land/ocean
7 to (from) the atmosphere. All units are in $\text{kgC m}^{-2} \text{yr}^{-1}$. Note the different scales in each panel. E_{FOS}
8 data shown is from GCP-GridFEDv2021.2. E_{LUC} data shown is only from BLUE as the updated
9 H&N2017 and OSCAR do not resolve gridded fluxes. S_{OCEAN} data shown is the average of GOBMs
10 and data-products means, using GOBMs simulation A, no adjustment for bias and drift applied to
11 the gridded fields (see Sections 2.4). S_{LAND} data shown is the average of DGVMs for simulation S2
12 (see Sections 2.5).



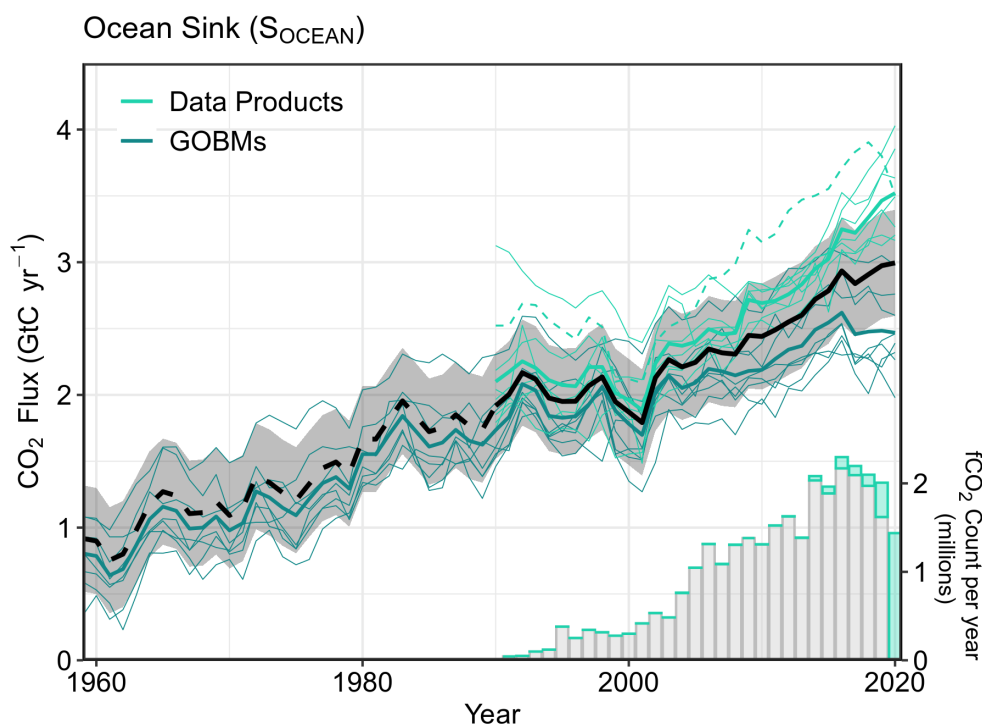
1

2 **Figure 7.** CO₂ exchanges between the atmosphere and the terrestrial biosphere as used in the
3 global carbon budget (black with $\pm 1\sigma$ uncertainty in grey shading in all panels). (a) CO₂ emissions
4 from land-use change (E_{LUC}) with estimates from the three bookkeeping models (yellow lines) and
5 DGVMs models (green) shown individually, with DGVMs ensemble means (dark green). The
6 dashed line identifies the pre-satellite period before the inclusion of peatland burning. (b) CO₂
7 gross sinks (positive, from regrowth after agricultural abandonment and wood harvesting) and
8 gross sources (negative, from decaying material left dead on site, products after clearing of
9 natural vegetation for agricultural purposes, wood harvesting, and for BLUE, degradation from
10 primary to secondary land through usage of natural vegetation as rangeland, and also from
11 emissions from peat drainage and peat burning) from the three bookkeeping models (yellow
12 lines). The sum of the gross sinks and sources is E_{LUC} shown in panel(a). (c) Land CO₂ sink (S_{LAND})
13 with individual DGVMs estimates (green). (d) Total atmosphere-land CO₂ fluxes ($S_{LAND} - E_{LUC}$), with
14 individual DGVMs (green) and their multi-model mean (dark green).



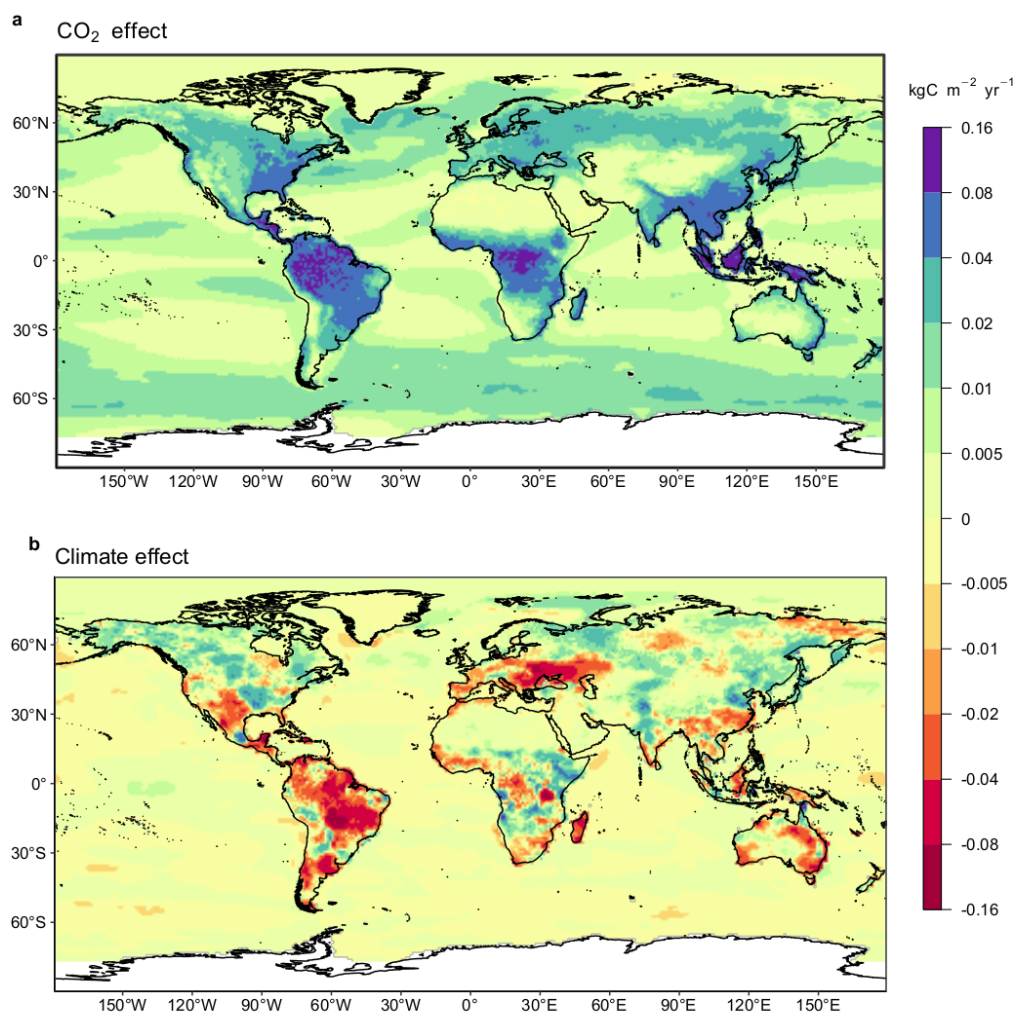
1

2 **Figure 8.** The partitioning of total anthropogenic CO₂ emissions ($E_{FOS} + E_{LUC}$) across (a) the
3 atmosphere (airborne fraction), (b) land (land-borne fraction), and (c) ocean (ocean-borne
4 fraction). Black lines represent the central estimate, and the coloured shading represents the
5 uncertainty. The grey dashed lines represent the long-term average of the airborne (44%), land-
6 borne (28%) and ocean-borne (24%) fractions during 1959-2020.



1

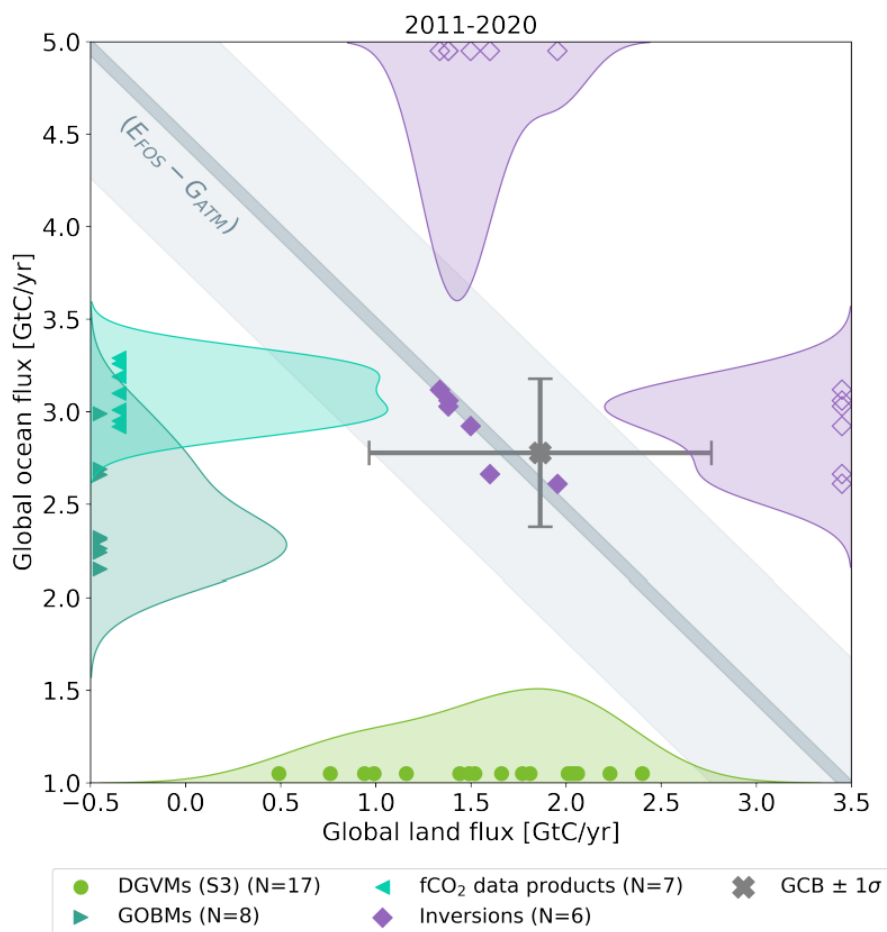
2 **Figure 9.** Comparison of the anthropogenic atmosphere-ocean CO₂ flux showing the budget values
3 of S_{OCEAN} (black; with the uncertainty in grey shading), individual ocean models (teal), and the
4 ocean fCO₂-based data products (cyan; with Watson et al. (2020) in dashed line as not used for
5 ensemble mean). The fCO₂-based data products were adjusted for the pre-industrial ocean source
6 of CO₂ from river input to the ocean, by subtracting a source of 0.61 GtC yr⁻¹ to make them
7 comparable to S_{OCEAN} (see Section 2.4). Bar-plot in the lower right illustrates the number of fCO₂
8 observations in the SOCAT v2021 database (Bakker et al., 2021). Grey bars indicate the number of
9 data points in SOCAT v2020, and coloured bars the newly added observations in v2021.



1

2 **Figure 10.** Attribution of the atmosphere-ocean (S_{OCEAN}) and atmosphere-land (S_{LAND}) CO₂ fluxes to
3 (a) increasing atmospheric CO₂ concentrations and (b) changes in climate, averaged over the
4 previous decade 2011-2020. All data shown is from the processed-based GOBMs and DGVMs. The
5 sum of ocean CO₂ and climate effects will not equal the ocean sink shown in Figure 6 which
6 includes the fCO₂-based data products. See Appendix C.3.2 and C.4.1 for attribution methodology.
7 Units are in kgC m⁻² yr⁻¹ (note the non-linear colour scale).

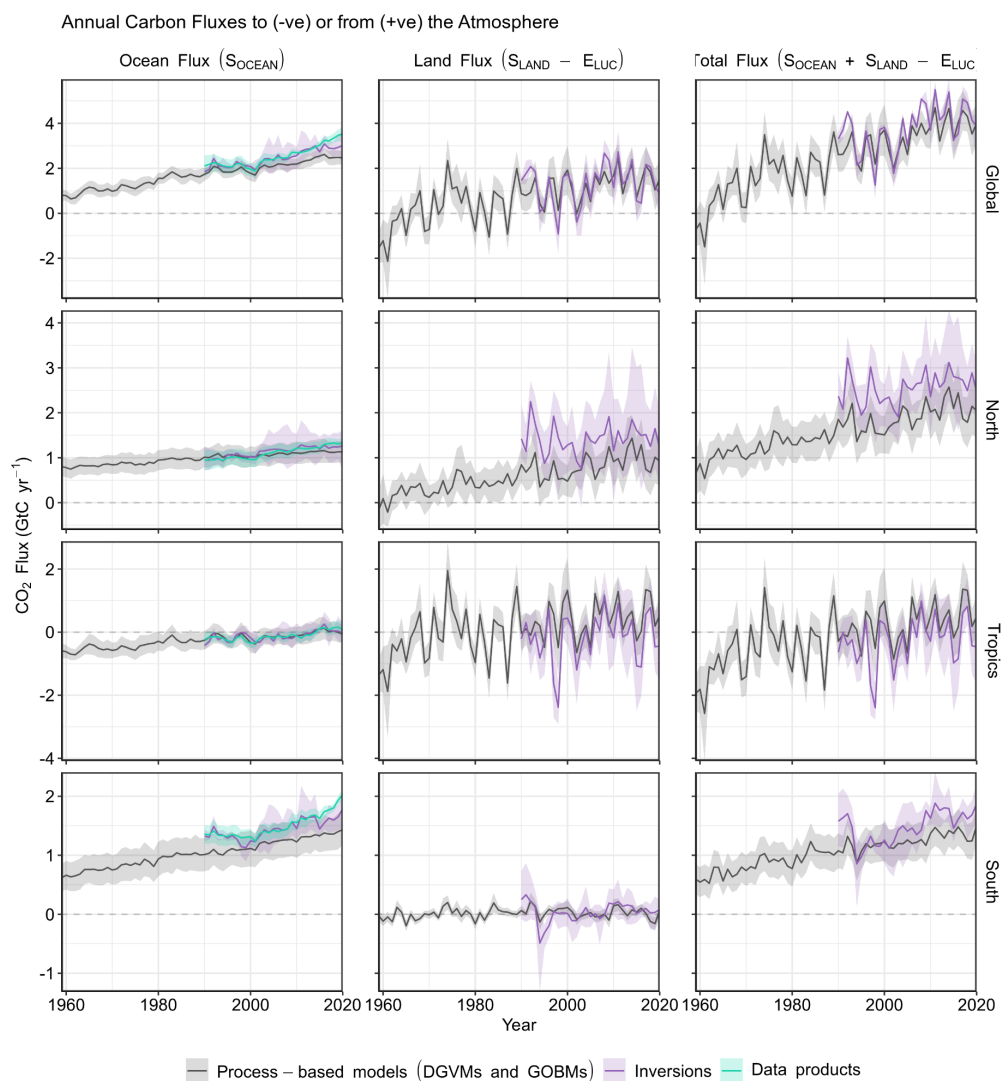
8



1

2 **Figure 11.** The 2011-2020 decadal mean net atmosphere-ocean and atmosphere-land fluxes
 3 derived from the ocean models and fCO₂ products (y-axis, right and left pointing blue triangles
 4 respectively), and from the DGVMs (x-axis, green symbols), and the same fluxes estimated from
 5 the six inversions (purple symbols on secondary x- and y-axis). The grey central point is the mean
 6 ($\pm 1\sigma$) of S_{OCEAN} and $(S_{\text{LAND}} - E_{\text{LUC}})$ as assessed in this budget. The shaded distributions show the
 7 density of the ensemble of individual estimates. The grey diagonal band represents the fossil fuel
 8 emissions minus the atmospheric growth rate from this budget ($E_{\text{FOS}} - G_{\text{ATM}}$). Note that positive
 9 values are CO₂ sinks.

10



1
 2 **Figure 12.** CO₂ fluxes between the atmosphere and the Earth's surface separated between land
 3 and oceans, globally and in three latitude bands. The ocean flux is S_{OCEAN} and the land flux is the
 4 net atmosphere-land fluxes from the DGVMs. The latitude bands are (top row) global, (2nd row)
 5 north (>30°N), (3rd row) tropics (30°S-30°N), and (bottom row) south (<30°S), and over ocean (left
 6 column), land (middle column), and total (right column). Estimates are shown for: process-based
 7 models (DGVMs for land, GOBMs for oceans); inversion models (land and ocean); and fCO₂-based
 8 data products (ocean only). Positive values indicate a flux from the atmosphere to the land or the
 9 ocean. Mean estimates from the combination of the process models for the land and oceans are



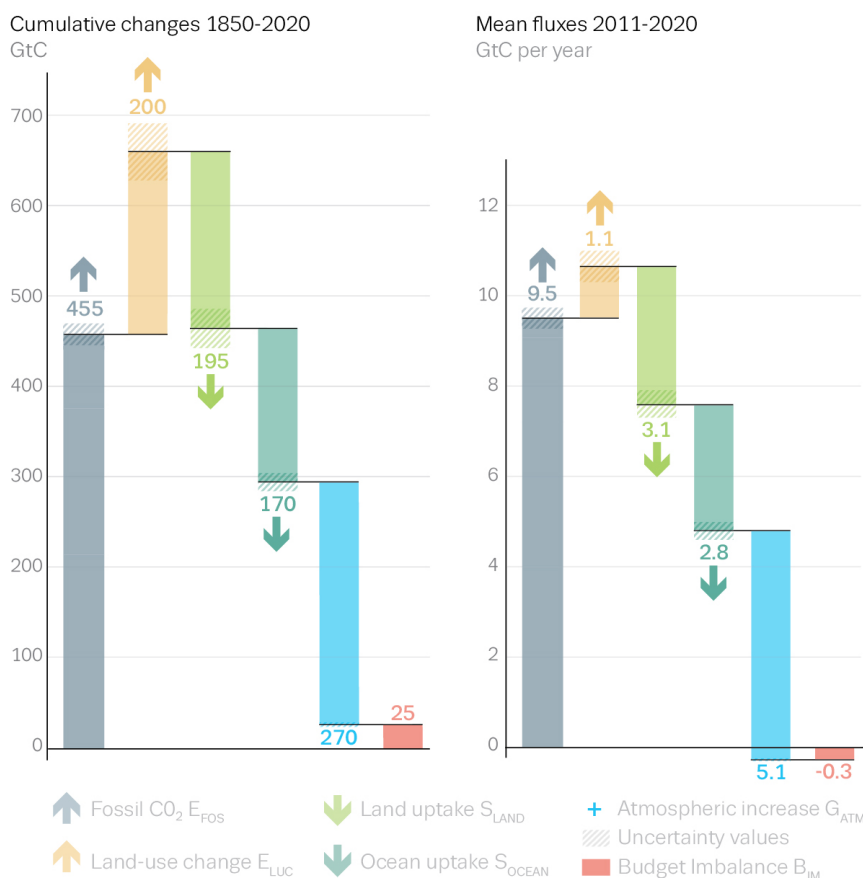
1 shown (black line) with ± 1 standard deviation (1σ) of the model ensemble (grey shading). For the
2 total uncertainty in the process-based estimate of the total sink, uncertainties are summed in
3 quadrature. Mean estimates from the atmospheric inversions are shown (purple lines) with their
4 full spread (purple shading). Mean estimates from the $f\text{CO}_2$ -based data products are shown for the
5 ocean domain (light blue lines) with their $\pm 1\sigma$ spread (light blue shading). The global S_{OCEAN} (upper
6 left) and the sum of S_{OCEAN} in all three regions represents the anthropogenic atmosphere-to-ocean
7 flux based on the assumption that the preindustrial ocean sink was 0 GtC yr^{-1} when riverine fluxes
8 are not considered. This assumption does not hold at the regional level, where preindustrial fluxes
9 can be significantly different from zero. Hence, the regional panels for S_{OCEAN} represent a
10 combination of natural and anthropogenic fluxes. Bias-correction and area-weighting were only
11 applied to global S_{OCEAN} ; hence the sum of the regions is slightly different from the global estimate
12 ($<0.06 \text{ GtC yr}^{-1}$).

13



1

Anthropogenic carbon flows



2

3 **Figure 13.** Cumulative changes over the 1850-2020 period (left) and average fluxes over
 4 the 2011-2020 period (right) for the anthropogenic perturbation of the global carbon cycle.
 5 See the caption of Figure 3 for key information and the methods in text for full details.

6



1



2

3

4 **Figure 14.** Kaya decomposition of the main drivers of fossil CO₂ emissions, considering population,
5 GDP per person, Energy per GDP, and CO₂ emissions per energy, for China (top left), USA (top
6 right), EU27 (middle left), India (middle right), Rest of the World (bottom left), and World (bottom
7 right). Black dots are the annual fossil CO₂ emissions growth rate, coloured bars are the
8 contributions from the different drivers. A general trend is that population and GDP growth put
9 upward pressure on emissions, while energy per GDP and more recently CO₂ emissions per energy
10 put downward pressure on emissions. The changes during 2020 led to a stark contrast to previous
11 years, with different drivers in each region.

12

13



1 Appendix A. Supplementary Tables

Table A1. Comparison of the processes included in the bookkeeping method and DGVMs in their estimates of ELUC and SLAND. See Table 4 for model references. All models include deforestation and forest regrowth after abandonment of agriculture (or from afforestation activities on agricultural land). Processes relevant for ELUC are only described for the DGVMs used with land-cover change in this study.																				
	Bookkeeping Models			DGVMs																
	H&N	BLUE	OSCAR	CABLE-POP	CLASSIC	CLM5.0	DLEM	IBIS	ISAM	ISBA-CTRIPI(h)	JSBA-CH	JULES-ES	LPJ-GU-ESS	LPJ	LPJ-Bern	OCNv2	ORCHIDEEv3	SDGVM	VISIT	YIBs
Processes relevant for ELUC																				
Wood harvest and forest degradation (a)	yes	yes	yes	yes	no	yes	yes	yes	yes	no	yes	no	yes	yes	no (d)	yes	yes	no	yes	no
Shifting cultivation / Subgrid scale transitions	no (b)	yes	yes	yes	no	yes	no	no	no	no	yes	no	yes	yes	no (d)	no	no	no	yes	no
Cropland harvest (removed, R, or added to litter, L)	yes (R) (p)	yes (R) (p)	yes (R)	yes (R)	yes (L)	yes (R)	yes	yes (R)	yes	yes (R+L)	yes (R+L)	yes (R)	yes (R)	yes (L)	yes (R)	yes (R+L)	yes (R)	yes (R)	yes (R)	yes (L)
Peat fires	yes	yes	yes	no	no	yes	no	no	no	no	no	no	no	no	no	no	no	no	no	no
fire as a management tool	yes (p)	yes (p)	yes (j)	no	no	no	no	no	no	no	no	no	no	no	no	no	no	no	no	no
N fertilization	yes (p)	yes (p)	yes (j)	no	no	yes	yes	no	yes	no	no	yes (k)	yes	no	yes	yes	yes	no	no	no
tillage	yes (p)	yes (p)	yes (j)	no	yes (g)	no	no	no	no	no	no	no	yes	no	no	no	yes (g)	no	no	no
irrigation	yes (p)	yes (p)	yes (j)	no	no	yes	yes	no	yes	no	no	no	yes	no	no	no	no	no	no	no
wetland drainage	yes (p)	yes (p)	yes (j)	no	no	no	no	no	yes	no	no	no	no	no	no	no	no	no	no	no
erosion	yes (p)	yes (p)	yes (j)	no	no	no	yes	no	no	no	no	no	no	no	no	no	no	no	yes	no
peat drainage	yes	yes	yes	no	no	no	no	no	no	no	no	no	no	no	no	no	no	no	no	no
Grazing and mowing Harvest (removed, r, or added to litter, l)	yes (r) (p)	yes (r) (p)	yes (r)	yes (r)	no	no	no	no	yes (l)	no	yes (l)	no	yes (r)	yes (l)	no	yes (r+l)	no	no	no	no
Processes also relevant for SLAND (in addition to CO2 fertilization and climate)																				
Fire simulation and/or suppression	N.A.	N.A.	N.A.	no	yes	yes	no	yes	no	yes	yes	yes	yes	yes	yes	no	no	yes	yes	no
Carbon-nitrogen interactions, including N deposition	N.A.	N.A.	N.A.	yes	no (f)	yes	yes	no	yes	no (e)	yes	yes	yes	no	yes	yes	yes	yes (c)	no	no (f)
Separate treatment of direct and diffuse solar radiation	N.A.	N.A.	N.A.	no	no	yes	no	no	no	no	no	yes	no	no	no	no	no	no	no	no
(a) Refers to the routine harvest of established managed forests rather than pools of harvested products.																				
(b) No back- and forth-transitions between vegetation types at the country-level, but if forest loss based on FRA exceeded agricultural expansion based on FAO, then this amount of area was cleared for cropland and the same amount of area of old croplands abandoned.																				
(c) Limited. Nitrogen uptake is simulated as a function of soil C, and Vcmax is an empirical function of canopy N. Does not consider N deposition.																				
(d) Available but not active.																				
(e) Simple parameterization of nitrogen limitation based on Yin (2002; assessed on FACE experiments)																				
(f) Although C-N cycle interactions are not represented, the model includes a parameterization of down-regulation of photosynthesis as CO2 increases to emulate nutrient constraints (Arora et al., 2009)																				



- (g) Tillage is represented over croplands by increased soil carbon decomposition rate and reduced humification of litter to soil carbon.
- (h) ISBA-CTRIP corresponds to SURFEXv8 in GCB2018
- (i) Bookkeeping models include the effect of CO₂-fertilization as captured by present-day carbon densities, but not as an effect transient in time.
- (j) as far as the DGVMs that OSCAR is calibrated to include it
- (k) perfect fertilisation assumed, i.e. crops are not nitrogen limited and the implied fertiliser diagnosed
- (m) fire intensity responds to climate and CO₂, but no fire suppression
- (z) Process captured implicitly by use of observed carbon densities.

1



1
 2
 3

Table A2. Comparison of the processes and model set up for the Global Ocean Biogeochemistry Models for their estimates of SOCEAN. See Table 4 for model references.

	NEMO-PlankTOM1 2	NEMO-PISCES (IPSL)	MICOM-HAMOCC (NorESM1-OCv1.2)	MPIOM-HAMOCC6	FESOM-2.1-REcoM2	NEMO3.6-PISCESv2-gas (CNRM)	MOM6-COBALT (Princeton)	CESM-ETHZ
SPIN-UP procedure								
Initialisation of carbon chemistry	GLODAPv1 corrected for anthropogenic carbon from Sabine et al. (2004)	GLODAPv2	GLODAP v1 (preindustrial DIC)	initialization from previous model simulations	GLODAPv2 alkalinity and preindustrial DIC	GLODAPv2	GLODAPv2 for Alkalinity and DIC. DIC is corrected to 1959 level for simulation A and C and corrected to pre-industrial level for simulation B using Khatiwala et al. (2009, 2013)	GLODAPv2 preindustrial
Preindustrial spin-up prior to 1850? If yes, how long?	spin-up 1750-1947	spin-up starting in 1836 with 3 loops of JRA55	1000 year spin up	yes, ~2000 years	50 years	long spin-up (> 1000 years)	Other biogeochemical tracers are initialized from a GFDL-ESM2M spin-up (> 1000 years)	spinup 1655-1849
atmospheric forcing for pre-industrial spin-up	looping NCEP year 1990	JRA55	CORE-I (normal year) forcing	spinup with omip climatology to reach steady state with the rivers	JRA55-do v.1.5.0 repeated year 1961	JRA55-do	GFDL-ESM2M internal forcing	COREv2 forcing until 1835, three cycles of conditions from 1949-2009. from 1835-1850: JRA forcing
atmospheric forcing for historical spin-up 1850-1958 for simulation A	1750-1947: looping NCEP year 1990; 1948-2020: NCEP	1836-1958 : looping full JRA55 reanalysis	CORE-I (normal year) forcing; from 1948 onwards NCEP-R1 with CORE-II corrections	NCEP 6 hourly cyclic forcing (10 years starting from 1948) with co2 at 278 ppm and rivers	JRA55-do-v1.5.0 repeated year 1961	JRA55-do cycling year 1958	JRA55-do-v1.5 repeat year 1959 (71 years)	JRA55 version 1.3, repeat cycle between 1958-2018.
atmospheric CO2 for historical spin-up 1850-1958 for simulation A	provided by the GCP; converted to pCO2 temperature formulation (Sarmiento et al., 1992), monthly	xCO2 as provided by the GCB, global mean, annual resolution, converted to pCO2 with sea-level	xCO2 as provided by the GCB, converted to pCO2 with sea level pressure and water vapor correction	provided by the GCB	xCO2 as provided by the GCB, converted to pCO2 with sea-level pressure and water vapour pressure,	xCO2 as provided by the GCB, converted to pCO2 with constant sea-level pressure and water vapour	xCO2 at year 1959 level (315 ppm), converted to pCO2 with sea-level pressure and water vapour pressure,	xCO2 as provided by the GCB (new version 2021), converted to pCO2 with atmospheric pressure,



	resolution	pressure and water vapour pressure			global mean, monthly resolution	pressure, global mean, yearly resolution	global mean, yearly resolution	and locally determined water vapour pressure from SST and SSS (100% saturation)
atmospheric forcing for control spin-up 1850-1958 for simulation B	1750-2020: looping NCEP 1990	1836-1958 : looping full JRA55 reanalysis	CORE-I (normal year) forcing	NCEP 1957 fixed forcing, co2=278 and rivers	JRA55-do-v1.5.0 repeat year 1961	JRA55-do-cycling year 1958	JRA55-do-v1.5 repeat year 1959 (71 years)	normal year forcing created from JRA-55 version 1.3, NYF = climatology with anomalies from the year 2001
atmospheric CO2 for control spin-up 1850-1958 for simulation B	constant 278ppm; converted to pCO2 temperature formulation (Sarmiento et al., 1992), monthly resolution	xCO2 of 286.46ppm, converted to pCO2 with constant sea-level pressure and water vapour pressure	xCO2 of 278 ppm, converted to pCO2 with seal level pressure and water vapor correction	278, no conversion, assuming constant standard sea level pressure	xCO2 of 278ppm, converted to pCO2 with sea-level pressure and water vapour pressure	xCO2 of 286.46ppm, converted to pCO2 with constant sea-level pressure and water vapour pressure	xCO2 of 278ppm, converted to pCO2 with sea-level pressure and water vapour pressure	xCO2 as provided by the GCB for 1850, converted to pCO2 with atmospheric pressure, and locally determined water vapour pressure from SST and SSS (100% saturation)
simulation A								
Atmospheric forcing for simulation A	NCEP	JRA55-v1.4 then 1.5 for 2020.	NCEP-R1 with CORE-II corrections	till 1948: continue from A_spinup with cyclic NCEP forcing (1948+10) and increasing CO2 => GCBA-1777-1948 -1948-2020 : with transient NCEP forcing and transient monthly CO2	JRA55-do-v1.5.0	JRA55-do	JRA55-do-v1.5.0 1959-2019 and JRA55-do-v1.5.0.1b for 2020	JRA-55 version 1.3
atmospheric CO2 for simulation A	provided by the GCP; converted to pCO2 temperature formulation (Sarmiento et al., 1992), monthly resolution	xCO2 as provided by the GCB, global mean, annual resolution, converted to pCO2 with sea-level pressure and	xCO2 as provided by the GCB, converted to pCO2 with sea level pressure and water vapor correction		xCO2 as provided by the GCB, converted to pCO2 with sea-level pressure and water vapour pressure, global mean,	xCO2 as provided by the GCB, converted to pCO2 with constant sea-level pressure and water vapour pressure,	xCO2 as provided by the GCB, converted to pCO2 with sea-level pressure and water vapour pressure, global mean,	xCO2 as provided by the GCB (new version 2021), converted to pCO2 with atmospheric pressure, and locally



		water vapour pressure			monthly resolution	global mean, yearly resolution	yearly resolution	determined water vapour pressure from SST and SSS (100% saturation)
simulation B								
Atmospheric forcing for simulation B	NCEP 1990	N/A	CORE-I (normal year) forcing	1948-2020: continue with B_spinup with fixed NCEP forcing 1957, co2=278 and rivers	JRA55-do-v1.5.0 repeat year 1961	JRA55-do-cycling year 1958	JRA55-do-v1.5.0 repeat year 1959	normal year forcing created from JRA-55 version 1.3, NYF = climatology with anomalies from the year 2001
atmospheric CO2 for simulation B	constant 278ppm; converted to pCO2 temperature formulation (Sarmiento et al., 1992), monthly resolution	N/A	xCO2 of 278 ppm, converted to pCO2 with sea level pressure and water vapor correction		xCO2 of 278ppm, converted to pCO2with sea-level pressure and water vapour pressure	xCO2 of 286.46ppm, converted to pCO2 with constant sea-level pressure and water vapour pressure	xCO2 of 278ppm, converted to pCO2 with sea-level pressure and water vapour pressure	xCO2 as provided by the GCB for 1850, converted to pCO2 with atmospheric pressure, and locally determined water vapour pressure from SST and SSS (100% saturation)
model specifics								
Physical ocean model	NEMOv3.6-ORCA2	NEMOv3.6-eORCA1L75	MICOM (NorESM1-OCv1.2)	MPIOM	FESOM-2.1	NEMOv3.6-GELATOv6-eORCA1L75	MOM6-SIS2	CESMv1.3 (ocean model based on POP2)
Biogeochemistry model	PlankTOM12	PISCESv2	HAMOCC (NorESM1-OCv1.2)	HAMOCC6	REcoM-2-M	PISCESv2-gas	COBALTv2	BEC (modified & extended)
Horizontal resolution	2o lon, 0.3 to 1.5o lat	1° lon, 0.3 to 1° lat	1° lon, 0.17 to 0.25 lat (nominally 1°)	1.5°	unstructured multi-resolution mesh. CORE-mesh, with 20-120 km resolution. Highest resolution north of 50N, intermediate in the equatorial belt and Southern Ocean, lowest in the subtropical gyres	1° lon, 0.3 to 1° lat	0.5° lon, 0.25 to 0.5° lat	Lon: 1.125°, Lat varying from 0.53° in the extratropics to 0.27° near the equator



Vertical resolution	31 levels	75 levels, 1m at the surface	51 isopycnic layers + 2 layers representing a bulk mixed layer	40 levels, layer thickness increase with depth	46 levels, 10 m spacing in the top 100 m	75 levels, 1m at surface	75 levels hybrid coordinates, 2 m at surface	60 levels (z-coordinates)
Total ocean area on native grid (km ²)	3.6080E+08	3.6270E+08	3.6006E+08	3.6598E+08	3.6475E+08	3.6270E+14	3.6110E+08	3.5926E+08
Ocean area on native grid (km ²) - NORTH	6.2646E+07		6.2049E+07	6.4440E+07		6.3971E+13		
Ocean area on native grid (km ²) - TROPICS	1.1051E+08		1.9037E+08	1.9248E+08		1.9025E+14		
Ocean area on native grid (km ²) - SOUTH	1.8766E+08		1.0765E+08	1.0986E+08		1.0848E+14		
gas-exchange parameterization	Quadratic exchange formulation (function of $T + 0.3 \cdot U^2$) * $(Sc/660)^{-0.5}$; Wanninkhof (1992, Equation 8); Sweeney et al. (2007)	see Orr et al. (2017): kw parameterized from Wanninkhof (1992), with $kw = a \cdot (Sc/660)^{-0.5} \cdot u_2 \cdot (1 - f_{ice})$ with a from Wanninkhof (2014)	see Orr et al. (2017): kw parameterized from Wanninkhof (1992), with $kw = a \cdot (Sc/660)^{-0.5} \cdot u_2 \cdot (1 - f_{ice})$ with $a=0.337$ following the OCMIP2 protocols	Gas transfer velocity formulation and parameter setup of Wanninkhof (2014), including updated Schmidt number parameterizations for CO ₂ to comply with OMIP protocol (Orr et al., 2017)	see Orr et al. (2017): kw parameterized from Wanninkhof (1992), with $kw = a \cdot (Sc/660)^{-0.5} \cdot u_2 \cdot (1 - f_{ice})$ with a from Wanninkhof (2014)	see Orr et al. (2017): kw parameterized from Wanninkhof (1992), with $kw = a \cdot (Sc/660)^{-0.5} \cdot u_2 \cdot (1 - f_{ice})$ with a from Wanninkhof (2014)	see Orr et al. (2017): kw parameterized from Wanninkhof (1992), with $kw = a \cdot (Sc/660)^{-0.5} \cdot u_2 \cdot (1 - f_{ice})$ with a from Wanninkhof (2014)	Gas exchange is parameterized using the Wanninkhof (1992) quadratic windspeed dependency formulation, but with the coefficient scaled down to reflect the recent 14C inventories. Concretely, we used a coefficient a of 0.31 cm hr ⁻¹ s ² m ⁻² to read $kw = 0.31 \text{ ws}^2 (1 - f_{ice}) (Sc=660)^{-1/2}$
time-step	96 mins	45 min	3200 sec	60 mins	45 min	15min	30 min	3757 sec
output frequency	Monthly	monthly	monthly/daily	monthly	monthly	monthly	monthly	monthly
CO ₂ chemistry routines	Following Broecker et al. (1982)	mocsy	Following Dickson et al. (2007)	as in Ilyina et al. (2013) adapted to comply with OMIP protocol (Orr et al., 2017).	mocsy	mocsy	mocsy	OCMIP2 (Orr et al., 2017)
river carbon input (PgC/yr)	60.24 Tmol/yr; 0.723 PgC/yr	0.61 PgC y-1	0	0.77 PgC/yr	0	-0.611 PgC y-1	-0.15 PgC y-1	0.33 Pg C yr-1
burial/net flux into the sediment (PgC/yr)	0.723 PgC/yr	0.59 GtC y-1	around 0.54	around 0.44 PgC/yr	0	-0.656 GtC y-1	-0.18 PgC y-1	0.21 Pg C yr-1

1
 2
 3



Table A3: Description of ocean data-products used for assessment of SOCEAN. See Table 4 for references.

	Jena-MLS	MPI-SOMFFN	CMEMS-LSCE-FFNN	CSIR-ML6	Watson et al	NIES-NN	JMA-MLR	OS-ETHZ-GRaCER
Method	<p>Spatio-temporal interpolation method where in a first step the global ocean is clustered into 16 biogeochemical provinces (one stand alone province for the Arctic Ocean - see Landschützer et al 2020) using a self-organizing map (SOM). In a second step, the non-linear relationship between available pCO₂ measurements from the SOCAT database (Bakker et al 2016) and environmental predictor data (SST, SSS, MLD, CHL-a, atmospheric CO₂ - references see Landschützer et al 2016) are established using a feed-forward neural network (FFN) for each province separately. The established relationship is then used to fill the existing data gaps (see Landschützer et al. 2013, 2016).</p>	<p>2-step neural network method where in a first step the global ocean is clustered into 16 biogeochemical provinces (one stand alone province for the Arctic Ocean - see Landschützer et al 2020) using a self-organizing map (SOM). In a second step, the non-linear relationship between available pCO₂ measurements from the SOCAT database (Bakker et al 2016) and environmental predictor data (SST, SSS, MLD, CHL-a, atmospheric CO₂ - references see Landschützer et al 2016) are established using a feed-forward neural network (FFN) for each province separately. The established relationship is then used to fill the existing data gaps (see Landschützer et al. 2013, 2016).</p>	<p>An ensemble of neural network models trained on 100 subsampled datasets from the Surface Ocean CO₂ Atlas v2021 (SOCATv2021, Bakker et al. 2021). Like the original data, subsamples are distributed after interpolation on 1x1 grid cells along ship tracks. Sea surface salinity, temperature, sea surface height, mixed layer depth, atmospheric CO₂ mole fraction, chlorophyll-a, pCO₂ climatology, latitude and longitude are used as predictors. The models are used to reconstruct sea surface pCO₂ and convert to air-sea CO₂ fluxes (see the proposed ensemble-based approach and analysis in Chau et al. 2020, 2021).</p>	<p>An ensemble average of six machine learning estimates of surface ocean pCO₂ using the approach described in Gregor et al. (2019) with the updated product using SOCAT v2021 (Bakker et al., 2016). All ensemble members use a cluster-regression approach. Two different cluster configurations are used: (1) based on K-means clustering; (2) Fay and McKinley (2014) 's CO₂ biomes. Three regression algorithms are used: (1) gradient boosted decision trees; (2) feed-forward neural network; (3) support vector regression. The product of the cluster configurations and the regression algorithms results in an ensemble with six members., hence the CSIR-ML6.</p>	<p>Derived from the SOCAT(v2021) pCO₂ database, but corrected to the subskin temperature of the ocean as measured by satellite, using the methodology described by Goddijn-Murphy et al. (2015). A correction to the flux calculation is also applied for the cool and salty surface skin. In other respects the product uses interpolation of the data using the two step neural network based on MPI-SOMFFN :in the first step the ocean is divided into a monthly climatology of 16 biogeochemical provinces using a SOM, In the second step a feed-forward neural network establishes non-linear relationships between pCO₂ and SST, SSS, mixed layer depth(MLD) and atmospheric xCO₂ in each</p>	<p>A feed forward neural network model was used to reconstruct monthly global surface ocean CO₂ concentrations 1x1 degree meshes and estimate air-sea CO₂ fluxes. The target variable is the per cruise weighted fCO₂ mean of SOCAT 2021. Feature variables include sea surface temperature (SST), salinity, chlorophyll-a, mixed layer depth, and the monthly anomaly of SST. See Zeng et al. (2014)</p>	<p>Fields of total alkalinity (TA) were estimated by using a multiple linear regressions (MLR) method based on GLODAPv2.2021 and satellite observation data. TA = f(SSDH, SSS) SOCATv2021 fCO₂ data were converted to total dissolved inorganic carbon (DIC) concentrations in combination with the TA, and then fields of DIC were estimated by using a MLR method based on the DIC and satellite observation data. DIC = f(SSDH, SST, SSS, log(Chl), log(MLD), time)</p>	<p>OceanSODA-ETHZ's Geospatial Random Cluster Ensemble Regression is a two-step cluster-regression approach, where multiple clustering instances with slight variations are run to create an ensemble of estimates (n_members=16). We use K-means clustering (n_clusters=21) for the clustering step and a combination of Gradient boosted trees (n_members=8) and Feed-forward neural-networks (n_members=8) to estimate SOCAT v2021 fCO₂. Clustering is performed on the following variables: SOCOM_pCO₂_climatology, SST_clim, MLD_clim, CHL_clim. Regression is performed on the following variables: xCO₂atm, SST, SST_anomaly, SSS, CHL, MLD, u10_wind, v10_wind, sea-</p>



					of the 16 provinces. Further description in Watson et al. (2020).			ice changes, SSH (note that the latter two variables are an update from Gregor and Gruber, 2021).
Gas-exchange parameterization	Quadratic exchange formulation $(k \cdot U^2 \cdot (Sc/660)^{-0.5})$ (Wanninkhof, 1992) with the transfer coefficient k scaled to match a global mean transfer rate of 16.5 cm/hr by Naegler (2009)	Quadratic exchange formulation $(k \cdot U^2 \cdot (Sc/660)^{-0.5})$ (Wanninkhof, 1992) with the transfer coefficient k scaled to match a global mean transfer rate of 16.5 cm/hr (calculated myself over the full period 1982-2020)	Quadratic exchange formulation $(k \cdot U^2 \cdot (Sc/660)^{-0.5})$ (Wanninkhof, 2014) with the transfer coefficient k scaled to match a global mean transfer rate of 16.5 cm/hr (Naegler, 2009).	Quadratic formulation $kw = a \cdot U^{10^2} \cdot (Sc/660)^{0.5}$ (J). We use scaled kw for ERA5 reanalysis wind data, which is scaled globally to 16.5 cm/hr (after Naegler 2009) like in Fay and Gregor et al. (2021) https://doi.org/10.5194/essd-2021-16	Nightingale et al. (2000) formulation : $K = ((Sc/600)^{-0.5}) \cdot (0.333 \cdot U + 0.222 \cdot U^2)$	$Kw = 0.251 \cdot Wnd \cdot \sqrt{Sc} / 660.0$ (Wanninkhof, 2014)	Quadratic exchange formulation $(k \cdot U^2 \cdot (Sc/660)^{-0.5})$ (Wanninkhof, 2014) with the transfer coefficient k scaled to match a global mean transfer rate of 16.5 cm/hr (Naegler, 2009) under fitted to the JRA55 wind field.	Quadratic formulation of bulk air-sea CO2 flux: $kw = a \cdot U^{10^2} \cdot (Sc/660)^{0.5}$ We use individually scaled kw 's for JRA55, ERA5, and NCEP-R1, which are all scaled globally to 16.5 cm/hr (after Naegler, 2009). See Fay and Gregor et al. (2021)
Wind product	JMA55-do reanalysis	ERA 5	ERA5	ERA5	CCMP wind product, 0.25 x 0.25 degrees x 6-hourly, from which we calculate mean and mean square winds over 1 x 1 degree and 1 month intervals. CCMP product does not cover years 1985-1987, for which we use a monthly climatology calculated as the means of 1988-1991.	ERA5	JRA55	JRA55, ERA5, NCEP1
Spatial resolution	2.5 degrees longitude * 2 degrees latitude	1x1 degree	1x1 degree	1 x 1	1 x 1 degree	1x1 degree	1x1 degree	1x1 degree



Temporal resolution	daily	monthly	monthly	monthly	monthly	monthly	monthly	monthly
Atmospheric CO2	Spatially and temporally varying field based on atmospheric CO2 data from 169 stations (Jena CarboScope atmospheric inversion sEXTALL_v20 21)	atmospheric pCO2_wet calculated from the NOAA ESRL marine boundary layer xCO2 and the NCEP sea level pressure with the moisture correction by Dickson et al 2007 (details and references can be obtained from Appendix A3 in Landschützer et al 2013)	Spatially and monthly varying fields of atmospheric pCO2 computed from CO2 mole fraction (Chevallier, 2013; CO2 atmospheric inversion from the Copernicus Atmosphere Monitoring Service), and atmospheric dry-air pressure which is derived from monthly surface pressure (ERA5) and water vapour pressure fitted by Weiss and Price (1980)	The NOAA's marine boundary layer product for the mole fraction of carbon dioxide (xCO2) is linearly interpolated onto a 1°x1° grid and resampled from weekly to monthly. Basically, xCO2 is multiplied by ERA5 mean sea level pressure (MSLP), and a water vapour pressure correction is applied to MSLP using the equation from Dickson et al. (2007). This results in monthly 1°x 1° atmospheric pCO2.	Atmospheric pCO2 (wet) calculated from NOAA marine boundary layer XCO2 and NCEP sea level pressure, with pH2O calculated from Cooper et al. (1998). (2019 XCO2 marine boundary values were not available at submission so we used preliminary values, estimated from 2018 values and increase at Mauna Loa.)	NOAA Greenhouse Gas Marine Boundary Layer Reference. https://gml.noaa.gov/ccgg/mbl/mbl.html	Atmospheric xCO2 fields of JMA-GSAM inversion model (Maki et al. 2010; Nakamura et al. 2015) were used. They were converted to pCO2 by using JRA55 sea level pressure. xCO2 fields in 2020 were not available at this stage, and we use observation data of obspack_co2_1_NRT_v6.1.1_2021-05-17 (Di Sarra et al. 2021) to estimate the increase from 2019 to 2020.	NOAA's marine boundary layer product for xCO2 is linearly interpolated onto a 1x1 degree grid and resampled from weekly to monthly. xCO2 is multiplied by ERA5 mean sea level pressure, where the latter corrected for water vapour pressure using Dickson et al. (2007). This results in monthly 1x1 degree pCO2atm.
Total ocean area on native grid (km2)	3.63E+08	3.63E+08	3.46E+08	3.48E+08	3.51E+08	3.28E+08 (3.23E+08 to 3.35E+08, depending on ice cover)	3.05E+08 (2.98E+08 to 3.15E+08, depending on ice cover)	3.55E+08
method to extend product to full global ocean coverage		Arctic and marginal seas added following Landschützer et al. (2020). previously applied coastal cut (1degree off coast) was dropped					We used the same method as Fay et al. (2021a)	Method has near full coverage
Ocean area on native grid (km2) - NORTH			5.4545E+07	5.0528E+07	5.0700E+07		3.90E+07 (3.75E+07 to 4.09E+07, depending on ice cover)	5.9771E+07
Ocean area on native grid (km2) - TROPICS			1.8875E+08	1.8933E+08	1.9230E+08		1.74E+08	1.8779E+08



Ocean area on native grid (km ²) - SOUTH			1.0241E+08	1.0767E+08	1.0868E+08		9.20E+07 (8.47E+07 to 1.02E+08, depending on ice cover)	1.0705E+08
--	--	--	------------	------------	------------	--	--	------------

- 1
- 2
- 3



1
2

Table A4. Comparison of the inversion set up and input fields for the atmospheric inversions. Atmospheric inversions see the full CO₂ fluxes, including the anthropogenic and pre-industrial fluxes. Hence they need to be adjusted for the pre-industrial flux of CO₂ from the land to the ocean that is part of the natural carbon cycle before they can be compared with SOCEAN and SLAND from process models. See Table 4 for references.

	CarbonTracker Europe (CTE)	Jena CarboScope	Copernicus Atmosphere Monitoring Service (CAMS)	UoE	CMS-Flux	NISMON-CO ₂
Version number	CTE2021	sEXTocNEET_v2021	v20r2	in-situ		v2021.1
Observations						
Atmospheric observations	Hourly resolution (well-mixed conditions) obspack GLOBALVIEWplus v6.1 and NRT_v6.1.1 (a)	Flasks and hourly from various institutions (outliers removed by 2-sigma criterion)	Hourly resolution (well-mixed conditions) obspack GLOBALVIEWplus v6.1 and NRT_v6.1.1 (a), WDCGG, RAMCES and ICOS ATC	Hourly resolution (well-mixed conditions) obspack GLOBALVIEWplus v6.1 and NRT_v6.1.1 (a)	ACOS-GOSAT v9 (6) retrievals between July 2009 and Dec 2014 and OCO-2 b10 (7) retrievals between Jan 2015 to Dec 2015. In addition, surface flask observations from remote sites were also assimilated from GLOBALVIEWplus v6.1 and NRT_v6.1.1.	Hourly resolution (well-mixed conditions) obspack GLOBALVIEWplus v6.1 and NRT_v6.1.1 (a)
Period covered	2001-2020	1957-2020	1979-2021	2001-2020	2010-2020	1990-2020
Prior fluxes						
Biosphere and fires	SIBCASA biosphere (b) with 2019-2020 climatological, GFAS fires	No prior	ORCHIDEE (climatological), GFEDv4.1s	CASA v1.0, climatology after 2016 & GFED4.0	yearly repeating CARDAMOM biosphere+fires	VISIT & GFEDv4.1s
Ocean	oc_v2020 (Rodenbeck et al., 2014), with updates, For 2020: climatology based on years 2015-2019	oc_v2021 (Rodenbeck et al., 2014) with updates	CMEMS Copernicus ocean fluxes (Denvil-Sommer et al., 2019), with updates	Takahashi climatology	MOM6	JMA global ocean mapping (Iida et al., 2015)
Fossil fuels	GCP-GridFEDv2021.1 (Jones et al., 2021b) for 2000-2018, GCP-GridFEDv2021.2 for 2019+2020 (c)	GCP-GridFEDv2021.2 (Jones et al., 2021b) (c)	GCP-GridFEDv2021.2 (Jones et al., 2021b) (c)	GCP-GridFEDv2021.2 (Jones et al., 2021b) (c)	GCP-GridFEDv2021.2 (Jones et al., 2021b) (c)	GCP-GridFEDv2021.2 (Jones et al., 2021b) (c)
Transport and optimization						
Transport model	TM5	TM3	LMDZ v6	GEOS-CHEM	GEOS-CHEM	NICAM-TM
Weather forcing	ECMWF	NCEP	ECMWF	MERRA2	MERRA-2	JRA55



Horizontal Resolution	Global: 3° x 2°, Europe: 1° x 1°, North America: 1° x 1°	Global: 4° x 5°	Global: 3.75° x 1.875°	Global: 4° x 5°	Global: 4° x 5°	isocahedral grid: ~225km
Optimization	Ensemble Kalman filter	Conjugate gradient (re- ortho- normalization) (d)	Variational	Ensemble Kalman filter	Variational	Variational
(a) (Cox et al., 2021; Di Sarra et al., 2021)						
(b) (van der Velde et al., 2014)						
(c) GCP-GridFEDv2021.2 (Jones et al., 2021b) is an update through the year 2020 of the GCP-GridFED dataset presented by Jones et al. (2021a).						
(d) ocean prior not optimised						

1
 2
 3
 4
 5
 6
 7
 8
 9
 10



1

Table A5 Attribution of fCO₂ measurements for the year 2020 included in SOCATv2021 (Bakker et al., 2016, 2021) to inform ocean fCO₂-based data products.

Platform name	Regions	No. of measurements	Principal Investigators	No. of data sets	Platform type
<i>1 degree</i>	North Atlantic, Coastal	8,652	Gutekunst, S.	2	Ship
<i>Allure of the Seas</i>	North Atlantic, Tropical Atlantic, Coastal	19,321	Wanninkhof, R.; Pierrot, D.	8	Ship
<i>Atlantic Explorer</i>	North Atlantic	15,665	Bates, N.	11	Ship
<i>Atlantic Sail</i>	North Atlantic, Coastal	25,082	Steinhoff, T.; Körtzinger, A.	6	Ship
<i>Aurora Australis</i>	Southern Ocean	14,316	Tilbrook, B.	1	Ship
<i>Bjarni Saemundsson</i>	Coastal	3,269	Benoit-Cattin A.; Ólafsdóttir, S. R.	1	Ship
<i>BlueFin</i>	North Pacific, Tropical Pacific, Coastal	76,505	Alin, S. R.; Feely, R. A.	12	Ship
<i>Cap San Lorenzo</i>	Tropical Atlantic, Coastal	12,417	Lefèvre, N.	2	Ship
<i>Celtic Explorer</i>	North Atlantic, Coastal	18,617	Cronin, M.	6	Ship
<i>Colibri</i>	North Atlantic, Tropical Atlantic, Coastal	13,402	Lefèvre, N.	2	Ship
<i>Equinox</i>	North Atlantic, Coastal	25,052	Wanninkhof, R.; Pierrot, D.	11	Ship
<i>F. G. Walton Smith</i>	Coastal	10,460	Rodriguez, C.; Millero, F. J.; Pierrot, D.; Wanninkhof, R.	6	Ship
<i>Finnmaid</i>	Coastal	253,894	Rehder, G.; Glockzin, M.	11	Ship
<i>Flora</i>	Tropical Pacific	4,099	Wanninkhof, R.; Pierrot, D.	2	Ship
<i>G.O. Sars</i>	Arctic, North Atlantic, Coastal	75,833	Skjelvan, I.	7	Ship
<i>GAKOA_149W_60 N</i>	Coastal	68	Cross, J. N.; Monacci, N. M.	3	Mooring
<i>Gulf Challenger</i>	Coastal	2,717	Salisbury, J.; Vandemark, D.; Hunt, C.	3	Ship
<i>Healy</i>	Arctic, North Pacific, Coastal	16,943	Sweeney, C.; Newberger, T.; Sutherland, S. C.; Munro, D. R.	4	Ship
<i>Henry B. Bigelow</i>	North Atlantic, Coastal	14,436	Wanninkhof, R.; Pierrot, D.	4	Ship
<i>Heron Island</i>	Coastal	768	Tilbrook B.	1	Mooring
<i>James Clark Ross</i>	Southern Ocean	2,000	Kitidis, V.	1	Ship
<i>James Cook</i>	North Atlantic, Tropical Atlantic, Coastal	46,710	Theetaert, H.	1	Ship
<i>KC_BUOY</i>	Coastal	1,983	Evans, W.	1	Mooring
<i>Laurence M. Gould</i>	Southern Ocean	25,414	Sweeney, C.; Newberger, T.; Sutherland, S. C.; Munro, D. R.	4	Ship
<i>Maria. S. Merian</i>	Tropical Atlantic, Coastal	35,806	Ritschel, M.	1	Ship
<i>Marion Dufresne</i>	Southern Ocean, Indian	4,709	Lo Monaco, C.; Metzl, N.	1	Ship
<i>Nathaniel B. Palmer</i>	Southern Ocean, Tropical Pacific	34,357	Sweeney, C.; Newberger, T.; Sutherland, S. C.; Munro, D. R.	3	Ship
<i>New Century 2</i>	North Pacific, Tropical Pacific, Tropical Atlantic, North Atlantic, Coastal	27,793	Nakaoka, S.-I.	14	Ship
<i>Nuka Arctica</i>	North Atlantic, Coastal	26,576	Becker, M.; Olsen, A.	6	Ship
<i>Oscar Dyson</i>	Arctic, North Pacific, Coastal	28,196	Alin, S. R.; Feely, R. A.	6	Ship
<i>Quadra Island Field Station</i>	Coastal	78,098	Evans, W.	1	Mooring
<i>Ronald H. Brown</i>	Southern Ocean, Tropical Atlantic, North Atlantic, Coastal	51,611	Wanninkhof, R.; Pierrot, D.	6	Ship



<i>Saildrone1030</i>	North Atlantic, Tropical Atlantic, Coastal	4,080	Skjelvan, I.; Fiedler, B.; Pfeil, B.; Jones, S. D.	1	Saildrone
<i>Sea Explorer</i>	Southern Ocean, Tropical Atlantic, North Atlantic, Coastal	89,896	Landschützer, P.; Tanhua, T.	6	Ship
<i>Sikuliaq</i>	Arctic, North Pacific, Coastal	36,278	Sweeney, C.; Newberger, T.; Sutherland, S. C.; Munro, D. R.	10	Ship
<i>Simon Stevin</i>	Coastal	16,448	Gkritzalis, T.	4	Ship
<i>Soyo Maru</i>	Coastal	46,280	Ono, T.	2	Ship
<i>Tangaroa</i>	Southern Ocean, Tropical Pacific	121,135	Currie, K. I.	13	Ship
<i>TAO110W_ON</i>	Tropical Pacific	1,518	Sutton, A. J.	3	Mooring
<i>Tavastland</i>	Coastal	4,214	Willstrand Wranne, A., Steinhoff, T.	5	Ship
<i>Thomas G. Thompson</i>	Southern Ocean, Tropical Atlantic	1,317	Alin, S. R.; Feely, R. A.	1	Ship
<i>Trans Carrier</i>	Coastal	24,135	Omar, A. M.	13	Ship
<i>Trans Future 5</i>	Southern Ocean, Coastal	16,404	Nakaoka, S.-I.; Nojiri, Y.	15	Ship
<i>Wakataka Maru</i>	North Pacific, Coastal	101,327	Tadokoro, K.; Ono, T.	7	Ship

1
 2
 3
 4
 5
 6
 7
 8
 9
 10
 11
 12
 13
 14
 15
 16



1
2
3

Site code	Measurement program name in Obspack	Specific doi	Data providers	used in 2021
AAO	Airborne Aerosol Observatory, Bondville, Illinois		Sweeney, C.; Dlugokencky, E.J.	yes
ACG	Alaska Coast Guard		Sweeney, C.; McKain, K.; Karion, A.; Dlugokencky, E.J.	yes
ACT	Atmospheric Carbon and Transport - America		Sweeney, C.; Dlugokencky, E.J.; Baier, B.; Montzka, S.; Davis, K.	yes
ALF	Alta Floresta		Gatti, L.V.; Gloor, E.; Miller, J.B.;	yes
AOA	Aircraft Observation of Atmospheric trace gases by JMA		ghg_obs@met.kishou.go.jp	yes
BGI	Bradgate, Iowa		Sweeney, C.; Dlugokencky, E.J.	yes
BNE	Beaver Crossing, Nebraska		Sweeney, C.; Dlugokencky, E.J.	yes
BRZ	Berezorechka, Russia		Sasakama, N.; Machida, T.	yes
CAR	Briggsdale, Colorado		Sweeney, C.; Dlugokencky, E.J.	yes
CMA	Cape May, New Jersey		Sweeney, C.; Dlugokencky, E.J.	yes
CON	CONTRAIL (Comprehensive Observation Network for TRace gases by AirLiner)	http://dx.doi.org/10.17595/20180208.001	Machida, T.; Matsueda, H.; Sawa, Y. Niwa, Y.	yes
CRV	Carbon in Arctic Reservoirs Vulnerability Experiment (CARVE)		Sweeney, C.; Karion, A.; Miller, J.B.; Miller, C.E.; Dlugokencky, E.J.	yes
DND	Dahlen, North Dakota		Sweeney, C.; Dlugokencky, E.J.	yes
ESP	Estevan Point, British Columbia		Sweeney, C.; Dlugokencky, E.J.	yes
ETL	East Trout Lake, Saskatchewan		Sweeney, C.; Dlugokencky, E.J.	yes
FWI	Fairchild, Wisconsin		Sweeney, C.; Dlugokencky, E.J.	yes
GSFC	NASA Goddard Space Flight Center Aircraft Campaign		Kawa, S.R.; Abshire, J.B.; Riris, H.	yes
HAA	Molokai Island, Hawaii		Sweeney, C.; Dlugokencky, E.J.	yes
HFM	Harvard University Aircraft Campaign		Wofsy, S.C.	yes
HIL	Homer, Illinois		Sweeney, C.; Dlugokencky, E.J.	yes
HIP	HIPPO (HIAPER Pole-to-Pole Observations)	https://doi.org/10.3334/CDIAC/HIPPO_010	Wofsy, S.C.; Stephens, B.B.; Elkins, J.W.; Hints, E.J.; Moore, F.	yes
IAGOS - CARIBIC	In-service Aircraft for a Global Observing System		Obersteiner, F.; Boenisch, H.; Gehrlein, T.; Zahn, A.; Schuck, T.	yes
INX	INFLUX (Indianapolis Flux Experiment)		Sweeney, C.; Dlugokencky, E.J.; Shepson, P.B.; Turnbull, J.	yes
LEF	Park Falls, Wisconsin		Sweeney, C.; Dlugokencky, E.J.	yes
NHA	Offshore Portsmouth, New Hampshire (Isles)		Sweeney, C.; Dlugokencky, E.J.	yes



	of Shoals)			
OIL	Oglesby, Illinois		Sweeney, C.; Dlugokencky, E.J.	yes
PFA	Poker Flat, Alaska		Sweeney, C.; Dlugokencky, E.J.	yes
RBA-B	Rio Branco		Gatti, L.V.; Gloor, E.; Miller, J.B.	yes
RTA	Rarotonga		Sweeney, C.; Dlugokencky, E.J.	yes
SCA	Charleston, South Carolina		Sweeney, C.; Dlugokencky, E.J.	yes
SGP	Southern Great Plains, Oklahoma		Sweeney, C.; Dlugokencky, E.J.; Biraud, S.	yes
TAB	Tabatinga		Gatti, L.V.; Gloor, E.; Miller, J.B.	yes
TGC	Offshore Corpus Christi, Texas		Sweeney, C.; Dlugokencky, E.J.	yes
THD	Trinidad Head, California		Sweeney, C.; Dlugokencky, E.J.	yes
WBI	West Branch, Iowa		Sweeney, C.; Dlugokencky, E.J.	yes

1



1
2

Table A7. Main methodological changes in the global carbon budget since first publication. Methodological changes introduced in one year are kept for the following years unless noted. Empty cells mean there were no methodological changes introduced that year.

Publication year	Fossil fuel emissions			LUC emissions	Reservoirs			Uncertainty & other changes
	Global	Country (territorial)	Country (consumption)		Atmosphere	Ocean	Land	
2006 (a)		Split in regions						
2007 (b)				ELUC based on FAO-FRA 2005; constant ELUC for 2006	1959-1979 data from Mauna Loa; data after 1980 from global average	Based on one ocean model tuned to reproduced observed 1990s sink		±1σ provided for all components
2008 (c)				Constant ELUC for 2007				
2009 (d)		Split between Annex B and non-Annex B	Results from an independent study discussed	Fire-based emission anomalies used for 2006-2008		Based on four ocean models normalised to observations with constant delta	First use of five DGVMs to compare with budget residual	
2010 (e)	Projection for current year based on GDP	Emissions for top emitters		ELUC updated with FAO-FRA 2010				
2011 (f)			Split between Annex B and non-Annex B					
2012 (g)		129 countries from 1959	129 countries and regions from 1990-2010 based on GTAP8.0	ELUC for 1997-2011 includes interannual anomalies from fire-based emissions	All years from global average	Based on 5 ocean models normalised to observations with ratio	Ten DGVMs available for SLAND; First use of four models to compare with ELUC	
2013 (h)		250 countries	134 countries and regions 1990-2011 based on GTAP8.1, with detailed estimates for years 1997, 2001, 2004, and 2007	ELUC for 2012 estimated from 2001-2010 average		Based on six models compared with two data-products to year 2011	Coordinated DGVM experiments for SLAND and ELUC	Confidence levels; cumulative emissions; budget from 1750
2014 (i)	Three years of BP data	Three years of BP data	Extended to 2012 with updated GDP data	ELUC for 1997-2013 includes interannual anomalies from fire-based emissions		Based on seven models	Based on ten models	Inclusion of breakdown of the sinks in three latitude bands and comparison with three atmospheric inversions



2015 (j)	Projection for current year based Jan-Aug data	National emissions from UNFCCC extended to 2014 also provided	Detailed estimates introduced for 2011 based on GTAP9			Based on eight models	Based on ten models with assessment of minimum realism	The decadal uncertainty for the DGVM ensemble mean now uses $\pm 1\sigma$ of the decadal spread across models
2016 (k)	Two years of BP data	Added three small countries; China's emissions from 1990 from BP data (this release only)		Preliminary ELUC using FRA-2015 shown for comparison; use of five DGVMs		Based on seven models	Based on fourteen models	Discussion of projection for full budget for current year
a Raupach et al. (2007)								
b Canadell et al. (2007)								
c GCP (2008)								
d Le Quéré et al. (2009)								
e Friedlingstein et al. (2010)								
f Peters et al. (2012b)								
g Le Quéré et al. (2013), Peters et al. (2013)								
h Le Quéré et al. (2014)								
i Le Quéré et al. (2015a)								
j Le Quéré et al. (2015b)								
k Le Quéré et al. (2016)								

1

2

3



1
2

Table A8: Mapping of scientific land flux definitions to the definition of the LULUCF net flux used in national reporting Note that estimates are based on the global carbon budget estimates from Friedlingstein et al (2020), which estimated higher emissions from the net land-use change flux (ELUC) and a larger natural terrestrial sink Non-intact lands are a proxy for "managed lands" in the country reporting

			2000-2009	2010-2019
ELUC from bookkeeping estimates (from Tab. 5)			1.44	1.61
SLAND	Total	from DGVMs	-2.90	-3.40
	on non-forest lands	from DGVMs	-1.05	-1.38
	on non-intact forest	from DGVMs	-1.39	-1.54
	on intact land (intact forest only for DGVMs)	from DGVMs	-0.46	-0.49
		from cohort-based ORCHIDEE	-1.29	-1.47
SLAND on non-intact lands plus ELUC		from DGVMs and bookkeeping ELUC	0.05	0.08
		from cohort-based ORCHIDEE	1.00	0.61
National greenhouse gas inventories (LULUCF)			0.00	-0.31
FAOSTAT (LULUCF)			0.39	0.20

3
4
5
6



1

Table A9. Funding supporting the production of the various components of the global carbon budget in addition to the authors' supporting institutions (see also acknowledgements).

Funder and grant number (where relevant)	Author Initials
Australia, Integrated Marine Observing System (IMOS)	BT
Australian National Environment Science Program (NESP)	JGC
Belgium, FWO (Flanders Research Foundation, contract IRI I001019N)	TG
BNP Paribas Foundation through Climate & Biodiversity initiative, philanthropic grant for developments of the Global Carbon Atlas	PC
Canada, Tula Foundation	WE
China, National Natural Science Foundation (grant no. 41975155)	XY
Commonwealth Scientific and Industrial Organization (CSIRO) - Climate Science Centre	JGC, JK
EC Copernicus Atmosphere Monitoring Service implemented by ECMWF on behalf of the European Commission	FC
EC Copernicus Marine Environment Monitoring Service implemented by Mercator Ocean	TTTC
EC H2020 (4C; grant no 821003)	PF, RMA, SS, GPP, PC, JIK, TI, LB, PL, LG, SL, NG
EC H2020 (CHE; grant no 776186)	MWJ
EC H2020 (CoCO2; grant no. 958927)	RMA, GPP
EC H2020 (COMFORT; grant no. 820989)	DCEB, LG
EC H2020 (CONSTRAIN; grant no 820829)	RS, PMF, TG
EC H2020 (CRESCENDO; grant no. 641816)	RS, EJ AJPS, TI
EC H2020 (ESM2025 – Earth System Models for the Future; grant agreement No 101003536).	RS, TG, TI, LB, BD
EC H2020 (EuroSea; grant no. 862626)	SDJ
EC H2020 (JERICO-S3; grant no. 871153)	GR
EC H2020 (QUINCY; grant no 647204)	SZ
EC H2020 (RINGO; grant no. 730944)	DCEB
EC H2020 (VERIFY; grant no. 776810)	MWJ, RMA, GPP, PC, JIK, NV, GG
Efg International	TT
EFG International	TT
European Space Agency Climate Change Initiative ESA-CCI RECCAP2 project 655 (ESRIN/4000123002/18/I-NB)	PF, SS, PC
European Space Agency OceanSODA project (grant no. 4000112091/14/I-LG)	LG
France, ICOS (Integrated Carbon Observation System) France	NL
France, Institut de Recherche pour le Développement (IRD)	NL
Germany, Blue Ocean and Federal Ministry of Education (BONUS INTEGRAL; Grant No. 03F0773A)	GR
Germany, Deutsche Forschungsgemeinschaft (DFG) under Germany's Excellence Strategy – EXC 2037 'Climate, Climatic Change, and Society' – Project Number: 390683824	TI
Germany, Federal Ministry for Education and Research (BMBF)	GR
Germany, GEOMAR Helmholtz Centre for Ocean Research	SKL
Germany, German Federal Ministry of Education and Research under project "DArgo2025" (03F0857C)	AK
Germany, Helmholtz Association ATMO programme	PA
Germany, Helmholtz Young Investigator Group Marine Carbon and Ecosystem Feedbacks in the Earth System (MarESys), grant number VH-NG-1301	JH, OG
Germany, ICOS (Integrated Carbon Observation System) Germany	GR, NL
Hapag-Lloyd	TT



Ireland, Marine Institute	MC
Japan, Environment Research and Technology Development Fund of the Ministry of the Environment (JPMEERF21S20810)	YN
Japan, Global Environmental Research Coordination System, Ministry of the Environment (grant number E1751)	SN, TO, CW
Kuehne + Nagel International AG	TT
Mediterranean Shipping Company (MSc)	TT
Monaco, Fondation Prince Albert II de Monaco	TT
Monaco, Yacht Club de Monaco	TT
NASA Interdisciplinary Research in Earth Science Program.	BP
Netherlands Organization for Scientific Research (NWO; grant no. SH-312, 17616)	WP
New Zealand, NIWA MBIE Core funding	KIC
Norway, Norwegian Research Council (grant no. 270061)	JS
Norway, Research Council of Norway, ICOS (Integrated Carbon Observation System) Norway and OTC (Ocean Thematic Centre) (grant no. 245927)	SKL, MB, SDJ
PEAK6 Investments	SKL
Saildrone Inc.	SKL
South Africa, Department of Science and Innovation	LD
South Africa, National Science Foundation	LD
Swiss National Science Foundation (grant no. 200020_172476)	SL
UK Royal Society (grant no. RP\R1\191063)	CLQ
UK, CLASS ERC funding	TG
UK, National Centre for Atmospheric Science (NCAS)	PCM
UK, Natural Environment Research Council (SONATA: grant no. NE/P021417/1)	DW
UK, Natural Environmental Research Council (NE/R016518/1)	LF
UK, Newton Fund, Met Office Climate Science for Service Partnership Brazil (CSSP Brazil)	AJWi
UK, Royal Society: The European Space Agency OCEANFLUX projects	AJWa
UK, University of Reading Research Endowment Trust Fund	PCM
USA, Department of Commerce, Office of Oceanic and Atmospheric Research (OAR)'s / National Oceanic and Atmospheric Administration (NOAA)'s Global Ocean Monitoring and Observation Program (GOMO)	DRM, CS, DP, RW, SRA, RAF, AIS, NRB
USA, Department of Commerce, Office of Oceanic and Atmospheric Research (OAR)'s / National Oceanic and Atmospheric Administration (NOAA)'s Ocean Acidification Program	DP, RW, SRA, RAF, AIS
USA, Department of Energy, Office of Science and BER prg. (grant no. DE-SC000 0016323)	AKJ
USA, Department of Energy, SciDac (DESC0012972)	GCH, LPC
USA, NASA Carbon Monitoring System program and OCO Science team program (80NMO018F0583) .	JL
USA, NASA Interdisciplinary Research in Earth Science (IDS) (80NSSC17K0348)	GCH, LPC
USA, National Science Foundation (grant number 1903722)	HT
USA, National Science Foundation (grant number PLR 1543457)	DRM, CS
USA, Princeton University Environmental Institute and the NASA OCO2 science team, grant number 80NSSC18K0893.	LR
Computing resources	
bwHPC, High Performance Computing Network of the State of Baden-Württemberg, Germany	PA
Cheyenne supercomputer, Computational and Information Systems Laboratory (CISL) at National Center for Atmospheric Research (NCAR)	DK
Deutsches Klimarechenzentrum (allocation bm0891)	JEMSN, JP
MRI (FUJITSU Server PRIMERGY CX2550M5)	YN

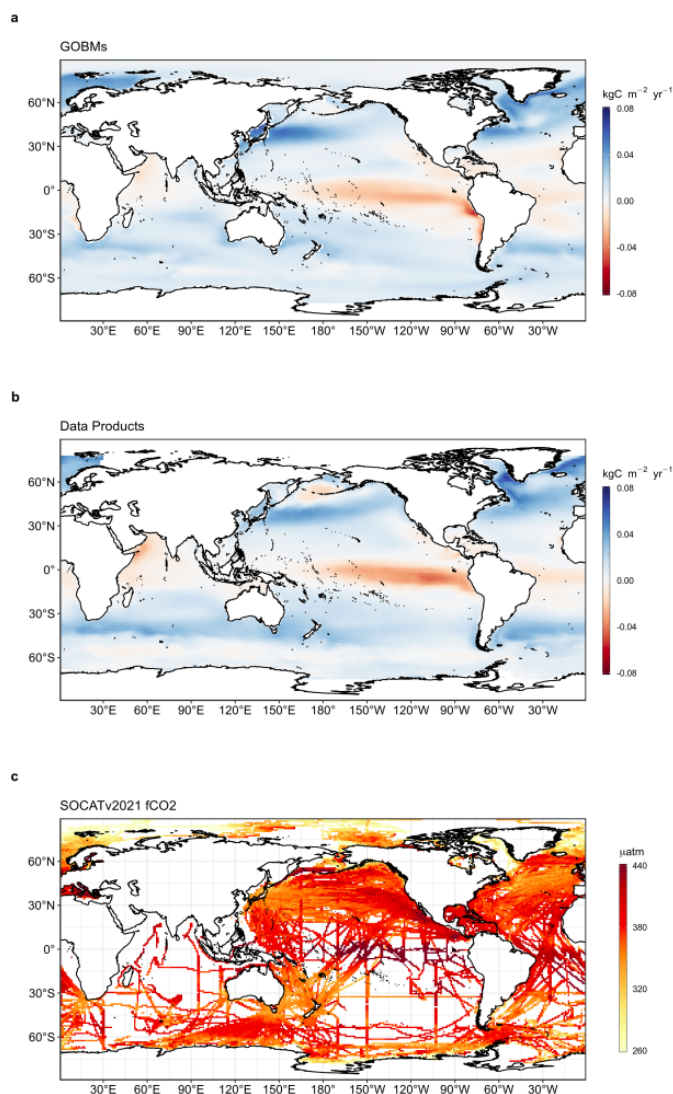


Netherlands Organization for Scientific Research (NWO; NWO-2021.010)	ITL
NIES (SX-Aurora)	YN
NIES supercomputer system	EK
supercomputer 'Gadi' of the National Computational Infrastructure (NCI), Australia	JK
Supercomputing time was provided by the Météo-France/DSI supercomputing center.	RS, BD
TGCC under allocation 2019-A0070102201 made by GENCI	FC
UEA High Performance Computing Cluster, UK	MWJ, CLQ, DRW
UNINETT Sigma2, National Infrastructure for High Performance Computing and Data Storage in Norway (NN2980K/NS2980K)	JS

1



1 Appendix B. Supplementary Figures



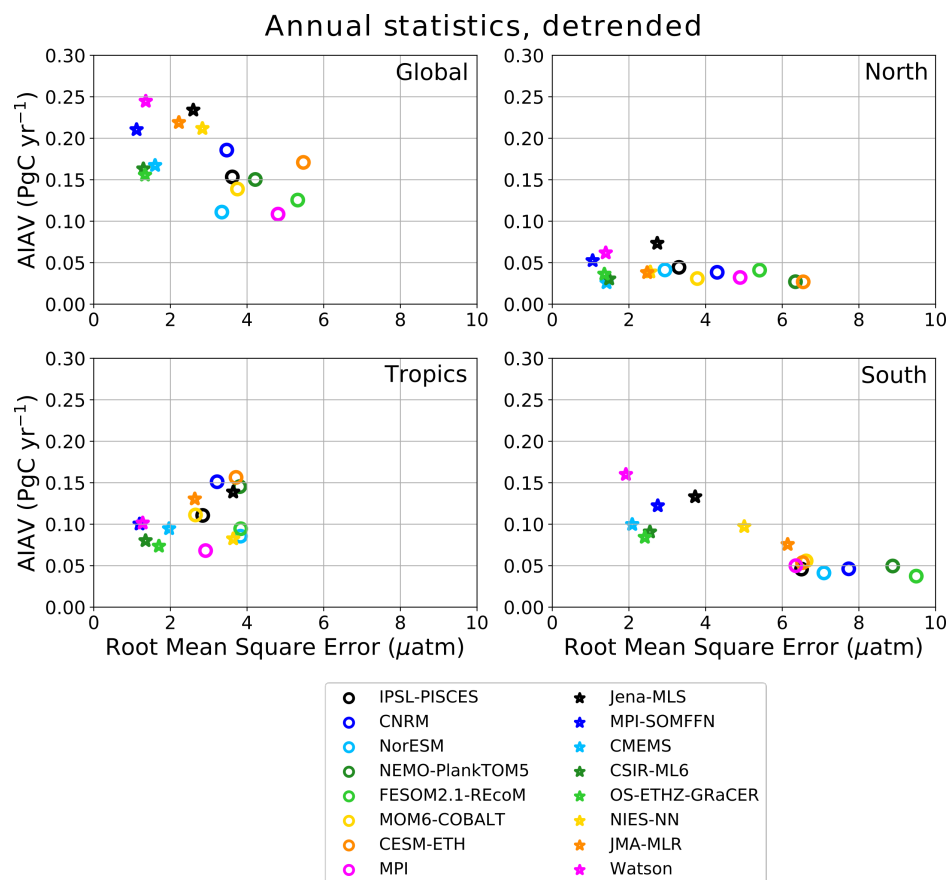
2

3 **Figure B1.** Ensemble mean air-sea CO₂ flux from a) global ocean biogeochemistry models and b)
4 fCO₂ based data products, averaged over 2011-2020 period (kgC m⁻² yr⁻¹). Positive numbers
5 indicate a flux into the ocean. c) gridded SOCAT v2021 fCO₂ measurements, averaged over the
6 2011-2020 period (µatm). In (a) model simulation A is shown. The data-products represent the
7 contemporary flux, i.e. including outgassing of riverine carbon, which is estimated to amount to
8 0.615 GtC yr⁻¹ globally.



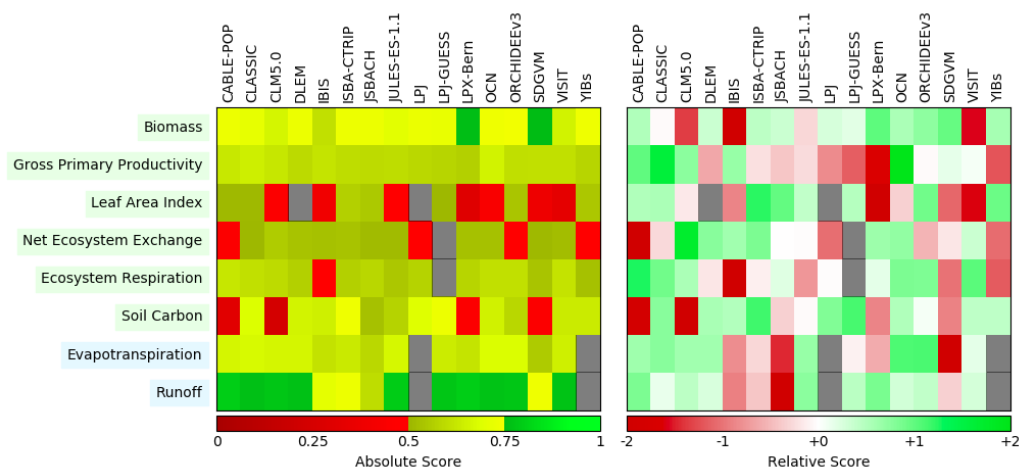
1

2



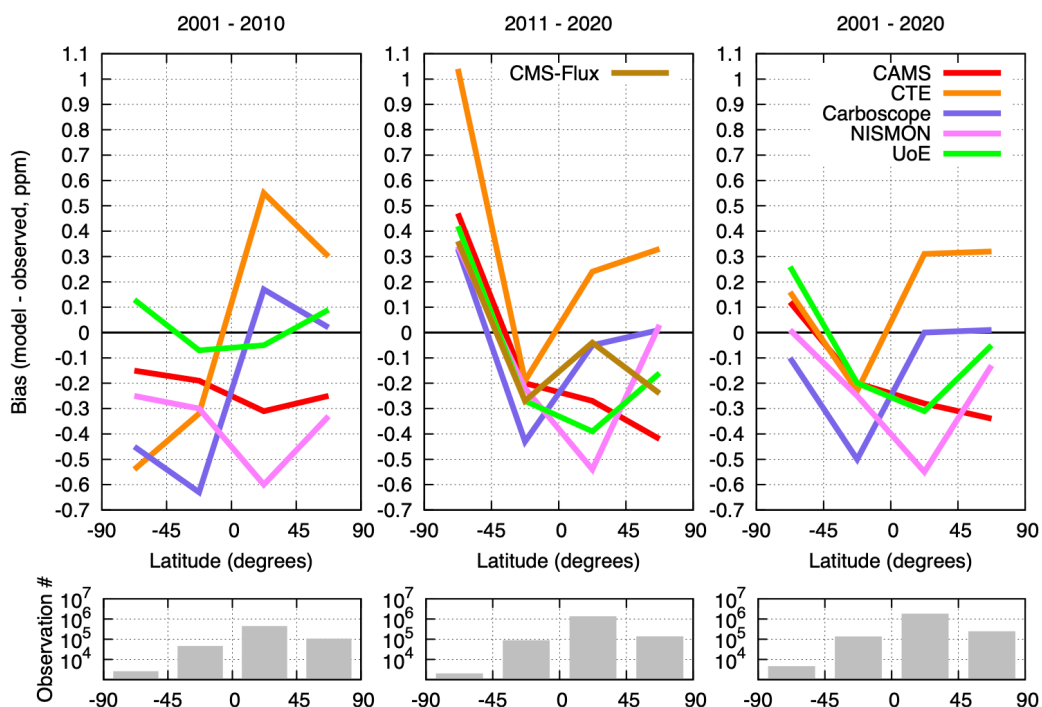
3

4 **Figure B2.** Evaluation of the GOBMs and data products using the root mean squared error (RMSE)
 5 for the period 1990 to 2020, between the individual surface ocean fCO₂ mapping schemes and the
 6 SOCAT v2021 database. The y-axis shows the amplitude of the interannual variability (A-IAV, taken
 7 as the standard deviation of a detrended time series calculated as a 12-months running mean over
 8 the monthly flux time series, Rödenbeck et al., 2015). Results are presented for the globe, north
 9 (>30°N), tropics (30°S–30°N), and south (<30°S) for the GOBMs (see legend circles) and for the
 10 fCO₂-based data products (star symbols). The fCO₂-based data products use the SOCAT database
 11 and therefore are not independent from the data (see section 2.4.1).

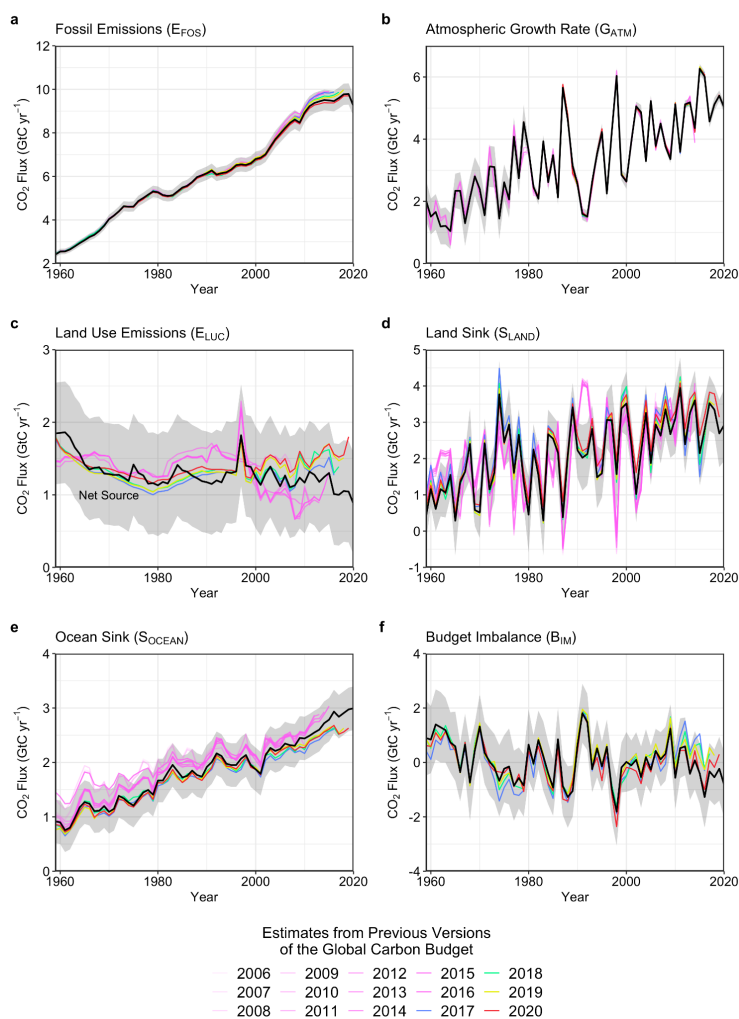


1

2 **Figure B3.** Evaluation of the DGVMs using the International Land Model Benchmarking system
 3 (ILAMB; Collier et al., 2018) (left) absolute skill scores and (right) skill scores relative to other
 4 models. The benchmarking is done with observations for vegetation biomass (Saatchi et al., 2011;
 5 and GlobalCarbon unpublished data; Avitabile et al., 2016), GPP (Jung et al., 2010; Lasslop et al.,
 6 2010), leaf area index (De Kauwe et al., 2011; Myneni et al., 1997), net ecosystem exchange (Jung
 7 et al., 2010; Lasslop et al., 2010), ecosystem respiration (Jung et al., 2010; Lasslop et al., 2010), soil
 8 carbon (Hugelius et al., 2013; Todd-Brown et al., 2013), evapotranspiration (De Kauwe et al.,
 9 2011), and runoff (Dai and Trenberth, 2002). For each model-observation comparison a series of
 10 error metrics are calculated, scores are then calculated as an exponential function of each error
 11 metric, finally for each variable the multiple scores from different metrics and observational data
 12 sets are combined to give the overall variable scores shown in the left panel. Overall variable
 13 scores increase from 0 to 1 with improvements in model performance. The set of error metrics
 14 vary with data set and can include metrics based on the period mean, bias, root mean squared
 15 error, spatial distribution, interannual variability and seasonal cycle. The relative skill score shown
 16 in the right panel is a Z-score, which indicates in units of standard deviation the model scores
 17 relative to the multi-model mean score for a given variable. Grey boxes represent missing model
 18 data.
 19



1
 2 **Figure B4.** Evaluation of the atmospheric inversion products. The mean of the model minus
 3 observations is shown for four latitude bands in three periods: (left) 2001-2010, (centre) 2011-
 4 2020, (right) 2001-2020. The six models are compared to independent CO₂ measurements made
 5 onboard aircraft over many places of the world between 2 and 7 km above sea level. Aircraft
 6 measurements archived in the Cooperative Global Atmospheric Data Integration Project (CGADIP;
 7 Cox et al., 2021) from sites, campaigns or programs that cover at least 9 months between 2001
 8 and 2020 and that have not been assimilated, have been used to compute the biases of the
 9 differences in four 45° latitude bins. Land and ocean data are used without distinction, and
 10 observation density varies strongly with latitude and time as seen on the lower panels.



1

2 **Figure B5.** Comparison of the estimates of each component of the global carbon budget in this
 3 study (black line) with the estimates released annually by the GCP since 2006. Grey shading shows
 4 the uncertainty bounds representing ± 1 standard deviation of the current global carbon budget,
 5 based on the uncertainty assessments described in Appendix C. CO₂ emissions from (a) fossil CO₂
 6 emissions (E_{FOS}), and (b) land-use change (E_{LUC}), as well as their partitioning among (c) the
 7 atmosphere (G_{ATM}), (d) the land (S_{LAND}), and (e) the ocean (S_{OCEAN}). See legend for the
 8 corresponding years, and Tables 3 and A7 for references. The budget year corresponds to the year
 9 when the budget was first released. All values are in GtC yr⁻¹.



1 **Appendix C. Extended Methodology**

2 **Appendix C.1 Methodology Fossil Fuel CO₂ emissions (E_{FOS})**

3 **C.1.1 Cement carbonation**

4 From the moment it is created, cement begins to absorb CO₂ from the atmosphere, a process
5 known as ‘cement carbonation’. We estimate this CO₂ sink, as the average of two studies in the
6 literature (Cao et al., 2020; Guo et al., 2021). Both studies use the same model, developed by Xi et
7 al. (2016), with different parameterisations and input data, with the estimate of Guo and
8 colleagues being a revision of Xi et al (2016). The trends of the two studies are very similar.
9 Modelling cement carbonation requires estimation of a large number of parameters, including the
10 different types of cement material in different countries, the lifetime of the structures before
11 demolition, of cement waste after demolition, and the volumetric properties of structures, among
12 others (Xi et al., 2016). Lifetime is an important parameter because demolition results in the
13 exposure of new surfaces to the carbonation process. The main reasons for differences between
14 the two studies appear to be the assumed lifetimes of cement structures and the geographic
15 resolution, but the uncertainty bounds of the two studies overlap. In the present budget, we
16 include the cement carbonation carbon sink in the fossil CO₂ emission component (E_{FOS}).

17 **C.1.2 Emissions embodied in goods and services**

18 CDIAC, UNFCCC, and BP national emission statistics ‘include greenhouse gas emissions and
19 removals taking place within national territory and offshore areas over which the country has
20 jurisdiction’ (Rypdal et al., 2006), and are called territorial emission inventories. Consumption-
21 based emission inventories allocate emissions to products that are consumed within a country,
22 and are conceptually calculated as the territorial emissions minus the ‘embodied’ territorial
23 emissions to produce exported products plus the emissions in other countries to produce
24 imported products (Consumption = Territorial – Exports + Imports). Consumption-based emission
25 attribution results (e.g. Davis and Caldeira, 2010) provide additional information to territorial-
26 based emissions that can be used to understand emission drivers (Hertwich and Peters, 2009) and
27 quantify emission transfers by the trade of products between countries (Peters et al., 2011b). The
28 consumption-based emissions have the same global total, but reflect the trade-driven movement
29 of emissions across the Earth’s surface in response to human activities. We estimate consumption-



1 based emissions from 1990-2018 by enumerating the global supply chain using a global model of
2 the economic relationships between economic sectors within and between every country (Andrew
3 and Peters, 2013; Peters et al., 2011a). Our analysis is based on the economic and trade data from
4 the Global Trade and Analysis Project (GTAP; Narayanan et al., 2015), and we make detailed
5 estimates for the years 1997 (GTAP version 5), 2001 (GTAP6), and 2004, 2007, and 2011
6 (GTAP9.2), covering 57 sectors and 141 countries and regions. The detailed results are then
7 extended into an annual time series from 1990 to the latest year of the Gross Domestic Product
8 (GDP) data (2018 in this budget), using GDP data by expenditure in current exchange rate of US
9 dollars (USD; from the UN National Accounts main Aggregates database; UN, 2021) and time
10 series of trade data from GTAP (based on the methodology in Peters et al., 2011a). We estimate
11 the sector-level CO₂ emissions using the GTAP data and methodology, include flaring and cement
12 emissions from CDIAC, and then scale the national totals (excluding bunker fuels) to match the
13 emission estimates from the carbon budget. We do not provide a separate uncertainty estimate
14 for the consumption-based emissions, but based on model comparisons and sensitivity analysis,
15 they are unlikely to be significantly different than for the territorial emission estimates (Peters et
16 al., 2012a).

17 **C.1.3 Uncertainty assessment for E_{FOS}**

18 We estimate the uncertainty of the global fossil CO₂ emissions at $\pm 5\%$ (scaled down from the
19 published $\pm 10\%$ at $\pm 2\sigma$ to the use of $\pm 1\sigma$ bounds reported here; Andres et al., 2012). This is
20 consistent with a more detailed analysis of uncertainty of $\pm 8.4\%$ at $\pm 2\sigma$ (Andres et al., 2014) and at
21 the high-end of the range of $\pm 5\text{-}10\%$ at $\pm 2\sigma$ reported by (Ballantyne et al., 2015). This includes an
22 assessment of uncertainties in the amounts of fuel consumed, the carbon and heat contents of
23 fuels, and the combustion efficiency. While we consider a fixed uncertainty of $\pm 5\%$ for all years,
24 the uncertainty as a percentage of emissions is growing with time because of the larger share of
25 global emissions from emerging economies and developing countries (Marland et al., 2009).
26 Generally, emissions from mature economies with good statistical processes have an uncertainty
27 of only a few per cent (Marland, 2008), while emissions from strongly developing economies such
28 as China have uncertainties of around $\pm 10\%$ (for $\pm 1\sigma$; Gregg et al., 2008; Andres et al., 2014).
29 Uncertainties of emissions are likely to be mainly systematic errors related to underlying biases of
30 energy statistics and to the accounting method used by each country.



1 C.1.4 Growth rate in emissions

2 We report the annual growth rate in emissions for adjacent years (in percent per year) by
3 calculating the difference between the two years and then normalising to the emissions in the first
4 year: $(E_{FOS}(t_0+1)-E_{FOS}(t_0))/E_{FOS}(t_0) \times 100\%$. We apply a leap-year adjustment where relevant to
5 ensure valid interpretations of annual growth rates. This affects the growth rate by about 0.3% yr-
6 1 (1/366) and causes calculated growth rates to go up approximately 0.3% if the first year is a leap
7 year and down 0.3% if the second year is a leap year.

8 The relative growth rate of E_{FOS} over time periods of greater than one year can be rewritten using
9 its logarithm equivalent as follows:

$$10 \frac{1}{E_{FOS}} \frac{dE_{FOS}}{dt} = \frac{d(\ln E_{FOS})}{dt} \quad (2)$$

11 Here we calculate relative growth rates in emissions for multi-year periods (e.g. a decade) by
12 fitting a linear trend to $\ln(E_{FOS})$ in Eq. (2), reported in percent per year.

13 C.1.5 Emissions projection for 2021

14 To gain insight on emission trends for 2021, we provide an assessment of global fossil CO₂
15 emissions, E_{FOS} , by combining individual assessments of emissions for China, USA, the EU, and
16 India (the four countries/regions with the largest emissions), and the rest of the world. We
17 provide full year estimates for two datasets: IEA (2021b) and our own analysis. This approach
18 differs from last year where we used four independent estimates including our own, because of
19 the unique circumstances related to the COVID-19 pandemic. This year's analysis is more in line
20 with earlier budgets.

21 Previous editions of the Global Carbon Budget (GCB) have estimated YTD emissions, and
22 performed projections, using sub-annual energy consumption data from a variety of sources
23 depending on the country or region. The YTD estimates have then been projected to the full year
24 using specific methods for each country or region. The methods described in detail below.

25 **China:** The method for the projection uses: (1) the sum of monthly domestic production of raw
26 coal, crude oil, natural gas and cement from the National Bureau of Statistics (NBS, 2021), (2)
27 monthly net imports of coal, coke, crude oil, refined petroleum products and natural gas from the
28 General Administration of Customs of the People's Republic of China (2021); proprietary monthly
29 estimates of sectoral coal consumption by the consultancy SX Coal (2021); and (3) annual energy



1 consumption data by fuel type and annual production data for cement from the NBS, using data
2 for 2000-2020 (NBS, 2021), with the last year being a preliminary estimate. We estimate the full-
3 year growth rate for 2021 using a Bayesian regression for the ratio between the annual energy
4 consumption data (3 above) from 2014 through 2019, and monthly production plus net imports
5 through August of each year (1+2 above) or the corresponding estimate from SX Coal for coal. The
6 uncertainty range uses the standard deviations of the resulting posteriors. Sources of uncertainty
7 and deviations between the monthly and annual growth rates include lack of or incomplete
8 monthly data on stock changes and energy density, variance in the trend during the last three
9 months of the year, and partially unexplained discrepancies between supply-side and
10 consumption data even in the final annual data.

11 Note that in recent years, the absolute value of the annual growth rate for coal energy
12 consumption, and hence total CO₂ emissions, has been consistently lower (closer to zero) than the
13 growth or decline suggested by the monthly, tonnage-based production and import data, and this
14 is reflected in the projection. This pattern is only partially explained by stock changes and changes
15 in energy content, and it is therefore not possible to be certain that it will continue in any given
16 year. For 2020 and 2021, COVID-19-related lockdown and reopening in China, similar but delayed
17 restrictions in major export markets, unusual amounts of flooding and extreme weather during
18 the summer months and extraordinarily high local and global prices of many energy products
19 imply that seasonal patterns and correlations between supply, stock changes and consumption
20 may be quite different this year than in the previous years that the regression is based on. Shocks
21 in the housing market and heightened perceptions of political risk among investors may also affect
22 consumption patterns. This adds a major but unquantified amount of uncertainty to the estimate.

23 **USA:** We use emissions estimated by the U.S. Energy Information Administration (EIA) in their
24 Short-Term Energy Outlook (STEO) for emissions from fossil fuels to get both YTD and a full year
25 projection (EIA, 2021). The STEO also includes a near-term forecast based on an energy
26 forecasting model which is updated monthly (last update with preliminary data through
27 September 2021), and takes into account expected temperatures, household expenditures by fuel
28 type, energy markets, policies, and other effects. We combine this with our estimate of emissions
29 from cement production using the monthly U.S. cement clinker production data from USGS for
30 January-June 2021, assuming changes in cement production over the first part of the year apply
31 throughout the year.



1 **India:** We use monthly emissions estimates for India updated from Andrew (2020b) through
2 August 2021. These estimates are derived from many official monthly energy and other activity
3 data sources to produce direct estimates of national CO₂ emissions, without the use of proxies.
4 Emissions from coal are then extended to September using a regression relationship based on
5 power generated from coal, coal dispatches by Coal India Ltd., the composite PMI, time, and days
6 per month. For the last 3-4 months of the year, each series is extrapolated assuming typical
7 trends.

8 **EU:** We use a refinement to the methods presented by Andrew (2021), deriving emissions from
9 monthly energy data reported by Eurostat. Some data gaps are filled using data from the Joint
10 Organisations Data Initiative (JODI, 2021). Sub-annual cement production data are limited, but
11 data for Germany and Poland, the two largest producers, suggest a small decline. For fossil fuels
12 this provides estimates through July. We extend coal emissions through September using a
13 regression model built from generation of power from hard coal, power from brown coal, total
14 power generation, and the number of working days in Germany and Poland, the two biggest coal
15 consumers in the EU. These are then extended through the end of the year assuming typical
16 trends. We extend oil emissions by building a regression model between our monthly CO₂
17 estimates and oil consumption reported by the EIA for Europe in its Short-Term Energy Outlook
18 (October edition), and then using this model with EIA's monthly forecasts. For natural gas, the
19 strong seasonal signal allows the use of the bias-adjusted Holt-Winters exponential smoothing
20 method (Chatfield, 1978).

21 **Rest of the world:** We use the close relationship between the growth in GDP and the growth in
22 emissions (Raupach et al., 2007) to project emissions for the current year. This is based on a
23 simplified Kaya Identity, whereby E_{FOS} (GtC yr⁻¹) is decomposed by the product of GDP (USD yr⁻¹)
24 and the fossil fuel carbon intensity of the economy (I_{FOS} ; GtC USD⁻¹) as follows:

$$25 \quad E_{FOS} = GDP \times I_{FOS} \quad (3)$$

26 Taking a time derivative of Equation (3) and rearranging gives:

$$27 \quad \frac{1}{E_{FOS}} \frac{dE_{FOS}}{dt} = \frac{1}{GDP} \frac{dGDP}{dt} + \frac{1}{I_{FOS}} \frac{dI_{FOS}}{dt} \quad (4)$$

28 where the left-hand term is the relative growth rate of E_{FOS} , and the right-hand terms are the
29 relative growth rates of GDP and I_{FOS} , respectively, which can simply be added linearly to give the
30 overall growth rate.



1 The I_{FOS} is based on GDP in constant PPP (Purchasing Power Parity) from the International Energy
2 Agency (IEA) up to 2017 (IEA/OECD, 2019) and extended using the International Monetary Fund
3 (IMF) growth rates through 2020 (IMF, 2021). Interannual variability in I_{FOS} is the largest source of
4 uncertainty in the GDP-based emissions projections. We thus use the standard deviation of the
5 annual I_{FOS} for the period 2009-2019 as a measure of uncertainty, reflecting a $\pm 1\sigma$ as in the rest of
6 the carbon budget.

7 **World:** The global total is the sum of each of the countries and regions.

8

9 **Appendix C.2 Methodology CO₂ emissions from land-use, land-use change and forestry (E_{LUC})**

10 The net CO₂ flux from land-use, land-use change and forestry (E_{LUC} , called land-use change
11 emissions in the rest of the text) includes CO₂ fluxes from deforestation, afforestation, logging and
12 forest degradation (including harvest activity), shifting cultivation (cycle of cutting forest for
13 agriculture, then abandoning), and regrowth of forests following wood harvest or abandonment
14 of agriculture. Emissions from peat burning and drainage are added from external datasets (see
15 section C.2.1 below). Only some land-management activities are included in our land-use change
16 emissions estimates (Table A1). Some of these activities lead to emissions of CO₂ to the
17 atmosphere, while others lead to CO₂ sinks. E_{LUC} is the net sum of emissions and removals due to
18 all anthropogenic activities considered. Our annual estimate for 1960-2020 is provided as the
19 average of results from three bookkeeping approaches (Section C.2.1 below): an estimate using
20 the Bookkeeping of Land Use Emissions model (Hansis et al., 2015; hereafter BLUE) and one using
21 the compact Earth system model OSCAR (Gasser et al., 2020), both BLUE and OSCAR being
22 updated here to new land-use forcing covering the time period until 2020, and an updated version
23 of the estimate published by Houghton and Nassikas (2017) (hereafter updated H&N2017). All
24 three data sets are then extrapolated to provide a projection for 2021 (Section C.2.5 below). In
25 addition, we use results from Dynamic Global Vegetation Models (DGVMs; see Section 2.5 and
26 Table 4) to help quantify the uncertainty in E_{LUC} (Section C.2.4), and thus better characterise our
27 understanding. Note that in this budget, we use the scientific E_{LUC} definition, which counts fluxes
28 due to environmental changes on managed land towards S_{LAND} , as opposed to the national
29 greenhouse gas inventories under the UNFCCC, which include them in E_{LUC} and thus often report



1 smaller land-use emissions (Grassi et al., 2018; Petrescu et al., 2020). However, we provide a
2 methodology of mapping of the two approaches to each other further below (Section C.2.3).

3 **C.2.1 Bookkeeping models**

4 Land-use change CO₂ emissions and uptake fluxes are calculated by three bookkeeping models.
5 These are based on the original bookkeeping approach of Houghton (2003) that keeps track of the
6 carbon stored in vegetation and soils before and after a land-use change (transitions between
7 various natural vegetation types, croplands, and pastures). Literature-based response curves
8 describe decay of vegetation and soil carbon, including transfer to product pools of different
9 lifetimes, as well as carbon uptake due to regrowth. In addition, the bookkeeping models
10 represent long-term degradation of primary forest as lowered standing vegetation and soil carbon
11 stocks in secondary forests, and include forest management practices such as wood harvests.

12 BLUE and the updated H&N2017 exclude land ecosystems' transient response to changes in
13 climate, atmospheric CO₂ and other environmental factors, and base the carbon densities on
14 contemporary data from literature and inventory data. Since carbon densities thus remain fixed
15 over time, the additional sink capacity that ecosystems provide in response to CO₂-fertilization
16 and some other environmental changes is not captured by these models (Pongratz et al., 2014).
17 On the contrary, OSCAR includes this transient response, and it follows a theoretical framework
18 (Gasser and Ciais, 2013) that allows separating bookkeeping land-use emissions and the loss of
19 additional sink capacity. Only the former is included here, while the latter is discussed in Appendix
20 D4. The bookkeeping models differ in (1) computational units (spatially explicit treatment of land-
21 use change for BLUE, regional-/ mostly country-level for the updated H&N2017 and OSCAR), (2)
22 processes represented (see Table A1), and (3) carbon densities assigned to vegetation and soil of
23 each vegetation type (literature-based for the updated H&N2017 and BLUE, calibrated to DGVMs
24 for OSCAR). A notable difference between models exists with respect to the treatment of shifting
25 cultivation. The update of H&N2017 changed the approach over the earlier H&N2017 version:
26 H&N2017 had assumed the "excess loss" of tropical forests (i.e., when FRA indicated a forest loss
27 larger than the increase in agricultural areas from FAO) resulted from converting forests to
28 croplands at the same time older croplands were abandoned. Those abandoned croplands began
29 to recover to forests after 15 years. The updated H&N2017 now assumes that forest loss in excess
30 of increases in cropland and pastures represented an increase in shifting cultivation. When the
31 excess loss of forests was negative, it was assumed that shifting cultivation was returned to forest.



1 Historical areas in shifting cultivation were extrapolated taking into account country-based
2 estimates of areas in fallow in 1980 (FAO/UNEP, 1981) and expert opinion (from Heinemann et al.,
3 2017). In contrast, the BLUE and OSCAR models include sub-grid-scale transitions between all
4 vegetation types. Furthermore, the updated H&N2017 assume conversion of natural grasslands to
5 pasture, while BLUE and OSCAR allocate pasture proportionally on all natural vegetation that
6 exists in a grid-cell. This is one reason for generally higher emissions in BLUE and OSCAR.
7 Bookkeeping models do not directly capture carbon emissions from peat fires, which can create
8 large emissions and interannual variability due to synergies of land-use and climate variability in
9 Southeast Asia, particularly during El-Niño events, nor emissions from the organic layers of
10 drained peat soils. To correct for this, the updated H&N2017 includes carbon emissions from
11 burning and draining of peatlands in Indonesia, Malaysia, and Papua New Guinea (based on the
12 Global Fire Emission Database (GFED4s; van der Werf et al., 2017) for fire and Hooijer et al. for
13 drainage. Further, estimates of carbon losses from peatlands in extra-tropical regions are added
14 from Qiu et al. (2021). We add GFED4s peat fire emissions to BLUE and OSCAR output as well as
15 the global FAO peat drainage emissions 1990-2018 from croplands and grasslands (Conchedda
16 and Tubiello, 2020), keeping post-2018 emissions constant. We linearly increase tropical drainage
17 emissions from 0 in 1980, consistent with H&N2017's assumption, and keep emissions from the
18 often old drained areas of the extra-tropics constant pre-1990. This adds 9.0 GtC for FAO
19 compared to 5.6 GtC for Hooijer et al. (2010). Peat fires add another 2.0 GtC over the same
20 period.

21 The three bookkeeping estimates used in this study differ with respect to the land-use change
22 data used to drive the models. The updated H&N2017 base their estimates directly on the Forest
23 Resource Assessment of the FAO which provides statistics on forest-area change and management
24 at intervals of five years currently updated until 2020 (FAO, 2020). The data is based on country
25 reporting to FAO and may include remote-sensing information in more recent assessments.
26 Changes in land-use other than forests are based on annual, national changes in cropland and
27 pasture areas reported by FAO (FAOSTAT, 2021). On the other hand, BLUE uses the harmonised
28 land-use change data LUH2-GCB2021 covering the entire 1850-2020 period (an update to the
29 previously released LUH2 v2h dataset; Hurtt et al., 2017; Hurtt et al., 2020), which was also used
30 as input to the DGVMs (Sec. 2.2.2). It describes land-use change, also based on the FAO data as
31 well as the HYDE3.3 dataset (Goldewijk et al., 2017a, 2017b), but provided at a quarter-degree



1 spatial resolution, considering sub-grid-scale transitions between primary forest, secondary forest,
2 primary non-forest, secondary non-forest, cropland, pasture, rangeland, and urban land (Hurt et
3 al., 2020; Chini et al., 2021). LUH2-GCB2021 provides a distinction between rangelands and
4 pasture, based on inputs from HYDE. To constrain the models' interpretation on whether
5 rangeland implies the original natural vegetation to be transformed to grassland or not (e.g.,
6 browsing on shrubland), a forest mask was provided with LUH2-GCB2021; forest is assumed to be
7 transformed to grasslands, while other natural vegetation remains (in case of secondary
8 vegetation) or is degraded from primary to secondary vegetation (Ma et al., 2020). This is
9 implemented in BLUE. OSCAR was run with both LUH2-GCB2021 and FAO/FRA (as used by
10 Houghton and Nassikas, 2017), where emissions from the latter were extended beyond 2015 with
11 constant 2011–2015 average values. The best-guess OSCAR estimate used in our study is a
12 combination of results for LUH2-GCB2021 and FAO/FRA land-use data and a large number of
13 perturbed parameter simulations weighted against an observational constraint. All three
14 bookkeeping estimates were extended from 2020 to provide a projection for 2021 by adding the
15 annual change in emissions from tropical deforestation and degradation and peat burning and
16 drainage to the respective model's estimate for 2020 (van der Werf et al., 2017, Conchedda &
17 Tubiello, 2020).

18 For E_{LUC} from 1850 onwards we average the estimates from BLUE, the updated H&N2017 and
19 OSCAR. For the cumulative numbers starting 1750 an average of four earlier publications is added
20 (30 ± 20 PgC 1750-1850, rounded to nearest 5; Le Quéré et al., 2016).

21 We provide estimates of the gross land use change fluxes from which the reported net land-use
22 change flux, E_{LUC} , is derived as a sum. Gross fluxes are derived internally by the three bookkeeping
23 models: Gross emissions stem from decaying material left dead on site and from products after
24 clearing of natural vegetation for agricultural purposes, wood harvesting, emissions from peat
25 drainage and peat burning, and, for BLUE, additionally from degradation from primary to
26 secondary land through usage of natural vegetation as rangeland. Gross removals stem from
27 regrowth after agricultural abandonment and wood harvesting. Gross fluxes for the updated
28 H&N2017 2016-2020 and for the 2021 projection of all three models were based on a regression
29 of gross sources (including peat emissions) to net emissions for recent years.

30 Due to an artifact in the HYDE3.3 data causing large abrupt transitions, an unrealistic peak in
31 emissions occurs around 1960 in BLUE and OSCAR. To correct for this, we replace the estimates



1 for 1959-1961 by the average of 1958 and 1962 in each BLUE and OSCAR. Abrupt transitions will
2 immediately influence gross emissions, which have a larger instantaneous component. Processes
3 with longer timescales, such as slow legacy emissions and regrowth, are inseparable from the
4 carbon dynamics due to subsequent land-use change events. We therefore do not adjust gross
5 removals, but only gross emissions to match the corrected net flux. Since DGVMs estimates are
6 only used for an uncertainty range of E_{LUC} , which is independent of land-use changes, no
7 correction is applied to the DGVMs data.

8 **C.2.2 Dynamic Global Vegetation Models (DGVMs)**

9 Land-use change CO_2 emissions have also been estimated using an ensemble of 17 DGVMs
10 simulations. The DGVMs account for deforestation and regrowth, the most important components
11 of E_{LUC} , but they do not represent all processes resulting directly from human activities on land
12 (Table A1). All DGVMs represent processes of vegetation growth and mortality, as well as
13 decomposition of dead organic matter associated with natural cycles, and include the vegetation
14 and soil carbon response to increasing atmospheric CO_2 concentration and to climate variability
15 and change. Most models explicitly simulate the coupling of carbon and nitrogen cycles and
16 account for atmospheric N deposition and N fertilisers (Table A1). The DGVMs are independent
17 from the other budget terms except for their use of atmospheric CO_2 concentration to calculate
18 the fertilization effect of CO_2 on plant photosynthesis.

19 DGVMs that do not simulate subgrid scale transitions (i.e., net land-use emissions; see Table A1)
20 used the HYDE land-use change data set (Goldewijk et al., 2017a, 2017b), which provides annual
21 (1700-2019), half-degree, fractional data on cropland and pasture. The data are based on the
22 available annual FAO statistics of change in agricultural land area available until 2015. The new
23 HYDE3.3 cropland/grazing land dataset which now in addition to FAO country-level statistics is
24 constrained spatially based on multi-year satellite land cover maps from ESA CCI LC. Data from
25 HYDE3.3 is based on a FAO which includes yearly data from 1961 up to and including the year
26 2017. After the year 2017 HYDE extrapolates the cropland, pasture, and urban data, based on the
27 trend over the previous 5 years, to generate data until the year 2020. HYDE also uses satellite
28 imagery from ESA-CCI from 1992 – 2018 for more detailed yearly allocation of cropland and
29 grazing land. The 2018 map is also used for the 2019-2020 period. The original 300 meter
30 resolution data from ESA was aggregated to a 5 arc minute resolution according to the
31 classification scheme as described in Klein Goldewijk et al (2017a). DGVMs that simulate subgrid



1 scale transitions (i.e., gross land-use emissions; see Table A1) also use the LUH2-GCB2021 data set,
2 an update of the more comprehensive harmonised land-use data set (Hurtt et al., 2020), that
3 further includes fractional data on primary and secondary forest vegetation, as well as all
4 underlying transitions between land-use states (850-2020; Hurtt et al., 2011, 2017, 2020; Chini et
5 al., 2021; Table A1). This new data set is of quarter degree fractional areas of land-use states and
6 all transitions between those states, including a new wood harvest reconstruction, new
7 representation of shifting cultivation, crop rotations, management information including irrigation
8 and fertilizer application. The land-use states include five different crop types in addition to the
9 pasture-rangeland split discussed before. Wood harvest patterns are constrained with Landsat-
10 based tree cover loss data (Hansen et al. 2013). Updates of LUH2-GCB2021 over last year's version
11 (LUH2-GCB2020) are using the most recent HYDE/FAO release (covering the time period up to
12 2021 included). We also use the most recent FAO wood harvest data for all years from 1961 to
13 2019. After the year 2019 we extrapolated the wood harvest data until the year 2020. The
14 HYDE3.3 population data is also used to extend the wood harvest time series back in time. Other
15 wood harvest inputs (for years prior to 1961) remain the same in LUH2.

16 DGVMs implement land-use change differently (e.g., an increased cropland fraction in a grid cell
17 can either be at the expense of grassland or shrubs, or forest, the latter resulting in deforestation;
18 land cover fractions of the non-agricultural land differ between models). Similarly, model-specific
19 assumptions are applied to convert deforested biomass or deforested area, and other forest
20 product pools into carbon, and different choices are made regarding the allocation of rangelands
21 as natural vegetation or pastures.

22 The difference between two DGVMs simulations (See Section C4.1 below), one forced with
23 historical changes in land-use and a second with time-invariant pre-industrial land cover and pre-
24 industrial wood harvest rates, allows quantification of the dynamic evolution of vegetation
25 biomass and soil carbon pools in response to land-use change in each model (E_{LUC}). Using the
26 difference between these two DGVMs simulations to diagnose E_{LUC} means the DGVMs account for
27 the loss of additional sink capacity (around 0.4 ± 0.3 GtC yr⁻¹; see Section 2.7.4, Appendix D4),
28 while the bookkeeping models do not.

29 As a criterion for inclusion in this carbon budget, we only retain models that simulate a positive
30 E_{LUC} during the 1990s, as assessed in the IPCC AR4 (Denman et al., 2007) and AR5 (Ciais et al.,
31 2013). All DGVMs met this criterion, although one model was not included in the E_{LUC} estimate



1 from DGVMs as it exhibited a spurious response to the transient land cover change forcing after
2 its initial spin-up.

3 **C.2.3 Mapping of national GHG inventory data to E_{LUC}**

4 For the first time, an approach is implemented to reconcile the large gap between E_{LUC} from
5 bookkeeping models and land use, land-use change and forestry (LULUCF) from national GHG
6 Inventories (NGHGI) (see Tab. A8). This gap is due to different approaches to calculating
7 “anthropogenic” CO_2 fluxes related to land-use change and land management (Grassi et al. 2018).
8 In particular, the land sinks due to environmental change on managed lands are treated as non-
9 anthropogenic in the global carbon budget, while they are generally considered as anthropogenic
10 in NGHGIs (“indirect anthropogenic fluxes”; Eggleston et al., 2006). Building on previous studies
11 (Grassi et al. 2021), the approach implemented here adds the DGVMs estimates of CO_2 fluxes due
12 to environmental change from countries’ managed forest area (part of the S_{LAND}) to the original
13 E_{LUC} flux. This sum is expected to be conceptually more comparable to LULUCF than simply E_{LUC} .
14 E_{LUC} data are taken from bookkeeping models, in line with the global carbon budget approach. To
15 determine S_{LAND} on managed forest, the following steps were taken: Spatially gridded data of
16 “natural” forest NBP (S_{LAND} i.e., due to environmental change and excluding land use change
17 fluxes) were obtained with S2 runs from DGVMs up to 2019 from the TRENDY v9 dataset. Results
18 were first masked with the Hansen forest map (Hansen et al. 2013), with a 20% tree cover and
19 following the FAO definition of forest (isolated pixels with maximum connectivity less than 0.5 ha
20 are excluded), and then further masked with the “intact” forest map for the year 2013, i.e. forest
21 areas characterized by no remotely detected signs of human activity (Potapov et al. 2017). This
22 way, we obtained the S_{LAND} in “intact” and “non-intact” forest area, which previous studies (Grassi
23 et al. 2021) indicated to be a good proxy, respectively, for “unmanaged” and “managed” forest
24 area in the NGHGI. Note that only 4 models (CABLE-POP, CLASSIC, YIBs and ORCHIDEE-CNP) had
25 forest NBP at grid cell level. Two models (OCN and ISBA-CTRIP) provided forest NEP and simulated
26 disturbances at pixel level that were used as basis, in addition to forest cover fraction, to estimate
27 forest NBP. For the other DGVMs, when a grid cell had forest, all the NBP was allocated to forest.
28 LULUCF data from NGHGIs are from Grassi et al. (2021) until 2017, updated until 2019 for Annex I
29 countries. For non-Annex I countries, the years 2018 and 2019 were assumed equal to the average
30 2013-2017. This data includes all CO_2 fluxes from land considered managed, which in principle



1 encompasses all land uses (forest land, cropland, grassland, wetlands, settlements, and other
2 land), changes among them, emissions from organic soils and from fires. In practice, although
3 almost all Annex I countries report all land uses, many non-Annex I countries report only on
4 deforestation and forest land, and only few countries report on other land uses. In most cases,
5 NGHGI include most of the natural response to recent environmental change, because they use
6 direct observations (e.g., national forest inventories) that do not allow separating direct and
7 indirect anthropogenic effects (Eggleston et al., 2006).

8 To provide additional, largely independent assessments of fluxes on unmanaged vs managed
9 lands, we include a DGVM that allows diagnosing fluxes from unmanaged vs managed lands by
10 tracking vegetation cohorts of different ages separately. This model, ORCHIDEE-MICT (Yue et al.,
11 2018), was run using the same LUH2 forcing as the DGVMs used in this budget (Section 2.5) and
12 the bookkeeping models BLUE and OSCAR (Section 2.2). Old-aged forest was classified as primary
13 forest after a certain threshold of carbon density was reached again, and the model-internal
14 distinction between primary and secondary forest used as proxies for unmanaged vs managed
15 forests; agricultural lands are added to the latter to arrive at total managed land.

16 Tab. A8 shows the resulting mapping of global carbon cycle models' land flux definitions to that of
17 the NGHGI (discussed in Sec. 3.2.2). Note that estimates in this table are based on the global
18 carbon budget estimates from Friedlingstein et al. (2020), which estimated higher emissions from
19 the net land-use change flux (E_{LUC}) and a larger natural terrestrial sink. ORCHIDEE-MICT estimates
20 for S_{LAND} on intact forests are expected to be higher than based on DGVMs in combination with
21 the NGHGI managed/unmanaged forest data because the unmanaged forest area, with about 27
22 mio km², is estimated to be substantially larger by ORCHIDEE-MICT than, with less than 10 mio
23 km², by the NGHGI, while managed forest area is estimated to be smaller (22 compared to 32 mio
24 km²). Related to this, S_{LAND} on non-intact lands plus E_{LUC} is a larger source estimated by ORCHIDEE-
25 MICT compared to NGHGI. We also show as comparison FAOSTAT emissions totals (FAO, 2021),
26 which include emissions from net forest conversion and fluxes on forest land (Tubiello et al., 2021)
27 as well as CO₂ emissions from peat drainage and peat fires.

28 **C.2.4 Uncertainty assessment for E_{LUC}**

29 Differences between the bookkeeping models and DGVMs models originate from three main
30 sources: the different methodologies, which among others lead to inclusion of the loss of



1 additional sink capacity in DGVMs (see Appendix D1.4), the underlying land-use/land cover data
2 set, and the different processes represented (Table A1). We examine the results from the DGVMs
3 models and of the bookkeeping method and use the resulting variations as a way to characterise
4 the uncertainty in E_{LUC} .

5 Despite these differences, the E_{LUC} estimate from the DGVMs multi-model mean is consistent with
6 the average of the emissions from the bookkeeping models (Table 5). However there are large
7 differences among individual DGVMs (standard deviation at around 0.5 GtC yr^{-1} ; Table 5), between
8 the bookkeeping estimates (average difference 1850-2020 BLUE-updated H&N2017 of 0.8 GtC yr^{-1} ,
9 BLUE-OSCAR of 0.4 GtC yr^{-1} , OSCAR-updated H&N2017 of 0.3 GtC yr^{-1}), and between the updated
10 estimate of H&N2017 and its previous model version (Houghton et al., 2012). A factorial analysis
11 of differences between BLUE and H&N2017 attributed them particularly to differences in carbon
12 densities between natural and managed vegetation or primary and secondary vegetation (Bastos
13 et al., 2021). Earlier studies additionally showed the relevance of the different land-use forcing as
14 applied (in updated versions) also in the current study (Gasser et al., 2020).

15 The uncertainty in E_{LUC} of $\pm 0.7 \text{ GtC yr}^{-1}$ reflects our best value judgment that there is at least 68%
16 chance ($\pm 1\sigma$) that the true land-use change emission lies within the given range, for the range of
17 processes considered here. Prior to the year 1959, the uncertainty in E_{LUC} was taken from the
18 standard deviation of the DGVMs. We assign low confidence to the annual estimates of E_{LUC}
19 because of the inconsistencies among estimates and of the difficulties to quantify some of the
20 processes in DGVMs.

21 **C.2.5 Emissions projections for E_{LUC}**

22 We project the 2021 land-use emissions for BLUE, the updated H&N2017 and OSCAR, starting
23 from their estimates for 2020 assuming unaltered peat drainage, which has low interannual
24 variability, and the highly variable emissions from peat fires, tropical deforestation and
25 degradation as estimated using active fire data (MCD14ML; Giglio et al., 2016). Those latter scale
26 almost linearly with GFED over large areas (van der Werf et al., 2017), and thus allows for tracking
27 fire emissions in deforestation and tropical peat zones in near-real time. During most years,
28 emissions during January-September cover most of the fire season in the Amazon and Southeast
29 Asia, where a large part of the global deforestation takes place, and our estimates capture
30 emissions until the end of September.



1

2 **Appendix C.3 Methodology Ocean CO₂ sink**

3 **C.3.1 Observation-based estimates**

4 We primarily use the observational constraints assessed by IPCC of a mean ocean CO₂ sink of $2.2 \pm$
5 0.7 GtC yr^{-1} for the 1990s (90% confidence interval; Ciais et al., 2013) to verify that the GOBMs
6 provide a realistic assessment of S_{OCEAN} . This is based on indirect observations with seven
7 different methodologies and their uncertainties, using the methods that are deemed most reliable
8 for the assessment of this quantity (Denman et al., 2007; Ciais et al., 2013). The observation-based
9 estimates use the ocean/land CO₂ sink partitioning from observed atmospheric CO₂ and O₂/N₂
10 concentration trends (Manning and Keeling, 2006; Keeling and Manning, 2014), an oceanic
11 inversion method constrained by ocean biogeochemistry data (Mikaloff Fletcher et al., 2006), and
12 a method based on penetration time scale for chlorofluorocarbons (McNeil et al., 2003). The IPCC
13 estimate of 2.2 GtC yr^{-1} for the 1990s is consistent with a range of methods (Wanninkhof et al.,
14 2013). We refrain from using the IPCC estimates for the 2000s ($2.3 \pm 0.7 \text{ GtC yr}^{-1}$), and the period
15 2002-2011 ($2.4 \pm 0.7 \text{ GtC yr}^{-1}$, Ciais et al., 2013) as these are based on trends derived mainly from
16 models and one data-product (Ciais et al., 2013). Additional constraints summarized in AR6
17 (Canadell et al., 2021) are the interior ocean anthropogenic carbon change (Gruber et al., 2019)
18 and ocean sink estimate from atmospheric CO₂ and O₂/N₂ (Tohjima et al., 2019) which are used
19 for model evaluation and discussion, respectively.

20 We also use eight estimates of the ocean CO₂ sink and its variability based on surface ocean fCO₂
21 maps obtained by the interpolation of surface ocean fCO₂ measurements from 1990 onwards due
22 to severe restriction in data availability prior to 1990 (Figure 9). These estimates differ in many
23 respects: they use different maps of surface fCO₂, different atmospheric CO₂ concentrations, wind
24 products and different gas-exchange formulations as specified in Table A3. We refer to them as
25 fCO₂-based flux estimates. The measurements underlying the surface fCO₂ maps are from the
26 Surface Ocean CO₂ Atlas version 2021 (SOCATv2021; Bakker et al., 2021), which is an update of
27 version 3 (Bakker et al., 2016) and contains quality-controlled data through 2020 (see data
28 attribution Table A5). Each of the estimates uses a different method to then map the SOCAT
29 v2021 data to the global ocean. The methods include a data-driven diagnostic method (Rödenbeck
30 et al., 2013; referred to here as Jena-MLS), three neural network models (Landschützer et al.,



1 2014; referred to as MPI-SOMFFN; Chau et al., 2021; Copernicus Marine Environment Monitoring
2 Service, referred to here as CMEMS-LSCE-FFNN; and Zeng et al., 2014; referred to as NIES-FNN),
3 two cluster regression approaches (Gregor et al., 2019; referred to here as CSIR-ML6; and Gregor
4 and Gruber, 2021, referred to as OS-ETHZ-GRaCER), and a multi-linear regression method (Iida et
5 al., 2021; referred to as JMA-MLR). The ensemble mean of the $f\text{CO}_2$ -based flux estimates is
6 calculated from these seven mapping methods. Further, we show the flux estimate of Watson et
7 al. (2020) who also use the MPI-SOMFFN method to map the adjusted $f\text{CO}_2$ data to the globe, but
8 resulting in a substantially larger ocean sink estimate, owing to a number of adjustments they
9 applied to the surface ocean $f\text{CO}_2$ data and the gas-exchange parameterization. Concretely, these
10 authors adjusted the SOCAT $f\text{CO}_2$ downward to account for differences in temperature between
11 the depth of the ship intake and the relevant depth right near the surface, and included a further
12 adjustment to account for the cool surface skin temperature effect. The Watson et al. flux
13 estimate hence differs from the others by their choice of adjusting the flux to a cool, salty ocean
14 surface skin. Watson et al. (2020) showed that this temperature adjustment leads to an upward
15 correction of the ocean carbon sink, up to 0.9 GtC yr^{-1} , that, if correct, should be applied to all
16 $f\text{CO}_2$ -based flux estimates. So far, this adjustment is based on a single line of evidence and hence
17 associated with low confidence until further evidence is available. The Watson et al flux estimate
18 presented here is therefore not included in the ensemble mean of the $f\text{CO}_2$ -based flux estimates.
19 This choice will be re-evaluated in upcoming budgets based on further lines of evidence.

20 The CO_2 flux from each $f\text{CO}_2$ -based product is either already at or above 98% areal coverage (Jena-
21 MLS, OS-ETHZ-GRaCER), filled by the data-provider (using Fay et al., 2021a, method for JMA-MLR;
22 and Landschützer et al., 2020, methodology for MPI-SOMFFN) or scaled for the remaining
23 products by the ratio of the total ocean area covered by the respective product to the total ocean
24 area ($361.9\text{e}6 \text{ km}^2$) from ETOPO1 (Amante and Eakins, 2009; Eakins and Sharman, 2010). In
25 products where the covered area varies with time (e.g., CMEMS-LSCE-FFNN) we use the maximum
26 area coverage. The lowest coverage is 93% (NIES-NN), resulting in a maximum adjustment factor
27 of 1.08 (Table A3, Hauck et al., 2020).

28 We further use results from two diagnostic ocean models, Khatiwala et al. (2013) and DeVries
29 (2014), to estimate the anthropogenic carbon accumulated in the ocean prior to 1959. The two
30 approaches assume constant ocean circulation and biological fluxes, with S_{OCEAN} estimated as a
31 response in the change in atmospheric CO_2 concentration calibrated to observations. The



1 uncertainty in cumulative uptake of ± 20 GtC (converted to $\pm 1\sigma$) is taken directly from the IPCC's
2 review of the literature (Rhein et al., 2013), or about $\pm 30\%$ for the annual values (Khaliwala et al.,
3 2009).

4 **C.3.2 Global Ocean Biogeochemistry Models (GOBMs)**

5 The ocean CO₂ sink for 1959-2019 is estimated using eight GOBMs (Table A2). The GOBMs
6 represent the physical, chemical, and biological processes that influence the surface ocean
7 concentration of CO₂ and thus the air-sea CO₂ flux. The GOBMs are forced by meteorological
8 reanalysis and atmospheric CO₂ concentration data available for the entire time period. They
9 mostly differ in the source of the atmospheric forcing data (meteorological reanalysis), spin up
10 strategies, and in their horizontal and vertical resolutions (Table A2). All GOBMs except one
11 (CESM-ETHZ) do not include the effects of anthropogenic changes in nutrient supply (Duce et al.,
12 2008). They also do not include the perturbation associated with changes in riverine organic
13 carbon (see Section 2.7.3).

14 Three sets of simulations were performed with each of the GOBMs. Simulation A applied historical
15 changes in climate and atmospheric CO₂ concentration. Simulation B is a control simulation with
16 constant atmospheric forcing (normal year or repeated year forcing) and constant pre-industrial
17 atmospheric CO₂ concentration. Simulation C is forced with historical changes in atmospheric CO₂
18 concentration, but repeated year or normal year atmospheric climate forcing. To derive S_{OCEAN}
19 from the model simulations, we subtracted the annual time series of the control simulation B from
20 the annual time series of simulation A. Assuming that drift and bias are the same in simulations A
21 and B, we thereby correct for any model drift. Further, this difference also removes the natural
22 steady state flux (assumed to be 0 GtC yr⁻¹ globally without rivers) which is often a major source of
23 biases. Simulation B of IPSL had to be treated differently as it was forced with constant
24 atmospheric CO₂ but observed historical changes in climate. For IPSL, we fitted a linear trend to
25 the simulation B and subtracted this linear trend from simulation A. This approach assures that
26 the interannual variability is not removed from IPSL simulation A.

27 The absolute correction for bias and drift per model in the 1990s varied between <0.01 GtC yr⁻¹
28 and 0.26 GtC yr⁻¹, with six models having positive biases, and one model having essentially no bias
29 (NorESM). The remaining model (MPI) uses riverine input and therefore simulates outgassing in
30 simulation B, i.e., a seemingly negative bias. By subtracting simulation B, also the ocean carbon



1 sink of the MPI model follows the definition of S_{OCEAN} . This correction reduces the model mean
2 ocean carbon sink by 0.03 GtC yr⁻¹ in the 1990s. The ocean models cover 99% to 101% of the total
3 ocean area, so that area-scaling is not necessary.

4 **C.3.3 GOBM evaluation and uncertainty assessment for S_{OCEAN}**

5 The ocean CO₂ sink for all GOBMs and the ensemble mean falls within 90% confidence of the
6 observed range, or 1.5 to 2.9 GtC yr⁻¹ for the 1990s (Ciais et al., 2013) after applying adjustments.
7 An exception is the MPI model, which simulates a low ocean carbon sink of 1.38 GtC yr⁻¹ for the
8 1990s in simulation A owing to the inclusion of riverine carbon flux. After adjusting to the GCB's
9 definition of S_{OCEAN} by subtracting simulation B, the MPI model falls into the observed range with
10 an estimated sink of 1.69 GtC yr⁻¹.

11 The GOBMs and data products have been further evaluated using the fugacity of sea surface CO₂
12 (fCO₂) from the SOCAT v2021 database (Bakker et al., 2016, 2021). We focused this evaluation on
13 the root mean squared error (RMSE) between observed and modelled fCO₂ and on a measure of
14 the amplitude of the interannual variability of the flux (modified after Rödenbeck et al., 2015).
15 The RMSE is calculated from detrended, annually and regionally averaged time series calculated
16 from GOBMs and data-product fCO₂ subsampled to open ocean (water depth > 400 m) SOCAT
17 sampling points to measure the misfit between large-scale signals (Hauck et al., 2020) The
18 amplitude of the S_{OCEAN} interannual variability (A-IAV) is calculated as the temporal standard
19 deviation of the detrended CO₂ flux time series (Rödenbeck et al., 2015, Hauck et al., 2020). These
20 metrics are chosen because RMSE is the most direct measure of data-model mismatch and the A-
21 IAV is a direct measure of the variability of S_{OCEAN} on interannual timescales. We apply these
22 metrics globally and by latitude bands. Results are shown in Fig. B2 and discussed in Section 3.5.5.

23 We quantify the 1- σ uncertainty around the mean ocean sink of anthropogenic CO₂ by assessing
24 random and systematic uncertainties for the GOBMs and data-products. The random
25 uncertainties are taken from the ensemble standard deviation (0.3 GtC yr⁻¹ for GOBMs, 0.3 GtC yr⁻¹
26 for data-products). We derive the GOBMs systematic uncertainty by the deviation of the DIC
27 inventory change 1994-2007 from the Gruber et al (2019) estimate (0.5 GtC yr⁻¹) and suggest
28 these are related to physical transport (mixing, advection) into the ocean interior. For the data-
29 products, we consider systematic uncertainties stemming from uncertainty in fCO₂ observations
30 (0.2 GtC yr⁻¹, Takahashi et al., 2009; Wanninkhof et al., 2013), gas-transfer velocity (0.2 GtC yr⁻¹,



1 Ho et al., 2011; Wanninkhof et al., 2013; Roobaert et al., 2018), wind product (0.1 GtC yr⁻¹, Fay et
2 al., 2021a), river flux adjustment (0.2 GtC yr⁻¹, Jacobson et al., 2007; Resplandy et al., 2018), and
3 fCO₂ mapping (0.2 GtC yr⁻¹, Landschützer et al., 2014). Combining these uncertainties as their
4 squared sums, we assign an uncertainty of ± 0.6 GtC yr⁻¹ to the GOBMs ensemble mean and an
5 uncertainty of ± 0.5 GtC yr⁻¹ to the data-product ensemble mean. These uncertainties are
6 propagated as $\sigma(S_{\text{OCEAN}}) = (1/2^2 * 0.6^2 + 1/2^2 * 0.5^2)^{1/2}$ GtC yr⁻¹ and result in an ± 0.4 GtC yr⁻¹
7 uncertainty around the best estimate of S_{OCEAN} .

8 We examine the consistency between the variability of the model-based and the fCO₂-based data
9 products to assess confidence in S_{OCEAN} . The interannual variability of the ocean fluxes (quantified
10 as A-IAV, the standard deviation after detrending, Figure B2) of the seven fCO₂-based data
11 products plus the Watson et al. (2020) product for 1990-2020, ranges from 0.16 to 0.26 GtC yr⁻¹
12 with the lower estimates by the three ensemble methods (CSIR-ML6, CMEMS-LSCE-FFNN, OS-
13 ETHZ-GRaCER). The inter-annual variability in the GOBMs ranges between 0.10 and 0.19 GtC yr⁻¹,
14 hence there is overlap with the lower A-IAV estimates of three data-products.

15 Individual estimates (both GOBMs and data products) generally produce a higher ocean CO₂ sink
16 during strong El Niño events. There is emerging agreement between GOBMs and data-products on
17 the patterns of decadal variability of S_{OCEAN} with a global stagnation in the 1990s and an extra-
18 tropical strengthening in the 2000s (McKinley et al., 2020, Hauck et al., 2020). The central
19 estimates of the annual flux from the GOBMs and the fCO₂-based data products have a correlation
20 r of 0.94 (1990-2020). The agreement between the models and the data products reflects some
21 consistency in their representation of underlying variability since there is little overlap in their
22 methodology or use of observations.

23

24 **Appendix C.4 Methodology Land CO₂ sink**

25 **C.4.1 DGVM simulations**

26 The DGVMs model runs were forced by either the merged monthly Climate Research Unit (CRU)
27 and 6 hourly Japanese 55-year Reanalysis (JRA-55) data set or by the monthly CRU data set, both
28 providing observation-based temperature, precipitation, and incoming surface radiation on a
29 0.5°x0.5° grid and updated to 2020 (Harris et al., 2014, 2020). The combination of CRU monthly
30 data with 6 hourly forcing from JRA-55 (Kobayashi et al., 2015) is performed with methodology
31 used in previous years (Viovy, 2016) adapted to the specifics of the JRA-55 data.



1 New to this budget is the revision of incoming short-wave radiation fields to take into account
2 aerosol impacts and the division of total radiation into direct and diffuse components as
3 summarised below.

4 The diffuse fraction dataset offers 6-hourly distributions of the diffuse fraction of surface
5 shortwave fluxes over the period 1901-2020. Radiative transfer calculations are based on
6 monthly-averaged distributions of tropospheric and stratospheric aerosol optical depth, and 6-
7 hourly distributions of cloud fraction. Methods follow those described in the Methods section of
8 Mercado et al. (2009), but with updated input datasets.

9 The time series of speciated tropospheric aerosol optical depth is taken from the historical and
10 RCP8.5 simulations by the HadGEM2-ES climate model (Bellouin et al., 2011). To correct for biases
11 in HadGEM2-ES, tropospheric aerosol optical depths are scaled over the whole period to match
12 the global and monthly averages obtained over the period 2003-2020 by the CAMS Reanalysis of
13 atmospheric composition (Inness et al., 2019), which assimilates satellite retrievals of aerosol
14 optical depth.

15 The time series of stratospheric aerosol optical depth is taken from the climatology by Sato et al.
16 (1993), which has been updated to 2012. Years 2013-2020 are assumed to be background years so
17 replicate the background year 2010. That assumption is supported by the Global Space-based
18 Stratospheric Aerosol Climatology time series (1979-2016; Thomason et al., 2018). The time series
19 of cloud fraction is obtained by scaling the 6-hourly distributions simulated in the Japanese
20 Reanalysis (Kobayashi et al., 2015) to match the monthly-averaged cloud cover in the CRU TS
21 v4.03 dataset (Harris et al., 2021). Surface radiative fluxes account for aerosol-radiation
22 interactions from both tropospheric and stratospheric aerosols, and for aerosol-cloud interactions
23 from tropospheric aerosols, except mineral dust. Tropospheric aerosols are also assumed to exert
24 interactions with clouds.

25 The radiative effects of those aerosol-cloud interactions are assumed to scale with the radiative
26 effects of aerosol-radiation interactions of tropospheric aerosols, using regional scaling factors
27 derived from HadGEM2-ES. Diffuse fraction is assumed to be 1 in cloudy sky. Atmospheric
28 constituents other than aerosols and clouds are set to a constant standard mid-latitude summer
29 atmosphere, but their variations do not affect the diffuse fraction of surface shortwave fluxes.



1 In summary, the DGVMs forcing data include time dependent gridded climate forcing, global
2 atmospheric CO₂ (Dlugokencky and Tans, 2021), gridded land cover changes (see Appendix C.2.2),
3 and gridded nitrogen deposition and fertilisers (see Table A1 for specific models details).
4 Four simulations were performed with each of the DGVMs. Simulation 0 (S0) is a control
5 simulation which uses fixed pre-industrial (year 1700) atmospheric CO₂ concentrations, cycles
6 early 20th century (1901-1920) climate and applies a time-invariant pre-industrial land cover
7 distribution and pre-industrial wood harvest rates. Simulation 1 (S1) differs from S0 by applying
8 historical changes in atmospheric CO₂ concentration and N inputs. Simulation 2 (S2) applies
9 historical changes in atmospheric CO₂ concentration, N inputs, and climate, while applying time-
10 invariant pre-industrial land cover distribution and pre-industrial wood harvest rates. Simulation 3
11 (S3) applies historical changes in atmospheric CO₂ concentration, N inputs, climate, and land
12 cover distribution and wood harvest rates.
13 S2 is used to estimate the land sink component of the global carbon budget (S_{LAND}). S3 is used to
14 estimate the total land flux but is not used in the global carbon budget. We further separate S_{LAND}
15 into contributions from CO₂ (=S1-S0) and climate (=S2-S1-S0).

16 **C.4.2 DGVM evaluation and uncertainty assessment for S_{LAND}**

17 We apply three criteria for minimum DGVMs realism by including only those DGVMs with (1)
18 steady state after spin up, (2) global net land flux ($S_{\text{LAND}} - E_{\text{LUC}}$) that is an atmosphere-to-land
19 carbon flux over the 1990s ranging between -0.3 and 2.3 GtC yr⁻¹, within 90% confidence of
20 constraints by global atmospheric and oceanic observations (Keeling and Manning, 2014;
21 Wanninkhof et al., 2013), and (3) global E_{LUC} that is a carbon source to the atmosphere over the
22 1990s, as already mentioned in section 2.2.2. All 17 DGVMs meet these three criteria.

23 In addition, the DGVMs results are also evaluated using the International Land Model
24 Benchmarking system (ILAMB; Collier et al., 2018). This evaluation is provided here to document,
25 encourage and support model improvements through time. ILAMB variables cover key processes
26 that are relevant for the quantification of S_{LAND} and resulting aggregated outcomes. The selected
27 variables are vegetation biomass, gross primary productivity, leaf area index, net ecosystem
28 exchange, ecosystem respiration, evapotranspiration, soil carbon, and runoff (see Fig. B3 for the
29 results and for the list of observed databases). Results are shown in Fig. B3 and discussed in
30 Section 3.6.5.



1 For the uncertainty for S_{LAND} , we use the standard deviation of the annual CO_2 sink across the
2 DGVMs, averaging to about $\pm 0.6 \text{ GtC yr}^{-1}$ for the period 1959 to 2019. We attach a medium
3 confidence level to the annual land CO_2 sink and its uncertainty because the estimates from the
4 residual budget and averaged DGVMs match well within their respective uncertainties (Table 5).

5 **Appendix C.5 Methodology Atmospheric Inversions**

6 Six atmospheric inversions (details of each in Table A4) were used to infer the spatio-temporal
7 distribution of the CO_2 flux exchanged between the atmosphere and the land or oceans. These
8 inversions are based on Bayesian inversion principles with prior information on fluxes and their
9 uncertainties. They use very similar sets of surface measurements of CO_2 time series (or subsets
10 thereof) from various flask and in situ networks. One inversion system also used satellite $x\text{CO}_2$
11 retrievals from GOSAT and OCO-2.

12 Each inversion system uses different methodologies and input data but is rooted in Bayesian
13 inversion principles. These differences mainly concern the selection of atmospheric CO_2 data and
14 prior fluxes, as well as the spatial resolution, assumed correlation structures, and mathematical
15 approach of the models. Each system uses a different transport model, which was demonstrated
16 to be a driving factor behind differences in atmospheric inversion-based flux estimates, and
17 specifically their distribution across latitudinal bands (Gaubert et al., 2019; Schuh et al., 2019).

18 The inversion systems prescribe same global fossil fuel emissions for E_{FOS} ; specifically, the GCP's
19 Gridded Fossil Emissions Dataset version 2021 (GCP-GridFEDv2021.2; Jones et al., 2021b), which is
20 an update through 2020 of the first version of GCP-GridFED presented by Jones et al. (2021a).
21 GCP-GridFEDv2021.2 scales gridded estimates of CO_2 emissions from EDGARv4.3.2 (Janssens-
22 Maenhout et al., 2019) within national territories to match national emissions estimates provided
23 by the GCP for the years 1959-2020, which were compiled following the methodology described in
24 Appendix C.1 based on all information available on 31st July 2021 (R. Andrew, *pers. comm.*).

25 Typically, the GCP-GridFED adopts the seasonal variation in emissions (the monthly distribution of
26 annual emissions) from EDGAR and applies small corrections based on heating or cooling degree
27 days to account for the effects of inter-annual climate variability on the seasonality emissions
28 (Jones et al., 2021a). However, strategies taken to deal with the COVID-19 pandemic during 2020
29 mean that the seasonality of emissions diverged substantially in 2020 from a typical year. To
30 account for this change, GCP-GridFEDv2021.2 adopts the national seasonality in emissions from
31 Carbon Monitor (Liu et al., 2020a,b) during the years 2019-2020 (Jones et al. 2021b).



1 The consistent use of GCP-GridFEDv2021.2 for E_{FOS} ensures a close alignment with the estimate of
2 E_{FOS} used in this budget assessment, enhancing the comparability of the inversion-based estimate
3 with the flux estimates deriving from DGVMs, GOBMs and fCO_2 -based methods. To account for
4 small differences in regridding, and the use of a slightly earlier file version (GCP-GridFEDv2021.1)
5 for 2000-2018 in CarbonTracker Europe, small fossil fuel corrections were applied to all inverse
6 models to make the estimated uptake of atmospheric CO_2 fully consistent. Finally, we note that
7 GCP-GridFEDv2021.2 includes emissions from cement production, but it does not include the
8 cement carbonation CO_2 sink (Xi et al., 2016; Cao et al., 2020; Guo et al. 2021) that is applied to
9 the GCB estimate of E_{FOS} in Table 6.

10 The land and ocean CO_2 fluxes from atmospheric inversions contain anthropogenic perturbation
11 and natural pre-industrial CO_2 fluxes. On annual time scales, natural pre-industrial fluxes are
12 primarily land CO_2 sinks and ocean CO_2 sources corresponding to carbon taken up on land,
13 transported by rivers from land to ocean, and outgassed by the ocean. These pre-industrial land
14 CO_2 sinks are thus compensated over the globe by ocean CO_2 sources corresponding to the
15 outgassing of riverine carbon inputs to the ocean, using the exact same numbers and distribution
16 as described for the oceans in Section 2.4. To facilitate the comparison, we adjusted the inverse
17 estimates of the land and ocean fluxes per latitude band with these numbers to produce historical
18 perturbation CO_2 fluxes from inversions. Finally, for the presentation of the comparison in Figure
19 11 we modified the FF-corrected and riverine-adjusted land sinks from the inversions further, by
20 removing a 0.2 GtCyr^{-1} CO_2 sink that is ascribed to cement carbonation in the GCB, rather than to
21 terrestrial ecosystems. The latter is not applied in the inversion products released through GCB or
22 the original data portals of these products.

23 All participating atmospheric inversions are checked for consistency with the annual global growth
24 rate, as both are derived from the global surface network of atmospheric CO_2 observations. In this
25 exercise, we use the conversion factor of 2.086 GtC/ppm to convert the inverted carbon fluxes to
26 mole fractions, as suggested by Prather (2012). This number is specifically suited for the
27 comparison to surface observations that do not respond uniformly, nor immediately, to each
28 year's summed sources and sinks. This factor is therefore slightly smaller than the GCB conversion
29 factor in Table 1 (2.142 GtC/ppm , Ballantyne et al., 2012). Overall, the inversions agree with the
30 growth rate with biases between $0.03\text{-}0.08 \text{ ppm}$ ($0.06\text{-}0.17 \text{ GtCyr}^{-1}$) on the decadal average.



1 The atmospheric inversions are also evaluated using vertical profiles of atmospheric CO₂
2 concentrations (Fig. B4). More than 30 aircraft programs over the globe, either regular programs
3 or repeated surveys over at least 9 months, have been used in order to draw a robust picture of
4 the model performance (with space-time data coverage irregular and denser in the 0-45°N
5 latitude band; Table A6). The six models are compared to the independent aircraft CO₂
6 measurements between 2 and 7 km above sea level between 2001 and 2020. Results are shown in
7 Fig. B4, where the inversions generally match the atmospheric mole fractions to within 0.6 ppm at
8 all latitudes, except for CT Europe in 2010-2020 over the more sparsely sampled southern
9 hemisphere.

10 **Appendix D Processes not included in the global carbon budget**

11 **Appendix D.1 Contribution of anthropogenic CO and CH₄ to the global carbon budget**

12 Equation (1) includes only partly the net input of CO₂ to the atmosphere from the chemical
13 oxidation of reactive carbon-containing gases from sources other than the combustion of fossil
14 fuels, such as: (1) cement process emissions, since these do not come from combustion of fossil
15 fuels, (2) the oxidation of fossil fuels, (3) the assumption of immediate oxidation of vented
16 methane in oil production. However, it omits any other anthropogenic carbon-containing gases
17 that are eventually oxidised in the atmosphere, such as anthropogenic emissions of CO and CH₄.
18 An attempt is made in this section to estimate their magnitude and identify the sources of
19 uncertainty. Anthropogenic CO emissions are from incomplete fossil fuel and biofuel burning and
20 deforestation fires. The main anthropogenic emissions of fossil CH₄ that matter for the global
21 (anthropogenic) carbon budget are the fugitive emissions of coal, oil and gas sectors (see below).
22 These emissions of CO and CH₄ contribute a net addition of fossil carbon to the atmosphere.

23 In our estimate of E_{FOS} we assumed (Section 2.1.1) that all the fuel burned is emitted as CO₂, thus
24 CO anthropogenic emissions associated with incomplete fossil fuel combustion and its
25 atmospheric oxidation into CO₂ within a few months are already counted implicitly in E_{FOS} and
26 should not be counted twice (same for E_{LUC} and anthropogenic CO emissions by deforestation
27 fires). Anthropogenic emissions of fossil CH₄ are however not included in E_{FOS}, because these
28 fugitive emissions are not included in the fuel inventories. Yet they contribute to the annual CO₂
29 growth rate after CH₄ gets oxidized into CO₂. Emissions of fossil CH₄ represent 30% of total
30 anthropogenic CH₄ emissions (Saunois et al. 2020; their top-down estimate is used because it is



1 consistent with the observed CH₄ growth rate), that is 0.083 GtC yr⁻¹ for the decade 2008-2017.
2 Assuming steady state, an amount equal to this fossil CH₄ emission is all converted to CO₂ by OH
3 oxidation, and thus explain 0.083 GtC yr⁻¹ of the global CO₂ growth rate with an uncertainty range
4 of 0.061 to 0.098 GtC yr⁻¹ taken from the min-max of top-down estimates in Saunois et al. (2020).
5 If this min-max range is assumed to be 2 σ because Saunois et al. (2020) did not account for the
6 internal uncertainty of their min and max top-down estimates, it translates into a 1- σ uncertainty
7 of 0.019 GtC yr⁻¹.
8 Other anthropogenic changes in the sources of CO and CH₄ from wildfires, vegetation biomass,
9 wetlands, ruminants, or permafrost changes are similarly assumed to have a small effect on the
10 CO₂ growth rate. The CH₄ and CO emissions and sinks are published and analysed separately in the
11 Global Methane Budget and Global Carbon Monoxide Budget publications, which follow a similar
12 approach to that presented here (Saunois et al., 2020; Zheng et al., 2019).

13 **Appendix D.2 Contribution of other carbonates to CO₂ emissions**

14 Although we do account for cement carbonation (a carbon sink), the contribution of emissions of
15 fossil carbonates (carbon sources) other than cement production is not systematically included in
16 estimates of E_{FOS}, except at the national level where they are accounted for in the UNFCCC
17 national inventories. The missing processes include CO₂ emissions associated with the calcination
18 of lime and limestone outside cement production. Carbonates are also used in various industries,
19 including in iron and steel manufacture and in agriculture. They are found naturally in some coals.
20 CO₂ emissions from fossil carbonates other than cement are estimated to amount to about 1% of
21 E_{FOS} (Crippa et al., 2019), though some of these carbonate emissions are included in our estimates
22 (e.g., via UNFCCC inventories).

23 **Appendix D.3 Anthropogenic carbon fluxes in the land-to-ocean aquatic continuum**

24 The approach used to determine the global carbon budget refers to the mean, variations, and
25 trends in the perturbation of CO₂ in the atmosphere, referenced to the pre-industrial era. Carbon
26 is continuously displaced from the land to the ocean through the land-ocean aquatic continuum
27 (LOAC) comprising freshwaters, estuaries, and coastal areas (Bauer et al., 2013; Regnier et al.,
28 2013). A substantial fraction of this lateral carbon flux is entirely 'natural' and is thus a steady
29 state component of the pre-industrial carbon cycle. We account for this pre-industrial flux where
30 appropriate in our study (see Appendix C.3). However, changes in environmental conditions and



1 land-use change have caused an increase in the lateral transport of carbon into the LOAC – a
2 perturbation that is relevant for the global carbon budget presented here.
3 The results of the analysis of Regnier et al. (2013) can be summarized in two points of relevance
4 for the anthropogenic CO₂ budget. First, the anthropogenic perturbation of the LOAC has
5 increased the organic carbon export from terrestrial ecosystems to the hydrosphere by as much as
6 $1.0 \pm 0.5 \text{ GtC yr}^{-1}$ since pre-industrial, mainly owing to enhanced carbon export from soils. Second,
7 this exported anthropogenic carbon is partly respired through the LOAC, partly sequestered in
8 sediments along the LOAC and to a lesser extent, transferred to the open ocean where it may
9 accumulate or be outgassed. The increase in storage of land-derived organic carbon in the LOAC
10 carbon reservoirs (burial) and in the open ocean combined is estimated by Regnier et al. (2013) at
11 $0.65 \pm 0.35 \text{ GtC yr}^{-1}$. The inclusion of LOAC related anthropogenic CO₂ fluxes should affect
12 estimates of S_{LAND} and S_{OCEAN} in Eq. (1) but does not affect the other terms. Representation of the
13 anthropogenic perturbation of LOAC CO₂ fluxes is however not included in the GOBMs and
14 DGVMs used in our global carbon budget analysis presented here.

15 **Appendix D.4 Loss of additional land sink capacity**

16 Historical land-cover change was dominated by transitions from vegetation types that can provide
17 a large carbon sink per area unit (typically, forests) to others less efficient in removing CO₂ from
18 the atmosphere (typically, croplands). The resultant decrease in land sink, called the ‘loss of
19 additional sink capacity’, can be calculated as the difference between the actual land sink under
20 changing land-cover and the counterfactual land sink under pre-industrial land-cover. This term is
21 not accounted for in our global carbon budget estimate. Here, we provide a quantitative estimate
22 of this term to be used in the discussion. Seven of the DGVMs used in Friedlingstein et al. (2019)
23 performed additional simulations with and without land-use change under cycled pre-industrial
24 environmental conditions. The resulting loss of additional sink capacity amounts to $0.9 \pm 0.3 \text{ GtC}$
25 yr^{-1} on average over 2009-2018 and $42 \pm 16 \text{ GtC}$ accumulated between 1850 and 2018 (Obermeier
26 et al., 2021). OSCAR, emulating the behaviour of 11 DGVMs finds values of the loss of additional
27 sink capacity of $0.7 \pm 0.6 \text{ GtC yr}^{-1}$ and $31 \pm 23 \text{ GtC}$ for the same time period (Gasser et al., 2020).
28 Since the DGVM-based ELUC estimates are only used to quantify the uncertainty around the
29 bookkeeping models' ELUC we do not add the loss of additional sink capacity to the bookkeeping
30 estimate.